THE VISUALLY EVOKED MAGNETIC RESPONSE (VEMR) TO A PATTERN ONSET/OFFSET STIMULUS.

A Thesis submitted for the degree of Doctor of Philosophy

by Christopher Degg

THE UNIVERSITY OF ASTON IN BIRMINGHAM

NOVEMBER 1993.

The University of Aston in Birmingham.

The visually evoked magnetic response (VEMR) to a pattern onset/offset stimulus.

Christopher Degg.

Submitted for the Degree of Doctor of Philosophy, November 1993

Thesis Summary.

This study characterizes the visually evoked magnetic response (VEMR) to pattern onset/offset stimuli, using a single channel BTi magnetometer. The influence of stimulus parameters and recording protocols on the VEMR is studied, with inferences drawn about the nature of cortical processing, its origins and optimal recording strategies.

Fundamental characteristics are examined, such as the behaviour of successive averaged and unaveraged responses; the effects of environmental shielding; averaging; inter- and intrasubject variability and equipment specificity.

The effects of varying check size, field size, contrast and refractive error on latency, amplitude and topographic distribution are also presented. Latency and amplitude trends are consistent with previous VEP findings and known anatomical properties of the visual system. Topographic results are consistent with the activity of sources organised according to the cruciform model of striate cortex. A striate origin for the VEMR is also suggested by the results to quarter, octant and annulus field stimuli.

Similarities in the behaviour and origins of the sources contributing to the CIIm and CIIIm onset peaks are presented for a number of stimulus conditions. This would be consistent with differing processing events in the same, or similar neuronal populations.

Focal field stimuli produce less predictable responses than full or half fields, attributable to a reduced signal to noise ratio and an increased sensitivity to variations in cortical morphology.

Problems with waveform peak identification are encountered for full field stimuli that can only be resolved by the careful choice of stimulus parameters, comparisons with half field responses or with reference to the topographic distribution of each waveform peak.

An anatomical study of occipital lobe morphology revealed large inter- and intrasubject variation in calcarine fissure shape and striate cortex distribution. An appreciation of such variability is important for VEMR interpretation, due to the technique's sensitivity to source depth and orientation, and it is used to explain the experimental results obtained.

Keywords : Neuromagnetism, Visually evoked magnetic response, Pattern onset/offset, Stimulus parameters, Topographic mapping.

FOR SARAH

ACKNOWLEDGEMENTS

I would like to express my gratitude to the following people:

To my supervisor, Professor G.F.A. Harding, for the initiation of this project, and the continued advice.

To my associate supervisor, Dr. R.A. Armstrong for his support, assistance and statistical advice.

To Dr. A. Slaven for her friendship throughout.

To Sarah Cadman for her patience and the innumerable hours spent sitting under the magnetometer.

To my parents for their continual encouragement.

To Dr. S. Swithenby of the Open University and Dr. B. Janday of Aston University for the source localisation performed on the 42 point mapping data (figure 6.41A).

To James Bedford for the localisation of the 20 point mapping data (figures 6.41B, 6.42 and 6.43).

To Gareth Barnes for writing the data acquisition computer programs used to record the unaveraged responses of section 5.33 and 5.36.

To everyone who acted as a subject.

I am indebted to the Department of Vision Sciences at Aston University for provision of a departmental studentship.

LIST OF CONTENTS

CHAPTER 3 - INTRODUCTION - THE VISUAL SYSTEM

CHAPTER 4 - METHODS

CHAPTER 5 - TECHNICAL CONSIDERATIONS

LIST OF TABLES

LIST OF FIGURES

CHAPTER 1

1.1 INTRODUCTION - GENERAL BACKGROUND.

The theoretical differences between magnetoencephalography and other neural imaging techniques currently available, offer potential advantages for its use in fundamental research and clinical studies. Surprisingly few authors have studied systematically the effects of varying stimulus parameters and recording protocols on the visually evoked magnetic response (VEMR). Such studies, with normal subjects, are an essential precursor to the clinical evaluation of any technique. A recent exception is provided by Slaven (1992), who studied the pattern reversal VEMR on normal subjects with a view to clinical evaluation.

The aim of this thesis is to characterise the visually evoked magnetic response to a pattern onset/offset stimulus. It is hoped that this will offer an insight into the underlying processing events, their cortical origins, and possible implications for recording in a clinical context.

Biomagnetism is the study of magnetic fields which originate in biological systems, while the magnetoencephalograph (MEG) specifically relates to fields produced by the ionic currents within neural tissue (Pizella and Romani 1990). The first biomagnetic recording was reported as early as 1963 by Baule and McFee. They measured cardiac activity using a detector consisting of several million turns of copper wire, wrapped around a ferrite core. Similar equipment was also used by Cohen (1968), who reported the first measurements of neural activity. The poor signal to noise conditions attainable with such crude equipment severely restricted the techniques availability and their application. This is not surprising, considering the amplitude of the evoked neuromagnetic signal is approximately 10^9 that of the earth's steady magnetic field, and 10^5 that of its fluctuations (Stok 1986). In subsequent years, the development of superconducting materials, cryogenics, gradiometer detection coils and shielded environments has greatly improved signal to noise conditions, making the technique more accessible. Using such equipment, the first measurements of the cortically evoked response to flash and patterned stimuli were made in 1975 by Cohen and Brenner respectively. Subsequently, MEG has been applied to a variety of biological systems (see chapter 2).

This chapter considers the technical aspects of magnetometry; its instrumentation, especially with respect to single channel systems; and the implications for data interpretation.

1.2 - CRYOGENICS AND DEWAR DESIGN.

The high sensitivity of the magnetometer to external magnetic fields relies upon the principle of superconductivity. Hence, certain materials lose all electrical resistance when cooled to liquid helium temperatures (-273° or 4.2K). Each material exhibits a critical temperature (Tc) at which superconductivity becomes possible. The disturbing effects of thermal energy decline as this temperature is lowered further, making it practical to operate systems at a temperature equivalent to 1/2 Tc. For niobium based superconducting quantum interference devices (SQUID's), such as those used in current magnetometers, the typical Tc is 9.3K while the operating temperature is below 4.7K (Fagaly 1990). Hence, the cryostat (or dewar) provides an environment in which such low temperatures can be maintained, without appreciably contributing to ambient noise levels.

Figure 1.2 shows a three dimensional representation of a single channel magnetometer. The space between the inner and outer dewar walls is evacuated to minimise heat loss by radiation, conduction or convection (Crum 1985). Conduction is further reduced by the choice of construction material, while making the surfaces shiny in the infrared portion of the spectrum lowers radiated heat transfer. Convection is prevented by sealing the top of the dewar from the atmosphere. Heat transfer can also occur by 'thermally driven acoustic oscillation', which can be prevented by making any tubes within the dewar open or closed at each end (Zimmerman 1982).

The vacuum space contains a thermal shield designed to further reduce heat transfer by radiation. This is commonly made of laminated plastic, with aluminium or copper wires running longitudinally. The use of metal sheet is avoided to minimise eddy current fields and Nyquist noise (see section 1.5) (Zimmerman 1982). Radiated heat is carried to the point where the shield joins the dewar neck, at which point it is transferred to the cold helium (Fagaly 1990).

The dewar must be transparent to magnetic fields (Fagaly 1990), with minimal electrical conductance (Zimmerman 1982).

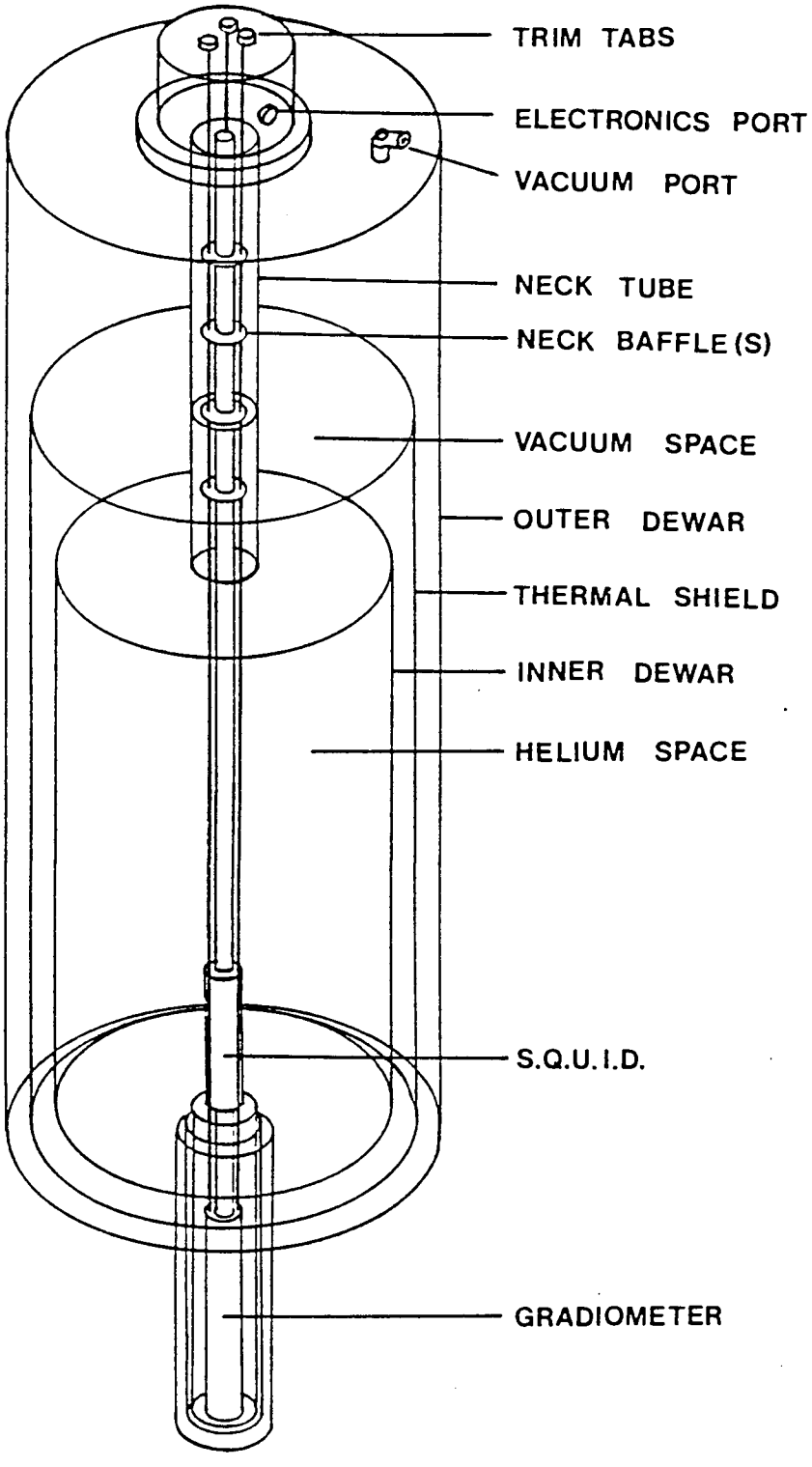

Figure 1.2 - Three dimensional representation of a single channel SQUID magnetometer.

The base of the dewar is elongated to form a tail section. The vacuum space and wall material are thinner in this region, to minimise the distance separating the gradiometer coils from the outer surface. When multiple channels are used, the increase in surface area of the tail usually requires thicker wall material. In extreme cases, the gradiometers may be incorporated within the vacuum space, to achieve an acceptable coil to scalp separation (Fagaly 1990).

The dewar neck allows access to the inner dewar (or helium space), for the magnetometer probe with its associated low temperature electronics (gradimeters, SQUID etc). It also provides the means for helium filling, and the venting of gaseous helium.

In all dewar designs, the liquid helium constantly evaporates, at a rate influenced by factors such as the cross sectional area of the neck, and the number of inserts. For a typical single channel system, approximately 1.3 litres of helium evaporate daily (Fagaly 1990). Hence, in the BTi magnetometer, helium gas is vented to atmosphere through a one way valve and a flow meter. The valve prevents atmospheric oxygen being drawn into the helium chamber. Oxygen is a possible source of noise, while air vapour could freeze within the dewar neck, risking blockage (Crum 1985). If helium cannot vent from the dewar, due to blockage or poor design, the resulting increase in interior pressure could result in an explosion.

The high cost of helium lost to evaporation, together with the inconvenience of regular fills is an undesirable aspect of magnetometry. An alternative is offered by closed cycle refrigeration, however, such techniques are prone to problems with magnetic noise and vibration (Williamson et al 1987). There are now multiple stage refrigeration techniques available, with non mechanical later stages to reduce noise fluctuations (Fagaly 1990).

1.3 - SQUID OPERATION.

Magnetometry relies upon the phenomenon of superconductivity, by which certain materials lose all electrical resistance when cooled below a critical transition temperature (Tc). At present, 28 metallic elements have been shown to demonstrate this property at varying values of Tc, while alloys have helped to raise this temperature (Gallop 1990). This section gives a brief

overview of magnetometer operation, a detailed description is provided by Gallop (1990).

The magnetometer essentially consists of a detector coupled to an input coil, (collectively called a flux transformer), and a superconducting quantum interference device (SQUID). Each of these are constructed from superconducting material and are maintained in a liquid helium environment (Figure 1.2). The associated output and feedback electronics operate at room temperature, being housed outside the dewar. Any magnetic flux applied to the detection coil induces a proportional current flow around the SQUID. circuit. This induces a magnetic field in the input coil, which is then detected by the SQUID. (Erne 1982). Although magnetic flux could be directly detected by the SQUID, the use of the flux transformer helps to reject unwanted noise, while amplifying the signal of interest (Fagaly 1990).

In order to understand the functioning of the SQUID, two fundamental principles have to be established. Firstly, if a closed ring of superconducting material is cooled below its critical temperature, in the presence of a magnetic field, flux remains trapped within the ring even after its source is removed. The flux is expelled from the bulk of the material however by a current flowing on the inner surface of the ring, which can flow indefinitely due to the lack of resistance. If another magnetic field approaches, its flux is prevented from entering the material by the creation of a shielding current in the outer surface of the ring. This exclusion of magnetic flux is known as the Meissner effect (Kaufman and Williamson 1980). If two superconducting rings are now considered, separated from each other by a thin layer of insulator, electrons can penetrate the surface of the material for a short distance as their energy decays. If a section of the insulator is thinned (~1-2nm), thereby creating a 'weak link' between superconductors, a situation can arise where electrons of sufficient energy tunnel through the insulator and interchange between the rings. The increased energy of the superconducting state occurring at this weak link (or Josephson Junction), is known as the Josephson coupling effect (Josephson 1965). With careful design, the superconducting state within the junction becomes ineffective when the ring attempts to shield out one flux quantum of magnetic field. This influx of a flux quantum, followed by the recovery of the superconducting state repeats periodically as long as the magnetic field applied increases (Kaufman and Williamson 1980).

The SQUID does not operate passively, but instead requires a biasing current at either a radio frequency (rf-SQUID) or a direct current (dc-SQUID). (Romani and Narici 1986). The rf-SQUID employs a single Josephson junction, and flux changes are detected by a 'resonant tank circuit' inductively coupled to the SQUID (Fagaly 1990). Such systems have been commercially available for longer that the dc-SQUID, being relatively inexpensive and reliable. The dc-SQUID differs from the rf in the nature of its biasing current, detection circuit and the use of two Josephson Junctions. (Figure 1.3). Its construction is more complex, as the characteristics of each junction must be matched, however the associated electronics are simpler (Gallop 1990). The dc-SQUID also has the advantage of a lower noise susceptibility, and greater signal sensitivity (Romani and Narici 1986).

A dc. bias current is fed to the SQUID ring, which develops a dc voltage across the junctions. This varies as a periodic function of any flux applied to the SQUID by the input coil (Gallop 1990). The output voltage is used to control a negative feedback circuit which causes a current to flow in a coil next to the SQUID, of sufficient field to cancel the effects of the input coil. (Fagaly 1990). The magnetometer output is taken from the feedback circuit, providing a current which is linearly proportional to the applied field (Kaufman and Williamson 1980).

The ability of the feedback circuit to monitor the operation of the SQUID requires it to be locked to a particular flux cycle. This state can be disrupted, (or flux jump), if the SQUID input varies more rapidly than the feedback circuit can track. The speed at which the system tracks flux is called its slew rate (Fagaly 1990), and commercial systems such as the BTi allow one of two rates to be chosen. Slow mode tracking is less affected by strong electrical transients and flux jumping, while the fast mode is less robust but allows more rapidly changing signals to be tracked.

The magnetometer can therefore be considered as a linear flux to current converter with low noise, and high gain (Fagaly 1990).

1.4 - GRADIOMETRIC DETECTION COILS.

Gradiometric input coils improve signal to noise conditions by the spatial discrimination between signals from origins of differing distance (Zimmerman et al 1971). The gradiometer is a single length of

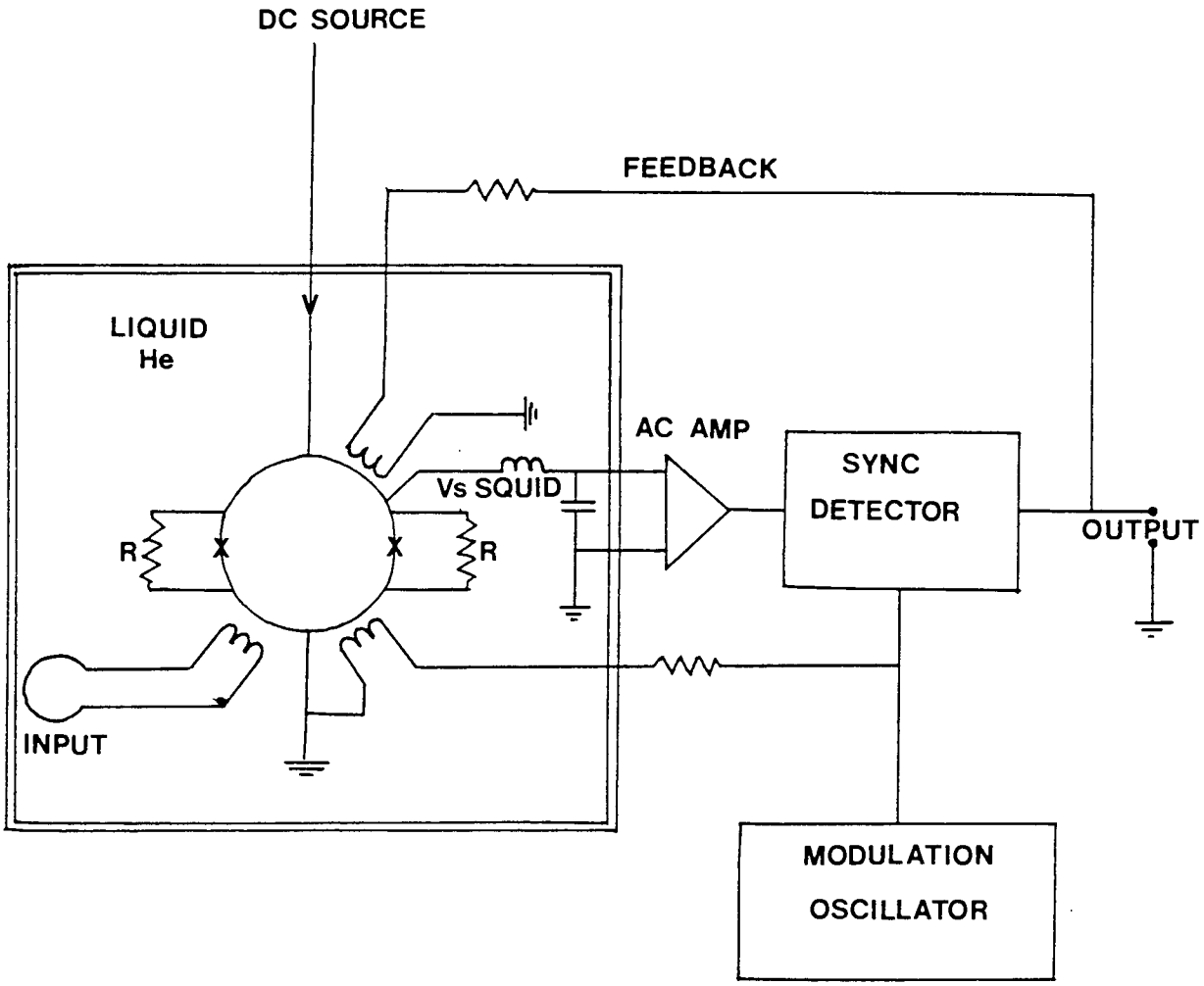

Figure 1.3 - The electronics associated with the D.C. SQUID magnetometer.

superconducting wire, usually niobium, whose discriminate properties depend upon coiling geometry. Most commercial gradiometers are axial (i.e. the plane of the coils lie parallel to the surface of the skin), and so preferentially detect radial field source components. Some groups (Ahlfors et al 1992) use planar gradiometers which measure the tangential field component, while it is also possible to monitor all three vector components simultaneously (Fagaly 1990). Although planar gradiometers can improve localisation accuracy and multiple source discrimination (Romani and Pizella 1990), the tangential field component is difficult to interpret since it constitutes a mixture of primary and secondary sources (Okada 1983).

The simplest detector is a single loop of wire (Figure 1.4A), however this is of limited value as it provides no discriminatory properties. The first order gradiometer has two parallel counter wound coils (Figure 1.4B). Fields threading the lower coil alone are registered, while those which thread both coils induce a current which is self cancelling. Such a detector is therefore insensitive to distant sources which tend to produce spatially uniform magnetic fields. Their use has proved sufficient only in shielded environments, due to the graded fields present in unshielded conditions. The second order gradiometer is essentially two first order coils arranged in series (Figure 1.4C). Its geometry allows for the rejection of spatially uniform fields, and fields with spatially uniform field gradients (Carelli et al 1982). Improvements in signal to noise ratio by a factor of 10^6 can be achieved over the signal loop detector (Fagaly 1990), and this has enabled the widespread application of the technique in unshielded environments. Higher order configurations can further improve noise cancellation, although the consequent increase in wire length is detrimental to the efficiency of flux transfer (Carelli et al 1982). In practice, gradiometers of increasing order detect progressively less signal strength from a source of fixed depth (Hari et al 1988). An important consideration for gradiometer design is the choice of baseline, or the distance separating the detection coil from the first compensation coil (Figure 1.4 BL). Sources which lie closer to the detection coil than the baseline produce fields which do not affect the compensation coils. Hence, the flux detected by the SQUID is proportional to field strength and not its gradient (Carelli et al 1982). A 3 to 4cm baseline provides optimal sensitivity for the detection of cortical sources (Kaufman et al 1987). Longer baselines can be used for deeper sources, at the expense of noise

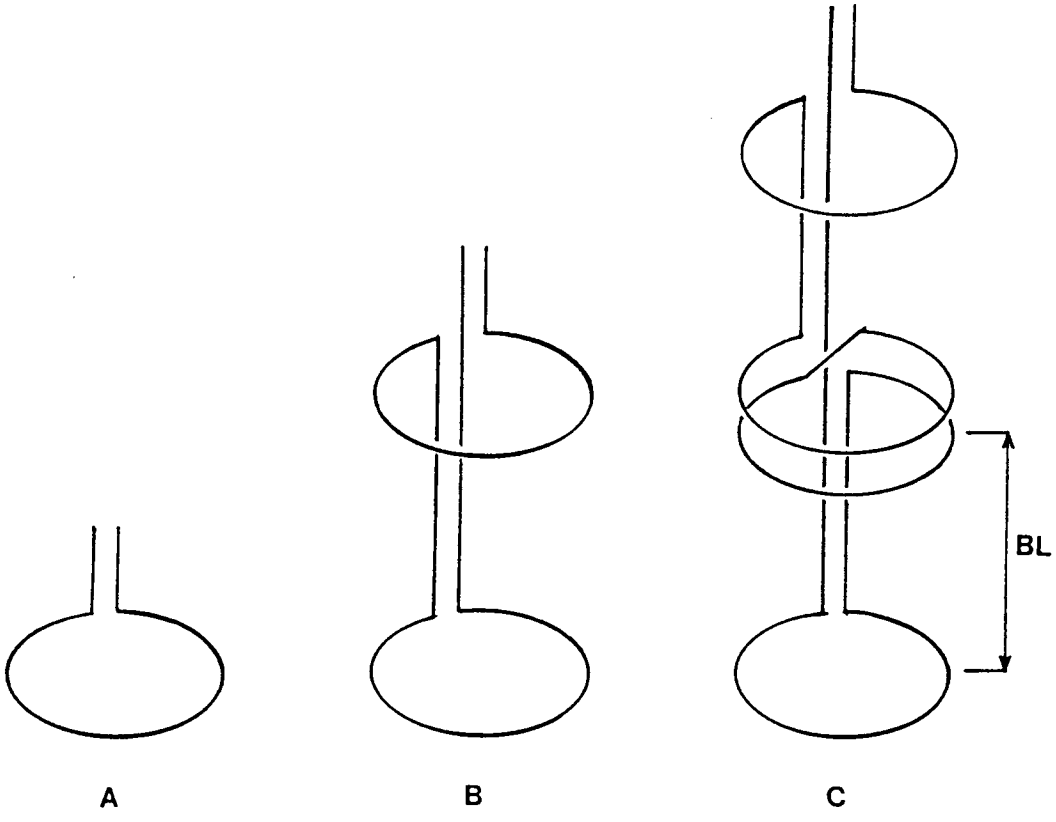

Figure 1.4 - Gradiometric pick up coil configurations.
A - a simple loop of wire. **B** - a single order gradiometer. **C** - a second order gradiometer.
BL - the baseline of the gradiometer, ie the distance between the detection coil and the first compensation coil.

discrimination. A second construction variable is coil diameter. Increasing coil area produces greater sensitivity to weaker sources (Fagaly 1990), with a reduction in spatial resolution, resulting in a blurred image of displaced maxima (Kaufman et al 1987). It is possible to overcome this by the use of asymmetric coils, hence a detector of smaller area but more turns than its compensation coil, will exhibit increased spatial resolution and sensitivity (Fagaly 1990).

It is not possible to manufacture gradiometers with coils of sufficiently accurate area and separation for optimal operation. As a consequence, most systems allow the shape of the coils to be adjusted from outside the dewar, by use of superconducting tabs fastened to the coil in orthogonal directions (Figure 1.2). In multichannel systems, where the complexity of such mechanical balancing is impractical, software noise cancellation is relied upon, with the use of three orthogonal noise detection coils (Romani and Narici 1986). The inefficiency of such systems however has restricted the use of multichannel magnetometry to shielded environments (Fenwick 1990).

1.5 - NOISE SOURCES AND THEIR EXCLUSION.

Problems encountered by all biological recording techniques is the separation of signals from noise. Table 1.5 lists some typical amplitudes and frequencies for fields of physiological origin, (Duret and Karp 1983). Noise can be of environmental, subject or instrumental origin. Environmental noise is dominant, with sources including the earth's magnetic field (30 - 100μT Gallop 1990); its fluctuations (Romani and Narici 1986); the interaction of solar winds with the magnetosphere (Fagaly 1990); distortion of the earth's field by large metallic structures; the electricity power frequency (Gallop 1990); and the presence of low frequency fields from nearby vehicles. Subject noise is a particular problem electrophysiologically, since myogenic activity produces large amplitude masking potentials. Magnetically, subject noise problems occur with ferromagnetic material, such as jewellery, watches and underwired bras. The effects of myogenic activity, minor movement and eye blinks are not particularly evident, although background brain activity, such as alpha rhythm can give problems when trying to record evoked activity (Cohen 1968). Intrinsic, or system noise, has many origins which can compound to produce untenable conditions. Nyquist noise results from

TABLE 1.5 - Some typical amplitudes and frequencies for magnetic fields of physiological origin. Source - Duret and Karp (1983).

random thermal fluctuations, particularly in metallic components of the dewar (Zimmerman 1982). Josephson noise is thermal noise associated with the resistance of the input coil and Josephson junctions (Gallop 1990). Johnson noise originates from eddy currents generated in the thermal shield, and its effects are pronounced due to the close proximity to the detector coils (Fagaly 1990). Noise can also occur from movements of the SQUID and its detector on their mountings, relative to ambient fields; mechanical deformations of the SQUID resulting from thermal fluctuations; thermoelectric currents induced in poorly designed superconducting shields during cooling (Gallop 1990); and vibration movements resulting from helium boil off (Zimmerman 1982). SQUID noise amplitude is frequency dependent, showing an inverse relationship with lower frequencies (1/F noise), and an invariant relationship at higher frequency (white noise) (Fagaly 1990).

The commonest approach to environmental noise reduction is the adoption of gradiometric pick up coils, which are insensitive to uniform fields, or fields of uniform gradient. Although such an approach has allowed recordings to be made in a variety of urban environments, this is achieved at the expense of reduced sensitivity (Romani and Narici 1986). A noise improvement of three orders of magnitude can be achieved by moving from an urban to rural environment (Carelli et al 1982). A third approach is in the use of electromagnetically shielded rooms, which although expensive, small (Romani and Narici 1986) and unportable (Fenwick 1990), are becoming more common. Eddy current shielding consists of copper or aluminium sheets welded together to form a sealed cube. Time varying magnetic fields induce circulatory currents in the metal, cancelling fields within the material and the inner space according to Lenzs law (Fagaly 1990). This is the cheapest form of shielding, best suited for high frequency attenuation, as lower frequencies require increasingly thicker walls (Gallop 1990). For low frequency attenuation, ferromagnetic materials such as mu-metal are used, due to their high permeability. Low frequency fields are diverted around the shield walls, following a path of lower resistance to that of the surrounding air (Erne 1982). For a given wall thickness, mu-metal shielding is more efficient if used in multiple layers. Hence, many commercial shielded rooms consist of a single layer of aluminium or copper, lined by 2-6 layers of mu-metal (Gallop 1990). Larger rooms are preferable, since thermal noise increases closer to the walls (Katila et al 1991). Mains interference can be reduced by limiting

ground loops, and the use of eddy current shields, notch filters, coaxial cables or battery powered equipment (Gallop 1990). Intrinsic noise can be reduced by careful dewar design. Rigid mounting of the SQUID prevents mechanical vibration and deformations (Gallop 1990). Johnson noise can be reduced by the use of resistive materials, at the cost of rf noise susceptibility (Fagaly 1990). Eddy current and Nyquist noise can be reduced by the use of electrically non conducting materials and the inclusion of vapour cooled radiation shields (Zimmerman 1982).

Signal enhancement can also be made during the data analysis stages, by the use of signal filtering, averaging and artefact rejection.

1.6 - SIGNAL RECORDING AND FILTERING.

The use of electronic filters to selectively remove signals of specific frequency has become a universally accepted method of improving signal to noise conditions. A description of signal filtering with respect to electrophysiological recordings is given by Regan (1989). Such filters can be analogue or digital, applied directly to the input signal (on-line), or to previously stored raw data (off-line). An appreciation of filter characteristics is essential for optimal experimental design, since the use of incorrect filter types and settings can produce latency and amplitude distortion (Skuse and Burke 1990).

Most recording devices produce an output of varying voltage, (analogue signal), which is converted to a numerical format by the averaging computer (Digitised or sampled). The choice of an appropriate sampling rate is important to prevent waveform distortions. The minimum sampling rate (or Nyquist criterion) should be more than twice that of the highest signal frequency, with frequencies greater than half the sampling rate removed by anti-aliasing filters. Filtering regimes remove unwanted noise by allowing only those signals within a specified frequency bandwidth to be analysed. This is achieved by the combination of low pass filters which set the upper frequency cut-off limit, high pass filters which set the lower limit and notch filters to remove signals of a specific fundamental frequency and their harmonics. Ideally, filters should produce amplitude attenuation independent of frequency within the pass band; an infinite attenuation outside this band; an infinitely steep transition between bands, and a phase response linearly

dependent on frequency, so as to produce a constant delay (Erne 1982). Such ideals are unattainable electronically however, and so the mathematical approximation of a filter to this ideal is referred to as its order (Erne 1982). Instead of an infinitely steep reduction in gain (voltage output/input) at the desired cut-off frequency, practical filters show a more gradual attenuation (filter roll-off). This is quantified by the frequency corresponding to a gain of $1/\sqrt{2}$, or 3dB below maximum. A steep roll off increases the attenuation of unwanted signal frequencies, while producing minimal latency distortion (Skuse and Burke 1990), however amplitude fluctuations can develop in the region near pass band frequency (Erne 1982).

All filters introduce a time delay between the input and output signal, and unless all frequencies are delayed uniformly, distortion of complex waveforms can result (Erne 1982). Such effects are more pronounced with low than high pass filters, a change from 100 to 30 Hz typically producing a 10ms delay (Regan 1989). Differences in filter performance may also affect latency, with two sets of apparently identical filters producing latency differences of 10ms or more (Armstrong et al 1991). High pass filters affect relative amplitude more than latency, resulting in variable waveform morphology. Latency distortion is influenced by the phase characteristics of each filter type (see Regan 1989). With a high pass filter, the input and output signals are in phase at high frequencies, but as frequency decreases, the output progressively leads the input. With low pass filters, lower frequencies are in phase, but as frequency increases the output lags the input. As notch filters affect phase relationships far from the notch frequency and introduce amplitude distortion, their use is not recommended unless essential. By using filters in series, the order of the resulting complex increases, producing roll off characteristics closer to the ideal. Although this is achieved at the cost of increased phase distortion, many commercial systems employ fourth order (4 pole) filters, equivalent to four single order filters in series.

Various types of analogue filter are available, (Butterworth, Chebyschev, Bessel and Gausian), each with differing characteristics. Bessel and Gausian filters show a linear phase response with frequency (Erne 1982), making them ideally suited for applications where absolute latency measures are of interest. Butterworth filters show good phase characteristics and a flat amplitude response with frequency, making them desirable for studies of signal power spectra (Erne 1982). Fourth order Butterworths were used throughout this

thesis, and also for the VEP onset studies of Ossenblok and Spekreijse (1991), Riemslag et al (1981) and Creel et al (1981). The latter three groups observed latency prolongation of 7, 9 and 14 ms respectively, the difference between them possibly attributable to the increasingly restrictive bandwidths used in each case (70 Hz, 0.5 to 75 Hz and 0.5 to 35 Hz respectively). This demonstrates that the pattern onset stimulus evokes cortical activity containing frequencies up to, or beyond 75Hz.

The characteristics described above are typical of analogue filters, while the problems of phase shifts and amplitude distortion can be significantly reduced by the adoption of digital filters (Skuse and Burke 1990). Despite their advantages, the use of digital filters is less prevalent, possibly due to past problems with availability and cost.

1.7 - MULTICHANNEL MAGNETOMETERS.

Use of the single channel magnetometer imposes restrictions in the study of the VEMR. With the development of multichannel systems, biomagnetic activity can be recorded topographically, without loss of spatial or temporal continuity. Initially up to 37 channels were commercially available, however this has now increased to 122 channels, with current research into the possibility of 200.

The type of magnetometer used is dependant upon its intended applications. A number of authors have stated that the shape of the tail is important, as each channel must be as close to the signals source as possible to maximise detectable amplitude (Romani and Narici 1986), and normal to the scalp to maintain primary/secondary source field contributions (Meijs et al 1987). This limits the flexibility of the resulting system, since cerebral studies ideally require the use of a spherically concave tail of approximately 10 cm radius (Romani and Narici 1986), while a flat tail would be better suited for cardiac and pulmonary studies. The increased surface area of the tail also imposes compromises between detector/source separation, temperature isolation and structural strength (Romani and Narici 1986). Within the tail, the detectors can be arranged in a Cartesian matrix to produce a simple, orthogonal grid, or hexagonally for optimal packing density (Romani and Pizzella 1990). Source depth influences the choice of total matrix area and the inter-coil separation, (2.5cm separation ideally suited for a 3cm deep source) (Romani and Pizzella

1990). The inter coil spacing used also influences the spatial resolution of the magnetometer, since fine field gradients, such as those produced by multiple source activity, ideally require increasingly dense detector arrays for adequate localisation (Fagaly 1990).

Most commercial multichannel systems use first order gradiometers with balancing achieved electronically. In large systems (50-100 channels), balancing problems can be reduced by the use of planar gradiometers (Romani and Narici 1986). As a result of the high noise susceptibility of first order gradiometers, and the inefficiency of software noise reduction for balancing, multichannel systems have been confined to shielded environments, increasing system costs while reducing flexibility (Fenwick 1990).

CHAPTER 2

INTRODUCTION - APPLICATIONS OF THE EVOKED RESPONSE.

2.1 - ORIGINS OF THE NEUROMAGNETIC FIELD.

The neurone consists of a cell body connected to dendritic projections with which impulses are received, and an axon to transmit them. Signals are transferred along axons by intracellular ionic current flow. At the axon terminal, impulses can be initiated in the dendritic and/or cell bodies of other neurones by means of synaptic transfer.

The mechanism of impulse propagation along axons takes the form of action potentials, facilitated by the action of energy dependent membrane pores (Hodgkin 1958). Hence, in its resting state, the potential within the axon is approximately -80mV relative to the extracellular medium. Any synaptic input which reduces the local extracellular potential to approximately +40mV initiates an action potential. First, pores within the membrane open, allowing the influx of sodium ions. The resulting depolarisation raises the intercellular potential to +30mV, causing a localised increase in positive charge at the leading edge of the propagation. An intracellular ionic current flows towards and past this leading edge (figure 2.1A IC), while transmembrane (figure 2.1A MC) and extracellular currents are also formed (figure 2.1A EC). The extracellular current returns to the initial point of depolarisation through the intercellular clefts. Following depolarisation, the sodium pores remain closed for a short time, while potassium pores open to facilitate repolarisation. The potassium ion outflux restores the intracellular resting potential, while also initiating intercellular, transmembrane and extracellular current flow of opposite polarity to those of the depolarisation. As the impulse is propagated along the fibre, the intra and extracellular ion concentrations are restored behind by the action of membrane bound ion pumps.

Current flow along dendrites occurs in the form of graded potentials whose amplitude, unlike action potentials, decreases more rapidly with time and distance from its point of origin (Okada 1983). The time course of graded potentials is also much slower than action potentials, between 10 and 100ms,

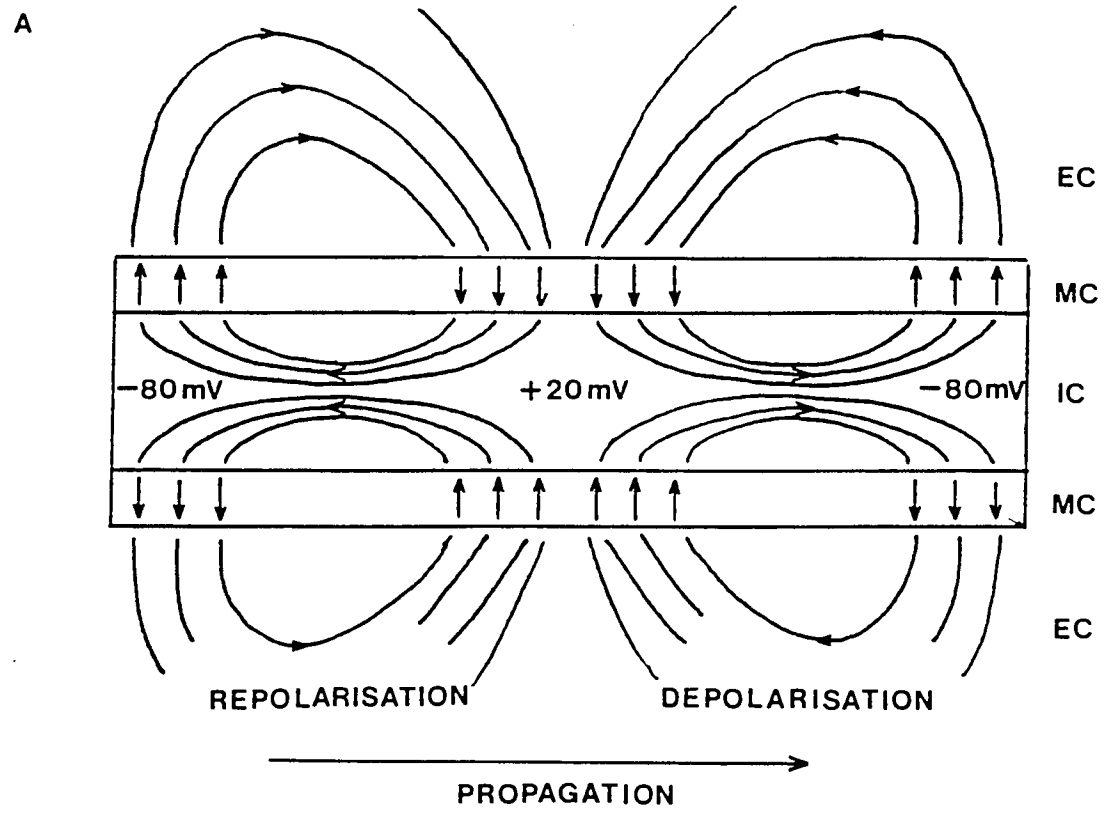

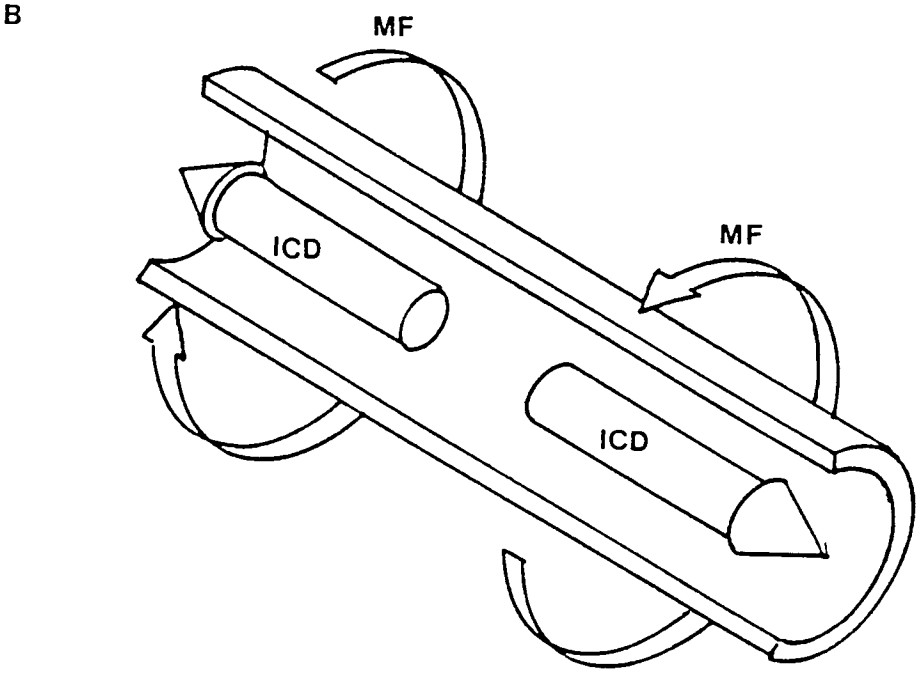

Figure 2.1 - Illustration of the ionic currents (**A**) and their associated magnetic fields (**B**), produced during an action potential propagation along a section of nerve axon.
IC - intracellular current. MC - membrane current. EC - extracellular current. ICD - intracellular current dipole. MF - magnetic field.

while the repolarisation front is insufficiently co-ordinated between neurones to be detected (Pizzella and Romani 1990).

For any current flow, the Biot-Savart law predicts that a magnetic field will be produced, with circular field lines centred at the current path, lying on a plane perpendicular to the direction of current (Tripp 1983). The rotational direction of this field can be predicted by Flemmings right hand rule. Of the currents mentioned previously, it is generally accepted that the extracranial, neuromagnetic fields originate from graded intracellular post-synaptic potentials, in the apical dendrites of pyramidal cells (Okada 1983). This has also been demonstrated practically by in-vitro and in-vivo animal studies (Barth and Sutherling 1990). Transmembrane current contributions are excluded due to the radial symmetry and thinness of the fibres, while extracellular current density is spread too diffusely throughout the poorly conducting intercellular clefts. Intracellular current density is raised by the boundary action of the membrane wall, while the medium within the fibre offers a path of relatively high conductivity. A graded field is more likely to be the origin of the magnetic field outside the head compared with the action potential, for a number of reasons. Since action potentials are more accurately modelled by a current quadrupole (figure 2.1B), and graded fields by a current dipole, the comparative differences in field interactions result in a more rapid attenuation of field strength with distance for the former (Wikswo 1983). In order to attain a suitably large signal strength to be detected above extraneous noise, simultaneous activity would be required in multiple fibres (See Okada 1982, Stok 1986). The exact number of neurones required would be dependant on the noise levels in which recordings were made. Such co-ordination would be less likely to occur with action potentials, since their short time course increases the probability of mutual field cancellation, between the asynchronous depolarisation and repolarisation fronts of adjacent neurones (Okada 1983).

Neurones have either an open or closed field configuration. The stellate and fussiform cells of cortical layers II, IV and VI have dendritic trees which ramify in all directions (closed field). Current flow within these does not produce a net magnetic field, due to mutual cancellation. However, the dendrites of most pyramidal cells are predominantly oriented perpendicular to the cortical surface (open field), producing a dipolar distribution when active (Okada 1983).

Synaptic input to the dendrites can occur at any point along their length. Input to the central portions initiate a current flow towards and away from the cell body simultaneously, producing a current quadrupole. Input to the apical regions produce a unidirectional current with dipole field characteristics (Okada 1982).

The magnetic fields produced by intracellular current flow are referred to as primary source fields, and it is these which are the major contributors to the radial component of the extracranial magnetic field (Okada 1982). Volume currents produce secondary sources at the boundaries between regions of differing conductivity, such as the brain and the skull. For a spherical conductor, the fields produced by these secondary sources are cancelled by those of the volume current. Where the conductor is not spherical however, as is the case in the cranium (Barth et al 1986) and to a greater extent the chest (Kaufman and Williamson 1982), the contribution of secondary sources to the radial field component increases.

2.2 - COMPARISONS BETWEEN NEUROIMAGING TECHNIQUES.

For neuromagnetometry to gain widespread acceptance, it must compete with a number of imaging techniques currently in use. Each has relative advantages and disadvantages, and it is these which will determine if biomagnetism can establish diagnostic uses.

The closest related technique to magnetoencephalography (MEG) is electroencephalography (EEG), which detects functional neural processing noninvasively, on a millisecond time scale. Positron emission tomography (PET) and single photon emission computed tomography (SPECT) measure the metabolism of functional processing. However, each of these methods are invasive, and the activity has to be averaged over a period of minutes. Magnetic resonance imaging (MRI), and computed axial tomography (CAT) provide structural, anatomical images, however these are also possibly invasive. MRI can also be used to provide information about functional processing, by exploiting the paramagnetic properties of deoxygenated blood (blood oxygen level dependent imaging BOLD).

The MEG and EEG differ theoretically and practically in the sources they detect, and the way in which this is achieved.

1. For a spherical conducting space, MEG detects the field components of sources lying tangentially with respect to the conductors surface (Okada 1982). Radial source fields are not detected due to cancellation from secondary sources created at the sphere boundary, according to Amperes law (Kaufman and Williamson 1982). The EEG detects the summated activity of both radial and tangential sources, with a slight dominance of the radial (Rose and Ducla-Soares 1990). Hence, MEG should theoretically detect the activity of sources within the walls of sulci preferentially, while the EEG would record those on gyral crests.

2. MEG field maxima are rotated by 90° with respect to those of the EEG, for the same tangentially oriented, dipolar source (Stok 1986).

3. The MEG field distribution is 1/3 smaller (more tight) than that of the corresponding EEG (Stok 1986). This occurs because the skull does not affect the passage of magnetic field through it. The volume currents detected by the EEG however are smeared at the boundaries of differing conductivity, such as the skull, scalp, dura etc. (Kaufman and Williamson 1982). As tissue thickness alters conductivity (Rose and Ducla-Soares 1990), the EEG is also influenced by inhomogenities in the tissue surrounding the brain. The tighter field distribution seen with MEG requires the use of increased spatial sampling (Spekreijse 1991), to accurately locate the position of field maxima and minima over the scalp, while also increasing the problems of locating a recording site of high signal to noise ratio with a single channel magnetometer (Harding et al 1991). The lack of smearing effects may increase MEG sensitivity to underlying pathology compared to the EEG (Armstrong et al 1991).

4. The magnetic transparency of biological tissue, combined with the insensitivity of MEG to volume currents, should theoretically allow greater spatial discrimination for multiple source activity with MEG localisation than EEG (Kaufman and Williamson 1982).

Practically, the EEG technique is cheaper to buy and run than the MEG, with the ability to allow prolonged, mobile monitoring studies to be undertaken (Rose and Ducla-Soares 1990). Evoked cortical activity measured using the MEG produces more intersubject latency and amplitude variability than that of the EEG (Armstrong et al 1991), while the EEG is more susceptible to volume current interference from myogenic activity (Rose and Ducla-Soares 1990).

PET and SPECT both use radioactively labelled molecules, injected or inhaled, to visualise neural processing. The molecules are taken up by the brain and

any increase in metabolic activity resulting from neural processing increases local blood flow, and causes an accumulation of radioactivity. Although PET scanning provides greater spatial resolution than SPECT, the equipment costs are greater (Fenwick 1990). The low levels of radioactivity involved minimise potential dangers to the subject, although it requires the response to be averaged over several minutes. This lowers temporal resolution compared to the MEG and EEG. In addition, each patient is limited to two PET scans per year. Although expensive, PET has become accepted by the clinical community.

The CAT scan is a well established method of obtaining structural brain images, although the use of X ray exposure is again slightly invasive and undesirable.

A more modern approach to structural imaging is provided by the MRI, which detects the proton spin resonance which follows exposure to a powerful magnetic field. The adverse effects of using such a field are not yet known, and so it must still be regarded as potentially invasive. The images produced provide excellent differentiation between white and grey matter, with the ability to distinguish the presence of sclerotic plaques and tumours, even in the absence of clinical or electrophysiological symptoms (Armstrong and Wastie 1987, Fenwick 1990). Such lesions are also transparent to the CAT scan. The MRI can detect clinically important lesions such as oedema and gliosis in acute and chronic cases of multiple sclerosis respectively (Ghilardi 1990). It is now possible to visualise functional activity within the brain to within an accuracy of 5mm (Geake 1992). This relies on the principle that deoxygenated blood is paramagnetic, and therefore disturbs the magnetic field around it, while oxygenated blood is not (blood oxygen level dependent imaging, or BOLD).

It has been stated that the cost of the 100 channel magnetometers is likely to be similar to that of the MRI (Fenwick 1990), and so definite diagnostic advantages would have to be established before MEG found clinical acceptance. For applications requiring good temporal resolution, MEG and EEG techniques would be desirable, while high spatial resolution would be fulfilled by the use of MRI or PET scanning. MRI is now being used in combination with functional techniques such as the EEG, CAT (Srebro and Purdy 1990), PET (Davidoff and Concar 1993) and MEG (Aine et al 1989 and Rogers et al 1991) to allow the localisation of specific processing events to be detected within the cortex. The combination of data from different techniques has proved difficult

however, since MRI is prone to technical problems such as spatial distortion of the images (Coffey et al 1992).

2.3 - MEG APPLICATIONS.

Few clinical applications of the MEG have been discovered or developed since its conception forty years ago. It has been applied to studies of most of the sensory modalities, and many of the conditions investigated by the EEG.

Action potential propagation's have been observed in isolated nerve preparations (Wikswo 1982), peripheral nerves and skeletal muscle (Roth 1990). These have contributed to an understanding of the origins of the neuromagnetic signal, while offering the potential for monitoring nerve injury intraoperatively (Roth 1990).

Studies of the visually evoked magnetic response (VEMR) have been published to flash (Teyler et al 1975), sinusoidal gratings (Brenner et al 1975, Maclin et al 1983), flashed pattern (Richer et al 1983), pattern reversal (Janday et al 1986, Armstrong et al 1991) and pattern onset/offset stimuli (Kouijzer et al 1985, Stok 1986, Aine et al 1989, Ahlfors et al 1992). These were concerned with the study of either source localisation, VEP comparisons, retinotopic projections or the influences of stimulus parameters. Armstrong et al (1991) presented normative data for the flash and pattern reversal VEMR, demonstrating greater variability than the corresponding VEP. This could be attributed to the detection of a more select neuronal population, however the authors also suggested that improvements might result from changes in recording protocol. Armstrong et al (1990) proposed that MEG could provide early detection of the neurodegeneration associated with Alzheimers disease. Hence, it is preferentially sensitive to the activity of sources within sulci, where the development of senile plaques and neurofibrillarly tangles is most pronounced. The potential localisation accuracy of MEG might also improve the detection of pathology causing visual field defects (Ahlfors et al 1992) and the presence of tumour calcification, oedema and infarcts (Armstrong and Janday 1989).

The magnetic equivalents to the electroretinogram and electrooculogram were reported by Katila and Varpula (1982), however no advantages could be found to justify the additional cost and complexity.

General studies of the somatosensory evoked field (Brenner et al 1978, Okada 1982, Rossini and Traversa 1990), and the somatotopic organisation of the cortex (Okada 1984, Narici et al 1991) have led to the possibility of spinal cord monitoring following injury and during recovery, and the preoperative localisation of functional cortex (Rose 1990).

Studies of the auditory evoked magnetic response dominate the literature (Pantev et al 1986, Reite et al 1978, Farrel et al 1980, Pelizzone and Hari 1986, Romani 1986, Rutten et al 1986). Clinical applications have been suggested for the postoperative monitoring of cochlea prosthesis function, lesion localisation and the evaluation of optimal surgical approaches (Makela and Hari 1990). Hoke et al (1989) and Pantev et al (1989) demonstrated that MEG could be used to provide a positive diagnosis of tinnitus, the M200 peak being diminished while the M100 enhanced in sufferers. A subsequent study by Jacobson et al (1991) could not substantiate these findings, although they suggested that this might be accounted for by differences in experimental paradigms, subject arousal or linguistic background.

The magnetocardiograph (MCG) has been investigated for longer than any other MEG field (Cohen and Cuffin 1975, Fenici 1982, Wikswo 1982), with applications proposed for the study of ventricular hypertrophies, bundle branch blocks, myocardial infarction, premature beats and Wolf-Parkinson White syndrome (Schmitz 1987, Mori and Nahaya 1987). MCG also offers advantages over its electrical counterpart in the measurement of foetal heart activity (FMCG), as it is relatively insensitive to interference from the maternal MCG (Kariniemi and Katila 1982).

The localisation accuracy theoretically attainable by the MEG and MEG/EEG techniques combined has provoked interest for their use in the presurgical delinearization of epilogenic foci (Rose et al 1987, Sutherling et al 1988, Ricci 1990, Sato 1990, Sutherling and Barth 1990). These offer greater precision than other noninvasive methods, while being cheaper and less dangerous than intracortical recording.

Fenwick (1990) has suggested a number of psychiatric conditions for which MEG could assist in the diagnosis and monitoring. These include paroxysmal behaviour disorders, schizophrenia, Parkinson's disease and Jacob-Creutzfeldt disease. All of these involve spike activity in deep structures such as the amygdala, hippocampus and septal regions, which do not necessarily propagate to the scalps surface. Problems with gradiometer baseline/noise

interaction, secondary source contributions and the depth inverse solution computation would have to be reduced before MEG could be exploited for such applications.

MEG applications have also been proposed for the study of migraine (Okada 1990), stroke (Vieth 1990), the steady fields of the bodies organs due to injury currents (Cohen 1982), the iron concentrations of the liver (Farrell 1982) and pulmonary dust contamination (Kalliomaki et al 1982).

Although many clinical applications have been proposed, few have achieved practical implementation. This could be attributed to limitations such as the poor signal to noise conditions attainable in most hospital settings (Nicholas et al 1983), the inconvenience and costs of regular helium fills, the prohibitive cost of equipment installation (Fenwick 1990) and until recently, the restriction to single channel recording. The advent of multichannel devices has not appreciably stimulated clinical interest either, possibly due to the increased complexity, the associated decrease in reliability and the requirement of a shielded environment. Magnetometry has historically been a product of the physics laboratory, where it is continually being developed. Although technical refinements are essential in the production of a practical technique, there must also be a transfer to the biological and clinical disciplines, where the products of such development can be exploited. It seems unlikely that widespread acceptance will be achieved within the clinical community until a degree of design stability has been reached.

2.4 - STIMULUS PRESENTATION.

Stimulation of the visual system can be achieved by a variety of methods, each displaying intrinsic advantages and disadvantages. The early intracellular recording studies of Hubel and Wiesel (1959) used spots and bars of light to delineate neuronal receptive fields, and determine their functional properties. The clinical use of light flashes has become well established (Adrian and Mathews 1934), offering a useful method of studying the integrity of peripheral retinal fibres and the luminance mediated visual pathways (Hughes et al 1987, Harding 1974). Of the many waveform peaks constituting the flash VEP, the P1 (at approximately 70ms), is said to represent activity of the primary visual cortex, via a geniculostriate pathway, while the P2 (approximately 125ms) arises from a retinotectal projection to extrastriate

cortex (Wright et al 1987, Harding and Wright 1986). Although prone to intersubject latency and amplitude variability (Kriss 1982), the response is relatively insensitive to subject refractive error, pupil diameter and fixation disparity (Harding 1982). Use of the pattern VEP was first reported by Spehlmann (1965), who produced a flashed onset/offset stimulus by the superposition of a checkerboard over a strobe light. This evokes a composite cortical response, being a mixture of pattern onset, offset and luminance activity (Richer et al 1983, Stok 1986). Although the presence of black checks effectively halves the luminance increase of the flash, the evoked response is generally of larger amplitude than any other stimulus type (Rietveld et al 1967, James and Jeffreys 1975). This can be attributed to the properties of cortical neurones, the majority of which are sensitive to contours of specific orientation, as opposed to changes in absolute luminance. These cells can be studied in isolation of luminance contamination by use of stimuli where the patterned screen is replaced by a blank offset screen of equal mean luminance. This approach also helps to reduce the intersubject variation experienced with luminance stimuli, thereby increasing its clinical acceptability (Kriss 1982). The use of a short onset duration helps to prevent component adaptation, however the resulting triphasic waveform is influenced by both pattern onset (peaks 1 and 2) and offset (peak 3), related activity (Jeffreys 1971). Increasing pattern duration beyond 100ms separates the onset and offset contributions (Wright 1983), the former producing a triphasic waveform, and the latter a single peak (Estevez and Spekreijse 1974, Jeffreys 1977). The onset waveform comprises three peaks within the first 200 ms post stimulus, CI (50 to 90ms), CII (90 to 120ms) and CIII (120 to 180ms), each of which are differentially influenced by changes in stimulus parameters (James and Jeffreys 1975). The onset/offset response is sensitive to changes in spatial contrast (Spekreijse et al 1977), reflecting activity of the geniculostriate pathways (Creel et al 1981), especially the transient cell system (Y pathway) (Kaufman and Williamson 1990). Although the precise location of the cortical generators for each waveform peak are disputed, it is generally accepted that they originate in different cell populations, under the influence of different aspects of the stimulus (Spekreijse et al 1977, Harding 1986).

Although the large amplitude of the pattern onset response makes it easier to record than that of the pattern reversal (Lesevre and Joseph 1979), problems with predictability and stability have diminished clinical acceptance (Wright

et al 1984, Harding and Wright 1986). The pattern reversal stimulus consists of a successive alternation of light and dark pattern elements, with a corresponding change in local contrast and luminance, but without any global changes. The pattern reversal stimulus has been shown to activate both motion (Spekreijse et al 1985) and contrast (Estevez and Spekreijse 1974, Dagnelie et al 1986) specific mechanisms within the visual system, with their relative contributions dependant upon the choice of stimulus parameters and the retinal regions stimulated. Signals are thought to be transferred predominantly via the central retinal fibres (Wright et al 1987), by the sustained (X cell) pathways (Kaufman and Williamson 1990). The cortical origins of the most prominent pattern reversal peak (P100) are disputed. Spekreijse et al (1985) attributed 96% of the response power to activity in striate cortex, while Creel et al (1981) proposed an association cortex origin. Comparisons between VEP pattern reversal and onset components have been drawn from their relative behaviour with alterations in stimulus parameters, and the use of stimuli which progressively change from an onset to reversal paradigm (Estevez and Spekreijse 1974, Spekreijse et al 1977). Using such approaches, the reversal P100 peak has been shown to be analogous to a combination of the onset CI and offset components (Estevez and Spekreijse 1974, Jeffreys 1977, Butler et al 1987), the activity of each attributed to a decrease in contrast. Pattern reversal does not however display any components corresponding to the onset CII and CIII (Jeffreys 1977). The waveform consistency of the P100 peak exceeds that of any other stimulus (Blumhardt 1987), and it is this to which can be attributed its universal clinical adoption.

A variety of patterned stimuli can be used in these presentation paradigms, including sine or square wave gratings (Brenner et al 1981. Aine et al 1990), checkerboards (Richer et al 1983, Kouijzer et al 1985, Stok 1986, Ahlfors et al 1992), dartboard segments or diamonds (Ermolaev and Kleinman 1983) and polka-dots (Harter 1971). Although grating stimuli are easily defined in terms of spatial frequency (Bodis-Wollner et al 1990) and fourier composition (DeValois et al 1979), the sluggish nature of the resulting waveform peaks has limited its clinical acceptance (Regan 1989). Their use has proved beneficial in the comparison between the body of psychophysical evidence already available about the visual system, and the results of VEP (Parker et al 1982, Musselwhite and Jeffreys 1985) and VEMR studies (Williamson et al 1978,

Kaufman and Williamson 1980, Okada et al 1982). The checkerboard has become the universally accepted clinical stimulus, due to its production of large amplitude, well defined waveform peaks (Smith and Jeffreys 1978, Lueders et al 1980, Kriss et al 1980, Blumhardt 1987, Harding 1990). The fundamental fourier components lie at angles of 45 and 135° to the check edges, with higher harmonics at different orientations. With rectangular checks, these angles vary according to the side length ratio (DeValois et al 1979). An appreciation of the fourier constituents of a given stimulus is important for response interpretation, since cortical neurones are preferentially sensitive to these orientations, as opposed to those of the contrast borders (DeValois et al 1979, Bodis-Wollner et al 1990). The larger amplitude responses of checkerboards compared to gratings could therefore be attributed to their more complex fourier composition. Calculation of spatial frequency is also more complex for checkerboards than gratings. Hence, for checks and bars of equal sidelength, the checkerboard spatial frequency is equivalent to $\sqrt{2}$ times that of the grating (DeValois 1979). The use of dartboard segment patterns increases peak amplitude, definition and intersubject stability, possibly due to a compensation for the effects of cortical magnification (Ermolaev and Kleinman 1983)

The rate of stimulus presentation also affects the nature of the evoked response. Stimuli presented at rates below 2/sec (Harding 1988) are said to elicit a transient response, in which the evoked activity from each stimulus presentation subsides before the following stimulus occurs. At rates above 4 to 10/sec (Harding 1988), a sustained response is obtained, in which successive stimuli occur before the response from the previous stimulus has subsided. Of the two techniques, transient stimulation tends to be favoured, since it offers the potential to study component amplitudes independently of each other (Smith and Jeffreys 1978).

2.5 - PATTERN ONSET / OFFSET STIMULATION.

Studies using the pattern onset/offset stimulus have attempted to address one of three problems. The most popular has been to determine the cortical origins of each waveform peak, either by reference to retinotopic projections (Jeffreys and Axford 1972 a and b, Parker et al 1982, Butler et al 1987), or the use of source localisation algorithms (Aine et al 1989, Ossenblok and Spekreijse

1991). Secondly, some authors have investigated the properties of each peak to variations in stimulus parameters (James and Jeffreys 1975, Jeffreys 1977). Finally, others have discussed clinical applications (Creel et al 1981, Galloway and Barber 1981, Riemslag et al 1981, Wright et al 1984, May et al 1991, Beers et al 1992).

The VEP to an onset stimulus produces a triphasic waveform within the first 200 ms, with peaks identified as CI (50 to 90ms), CII (90 to 120ms) and CIII (120 to 180ms), of surface positive, negative and positive polarity respectively (Jeffreys and Axford 1972 a and b, Ermolaev and Kleinman 1983). An extra peak has also been observed at approximately 60 ms by Lesevre and Joseph (1979) (wave 0), and Drasdo (1980) (C0), occurring with the use of foveal stimuli and high spatial frequencies. The onset VEMR is biphasic, with peaks of opposite polarity at approximately 120 and 180ms, referred to as either M120 and M180 (Richer et al 1983) or type I and II (Stok 1986). Comparative studies between VEP and VEMR waveforms (Kouijzer et al 1985, Aine et al 1990), and scalp topographies (Richer et al 1983), have suggested common cortical generators for VEP and VEMR peaks of similar latency. There is no magnetic equivalent of the VEP CI apparent in the averaged response however, possibly due to its predominantly radial orientation relative to the scalp, as shown for the flashed pattern (Richer et al 1983) and pattern onset stimuli (Ossenblok and Spekreijse 1991) (see chapter 5).

Interest in the localisation of component generators should provide a more detailed understanding of visual processing. The results of various authors have been contradictory, possibly reflecting differences in stimulus parameters, and the complexity of visual cortex anatomy. It has been commonly assumed that each waveform peak reflects the activity of a single cortical generator. However the work of several authors has disputed this assertion (Lesevre and Joseph 1979, Stok 1986, Maier et al 1987, Van Dijk and Spekreijse 1990, Ossenblok and Spekreijse 1991). Hence, the contribution of several spatially discrete cortical regions to each peak could prevent simplistic interpretation.

The VEP CI component may originate in striate (Jeffreys and Axford 1972 a, James and Jeffreys 1975, Jeffreys 1977, Smith and Jeffreys 1978, Darcey et al 1980, Parker et al 1982, Butler et al 1987) or extrastriate cortex (Lesevre and Joseph 1979, Drasdo 1980, Drasdo and Edwards 1989, Van Dijk and Spekreijse 1990). Butler et al (1987) encountered problems in attributing foveal CI

activity to striate cortex, due to its unpredictable surface positive distribution. This was explained by the presence of lateral calcarine sulci, or an opposing direction of micropotential flow for foveal and extrafoveal responses. The CII component has been attributed to activity in striate (Darcey et al 1980, Van Dijk and Spekreijse 1990) or extrastriate cortex (Jeffreys and Axford 1972 a, Jeffreys 1977, Spekreijse et al 1977, Smith and Jeffreys 1978, Lesevre and Joseph 1979, Drasdo and Edwards 1989), while the CIII is said to originate from extrastriate regions different to those of the CII (Jeffreys and Axford 1972 b, Jeffreys 1977, Smith and Jeffreys 1978, Lesevre and Joseph 1979). Several authors have found response interpretation less simple. Maier et al (1987) used a principal component analysis technique and attributed onset activity to two temporally overlapping cortical sources. The first contributed to both CI and CII, originating in striate cortex, while the second, extrastriate component contributed to the latter portion of the CII. Ossenblok and Spekreijse (1991) used a similar analysis approach and found activity equivalent to the CI peak in extrastriate regions, on the outer lobe surfaces (area 18), and activity more laterally (area 19) corresponding to the CIII. Vassilev et al (1983) and Srebro (1985) each considered the onset response too complex to interpret.

Localisation of VEMR data has proved less variable, with the 100ms peak originating from retinotopically organised cortex (Ahlfors et al 1992), in the contralateral hemisphere to that of the visual stimulus, at a position below O1 or O2 and a depth between 12 and 24mm (Richer et al 1983, Kouijzer et al 1985). Aine et al (1990) attributed the onset response to the activity of two equivalent dipoles, one at 90ms in striate cortex, and the second in extrastriate cortex at 110ms. Similarities in source origins have been drawn between the 120 and 180ms peaks, except with an opposing direction of current flow (Richer et al 1983) and also between the onset and offset responses (Kouijzer et al 1985).

An understanding of the effects of varying stimulus parameters is useful for the determination of cortical origins and the development of clinical stimulus regimes. Using such approaches, the onset response has been attributed to transient and sustained components of the stimulus, while the offset is a purely transient phenomena (Vassilev et al 1983). Onset/offset differences have also been observed in topographic distributions (Spekreijse et al 1972, Jeffreys 1977, Spekreijse et al 1977), with the offset enhanced more by binocular presentation (Spekreijse et al 1972) and influenced less by spatial frequency variation (Spekreijse et al 1973). Different behaviour has also been

reported to contrast changes, the onset sensitive to standing contrast (Spekreijse et al 1973), while the offset responds to the absolute magnitude of contrast change.

The VEP CI component is thought to reflect pre-processing events leading to the CII (Spekreijse et al 1977), being influenced by both stimulus contour (Jeffreys 1977) and contrast (Jeffreys 1977, Lesevre and Joseph 1979). Its amplitude is enhanced by the use of large checks (Barber and Galloway 1981, Ossenblok and Spekreijse 1991), and saturates at higher contrast levels than later peaks (Jeffreys 1977). Unlike the CII and CIII, the CI is unattenuated by stimulus blur, or the brief pre-exposure of the pattern (Jeffreys 1977). It can be attenuated by longer pre-exposure to patterns of similar size and orientation (Smith and Jeffreys 1978).

The VEP CII component is thought to represent the processing of local contour and form (Smith and Jeffreys 1978), as it is edge specific (Lesevre and Joseph 1979, Manahilov et al 1992), and influenced by contour sharpness (Harding 1988, James and Jeffreys 1975, Jeffreys 1977). Unlike the CI and CIII, it is attenuated by the presence of steady outlines which match the orientation of the pattern edges (James and Jeffreys 1975, Jeffreys 1977).

The VEP CIII also represents a contour specific mechanism (Jeffreys 1977), responding in a similar way to the CII regarding pre-exposure, stimulus clarity and the presence of discontinuous contours (James and Jeffreys 1975, Jeffreys 1977). Its activity is also enhanced by binocular presentation (Ossenblok and Spekreijse 1991) and the use of small check sizes (Barber and Galloway 1981). The behaviour of both CII and CIII peaks with changes in contrast parallel the subjective impression of contour clarity (Jeffreys 1977), hence saturation occurs when the pattern is clearly distinguishable throughout the visual field. Extrapolation of VEP amplitude with changing contrast, back to 0uV produces a close correlation with the thresholds obtained from psychophysical studies. For stimulus presentations below 70 ms duration, CI and CII peaks obey Bloch's law, hence their amplitude is linearly related to the log(contrast x duration) product (Spekreijse 1973).

Fewer studies have reported the influence of stimulus parameters on the onset VEMR components. Variation in spatial frequency has been shown to alter the apparent depth, position and orientation of the underlying sources (Aine et al 1990).

2.6 - CLINICAL APPLICATIONS OF THE PATTERN ONSET VEP.

The clinical applications of the visually evoked potential have concentrated primarily on the use of pattern reversal and/or flash stimuli. The pattern onset CII component has been shown to exhibit greater intersubject latency and amplitude variability; greater sensitivity to refractive error; a larger delay with increasing age; greater hemispheric asymmetry and more difficult identification in the 10-19 year old, than the corresponding pattern reversal P100 (Wright et al 1984, Wright et al 1985, Harding and Wright 1986). Hence, although a stable response in the normal population is an essential prerequisite for the detection of abnormalities, each of these variables progressively erode such stability.

Extensive reviews of the clinical applications of the VEP are provided by Lueders et al (1980), Blumhardt (1987), Ghilardi et al (1990) and Harding (1990). These include studies of ocular conditions such as refractive error, lens and media opacities, amblyopia, glaucoma and retinal and macula disease. The optic projections can be monitored for prechiasmal, chiasmal and postchiasmal lesions, associated with optic neuritis (Halliday et al 1972, Wright et al 1987), multiple sclerosis (Halliday et al 1972, Hughes et al 1987, Kjaer 1982), toxic optic neuropathies and hereditary optic atrophies (Harding et al 1980). Neurodegenerative processes associated with diseases such as dementia (Harding et al 1981, Wright et al 1984), Parkinson's and Jakob-Creutzfeldt can also be diagnosed. Briefly, by examination of latency, amplitude and topographic information, obtained from techniques such as the VEP, ERG and EOG, lesions can be located to specific portions of the visual pathways, and visual disorders diagnosed or excluded. The accuracy of VEP findings can also prove superior to techniques such as the MRI and CT scans, for example in the early diagnosis of dementia (Harding et al 1985). Although the pattern onset stimulus has not received widespread clinical acceptance, advantages have been reported for a number of conditions. Beers et al (1992) exploited its sensitivity to stimulus clarity by using it as an objective measure of visual acuity. It has proved useful in the identification of sensory deficits in children with reading difficulties (May et al 1991) and the detection of visual field loss associated with glaucoma (Galloway and Barber 1981). It provides a higher detection rate for multiple sclerosis than that of the pattern reversal (Riemslag et al 1981) and offers greater efficiency in the detection of

misrouted optic fibres (Creel et al 1981). Positive advantages can also be offered over pattern reversal for studies of patients in which steady fixation is a problem, such as the very young, those with nystagmus and those with a neurological deficit.

2.7 - RETINOTOPIC PROJECTIONS AND THE CRUCIFORM MODEL.

Information is transferred from the eyes to the visual cortices, via intermediary structures, using a system of precisely organised fibres, which preserve the spatial integrity of the visual scene. A simplified account of these projections is provided by the cruciform model (Jeffreys and Axford 1972 a), which is based on the earlier findings of Holmes (1945) and Spalding (1952). The striate cortex is modelled as a cross, the calcarine fissure of each hemisphere assumed to lie at right angles to the longitudinal fissure, projecting perpendicularly from the surface of the scalp (figure 2.7). Stimulation of the left visual field of each eye projects to the contralateral (right) hemisphere, and vice-versa, while stimuli in the upper and lower fields project to cortical regions below and above the calcarine fissure respectively. Activity next to the vertical meridian activate sources lining the medial surfaces of the longitudinal fissure, while that next to the horizontal meridian project to sources within the calcarine walls. As retinal stimuli become increasingly eccentric, projection progresses in a posterior to anterior direction along the fissure complex.

Theoretically, a component of striate cortical origin should produce a response of reverse electrical polarity for upper verses lower, and right verses left peripheral quarter or hemifield stimulation. A topography which reverses polarity for upper and lower field stimuli, but not left to right, is usually interpreted as arising from extrastriate cortex on the lateral surface of the occipital lobes (Jeffreys 1977). Striate activity should also produce activity from stimulation of the central 1° of the visual field; with the response from peripheral stimuli centred close to the cortical midline; showing dipolar VEP distributions for left and right half fields and monopolar for upper and lower fields (Jeffreys and Axford 1972 a). Such projections have been confirmed using positron emission tomography with a patterned stimulus (Fox and Raichle 1984), while the model has proved sufficient to explain the VEP and VEMR data of several authors (Jeffreys and Axford 1972 a, Darcey et al 1980,

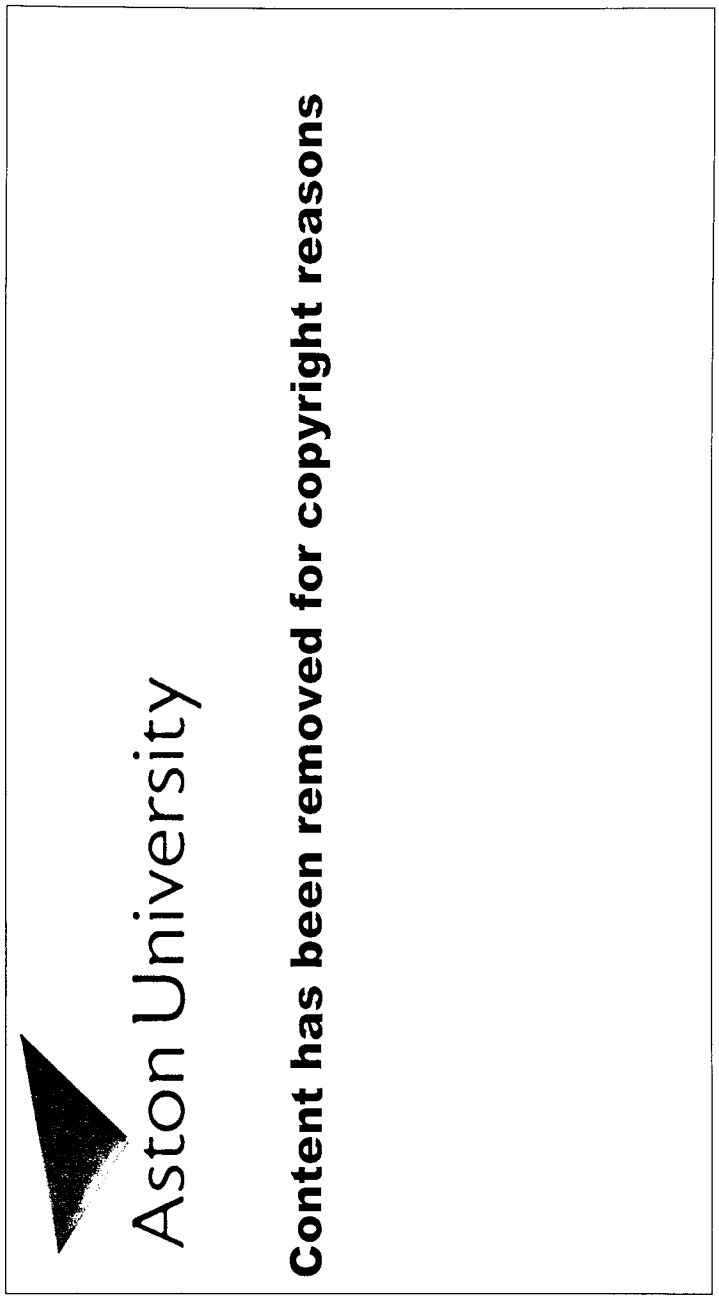

Figure 2.7 - Retinotopic projection of the visual field onto the cortex, assuming the cruciform model of striate cortex (Jeffreys and Axford 1972 I).

Brenner et al 1981, Parker et al 1982, Maclin et al 1983, Butler et al 1987, Aine et al 1990, Harding et al 1991, Kaufman et al 1991 and Ahlfors et al 1992). Others have found exceptions however (Halliday and Michael 1970, Jeffreys and Axford 1972 a, Lehmann et al 1977, Parker et al 1982, Butler et al 1987, Ossenblok and Spekreijse 1991, Ahlfors et al 1992), each attributing their problems to the over simplistic representation of fissure distribution. Jeffreys and Axford (1972 a) did explain that the model does not address the large interhemispheric, and intersubject variation in striate cortex morphology, particularly at the posterior extremities.

The ability to differentiate between differing retinotopic projection has proved clinically beneficial for the detection of misrouted optic fibres (Creel et al 1981), visual field defects (Galloway and Barber 1981) and the localisation of lesions along the visual pathways (Kelly 1985, Blumhardt 1987, Ghilardi et al 1990, Harding 1990).

2.8 - SOURCE LOCALISATION.

The distribution of magnetic field gradients over the scalp are often used to predict the source origins of underlying current generators, (the inverse problem). In the case of a dipolar distribution, a single equivalent current source is assumed, lying at a position midway between the field maxima; at a depth equal to the maxima separation divided by $\sqrt{2}$ (Kaufman and Williamson 1982); with an orientation given by Flemmings right hand rule. Another approach is provided by source localisation algorithms. These attempt to solve the inverse problem by matching the recorded field distribution with one computed theoretically, from a known source configuration, (the forward problem). The use of such algorithms have become prevalent in neuromagnetometry, in an attempt to exploit the theoretical differences between MEG and EEG techniques. Subsequent studies have examined the relative advantages of various mathematical approaches to the problem, and their practical application (Meijs et al 1987, Ossenblok and Spekreijse 1991, Ahlfors et al 1992).

It is universally accepted that the inverse problem is ill posed, hence it has no unique solution, since an infinite number of different source combinations can produce the same summated distribution (Kaufman and Williamson 1982, Balish and Muratore 1990). Constraints are often introduced therefore

regarding source type, the conducting space properties and the measurement procedure (the restricted inverse problem Stok 1986) to increase the significance of the resulting analysis.

The pickup coil area, gradiometer baseline, intercoil separation and the overall size of the measurement grid, all affect localisation accuracy (Romani and Leoni 1984). In addition, variables such as detector location and head model size must also be considered (Cuffin 1986).

The current source can be assumed to be a single dipole or alternatively an array of distributed sources of fixed position and orientation (Balish and Muratore 1990, Kaufman et al 1991, Bedford 1992). For the latter, a priori assumptions have to be made regarding the number of sources to include in the analysis, their orientations, positions and relative contributions. In all cases, the EEG current source has six degrees of freedom, two for orientation, three for position and one for strength. That of the MEG requires only five, since the technique is insensitive to radially oriented dipoles (Spekreijse 1991).

Most studies use a rotationally symmetric volume as the head model, as it is relatively simple to compute while adequately representing the shape of the occipital region of the head (Spekreijse 1991). As a consequence of the spherically symmetric model, only the radial field component of the source is important, without consideration of volume current effects (Van Dijk and Spekreijse 1990). The nonhomogeneous spherical model incorporates multiple concentric layers of differing conductivity, representing the dura, skull and scalp. This allows the influence of volume currents to be modelled for the EEG, while the spherical shape excludes their effects on the MEG (Gryzpan and Geselowitz 1973). EEG localisation accuracy is greatly affected by model parameters, since changes in sphere radii and conductivity of as little as 20% can introduce amplitude variations of up to 60% (Stok 1986). As the head is not truly spherical, the influences of secondary sources on the MEG cannot be dismissed (Barth et al 1986). This is especially important when studying frontal and temporal lobe activity, where the deviation from spherical is considerable (Hamalainen and Sarvas 1987). Realistic head shape models have been developed with reference to MRI data, which accurately define the shape of the various conducting regions (Balish and Muratore 1990). Comparisons between results for a spherical and a four component realistic head model have revealed differences in localisation accuracy of up to 16 mm (Meijs et al

1987). Although the conductivity within the skull is influenced by the presence of fissures and ventricles (Barth et al 1986), their effects on localisation accuracy is minimal (Cuffin 1985). Consequently, head models are assumed to be homogeneous conductors for simplicity.

The most common source localisation approach assumes a single equivalent current dipole (ECD), located in a homogeneous spherical conductor. The dipole is positioned at random within the sphere and the surface field it would produce calculated (forward problem). This is compared to the recorded distribution by a least squares fit routine. The process is repeated iteratively, with minor changes to the model, until a reasonable fit is achieved (Barth et al 1987). This assumes that activity is restricted to a single, small area of cortex (Aine et al 1989), with dipolar current properties. If a fit is not achieved, it may suggest the presence of noise in the data, or the activity of multiple sources (Romani and Pizella 1990). More complex techniques have been developed for the localisation of multiple sources, including the use of principal component analysis (PCA)(Maier 1987, Ossenblok and Spekreijse 1991), the minimum norm estimate (MNE) (Aine et al 1989, Ahlfors et al 1991) and the minimum mean square (MMS) methods (Sencaj and Aunon 1982). Each of these attempt to resolve the recorded distribution mathematically into a number of discrete dipolar sources. The MNE and MMS methods are less susceptible to the effects of noise than the ECD, to an extent where localisation can be achieved with unaveraged data (Ahlfors et al 1991). This is particularly desirable since the averaging process results in a loss of temporal information about the processing events (Nunez 1986).

All analysis techniques face problems when attempting to separate the activity of closely spaced sources, due to the superposition theorem (Stok 1986). Hence, adjacent dipolar sources can produce a single, summated dipolar field distribution. Under optimal conditions, MEG should theoretically be capable of detecting the activity of superficial, non-simultaneous sources, separated by only a few mm (Hari et al 1988). In practice, the separation between two sources can be detected if it exceeds 1 to 2 cm (Okada 1984), or if the angular separation between them is increased (Balish and Muratore 1990). Multiple source activity can be distinguished by localisation at successive latencies, appearing as discontinuous changes in the dipole position or orientation with time (Ioannides et al 1990).

The development of physiologically and clinically useful applications for MEG should be greatly enhanced by the combination of multichannel systems, realistic head modelling and source localisation approaches. These, together with MRI data should enable the accurate pinpointing of specific cortical regions responsible for a given neural process. Greater information might also be attainable if signal averaging could be dispensed with. Although MEG is capable of more accurate localisation than the EEG (Spekreijse 1991), the ability of the EEG to detect magnetically silent sources would also prove beneficial if used in combination.

CHAPTER 3

3.1 INTRODUCTION - THE VISUAL SYSTEM.

Of the five human senses, vision is the most highly developed. It provides information about shape, texture, colour, movement and three dimensional relationships. Much of the fundamental work into visual function has been performed using invasive intracellular recording on primates and cats. Comparisons with humans have been achieved by observations on patients with visual dysfunction resulting from known neural injury, while the advent of neuroimaging techniques such as MRI and MEG offer the potential for detailed noninvasive investigations. Comprehensive reviews of visual system anatomy and function are provided by Regan (1989), Carpenter (1984) and Zeki (1992).

Figure 3.1A and B show two aspects of the brain, with the visual pathways illustrated. Light entering the eye is converted into electrical impulses which are transmitted down the optic nerves (ON) to the optic chiasm (OC), where fibres from the nasal half of each eye dissociate (figure 3.1B, OC). Hence, each cerebral hemisphere receives information primarily from the contralateral visual field. Following dissociation, the fibres pass to the lateral geniculate bodies (LGB) via the optic tracts (OT), and then along the optic radiations (OR) to the occipital cortices (OCC). Signals are also passed from the retina and cortex to the superior colliculus (SC), a pathway that controls pupil size, accommodation, eye and head movements.

3.2 - THE EYE.

Light enters the eye through the cornea, a transparent protective layer, kept clean by the combined action of tear glands and eyelids. Behind this lies the iris, whose aperture varies automatically to control the amount of light passing through the crystalline lens. The curvature and thickness of this lens also varies under muscular control, effectively altering the focal length of the eye. The combined effects of these optics is to produce a focused image of acceptable mean luminance on the retinal cells lining the rear of the eye. The retina consists of a number of different cell types, organised into distinct, interconnected layers. The most distal of these is a tightly packed array of

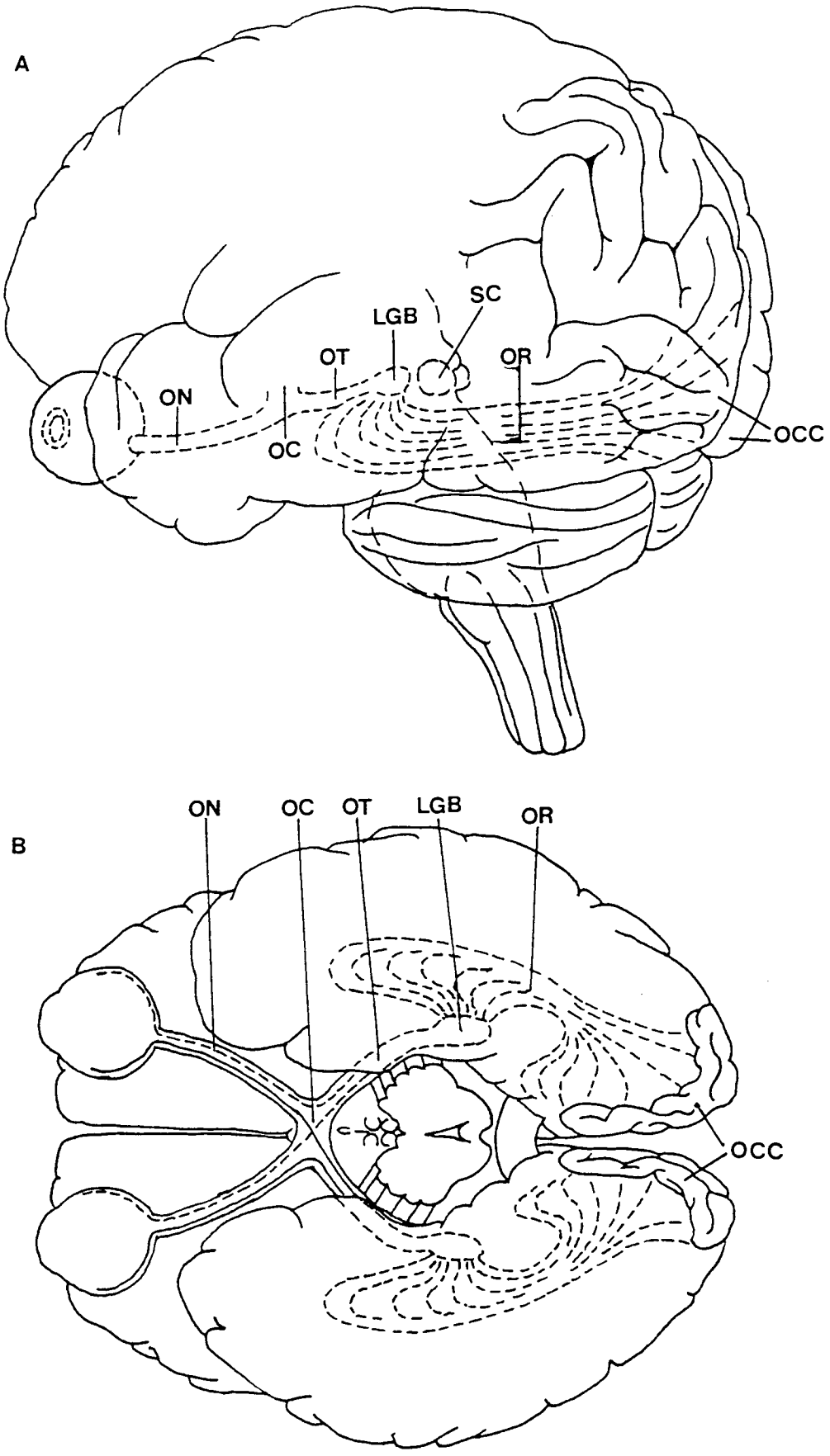

Figure 3.1 - Visual pathways as viewed from the lateral (**A**) and inferior (**B**) aspects of the brain. Structures below the surface are drawn with dotted lines.
ON - optic nerve. OC - optic chiasm. OT - optic tract. LGB - lateral geniculate body. SC - superior colliculus. OR - optic radiation. OCC - occipital cortex.

receptors which contain the photosensitive chemicals responsible for light conversion. These can be divided into two structural and functional groups, the rods and cones. Rods are involved in scotopic vision (or low ambient light levels), being primarily sensitive to the blue part of the spectrum. Cones respond to higher light levels (or photopic conditions), with three subgroups producing trivariant colour vision. This is achieved by the use of photosensitive chemicals, differentially sensitive to red (566nm), green (535nm) or blue (415 to 420nm) wavelengths of light. Cones also differ from rods in being directionally sensitive to the angle of light approach, having faster response times and less convergence for increased image quality. Signals initiated in the receptors pass anteriorly to other cell types, travelling in the opposite direction to the incoming light. These include bipolar, amacrine, horizontal, interplexiform and ganglion cells, each of which can be subdivided further into classes. The most direct route through the retina is from the receptor to the ganglion cells via the bipolars. Alternatively, lateral connections can be involved, with horizontal cells between the receptors and bipolars and/or amacrines between the bipolars and ganglion cells. Each of these contribute to the centre/surround receptive field organisation of the retina to be described later (Kuffler 1953, Baylar et al 1971). Ganglion cells can also be divided into X, Y and W in cats (Enroth-Cugell and Robson 1966) and M and P in primates (Gouras 1969, Sherman et al 1976). The W cells have small cell bodies which project to the superior colliculus; X cells, constituting 80% of the total, have medium sized cell bodies which project to the LGB; and Y cells (10% of the total) have large cell bodies projecting to both the SC and LGB. The ganglion cell axons travel across the surface of the retina to the optic disc, at which point they become myelinated and leave the eye as the optic nerve.

Variations in the distribution of each cell type has been used to segregate retinal regions of specific eccentricity. The fovea (central 3°) is recognised by reduced retinal thickness, pitted shape and lack of rods. The foveola (1.2°) contains only photoreceptors, glial and Müller cells. The parafovea and perifovea show increased concentrations of rods, with fewer cones than the central fovea, while the parafovea also shows the densest accumulation of neurons within the retina. The receptor cells of the central fovea are connected to individual, or even multiple ganglion cells, while at greater eccentricities, each ganglion cell is connected to several receptors. The number of receptors forming the input to each ganglion cell determines its

receptive field size, which range from a few minutes of arc in the central fovea, to 3 to 5° in the periphery (Kuffler 1953), with a corresponding decrease in spatial resolution. The receptive fields are further organised into the form of a central core area with an antagonistic surround, classified as either on- or off-centre (Kuffler 1953). For the former, a maximal excitatory response is obtained if a light stimulus falls on the central area alone, while for the latter, the stimulus has to fall in the periphery. The fields of adjacent cells form a dense overlapping array across the retina, whose organisation allows for the detection of movement and the edges of stimulus elements (Leventhal 1985). The use of centre/surround antagonism is particularly useful since it allows vision to operate over a wide range of ambient luminance levels (Luminance gain). This is achieved by the measurement of the relative difference in luminance between adjacent retinal locations, and not absolute luminance.

3.3 - THE LATERAL GENICULATE BODIES.

The lateral geniculate bodies (figure 3.1 LGB) form a thalamic relay station for visual signals as they pass from the eye to the cortex. Their structure has six layers, each separated by intervening axons and dendrites. The four dorsal layers are called the parvocellular laminae due to the predominance of small cell bodies, while those of the two thinner, ventral layers are larger (Magnocellular). Magno- and parvocellular laminae can also be classified according to the nature of their inputs, processing and outputs (See Kaplan et al 1991). Input to all layers is highly segregated, with axons from contralateral and ipsilateral eyes projecting exclusively to successive layers (Hubel and Wiesel 1977). For parvocellular laminae, two layers have a predominance of on-centre ganglion cell inputs, while the other two are of the off-centre type (Schiller and Colby 1983). Retrograde inputs are also received from the brainstem reticular formation, and layer IV of the visual cortex.

Functional properties also differ between magno- and parvocellular laminae, the parvo layers demonstrating smaller receptive fields (Derrington and Lennie 1984); a more sustained response (Gouras 1969); increased linear summation; lower conduction velocity inputs and outputs, and lower contrast sensitivity (Shapley et al 1981). Parvocellular layers also display colour

opponent receptive fields, unlike those of the achromatic magnocellular layer (Gouras 1969, Shapley et al 1981). These functional differences suggest that the LGB could be used to separate contrast and colour information transmitted by the retina. LGB cells are also known to be organised with centre surround antagonism, weak orientation tuning properties (DeValois et al 1982), but no binocular fusion.

3.4 - CORTICAL MORPHOLOGY AND PROCESSING.

Each cerebral hemisphere can be divided into two morphologically distinct regions. The central, white matter, consists of tracts of myelinated nerve axons, used to transfer information, both between different cortical regions, and the rest of the body. The cortical surface is a 1.5 to 4.5mm thick layer of densely packed neurons (Polyak 1953), whose interconnections perform the mechanisms of neural processing. The folding of the cortex into gyri and sulci allows a relatively large surface area (approximately 1ft sq. Hubel 1988) to be accommodated within the restricted volume of the skull.

Studies of humans with known neurological damage (Barber et al 1993, Plant et al 1993), and intracellular recording on animals, have shown that well defined regions of the cortex are responsible for specific functions. Each of these were classified in the early 1900's by workers such as Cambell and Brodmann (Von Bonin 1950). Of the 50+ regions identified, at least twenty cortical areas are thought to be involved in visual processing (Van Essen 1985). Each is extensively interconnected either directly, or indirectly, via subcortical nuclei. Most visual information passes first to striate cortex (Brodmann 17 or V1 in primates), located in the walls of the calcarine fissure, the cuneal and lingual gyri and on the lateral lobe surfaces (Polyak 1953). This acts as a relay station for passage to other visual areas, itself being sensitive to stimulus colour and form (Livingstone and Hubel 1984). The prestriate cortex (Brodmann area 18 and 19, or primate areas V2 and V4) processes information about stimulus form, orientations and movement, with V4 showing a preference for colour processing (Zeki and Ship 1988). Subsequent interconnections link the prestriate regions with those of the inferotemporal lobe (areas 20 and 21). Human PET studies have localised colour processing to area V4 (Brodmann 18), and achromatic check movement to area V5 (the midtemporal lobe) (Zeki 1992). Visual processing is therefore

achieved by a progressive alteration of the incoming parallel signals at different cortical locations, the results of which are transferred back to areas V1 and V2 for mapping onto the visual field (Zeki 1992).

The cortex is composed primarily of pyramidal, stellate and fusiform neurons, whose arrangement, interconnections and relative densities produce six distinct layers. The fourth layer below the pia surface can be further subdivided into four layers (figure 3.4), IVc appearing as a dense white band (Band of Gennari) in regions of primary visual cortex (Polyak 1953). Striate cortical neurons are grouped into vertical columns, running from the pia to the white matter, according to their functional properties to various parameters of the visual stimulus. The early intracellular recording studies of Hubel and Wiesel (1959, 1962) on cats, demonstrated the presence of such columns, sensitive to the orientation of lines within the visual field and the eye from which these signals originate (Ocular dominance columns). Other columns have also been identified for stimulus spatial frequency in cats, using activity dependent 2(14C) deoxy-D-glucose (Tootell et al 1981). Figure 3.4 shows a diagrammatic representation of cortical organisation, the top of the cube corresponding to the pia. The nearest quadrant of the cube represents a cortical hypercolumn, comprising a set of ocular dominance columns (one for each eye) and a complete set of orientation columns. The latter are between 30 and 100μm wide, with the angle of preferred orientation changing systematically between successive columns by approximately 10° (Hubel and Wiesel 1977, 1979). The hypercolumns contain sufficient orientation units to account for line rotations of 360°. Ocular dominance columns are approximately 250 to 500μm wide, each receiving input exclusively from one eye (Hubel and Wiesel 1977). Staining cortical sections with mitochondrial enzyme cytochrome oxidase has revealed distinct areas which take up stain readily (the blobs), surrounded by lightly stained regions (interblobs) (Livingstone and Hubel 1988). The blobs are represented in figure 3.4 by the cylindrical structures, which appear only in cortical regions above and below layer IV. The blobs contain cells which are wavelength selective, and therefore sensitive to colour. Although they do not exhibit orientation specific properties (Livingstone and Hubel 1984), they can determine the edges of shapes by differences in colour and brightness (Livingstone 1990). The interblob regions have cells which are orientation specific, responding to

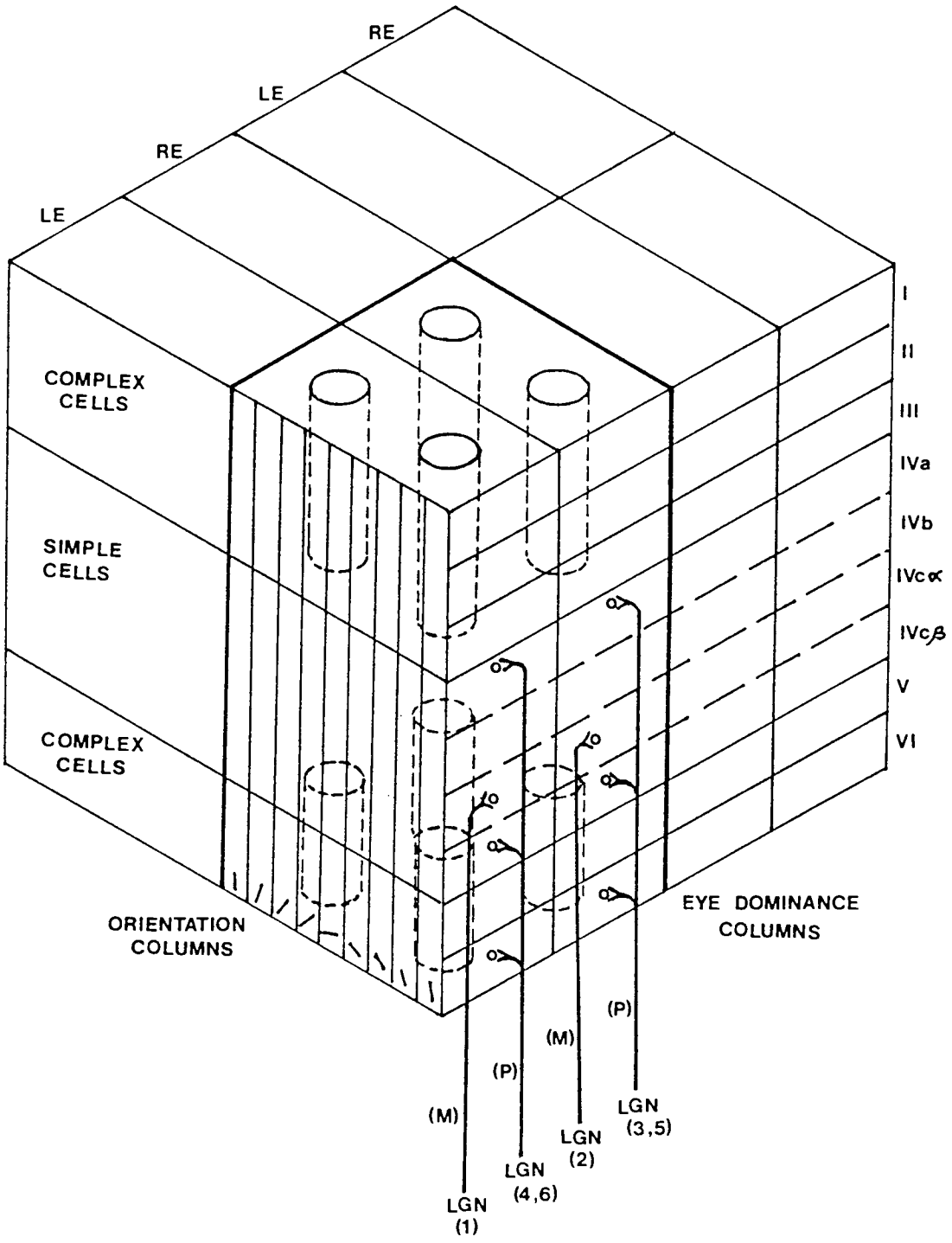

Figure 3.4 - Schematic diagram of a visual cortex hypercolumn (adapted from Hubel 1988). Dashed pegs represent cortical blob regions surrounded by interblobs. Columns are shown for orientation and eye dominance preferences (LE - left eye, RE - right eye). The various horizontal cell layers of the cortex are numbered to the right, the top of the cube corresponding to the pia suface. Also shown are lateral geniculate nucleus (LGN) inputs to the various cortical layers. The inputs originate from either magnocellular (M) or parvocellular (P) LGN systems, the numbers indicating precisely which LGN layer they are from.

contours generated by differences in wavelength or luminance (Livingstone and Hubel 1984).

The receptor field properties of cortical neurons are more complex than those of the eye or LGB, since few show simple circular field antagonism. Hubel and Wiesel (1962), classified cortical cells in cats as either simple or complex according to their functional properties. Simple cells, found predominantly in layer IV of striate cortex (figure 3.4), have a rectangular antagonistic centre surround arrangement which respond optimally to light slits with the same orientation as its field axis. Flashed or moving lines increase this response, while non-optimal stimuli (regarding orientation, length, spatial frequency or velocity), result in non linear inhibition (Kulikowski and Murray 1985). Leventhal (1985) proposed that the orientation preferences of such cells were formed during cortical maturation, under the influence of orientation sensitive LGB and retinal ganglion afferents. The more highly tuned nature of the cortical cells was attributed to enhancements from intracortical inhibition and/or excitatory convergence.

Complex cells are found above and below layer IV (figure 3.4), again showing a preference for stimuli of slits, bars or edges of specific orientation. They are assumed to be composed of cells which receive input from several simple cells, each of the same axis. Their properties differ from simple cells however, since they do not show precise antagonistic on/off regions and they respond to a variety of stimulus characteristics such as novelty, contour movement and texture. Different subgroups of complex cell have been identified (See Hubel 1988), those of layers I and II respond proportionally to increasing line length; those of layer IV have an optimal upper length (end capped); while those of layer V show no preference. Leventhal (1985) proposed that the orientation specificity of layer II and III complex cells occurs due to the excitatory input from layer IV simple cells; while those of layers V and VI are influenced by intracortical inhibitory connections from the complex cells of layers II and III of the same column.

Cortical interconnections have been described in detail by Van Essen (1985), Zeki and Ship (1988), and Zeki (1990, 1992). Afferent fibres to the cortex make synaptic contact with neurons in specific layers, dependent upon their origins. Retinocortical fibres from the magnocellular layers of the LGB (LGB 1 and 2, figure 3.4) terminate in layers IVca and the upper parts of IVcb, while those from the parvocellular laminae (LGB 3 to 6), project to layers IVcb, IVa

and VI. In all cases, inputs to layer IV preserve monocular separation, with convergence occurring in superficial layers. Magno- and parvocellular inputs also remain segregated until the interblob regions of layers II and III are reached (Van Essen 1985).

Afferent fibres of thalamic origin, and collateral fibres from other cortical regions, synapse with the neurons of layer IV and III. Neurons of layer IVc make axonal contact with the apical dendrites in layers II and III, which in turn project to those in layer V, then VI and back to layer IV (Gilbert and Wiesel 1979, Singer 1979).

Cortical efferents are produced by all layers with the exception of I, IVa and IVc. Neurons of layer II and III send collaterals to higher cortical areas, such as the prestriate cortex. Cells of layer V project to the superior colliculus, while those of layer VI return to the LGB. Magno- and parvocellular striate cells are also known to produce efferent axons. The magnocellular neurons project to the thick, stripe region of cortical area V2, concerned with binocularity; the parvocellular cells from blob regions project to the thin stripe region of V2, concerned with colour; while the interblob parvocellular cells connect with the interstripe regions of V2, associated with stimulus form (Livingstone and Hubel 1984, Zeki and Ship 1988).

3.5 - PARALLEL PROCESSING.

Information about different aspects of the visual scene are transferred from the eye to the occipital cortex and beyond via separate pathways, acting in parallel (Zeki and Shipp 1988). These are referred to as the W, X and Y systems in cats (Enroth-Cugell and Robson 1966), and the M and P pathways in primates. For recent detailed reviews see Kaplan et al 1991 and Zeki 1990, 1992. Evidence from psychophysical studies have suggested that man also possess sustained and transient detection systems (Kulikowski and Tolhurst 1973, Tolhurst 1975). Although the interspecies differences are often ignored, the cat and primate systems differ. Hence, the geniculate neurons project exclusively to the striate cortex in primates but also to extrastriate regions in the cat (Sherman 1985), and so care must be taken when drawing comparisons from the literature.

Segregation of visual information occurs as early as the retinal ganglion cells and the pathways remain distinct through the lateral geniculate bodies,

into the striate cortex and even to association regions beyond (Zeki 1992). In cats, the various pathways are identified according to their functional and anatomical properties. The W system accounts for 15 to 20% of the retinal ganglion cells, and although the fibres project to striate and extrastriate cortex, they respond poorly to visual stimuli (Sur and Sherman 1982). The X, or sustained system, produces a sustained response to prolonged stimulation. X type cells account for 50 to 60% of the total retinal ganglion cells, and they project solely to the striate cortex, with the majority of synapses occurring in layers IV and VI of a single ocular dominance column. The X system is sensitive to high spatial frequency patterns, contributing to detailed acuity analysis, while also being essential for stereopsis. The Y, or transient system, involves only 5% of retinal ganglion cells, however their projections are amplified centrally to dominate striate and extrastriate cortical afferents. Synapse again occurs in layers IV and VI, however the precise locations differ from those of the X system, and several ocular dominance columns of the same eye are involved (Sherman 1985). The Y cell axons display faster conduction than those of the X (Parker and Salzen 1977), while they are stimulated preferentially by lower spatial frequencies (Lehmkuhle et al 1980).

The properties of the M and P processing systems in primates (table 3.5), show similarities with the cat Y and X systems respectively. The P cell system can be subdivided into those cells which receive input from red/green sensitive axons and those from the blue/green cones. The M system is characterised by cells sensitive for motion and stereoscopic depth. It is responsive to flicker, and is able to perceive pattern and higher order pattern such as shading (Kaplan et al 1991). The P system carries information about colour and fine detail at high contrast, and is probably responsible for the detection of form and shape (Kaplan et al 1991 and Livingstone 1990).

Zeki (1992) in his review of parallel processing, suggested that four parallel systems are involved in visual processing, one for motion, one for colour and two for form. The motion sensitive M cell pathways project from the retina to magnocellular layers of the LGB, then to layer IVb of striate cortex, and then to area V5 either directly or via the stripe region of V2 (Livingstone and Hubel 1984). The colour sensitive P system projects from the eye to parvocellular LGB layers, and then to the blob region of striate cortex, before passing to the V4 area directly and via the thin stripe of V2. The processing of form occurs via both P and M systems, being colour dependent and independent

TABLE 3.5 - Properties of the M and P cell visual processing systems in primates (Lennie 1982, Livingstone 1990, Kaplan et al 1991, Zrenner 1991).

respectively. The P pathways project from the LGB to the interblob regions of striate cortex, and then to the interstripe region of V2. The M pathways project to layer IVb of the striate cortex, then to area V3 directly and via the thick stripe region of V2.

The effects of human parallel processing channels have been used to explain electrophysiological (Parker and Salzen 1977, Halliday 1982, Vassilev et al 1983) and psychophysical reaction time results (Breitmeyer 1975, Vassilev et al 1983). Hence, the increase in latency and reaction time observed with increasing spatial frequency has been attributed to a transfer of activity from the fast conducting transient system (Y), to that of the slower, sustained pathways (X) (Vassilev et al 1983). Alternatively, Parker and Salzen (1977), proposed that such a change could occur within the transient system alone.

As M and P processing streams (or their human equivalents), operate in combination, the resulting cortical activity is dependant upon their relative contributions (Aine et al 1990, Ahlfors et al 1992). The activity of each system can be enhanced by careful stimulus design, with transient channel activity increased by large check sizes (56', Harding and Wright 1986), rapid temporal changes (Legge 1978) and low contrast or luminance (Kaplan et al 1991). The sustained system is preferentially activated by low spatial frequencies (12c/deg, Harding and Wright 1986), steady or slowly changing stimuli (Legge 1978) and coloured, isoluminant pattern elements (Krauskopf et al 1989). The tailoring of stimuli for specific visual pathways would be useful in the localisation of specific cortical regions, with potential clinical applications, since diseases such as Alzheimers, glaucoma and multiple sclerosis are thought to preferentially influence the M cell pathways (Johnson et al 1987 and Quigley et al 1988).

CHAPTER 4

METHODS

4.1 - EQUIPMENT.

THE MAGNETOMETER.

Throughout this thesis, magnetic fields were measured using a BTi magnetometer (Model 601). The device was a single channel dc SQUID, second order gradiometer, with a pick-up coil diameter of 2cm, located 12mm from the outer surface of the dewar tail, and a baseline of 5cm. The system had an intrinsic noise level of 16.6fT/$\sqrt{Hz}$ at 5Hz.

THE STIMULATOR.

The pattern onset stimulus was provided by a Bio-Logic VM 4515 monitor (60 Hz refresh rate), controlled by a Medelec OS5 unit.

TV systems have become widely accepted as a means of stimulus presentation (Shagass et al 1976, Skrandies et al 1980, Parker et al 1982, Stok 1986, Butler et al 1987, Maier et al 1987, Ossenblok and Spekreijse 1991, Beers et al 1992), as they allow a variety of pattern types to be used (Harding 1990), with precisely controllable temporal and spatial frequencies (Yoshii et al 1991). Such systems do have problems however:-

1. Raster systems have been shown to produce an average latency delay of 8.33ms between pattern appearance at the top and bottom of the screen. This value decreases at refresh rates greater than 60Hz (Lueders et al 1980, Regan 1989).
2. Most commercial monitors cannot maintain a constant luminance between pattern on and offset, particularly at higher contrast levels (Lavasik and Ahmedbhai 1985, Yoshii et al 1991).
3. TV systems tend to increase intertrial variability, absolute latency and latency variability compared to that attainable with optical systems (Stokard et al 1979).

Optical stimulators, using a projector and shutter arrangement (Spekreijse et al 1973, Lesevre and Joseph 1979, Drasdo 1980, 1981 and 1982), maintain space average luminance (Drasdo 1982, Yoshii et al 1991), while allowing for the adjustment of contrast and pattern rise time (Drasdo 1982). Their use was

precluded however, due to the unacceptable environmental noise levels generated by the electro magnetic shutter drive.

The averager was not locked to the stimulus frame rate, hence averaging did not always coincide with the beginning of the screen refresh. While this can help to reduce the problems of noise associated with the monitors vertical deflection of the raster scan, it also results in a reduction in signal amplitude, and an increased latency variability (Haywood and Mills 1980).

STIMULUS PARAMETERS.

1. Unless otherwise stated, the full field stimulus subtends an angle of 7°20' (horizontal) x5°43' (vertical) to the eye, with a half field of 3°40'x5°43'. This was achieved with the monitor placed 2.5m from the subject to minimise electronic interference.

2. Most recordings were performed with a check size of 38'x27' and a contrast of 65%. The edges between the black and white squares had a square contrast change, rather than a sinusoidal modulation.

3. The luminance of the offset grey screen was 74Cd/m^2. Upon pattern onset, the mean luminance of the checkerboard caused an increase of 0.03, 5.82 and 47.14Cd/m^2, (or 0.04, 7.84 and 63.48%) for contrast levels of 15, 65 and 93% respectively. Since the monitor system had no provision for luminance correction, the majority of the recording was performed using the 65% contrast, as opposed to 93%. The problem with non-linear monitor phosphors has been mentioned previously by Duwaer and Spekreije (1978), who experienced a luminance modulation of 10%.

4. The stimulus rate was 1Hz, hence the checkerboard appeared abruptly, and was replaced 200ms later by a blank grey screen, which remained for 800ms. The interstimulus period was not randomised. A pattern duration of 200ms was adopted, as it has been shown to be the minimum time required to produce separation of the onset and offset response components (Parker et al 1982).

5. Binocular stimulation was used throughout. Binocular onset responses have been shown to produce greater amplitudes than monocular (Harding et al 1991), with similar topographic distributions (Jeffreys and Axford 1972 b, Creel et al 1981).

4.2 - RECORDING PROTOCOLS.

SUBJECTS.

1. All subjects who participated in this study were consenting volunteers, without ophthalmological disorders. Where required, visual acuities were corrected to 6/6 or better using a trial frame and lens set of non-ferrous construction.
2. Subjects were relaxed as much as possible prior to recording by explaining the nature of the equipment and experiment. This helped to reduce myogenic artifacts.
3. Subjects were asked to remove all objects which could provide sources of noise, such as jewellery and watches. Particular noise problems were encountered with necklaces and underwired bras which move with the chest during respiration.
4. It was found more convenient and comfortable to record from seated subjects, rather than those lying prone. This also removed the problem of breathing artifacts found commonly with subjects lying on their chests.
5. The subject was asked to fixate on a small dark focal spot on the monitor (less than 30' diameter), and mentally count the number of pattern appearances. The latter instruction was given to help maintain concentration, and so diminish alpha activity and fixation disparity (Carelli et al 1982).
6. Where multiple recordings were required within any given session, the subject was asked to relax following each run, so as to minimize fatigue (Regan 1989).
7. The temporal variability studies of chapter 5 required ten consecutive recordings to be made in a given session. To remove any variation resulting from probe positioning errors, an experienced subject was used (CD), who could maintain the same position for all ten recordings, without moving.
8. The mean luminance of the room was maintained at $20Cd/m^2$ for all experiments, and noncycloplegic conditions were used throughout.
9. The study was approved by the University Ethical Committee.

TOPOGRAPHIC MAPPING.

The majority of the topographic maps presented in this study were recorded from an array of twenty locations over the occipital scalp, consisting of four rows of five positions (figure 4.2A). This allowed a sufficiently large area of

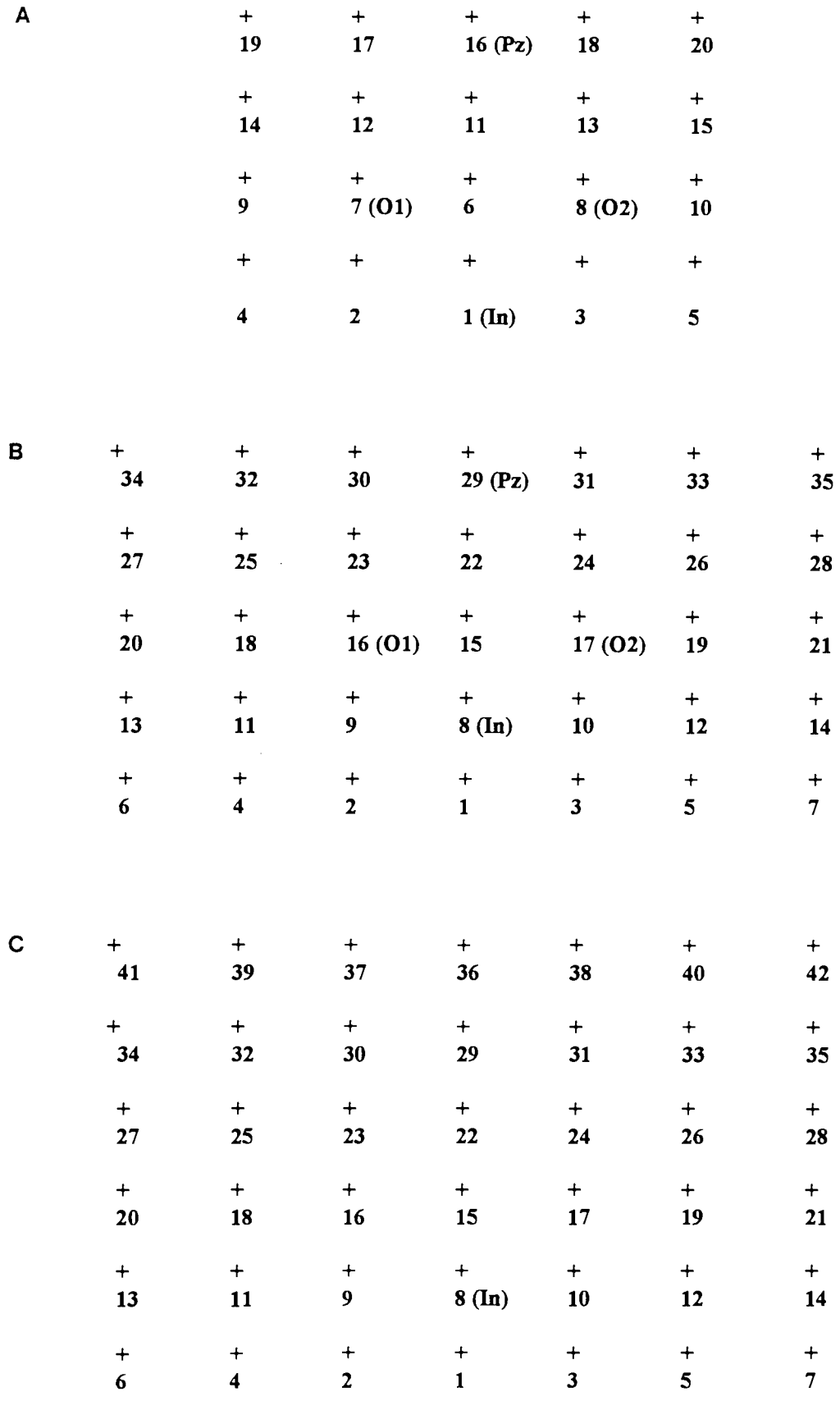

Figure 4.2 - Illustration of the three recording matrices used throughout this thesis, and their relationship to the international 10/20 system of electrode placement. The numbers below each point indicate the order in which they were recorded.
A - 20 point array. **B** - 35 point array. **C** - 42 point array.

the scalp to be sampled, while limited the time required to complete each session to approximately 40 to 50 minutes.

RECORDING MATRIX.

Figure 4.2A shows how the twenty point matrix corresponded to the 10/20 electrode placement system. The space separating each point from its nearest neighbour was equivalent to 10% of the half circumference of the head, from nasion to inion. Such a relative separation was used to take account of the intersubject variations in head size. These positions were measured, and marked on the scalp with a chinagraph pencil prior to recording. The number printed below each point corresponds to the order in which it was recorded.

Figure 4.2B shows a 35 point matrix, used to more fully delineate the full field response of subject SC. The array has that of figure 4.2A at its core, with the addition of an extra row of points below the inion line, and at either side.

Figure 4.2C shows a 42 point matrix, used in the source localisation of three separate recordings. Each point is separated from its nearest neighbour by a fixed distance of 2cm, the inion corresponding to the central position on the penultimate row from the bottom. The increased spatial sampling was used to increase the accuracy and statistical significance of source localisation procedures. The grid spacing chosen for source localization is related to the source depth below the scalp (D) and the distance from the pickup coil to the scalp (d), by the equation:-

$$\text{Grid spacing} = 0.7\ (D+d)$$ (Romani and Leoni 1984).

In general, increasing the number of recording locations improves the resolution of recordings made within a fixed area (Hari et al 1988), or under worsening signal to noise conditions (Stok 1986). In practice, most authors use approximately 40 recording positions, separated by 2cm (Darcey et al 1980, Richer et al 1983, Kouijzer 1985, Stok 1986, Spekreijse 1991).

PROBE POSITIONING AND MAPPING APPROACH.

The centre of the dewar tail was located over each of the pre-marked scalp positions in turn, and oriented normal to the scalps surface. Although the positioning accuracy is likely to be lower than that attainable using reference

transmitters fastened to the head, the intertrial topographic stability obtained suggested that this was not a significant source of error (see chapter 5). Various mapping approaches have been adopted by different authors, either moving the magnetometer over the scalp in a flat plane (Kouijzer et al 1985, Stok 1986), a sphere (Meijs et al 1987), or normal to the scalp (Romani and Narici 1986, Meijs et al 1987, Harding et al 1991). The planar method allows for precise positioning (Stok et al 1986), although it also has disadvantages. The subject has to lie prone (Kouijzer et al 1985), while the increased distance and angle between the scalp and probe, for the outer recording positions, decreases signal to noise conditions and increases the contributions from secondary sources (Meijs et al 1987). For a spherical recording surface, the effects of secondary sources on the radial field component are minimal (Meijs et al 1987), so simplifying computer algorithms (Barth et al 1986). Variations in scalp to probe distance between different locations reduce signal to noise conditions (Barth et al 1986), while accurate localisation requires the gantry to be under computer control. Mapping with the probe placed normal to the scalp provides an acceptable compromise between the two previous methods. The minimal probe/scalp distance maximises detectable signal strength (Romani and Narici 1986), and requires only simple gantries. Although secondary sources influence the recorded field distribution, their effects are less than those encountered when recording over a flat plane (Meijs et al 1987).

SEQUENTIAL MAPPING.

Due to the restrictions imposed by single channel recording, the topographic distributions presented in this thesis were obtained by combining the data from twenty sequential recordings, each made from a separate scalp location. This makes the assumption that the underlying current activity remains in a constant position and orientation during the recording session, and that the effects of background noise are unrelated to the evoked signal (Kaufman et al 1991). The problems of such an approach include the loss of temporal continuity of the data, the increased time required to complete a recording session (Romani and Narici 1986), and the susceptibility to probe positioning errors (Hari et al 1988).

4.3 - DATA ACQUISITION AND INTERPRETATION.

ACQUISITION.

Signals from the magnetometer were recorded at a sensitivity of x1000 (89pT/V, flux to voltage), filtered between 0.3 and 30Hz by four pole Butterworth filters (24dB/octave roll off), and passed through a 50Hz comb filter. The low pass filter had to be set at 30Hz to remove high frequency noise in the unshielded environment. As discussed in section 1.6, the onset evoked cortical response contains frequencies up to, or beyond 75Hz, therefore the use of a 30Hz low pass filter would have the effect of removing signal information as well as noise, which although undesirable was unavoidable. Several authors have also adopted a similar filtering regime for studies of the pattern onset VEP (Darcey et al 1980, Barber and Galloway 1981, Creel et al 1981, Edwards and Drasdo 1987, May et al 1991).

Signals were attenuated by a factor of 100 so as to produce an input signal whose amplitude was within the operating range of the analogue to digital converters. Attenuation had to be performed, since the magnetometer system offered a limited range of signal amplification values. Signals were then sampled at a rate of 256Hz and averaged on a Bio-Logic Traveler signal processor, incorporating artifact rejection. Fifty signals were averaged from each scalp location, with a time base of 500ms.

Waveform amplitudes were measured from peak to baseline. The baseline set by the averager was a technical zero baseline as opposed to a biological baseline, hence an equivalent value to that which would be obtained by short circuiting the preamplifier input (Lehman and Brown 1980). Various other methods of peak measurement have been used by previous authors; including peak to peak amplitude (Edwards and Drasdo 1987); peak to baseline, with the baseline taken as the amplitude at the beginning of the averaging epoch (Ermolaev and Kleinman 1983), or the average amplitude of a short pre-stimulus (Jeffreys and Axford 1972 a and b, Butler et al 1987) or post-stimulus period (Barber and Galloway 1981). Lehman and Brown (1980) advocated the use of a technical zero baseline, since they considered peak to peak measures inappropriate where individual peaks varied independently with stimulus parameters. They also questioned the use of a pre stimulus baseline, due to the assumption that no time locked neural activity occurred during this period. The technical zero baseline is however susceptible to direct current (DC)

shifts, in which any DC potential that occurs during data acquisition can displace the waveform with respect to the baseline. This can result in variation in peak amplitude, or in extreme cases, polarity. Amplitude alterations resulting from DC offsets is an additional source of variation, which when combined with noise fluctuations and the adverse effects of single channel recording, restrict the conclusions which can be drawn from the topographic data.

ANALYSIS.

The coloured topographic contour distributions used throughout this thesis were calculated and printed by a Nicolet Pathfinder II, using linear interpolation. Two colour scales are used, the first represents areas of zero magnetic field as yellow, with increasing strengths of magnetic flux flowing out of the head shown as red to white, and inward flowing flux as green to blue. The second is used for standard deviation and coefficient of variance (CV) plots, and changes from blue to white, via red, as values increase.

The coefficient of variance (CV) maps were calculated from the mean and standard deviation (SD) values for each recording position, from the equation CV = SD/Mean x 100, with values given as a percentage. A large CV value will occur in situations where the standard deviation is large with respect to the mean. With the mean topographic data shown here therefore, large CV values tend to occur at recording positions where the constituent maps show magnetic fields of opposite polarity. Hence if one map shows an area of outward flowing field, in the same position and of similar amplitude to an area of inward flowing field on the second map, the mean field would be small while the SD and CV values would be high. The advantage of using the CV value as compared to the SD is that the CV takes account of the size of the mean on the variation.

The line contour plots presented in chapter 7 were calculated using spline interpolation by the PC based package "SURFER".

Unless otherwise stated, the units of amplitude displayed in the figures and graphs can be converted to fT by multiplying by a factor of 6.7.

The 42 point topographic data for the right half field response of one subject was used as input for two different source localization approaches;-

1. A single dipole in a sphere model (Janday et al 1989), performed at the Open University.

2. A distributed source space, based on the idealised cruciform model of the visual cortices (Jeffreys and Axford 1972 a), containing 42 current elements oriented normally to the respective cortical surfaces. This was contained within a spherical conductivity model of the head (Bedford 1992).

The latter of these was also used to localise the 20 point mean half field data from ten subjects.

RESPONSE INTERPRETATION.

Throughout this thesis, responses are interpreted with regards waveform morphology, peak latency, amplitude and/or topographic distribution. Where possible, topographic data has been quantified by the inclusion of mean, standard deviation or coefficient of variance distributions. Alternatively, similarities between topographic distributions have been quantified by average standard deviation (SD) figures, calculated as the sum of the standard deviations between corresponding recording locations of the constituent topographies, divided by the number of positions. Hence, the average SD is given as a value per recording location. These approaches can be used to quantify similarities and differences between a series of topographic distributions, however they cannot quantify the changes in topography which occur with changing stimulus parameters. Quantification of such data in this thesis is also hindered by the presence of multiple field areas resulting from full field stimulation and the problems associated with single channel recording. Analysis of such data is therefore made by visual inspection of the distributions, and so the subjective element to analysis must be considered when interpreting the implications of the findings.

CHAPTER 5

5.1 - TECHNICAL CONSIDERATIONS.

Before examining how the visually evoked magnetic response (VEMR) to a pattern onset stimulus is affected by variations in stimulus parameters, such as check and field size, it is first necessary to establish its intrinsic variability.

The following studies examine the inter- and intrasubject latency and amplitude variation of the major peaks following pattern onset. The effects of averaging, shielding, equipment specificity and subject refractive error are also considered. The study of such variables is useful for both research and clinical applications, as it provides a baseline of normal response, against which the effects of changes in stimulus parameters and pathology can be compared. Few studies of this nature have been reported in the literature for the VEMR (Lewis et al 1984, Kouijzer et al 1985, Armstrong et al 1991, Harding et al 1991, Ahlfors et al 1992).

5.2 - CRITERIA FOR COMPONENT IDENTIFICATION.

Throughout this study, the three major peaks following pattern onset are referred to as the CIm, CIIm and CIIIm (figure 5.421). Identification is made by visual inspection of the waveforms, with consideration given to peak latency, morphology, relative amplitude and topography. Each peak is likely to represent the activity of several neural generators, with overlapping activity (Lesevre and Joseph 1979), especially when using half and full field stimuli. Hence, where the term 'component' is used, it refers to the co-ordinated activity of a group of sources, as opposed to that of an individual population of neurones. Techniques such as principal component analysis have been used to separate the multiple sources contained in the pattern onset VEP (Maier et al 1987, Ossenblok and Spekreijse 1991). Assigning latencies to waveform peaks by visual inspection alone has problems. The method is subjective and difficulties arise when recording at positions of low signal to noise ratio, where broad or multiple peaks often result. More objective methods for peak identification can be used, such as the measurement of the area below the peak, which reduces the problems of noise and latency variation. The

technique is sensitive however, to the choice of baseline, and the overlapping activity of different peaks (Regan 1989).

For all single point studies, a scalp position of known high signal strength, as determined by previous mapping studies, was chosen for probe location. Such a position was accepted as one producing a magnetic field whose averaged amplitude was greater than twice that of the background noise (Aine et al 1990). Background noise varied according to the time of day, from 30 to 40 fT (measured peak to peak) in the early mornings and late evenings, to 80 to 110 fT during the day. In the case of the temporal variability studies on subject CD, recordings were made 6cm to the right of the inion. This corresponds to the positive field maxima for a full field stimulus. For the intersubject study, since topographic distributions were not available for each individual, a half field stimulus was employed, due to the predictable nature of its evoked topography (See section 6.2). Recordings were made 6cm above the inion, either over the midline or 3cm to the left. This coincides with the position of inward flowing field over the scalp for right half field stimulation, and in all cases a high amplitude signal was obtained with a single positioning of the probe.

The VEMR waveform displays two prominent peaks within the first 180ms post stimulus, the most dominant of which occurs between 100 and 120ms (the CIIm). This is followed by a more rounded peak, of similar amplitude but opposite field direction, (the CIIIm). Both peaks are seen consistently in different subjects, even in areas of poor signal to noise ratio. Peaks of similar latency and topographic distribution have been described by other authors, the type I and II onset responses of Stok (1986) and the flashed pattern M120 and M180 of Richer et al (1983). A peak is sometimes seen preceding the CIIm, being of low amplitude, opposite field direction and poor morphology (CIm), however this occurs in only 5 to 10% of averaged responses from different subjects and recording locations. Stimulus offset is marked by a large peak of symmetrical morphology, appearing at approximately 140ms post stimulus. The polarity of this peak is usually opposite to that of the onset CIIm. The opposite polarity for the onset and offset responses suggests that they could be generated primarily by a contrast and/or contour mechanism, as opposed to a luminance specific process (Spekreijse et al 1973).

5.3 - THE UNAVERAGED ONSET RESPONSE AND THE EFFECTS OF AVERAGING.

5.31 - UNAVERAGED DATA.

Unlike the VEMR to pattern reversal or flash stimuli (Slaven 1993), the onset responses produce waveform peaks which are visible in individual sweeps. Observations of successive, unaveraged waveforms suggest that the latencies and amplitudes of each peak fluctuate with time. In order to determine if these variations are random, chaotic or cyclic, the following study was performed.

5.32 - METHODS.

Consecutive unaveraged waveforms were recorded using a PC based computer program (Mr. G Barnes, Aston University), and stored for subsequent analysis. Three runs were made on subject CD to a full field stimulus of check size 38'x27' and a contrast of 65%. Runs one and two stored the initial 50 and 100 consecutive responses respectively. For the third, the subject observed 151 pattern appearances, with only the last 100 being saved. The latter was intended to observe any effects of response habituation. Recordings were made in a shielded environment, fitted with eddy current and mu-metal shielding (See section 5.5).

In each case, the CIm, CIIm and CIIIm peaks were identified from each consecutive response, and the latency and amplitude of each measured.

In order to determine if consecutive responses varied temporally, the latency and amplitude data for each peak (CIm, CIIm and CIIIm) of the three runs, were examined using pattern analysis by linear regression (Yarranton 1969). This analysis can be applied to any set of consecutive data, to determine the presence and scale of 'non randomness'.

The variable under consideration (for example CIIm latency), was measured from successive waveforms, and recorded sequentially. Linear regression coefficients were calculated for pairs of adjacent values and then with an increasing degree of separation along the transect i.e. separation by 1,2,3,4....n. Hence, the number of pairs included in the regression decreased with increasing separation between the values. The regression coefficient was then plotted against the degree of separation of the samples.

Regression analysis was performed on a BBC microcomputer, the results being displayed in the format of the block size under test, the regression coefficient, the standard error and the significance value of the test (T). Significant negative or positive values of T indicate non randomness within the data set. The block size which produces the first significant negative T value corresponds to the size of clusters within the data, while the first significant positive T value corresponds to the distance separating the centre of each cluster, or the cluster frequency. Significant T values at subsequent block sizes indicate the presence of clustering on a larger scale (Armstrong 1993).

5.33 - RESULTS AND IMPLICATIONS.

Figure 5.331 shows six consecutive, unaveraged waveforms. The CIIm and CIIIm peaks are visible on each, the CIIIm of poorer morphology, while the CIm is apparent on four waveforms. Almost all unaveraged responses display large amplitude CIIm and CIIIm peaks, while many also show CIm peaks of similar amplitude and poorer morphology.

Figure 5.332 shows latency versus amplitude plots for each peak of the 248 unaveraged responses recorded. The CIIm and CIIIm clusters are similarly distributed, except with a slightly greater variation in CIIIm latency.

Peaks which show latency variation from moment to moment tend to become 'flattened' in the averaging process (see section 5.34). If the peaks are also of comparatively low amplitude, then they may not be present on the averaged waveform. Problems with averaging, coupled with the intermittent appearance of the unaveraged CIm, might provide an explanation for its absence from the averaged waveform. This would also suggest that the VEMR CIm peak has different origins from those of the VEP CI, since the latter has been shown to arise from predominantly radially oriented sources (Ossenblok and Spekreijse 1991), whose activity should not be apparent in the averaged or unaveraged VEMR. Similar problems could also explain the broad appearance of the averaged CIIIm peak relative to the CIIm. The absence of the CIm peak from some unaveraged sweeps, may be due to the intermittent activity of the contributory sources. Alternatively, CIm source activity could be periodically suppressed by sources which contribute to the later components. Of the 215 unaveraged waveforms displaying a CIm peak, five showed a positive

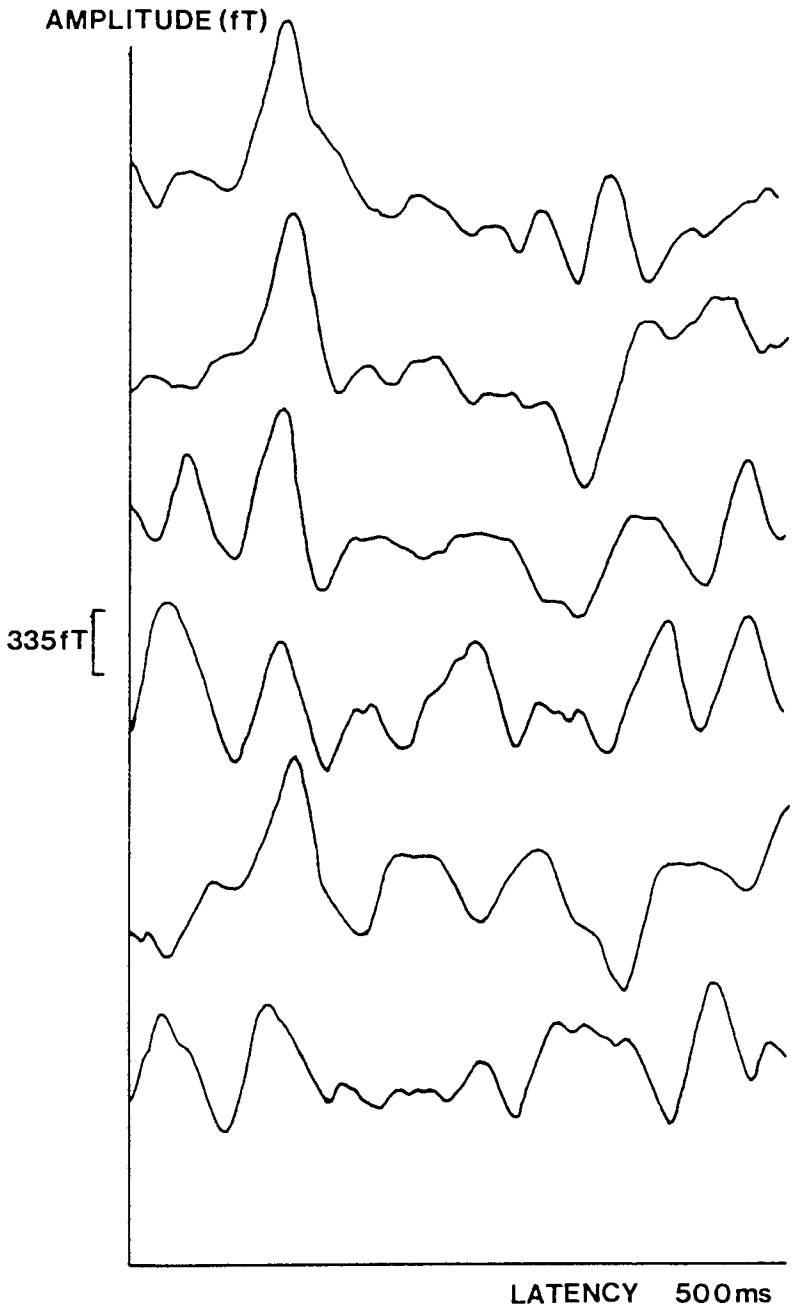

Figure 5.331 - Six consecutive, unaveraged onset waveforms of subject CD. An upward deflection (or waveform peak) corresponds to magnetic field flowing out from the scalp, and vice versa.

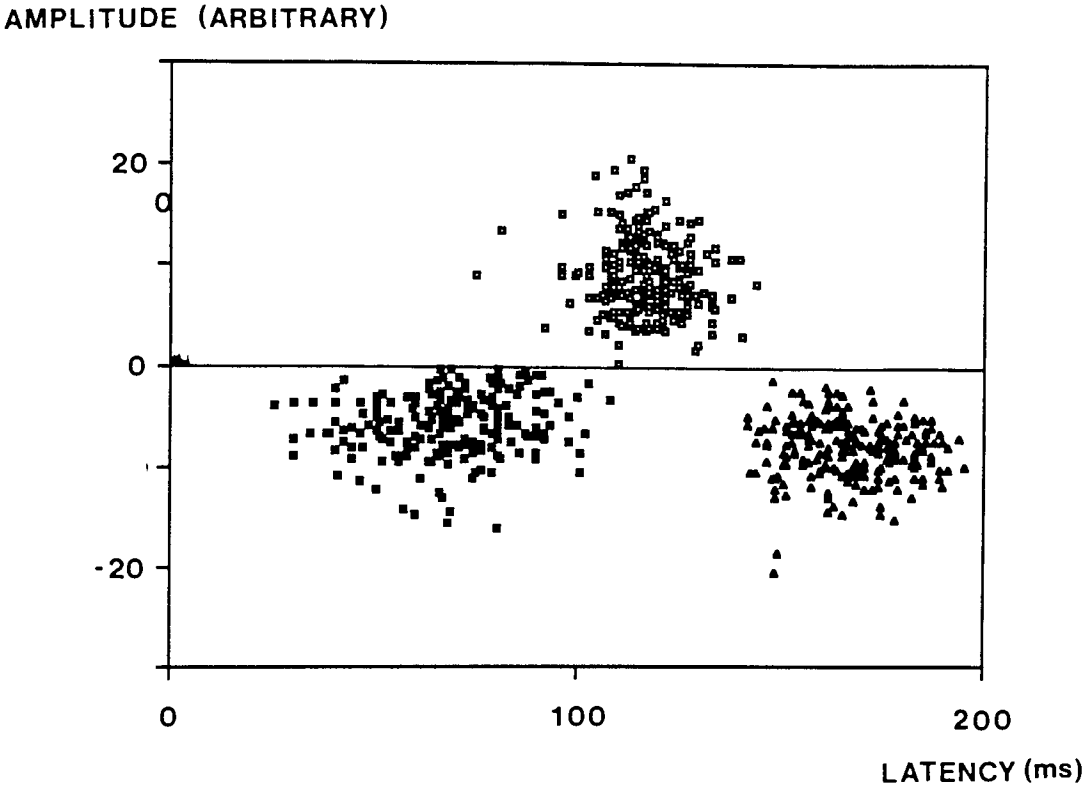

Figure 5.332 - Latency versus amplitude scatter plots for the three most prominant waveform peaks of subject CD following pattern onset. The data from 250 unaveraged responses recorded in the double shielded environment are shown.

amplitude. This could have occured due to the effects of DC drifts, and hence, the five responses were omitted from further analysis (See section 4.3).

Table 5.333 shows the mean, standard deviation and coefficient of variance (CV) for the latency and amplitude of each peak, shown graphically by the latency/amplitude scatter plots of Figure 5.334. CV values are similar whether fifty or one hundred responses were recorded. Increasing the stimulus period by the inclusion of fifty stimuli prior to recording, results in an increased CV for CIIIm amplitude and the latency of CIIm and CIIIm. This could represent the effects of habituation, or poor fixation resulting from fatigue.

Table 5.335 shows the cluster and frequency results for the pattern analysis by linear regression, performed on each onset peak. Non random behaviour is apparent for both latency and amplitude measures of several peaks, with multiple clustering suggested particularly with the larger sample sizes. Such clustering could represent cyclic processing events, such as the activity of negative feedback mechanisms; the effects of noise from cycling generators; or the contribution from rhythmic brain activity. This latter possibility has been proposed by Cignek (1969), to explain the variability seen with the unaveraged flash VEP. Variations in cortical excitability to various stimuli have also been attributed to the simultaneously occurring background alpha activity (Jansen and Brandt 1991).

This technique has a number of limitations, and the results should be interpreted accordingly. Firstly, if clusters of constant size and separation are present in the data, the analysis will indicate the presence of clustering on multiple scales. Such a possibility was mentioned by Yarranton (1969). Secondly, if T values are obtained which fall just below significance level, (possibly due to a small data set), their exclusion could greatly effect the interpretation of cluster size and repetition. Finally, the interrelationships between successive clusters of equal size are not provided. Although the presence of clusters is indicative of co-ordinated, repeating activity, it would be impossible to determine the spatial interrelationship between the clusters. A similar approach has been reported by Zerlin and Davis (1967), who studied the unaveraged vertex sharp potential waves in one subject, to investigate possible sequential effects of cyclic recurring patterns. In this case the data were analysed by auto correlation techniques. They did not observe any cyclic behaviour, but concluded that although EEG noise was likely to contribute to amplitude variability, it could not account for all the variation found in the

TABLE 5.333. - Mean, standard deviation and coefficient of variance values for the latency and amplitude of the sequential unaveraged CIm, CIIm and CIIIm onset peaks.

RUN 1 - UNAVERAGED RESPONSES 1 TO 50.

COMPONENT	LATENCY (ms)	VARIANCE (%)	AMPLITUDE (arbitary)	VARIANCE (%)	SAMPLES
CIm	64.98 ± 16.33	25.14	-48.2 ± 30.3	72.75	47
CIIm	114.26 ± 5.57	4.87	+113.8 ± 33.6	25.09	50
CIIIm	163.19 ± 11.23	6.88	-75.5 ± 25.1	33.29	48

RUN 2 - UNAVERAGED RESPONSES 1 TO 100.

COMPONENT	LATENCY (ms)	VARIANCE (%)	AMPLITUDE (arbitary)	VARIANCE (%)	SAMPLES
CIm	68.47 ± 14.58	21.29	-66.5 ± 29.4	44.23	83
CIIm	117.34 ± 7.67	6.54	+80.7 ± 31.7	39.25	99
CIIIm	167.00 ± 11.54	6.91	-96.7 ± 29.5	30.50	90

RUN 3 - UNAVERAGED RESPONSES 51 TO 150.

COMPONENT	LATENCY (ms)	VARIANCE (%)	AMPLITUDE (arbitary)	VARIANCE (%)	SAMPLES
CIm	69.84 ± 17.85	25.56	-58.4 ± 30.3	51.80	80
CIIm	117.85 ± 11.72	9.94	+80.2 ± 30.3	37.77	99
CIIIm	169.12 ± 15.00	8.87	-71.9 ± 25.0	34.69	91

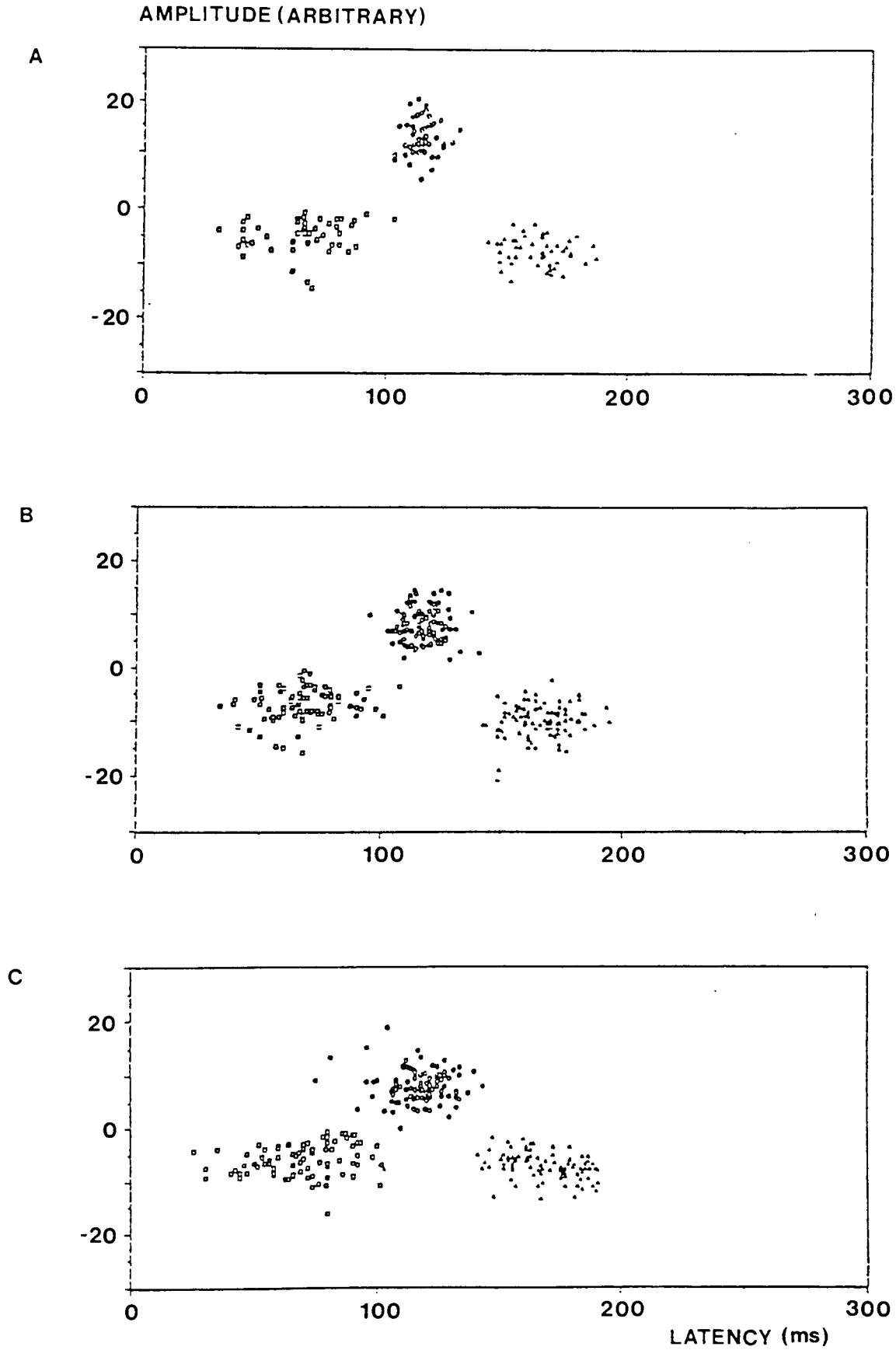

Figure 5.334 - Latency versus amplitude scatter plots for the three most prominant waveform peaks following pattern onset. Results show 50 (**A**) and 100 (**B**) consecutive, unaveraged responses, as well as 100 responses recorded following pre-exposure of the subject to 50 onsets of the stimulus (**C**).

TABLE 5.335 - Data for the pattern analysis by regression of the sequential unaveraged CIm, CIIm and CIIIm onset peaks. The size of clusters of similar values and the frequency of their repetition is shown.

RUN 1 - UNAVERAGED RESPONSES 1 TO 50.

	CIm		CIIm		CIIIm	
	CLUSTER	FREQ.	CLUSTER	FREQ.	CLUSTER	FREQ.
LATENCY	6, 13	24	8, 20	24	8	23, 30
AMPLITUDE	----	----	----	----	22, 30	----

RUN 2 - UNAVERAGED RESPONSES 1 TO 100.

	CIm		CIIm		CIIIm	
	CLUSTER	FREQ.	CLUSTER	FREQ.	CLUSTER	FREQ.
LATENCY	27	----	2, 45	3,7	20	----
AMPLITUDE	----	----	16, 17, 18, 21	34	----	3, 34

RUN 3 - UNAVERAGED RESPONSES 51 TO 151.

	CIm		CIIm		CIIIm	
	CLUSTER	FREQ.	CLUSTER	FREQ.	CLUSTER	FREQ.
LATENCY	6, 41	36, 47 52	2, 7, 8	43, 44 58	----	60
AMPLITUDE	----	----	47	----	1, 53	----

data. They did however notice a negative trend in amplitude with time, attributed to fatigue or habituation.

Where similar cluster sizes and frequencies occur between different components, it would be interesting to determine their relative phase characteristics. Signals in phase could be indicative of a common source generator. Data from pairs of components were plotted, and regression lines fitted to see if any correlations existed. Negative and positive correlations would suggest activity out of, and in phase respectively. No correlations were found between the amplitudes of any components. For the latencies, a significant, positive linear correlation was evident between the CIm and CIIm ($p<0.01$ to <0.001) and the CIIm and CIIIm ($p<0.02$ to <0.001), of all runs except the CIIm/CIIIm of run 2. No correlations were found between CIm and CIIIm latencies.

The limitations of this technique, restrict the implications which can be drawn from the results. There is the suggestion of non random behaviour between consecutive onset neural responses, with positive correlations between the generators of the CIm/CIIm and CIIm/CIIIm peaks. This could suggest similarities between the VEMR onset components of this study, and those of the onset VEP described by Ossenblok and Spekreijse (1991). These authors analysed onset VEP responses using principal component analysis and source localisation algorithms. They concluded that the triphasic VEP waveform could be resolved into the overlapping activity from two separate cortical sources. Activity from the first produced the first positive waveform peak (CI), and the initial part of the following negativity (CII). The second source contributed to the latter stages of this negativity (CII), and to the following positivity (CIII). If the VEMR and VEP results are analogous, then their data suggests that the activity recorded in this study could be from extrastriate cortical regions. With refinement of the pattern analysis by regression technique, combined with the large amplitude pattern onset VEMR, the possibility exists to study visual processing on a millisecond time scale, without the information loss encountered with signal averaging. If such an approach were to be implemented, the influence of factors such as sampling rate would have to be investigated in order to maximise waveform resolution.

5.34 - EFFECTS OF AVERAGING.

Individual evoked responses cannot normally be studied because of poor signal to noise ratio (Squires et al 1976). Noise can be defined as any signal other than that under observation, and it can arise from the environment, instrumentation and the subjects background brain activity. Early attempts to separate the evoked signals from noise included photographic superposition (Dawson 1947), but this was superseded by various averaging techniques. It is possible to enhance the amplitude of a desired signal by optimising interstimulus intervals, or by using optimal passband filters for the frequency content of the given signal (Hari et al 1988). Although this can be useful, prior knowledge of signal characteristics is required, and so averaging has remained the universally accepted method of data acquisition.

The averaging process operates by storing successive response waveforms in separate memory registers, and then performing a summation of the amplitude values at corresponding latencies of each. Consequently, neural activity occurring at the same time with relation to the stimulus becomes progressively larger on the resultant waveform (average in), while random noise has a tendency to diminish (average out). The interpretation of an averaged waveform therefore makes the assumption that identical stimuli produce identical responses, whose latencies do not vary from trial to trial. It also assumes that the noise is not related to the evoked signal, but instead occurs at random intervals. If these criteria are met, then the signal to noise ratio improves as a function of $\sqrt{N}$, where N is the number of responses included in the average (Regan 1989). It has been shown however that identical stimuli do not produce identical responses (McGillem and Aunon 1977), and that noise, particularly background brain activity such as alpha rhythm, can become time locked to the stimulus. Also, variations in the latency of successive unaveraged responses can result in an average response of prolonged latency, reduced amplitude, or which is completely absent (Brazier 1964). This is of particular importance in extended recording sessions, as subject fatigue can increase latency variation.

To reduce these problems, various adaptations have been made to the basic averaging process. However each has its own advantages and disadvantages. Donchin (1969) used stepwise discriminate analysis, in which waveforms could be pre-sorted prior to averaging, according to differences in their behaviour

to specific stimulus characteristics. However, this method is dependent upon the selection criteria adopted. Woody (1967), introduced crosscorrelation averaging in an attempt to avoid the problems of unaveraged latency variation. This process identifies the peak of interest for each unaveraged response and then adjusts the entire waveform to align these peaks prior to averaging. Although the definition of the given peak is improved, other peaks on the waveform tend to diminish due to the questionable assumption that the entire waveform varies uniformly with time (McGillem and Aunon 1977, Aunon and McGillem 1979, Aunon and Sencaj 1978). The method of latency corrected averaging introduced by Aunon and Sencaj (1978) attempted to rectify this problem by identifying and separating each peak of the unaveraged responses, and aligning them separately prior to averaging. Although each peak is retained in the average, large assumptions are again made as to what constitutes a peak and what is noise. In addition, there is also a tendency for the largest peak to dominate the average. Such a method may be useful to establish if the absence of the CIm in the averaged waveform were due to latency variation, or factors such as source orientation.

As a result of these problems, a method to determine the number of responses required to produce an averaged waveform of minimal distortion is needed.

5.35 - METHODS.

Recordings were made on subject CD to a full field stimulus of 38'x27' checks at 65% contrast. The PC based data acquisition program from section 5.32 was adapted to record each successive response, average it with those recorded previously, and store the result. Consequently, waveform number 1 represented the unaveraged response to the first stimulus onset, number 2 was the average of the first and second responses, three was the average of the first three responses, and so on. The latency and amplitude of each peak was then plotted as a function of the number of individual responses included in the average. Four recordings were made, two directly over the positive field maxima, and the other two at 3 and 6cm intervals to the left. All measurements were made in a room fitted with eddy current, and mu-metal shielding. (See section 5.5)

5.36 - RESULTS AND IMPLICATIONS.

Figures 5.361, 5.362 and 5.363 show the effects of increasing the number of responses per average on the latency and amplitude of each peak, recorded over the position of maximal field strength, 3cm and 6cm to the left respectively. When recording over the maxima, the latency of all three peaks stabilises after ten responses, after which the CIm varies by 5ms, the CIIm by 1ms and the CIIIm by 6ms. The amplitude of the CIm is less stable, varying continuously up to 50 samples. The amplitude of the CIIm and CIIIm peaks decline initially, before stabilising after 30 and 20 samples respectively. When recording 3cm from the maxima, (figure 5.362), the latency and amplitude behaviour of the CIm and CIIIm peaks remain similar to that seen previously. For the CIIm, the latency is slightly more variable. After 11 samples, a variation of approximately 4ms is achieved. Stable amplitudes are obtained after 15 samples. At a distance of 6cm from the maxima (figure 5.363), the CIm latency peaked after 15 samples, but does not stabilise, while amplitude stabilises after 20 samples. The CIIm amplitude stabilises after 15 samples. Latency varies continuously up to 50 samples per average, the rate of change becoming slower after approximately 40 responses. The CIIIm amplitude becomes stable after 5 samples, while its latency behaves in a similar way to that of the CIIm.

Hence, approximately 10 to 15 responses per average would be sufficient to obtain CIIm and CIIIm peaks of stable latency and amplitude, if recordings were made within 3cm of the field maxima. Also, increasing the number of responses in the average can be detrimental, as the amplitude may begin to decline due to variability introduced as a result of subject fatigue. The use of such a small number of responses per average would be of limited use with a single channel magnetometer system, as the position of the field maxima would have to be known to within a 3cm radius. Such accuracy may be possible using half field stimuli (See chapter 6). With a multichannel system, the larger area of scalp covered in each recording should allow at least one channel to lie within this area. The differences in amplitude behaviour for the CIm, as compared to the CIIm and CIIIm could suggest a contrast type origin for the former, and a contour specific mechanism for the latter. Hence, Barber and Galloway (1979) demonstrated that contour specific mechanisms

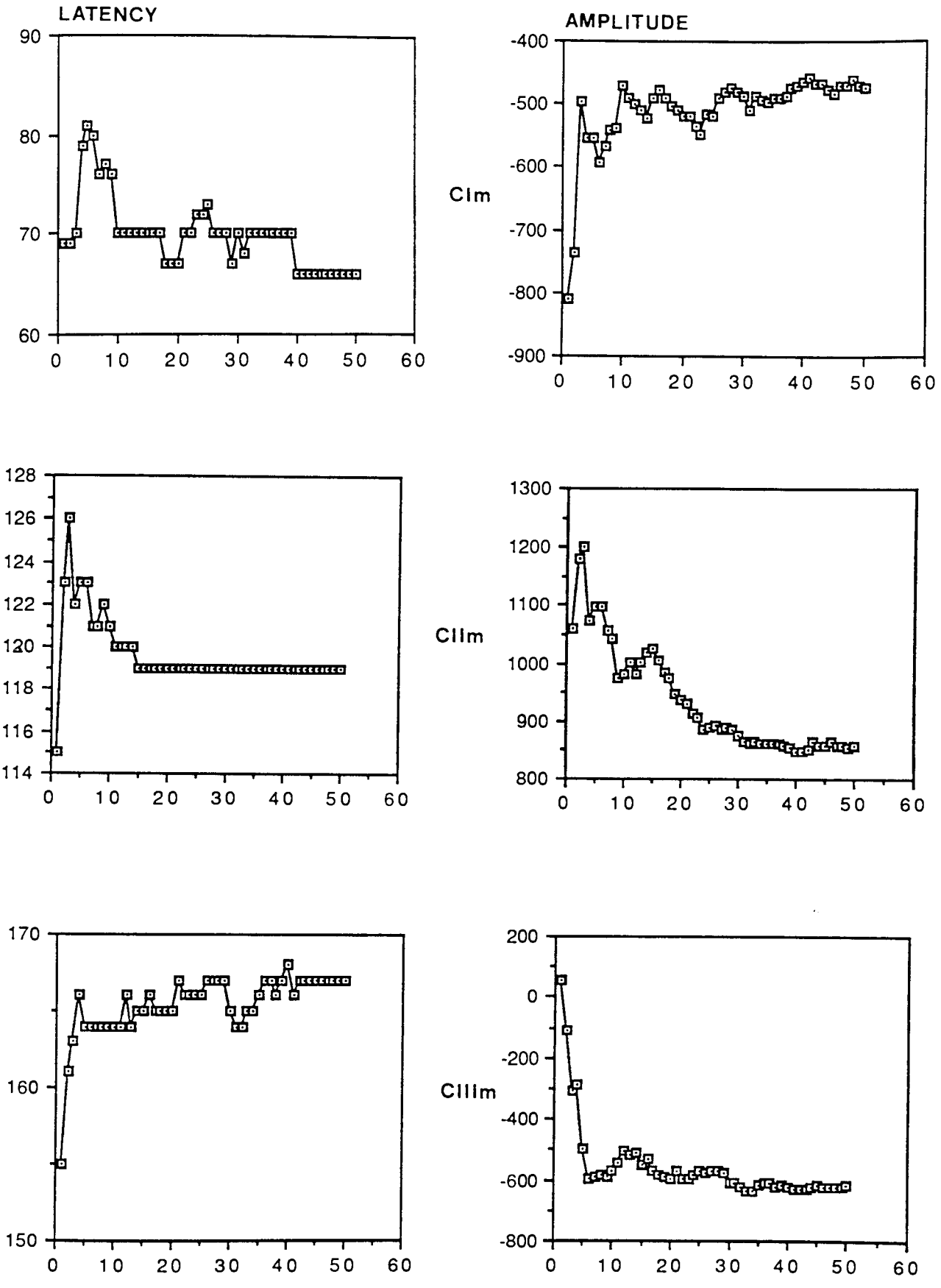

Figure 5.361 - The effects of increasing the number of responses included in the average on the latency and amplitude of the three most prominant waveform peaks following pattern onset. Recordings were made on subject CD from a scalp location of maximal field response. The number of responses included in the average are show along the horizontal axis, while the vertical axis shows the response latency in milliseconds (left hand graph in each case), or amplitude (right hand graph). The units of amplitude were not calibrated in μV or fT, and so cannot be compared with those used throughout the rest of the thesis, however all responses shown in this section are comparable.

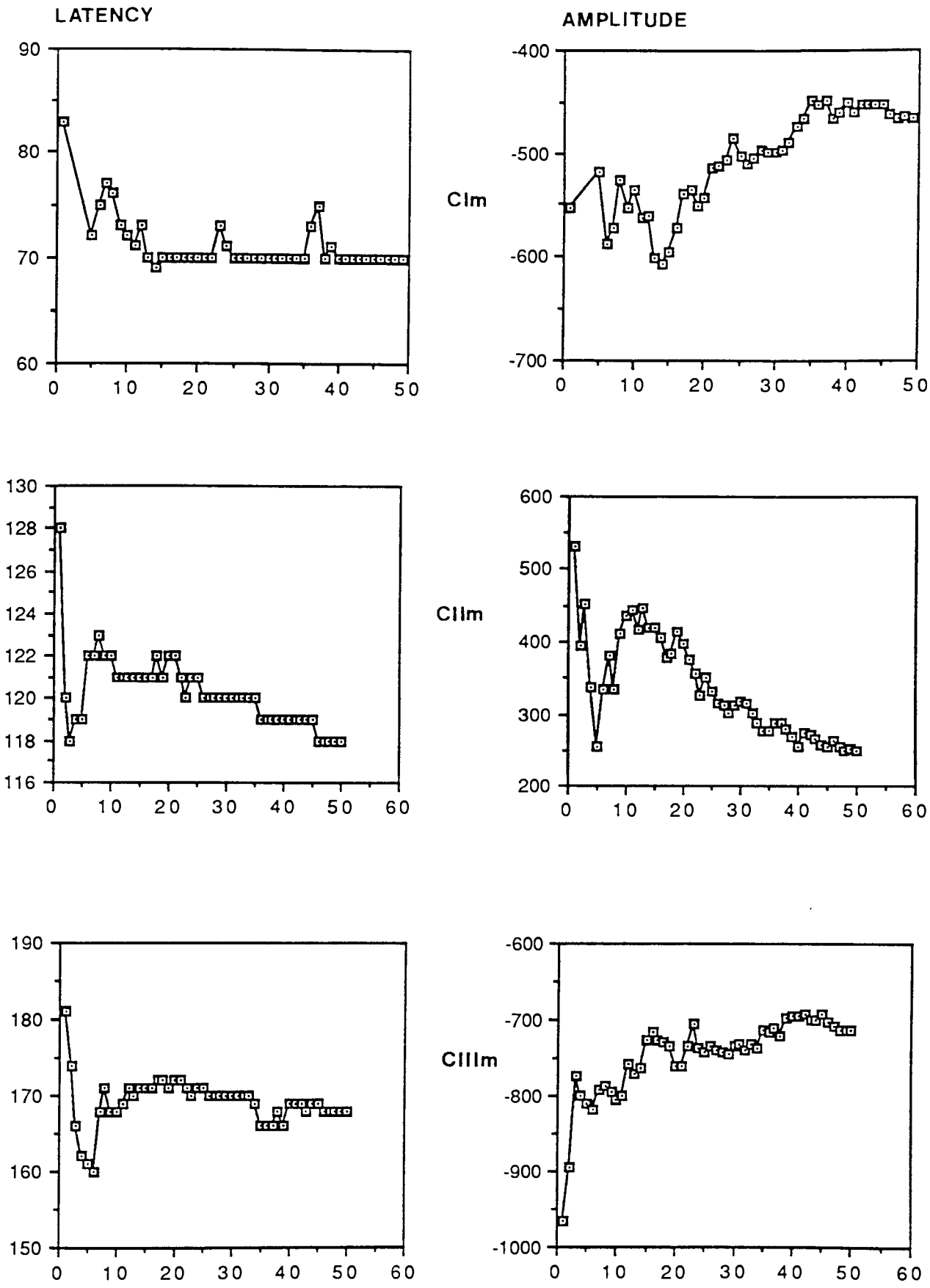

Figure 5.362 - The effects of increasing the number of responses included in the average on the latency and amplitude of the three most prominant waveform peaks following pattern onset. Recordings were made on subject CD from a scalp location 3cm to the left of the maximal field response. The number of responses included in the average are show along the horizontal axis, while the vertical axis shows the response latency in milliseconds (left hand graph in each case), or amplitude (right hand graph). The units of amplitude were not calibrated in μV or fT, and so cannot be compared with those used throughout the rest of the thesis, however all responses shown in this section are comparable.

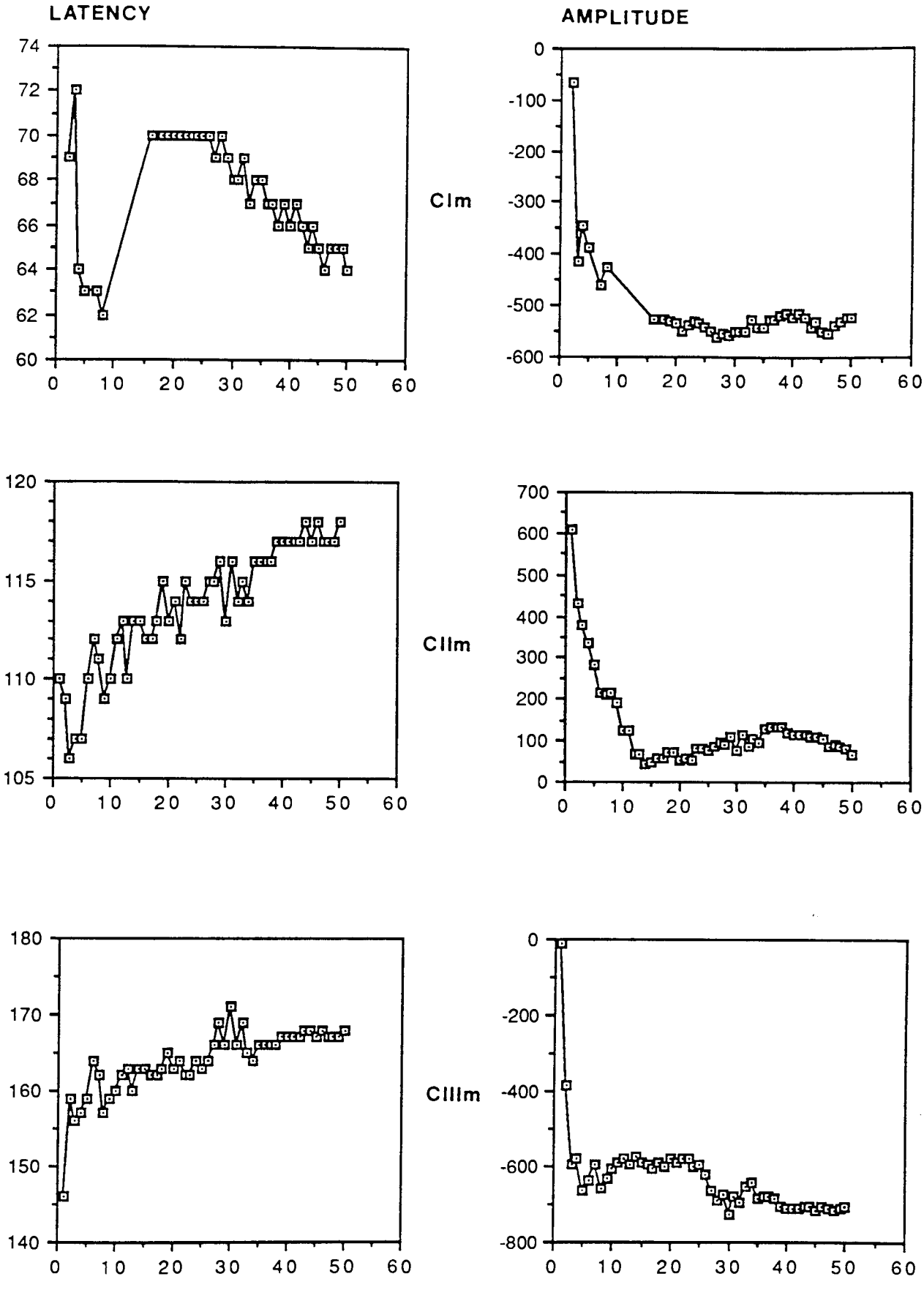

Figure 5.363 - The effects of increasing the number of responses included in the average on the latency and amplitude of the three most prominant waveform peaks following pattern onset. Recordings were made on subject CD from a scalp location 6cm to the left of the maximal field response. The number of responses included in the average are show along the horizontal axis, while the vertical axis shows the response latency in milliseconds (left hand graph in each case), or amplitude (right hand graph). The units of amplitude were not calibrated in μV or fT, and so cannot be compared with those used throughout the rest of the thesis, however all responses shown in this section are comparable.

undergo amplitude attenuation with repeated pattern presentation, while contrast specific processing is unaffected by adaptation.

These findings compare well with those of Duffy and Rengstorff (1971), who examined the possibility of using the VEP to a flashed pattern as an objective test for refractive error. They observed that 10 to 15 responses per average were sufficient to obtain an accuracy of ±2.5 dioptres of blur. Lewis et al (1984) used a flashed pattern stimuli to observe the effect of averaging on the VEMR. They compared the responses to 20 and 40 samples per average and found no difference in latency, but a lower amplitude with the larger average, as would be predicted from the results presented here. However, Stok (1986) and Kouijzer et al (1985) both used 200 responses per average in their studies of the pattern onset and flashed pattern VEMR, but the rationale for this number was not explained.

As mentioned previously, the use of a small response number per average with a single channel system would have limited use if the position of maximal field was not known. This would not be a problem for mapping studies. If a topographic map were constructed using a minimum number of responses per average, the distribution obtained would presumably show the position of the field maxima unchanged, as problems with noise should occur only as the probe is moved into the transitional areas between maxima. In order to test this hypothesis, a series of four full field, twenty point maps were recorded on subject SC, using 50, 30, 20 and 10 responses per average. The gross waveform morphology recorded at the scalp location of maximal field strength remains consistent regardless of the number of responses per average (figure 5.364). Decreases in the sample size result in amplitude increases and decreases in different peaks, depending upon which scalp location is examined. The largest amplitude peaks, with clearest morphology, are obtained using 20 responses per average, while with 10, the peaks are still visible but the noise is greater. Figure 5.365 shows the topographic distributions of the three prominent peaks for each recording condition. As the number of responses included in the average is reduced, the regions of inward and outward flowing field (for each waveform peak latency) show gross similarities. Variations do occur in the exact positions of the negative and positive field maxima, however this could be confounded by the problems of single channel mapping (See section 4.2). Figure 5.366 shows the mean and standard deviation topographies for each of the three peaks. Peaks 1 and 2 show most variation over the left hemisphere,

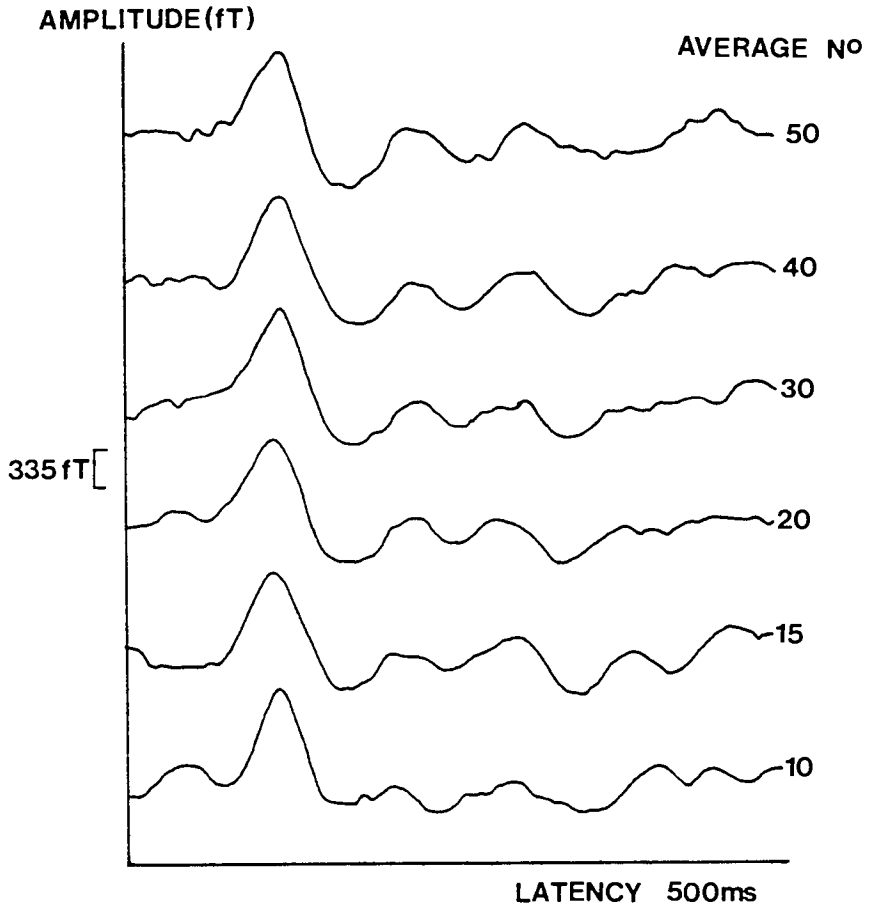

Figure 5.364 - A series of averaged onset waveforms from subject SC consisting of 10, 15, 20, 30, 40 and 50 responses per average respectively.

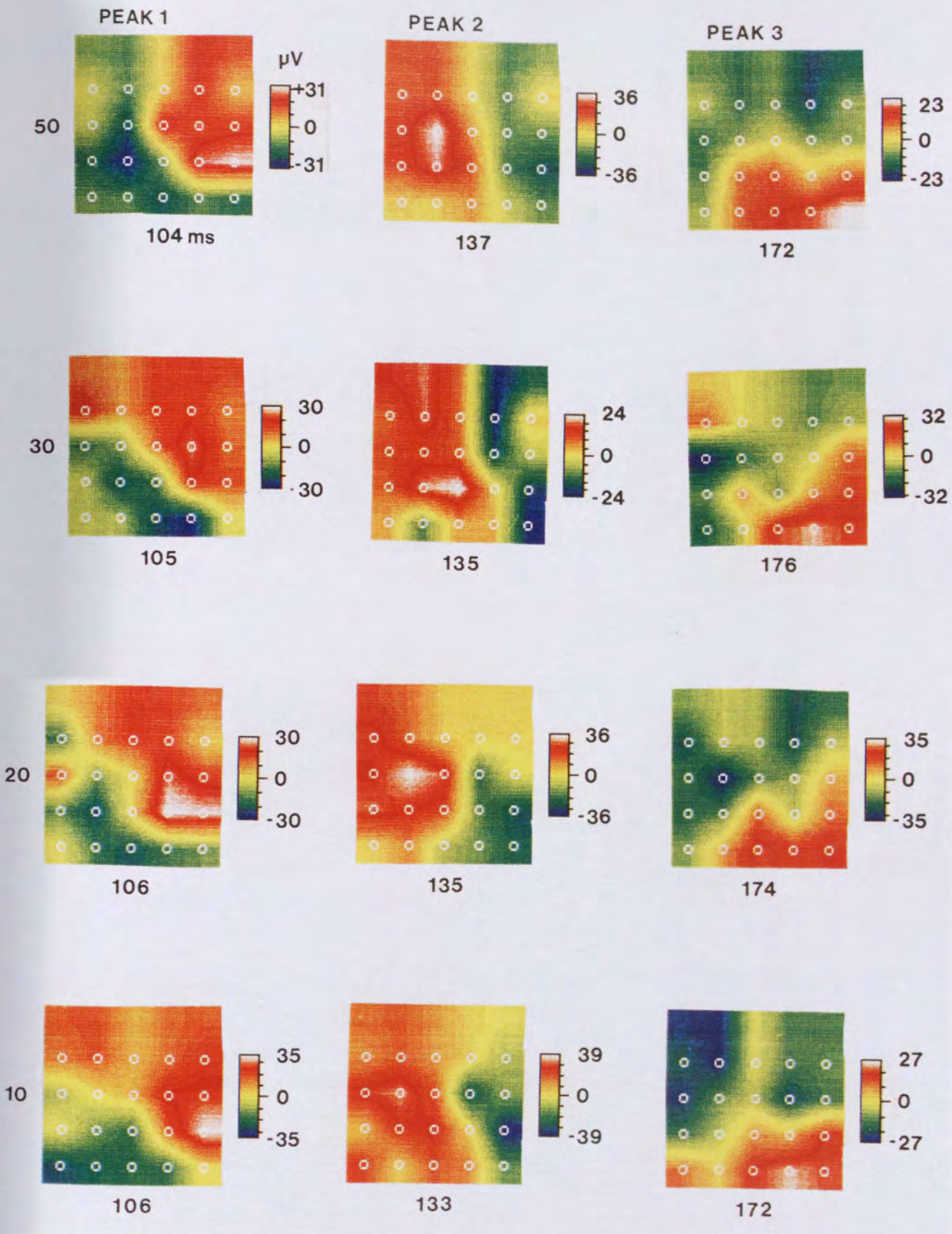

Figure 5.365 - The topographic distributions of the three most prominant waveform peaks following pattern onset for subject SC, recorded using 50, 30, 20 and 10 responses per average respectively.

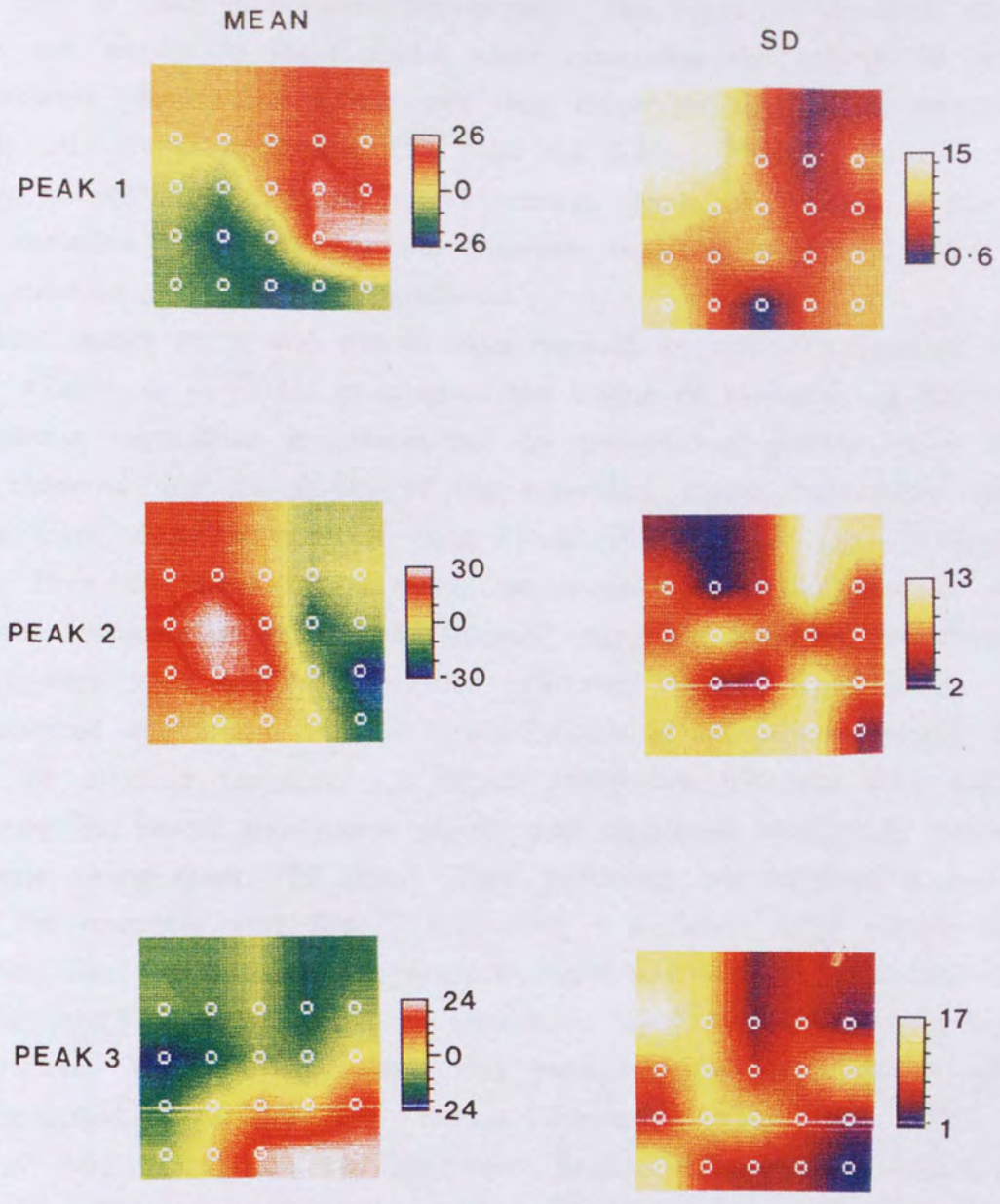

Figure 5.366 - Mean and standard deviation topographies of the full field data presented in figure 5.365.

while that of peak 3 is more widespread. The range of standard deviation values are similar to those found when examining the effects of repeated measurement (figure 5.432), but less than those for intersubject comparisons of full field responses (figures 6.81, 6.82 and 6.83). Hence, alterations in the number of responses included in the average (from 10 to 50), produces no more variation than that apparent between repeated recordings made with fixed stimulus and recording parameters.

Recent studies by several authors have reported the use of unaveraged VEMR data. Ahlfors et al (1992) investigated the effects of averaging in combination with source localization procedures for the multichannel pattern onset VEMR. They observed that the results of the equivalent dipole localisation did not change significantly when more than 15 to 20 responses per average were used. They also noted that a single, unaveraged 24 channel response gave a reasonable estimate of the source locations, using the minimum norm estimate method, even when the more common equivalent dipole routine failed. This was achieved due to the different susceptibilities of the two techniques to the effects of noise in the data. A similar observation has also been described previously by Sencaj and Aunon (1982) who examined localisation procedures on single sweep onset VEP data. They concluded that localisation was poor unless the responses were first filtered using a minimum mean square method. Following this, 70% of their data could be fitted with a single equivalent dipole, most of which showed orientations similar to those seen with averaged data. Single sweep MEG responses have also been used in the study of epilepsy migraine (Okada 1990) and focal ischemia following a stroke (Vieth 1990). The work of Sato (1990) and Sutherling and Barth (1990) on unaveraged, MEG recordings of spontaneous brain activity, provides a good example of how single sweep mapping can offer practical advantages over that of averaged data. The problem with localising epileptic foci from averaged responses is that the information obtained only indicates the 'centroid' of activity. If several single spikes are localised individually, and overlaid, the volume of abnormal activity can be defined, allowing more accurate surgical intervention.

Given the large signal to noise ratio found with the onset stimulus and the MEG technique, the use of unaveraged recording of evoked cortical responses could be useful for certain studies. The speed of recording could be beneficial when examining patients in whom prolonged fixation was not possible. These

might include accident victims, those with neurological disorders such as Alzheimers disease, young children and premature babies. This latter group would be promising as previous VEP studies have found that neonates produce the largest amplitude flash responses of any other age group (Shagass 1972). Ellingson (1964), also found identifiable evoked potentials to single flash stimuli in 50% of neonates, which he attributed to the low amount of background brain activity (Shagass 1972). Removing the requirement for signal averaging would also be beneficial in the studies of visual processing, since information is lost when consecutive responses are combined.

5.4 - TEMPORAL VARIABILITY.

Clinically, VEP abnormalities are often detected by comparing the latency and/or amplitude of a given waveform peak, with normative variation values calculated from a large population of 'normal' subjects. It is also important to quantify how the signal of interest varies temporally for a given subject.

Knowledge of such temporal variation can also be beneficial as it is becoming increasingly popular to monitor the progress of disease, and the effects of drug treatment by serial recording. Such studies involve the recording of data on different occasions, possibly in different locations and with different equipment. Serial studies have been reported previously for the monitoring of patients with multiple sclerosis (Cohn et al 1982), optic neuritis (Harding et al 1986) and Alzheimers disease (Harding et al 1981, Orwin et al 1986 and Wright et al 1984). Other studies have reported the effects of circadian variation on the evoked responses to flash (Were and Smith 1964), pattern reversal (Oken et al 1987, Lu and Safford 1989, Padhiar and Harding 1991), auditory brainstems (Marshall and Donchin 1981) and patterned electroretinograms (Bartel et al 1991). Factors which affect response reproducibility have also been characterised, such as the phase of the prestimulus alpha rhythm (Jansen and Brandt 1991); fatigue, stimulus artifacts, accommodation, pupil size, age, attention span and concentration (Lu and Safford 1989); habituation (Shagass 1972) and the changes in neuronal excitation and inhibition (Sencaj and Aunon 1982). Although the temporal reproducibility of the pattern onset VEMR has been mentioned previously (Kouijzer et al 1985, Ahlfors et al 1992), no systematic studies have been presented.

This study examines the intrasubject variation between consecutive, averaged onset VEMR responses, variation between occasions, the effects of refractive error, environmental shielding levels and equipment specificity.

5.41 - METHODS.

The recording protocols used are the same as those reported by Armstrong et al (1991) for the pattern reversal VEMR. In all cases, recordings were made on subject CD to a full field stimulus, with the probe positioned over the area of maximal outward flowing field for the CIIm component.

Ten consecutive recordings, of fifty averages each, were made, without movement of the subject. This obviated the need for repositioning of the probe, and the errors which this could introduce. Recordings were made at similar times in the morning and afternoon for five days.

The procedure was repeated with two separate BTi single channel magnetometer systems, the only common features between the two being the dewar, averager and stimulator. Repetitions were also made with one of the systems in an unshielded environment; in a room fitted with aluminium eddy current shielding (Vacuumschmelze); and again in the same room with an extra, single shell of mu-metal shielding (Vacuumschmelze).

Latencies and amplitudes of each peak were analysed by linear interpolation, to determine if there were any trends within each run of ten consecutive responses. The data were also analysed by analysis of variance (ANOVA) to partition the sources of variance. As the scalp probe position was optimal for recording the CIIm and CIIIm peaks, but not necessarily the CIm, this latter peak might be affected to a greater extent by noise.

5.42 - RESULTS AND IMPLICATIONS.

Figure 5.421 shows an averaged evoked onset waveform, below which there is a series of sixteen responses superimposed. These display greater consistency than the onset waveforms presented by Stok (1986) and Ahlfors et al (1992).

The latency of each group of ten consecutive CIIm responses recorded at each morning and afternoon session varied by between 0.8 and 3.8ms, while amplitudes varied by between 11.7 and 77.1fT. No consistent latency or amplitude differences were seen between recordings made in the morning or

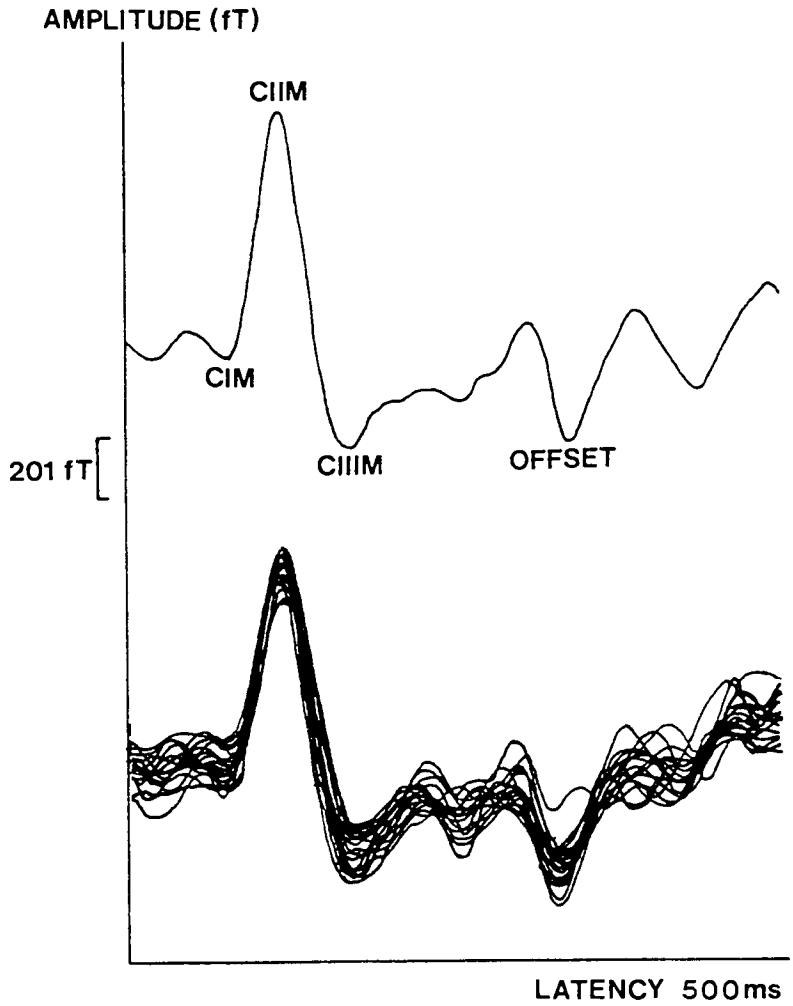

Figure 5.421 - A typical waveform of subject CD showing three onset peaks (CIm, CIIm and CIIIm) and an offset peak. Below are sixteen averaged waveforms, recorded from subject CD as two series of eight consecutive recordings, taken over a period of 48 hours.

afternoon. This compares favourably with the latency variation of between 8 and 11ms reported for the pattern reversal VEMR under similar conditions (Armstrong et al 1991). The CIIm peak latency was consistently less variable, and the amplitudes larger than those of the pattern reversal P100m (Armstrong et al 1991). They also reported that variation was greater in the afternoons, which was attributed to the effects of noise. The reduced latency variability of the onset response might be a product of the increased signal to noise ratio. This data also compares well with the findings of Cohn et al (1985), who reported an intersession latency variation of 10ms or more for the pattern reversal VEP.

Regression lines were fitted to the sets of ten consecutive responses in order to determine if any sequential trends were evident, as might result from fatigue or habituation. Significant fits were found in 32% of the data for latency and in 24% for amplitude. These were either linear or curvilinear, but a consistent pattern was not apparent. A greater proportion of significant fits were obtained for the double shielded environment. Hence, reduction in the environmental noise could have been sufficient to allow the detection of more subtle trends in successive responses than was previously possible. Although Armstrong et al (1991) could not detect any latency trends for the consecutive pattern reversal responses, this may be due to the lower amplitudes of their signals, and therefore poorer signal to noise ratio (Harding et al 1991). Significant trends within sequential recordings have been reported previously. Stoltz et al (1988) demonstrated that the pattern reversal VEP latency decreased during a recording session. Other flash VEP studies have dismissed the effects of fatigue, habituation or attention level on the latency of consecutive responses, (Werre and Smith 1964, Lueders et al 1980)

Table 5.422 shows the latency and amplitude variation for each onset peak for all conditions. Of the 218 averaged responses in which a CIm peak was present, 6 had positive amplitudes. This could have occured due to the effects of DC drifting (See section 4.3), hence these values were excluded from further analysis. By comparing the averaged latency values of table 5.422 II with those of the unaveraged responses in figure 5.333, it is apparent that all peaks show a later latency following averaging, which is consistent with the problems produced by the averaging process mentioned earlier (Brazier 1964).

Table 5.423 shows the results of the analysis of variance (ANOVA), for the CIIm peak in each recording situation. In all cases, more latency variation

CV = COEFFICIENT OF VARIANCE. n = NUMBER OF AVERAGED RESPONSES.

I : UNSHIELDED ENVIRONMENT. MAGNETOMETER SYSTEM A : 1unit = 5.0fT.

CIm	MEAN LATENCY	=	66.60	ms	±8.71	n = 64	CV = 13.07%
	MEAN AMPLITUDE	=	-9.93	units	±6.39	n = 64	CV = 64.41%
CIIm	MEAN LATENCY	=	113.06	ms	±2.60	n = 70	CV = 2.30%
	MEAN AMPLITUDE	=	+33.06	units	±7.78	n = 70	CV = 23.53%
CIIIm	MEAN LATENCY	=	174.21	ms	±13.38	n = 70	CV = 7.68%
	MEAN AMPLITUDE	=	-28.73	units	±9.29	n = 70	CV = 32.34%

II : UNSHIELDED ENVIRONMENT. MAGNETOMETER SYSTEM B : 1unit = 6.7fT.

CIm	MEAN LATENCY	=	77.00	ms	±6.00	n = 64	CV = 7.79%
	MEAN AMPLITUDE	=	-21.30	units	±9.02	n = 64	CV = 42.44%
CIIm	MEAN LATENCY	=	121.29	ms	±2.66	n = 100	CV = 2.19%
	MEAN AMPLITUDE	=	+58.67	units	±12.69	n = 100	CV = 21.63%
CIIIm	MEAN LATENCY	=	177.82	ms	±10.60	n = 96	CV = 5.96%
	MEAN AMPLITUDE	=	-52.37	units	±13.69	n = 96	CV = 26.15%

III : EDDY CURRENT SHIELDING. MAGNETOMETER SYSTEM B.

CIm	MEAN LATENCY	=	76.51	ms	±4.15	n = 32	CV = 5.42%
	MEAN AMPLITUDE	=	-37.30	units	±12.60	n = 32	CV = 33.78%
CIIm	MEAN LATENCY	=	123.72	ms	±2.06	n = 70	CV = 1.67%
	MEAN AMPLITUDE	=	+67.76	units	±8.23	n = 70	CV = 12.15%
CIIIm	MEAN LATENCY	=	183.42	ms	±6.56	n = 57	CV = 3.58%
	MEAN AMPLITUDE	=	-64.43	units	±10.64	n = 57	CV = 16.51%

IV : EDDY CURRENT AND MU-METAL SHIELDING. MAGNETOMETER SYSTEM B

CIm	MEAN LATENCY	=	75.67	ms	±4.05	n = 52	CV = 5.35%
	MEAN AMPLITUDE	=	-23.21	units	±6.47	n = 52	CV = 27.86%
CIIm	MEAN LATENCY	=	120.16	ms	±1.48	n = 100	CV = 1.23%
	MEAN AMPLITUDE	=	+66.85	units	±8.65	n = 100	CV = 12.95%
CIIIm	MEAN LATENCY	=	173.25	ms	±6.63	n = 99	CV = 3.82%
	MEAN AMPLITUDE	=	-65.51	units	±9.43	n = 99	CV = 14.40%

Figure 5.422 - Mean, standard deviation and coefficient of variance data for the latency and amplitude of the CIm, CIIm and CIIIm onset peaks. Results were recorded on two separate magnetometer systems (I and II); with system II in an eddy current shielded room (III); and condition III with the addition of mu-metal shielding.

TABLE 5.423 - Analysis of variance (ANOVA) for the latency and amplitude of the CIIm onset peak recorded in conditions I to IV, (as in Figure 5.422).

MIN	=	Variance between determinations. Minute to minute.
AM/PM	=	Variance between morning and afternoon, AM/PM.
DAYS	=	Variance between days.
I	=	Magnetometer A. Unshielded environment.
II	=	Magnetometer B. Unshielded environment.
III	=	Magnetometer B. Eddy current shielding.
IV	=	Magnetometer B. Eddy current and Mu-metal shielding.

CIIm LATENCY ANOVA

	I	II	III	IV
Mean latency (ms)	113.06	121.29	123.72	120.16
MIN	5.62	5.62	3.52*	1.42
AM/PM	1.55	0.85	0.54*	0.87
DAYS	-0.76	0.82	-0.18*	-0.03

* = not significant

CIIm AMPLITUDE ANOVA

	I	II	III	IV
Mean amplitude (units)	32.97	58.67	67.76	66.85
MIN	13.67	22.20	39.16	22.33
AM/PM	31.67	76.89	19.43	30.63
DAYS	24.49	82.88	17.46	30.59

occurs between determinations than from morning to afternoon. In most cases, variance between days is negligible. These findings are similar to those described for the pattern reversal VEMR, (Armstrong et al 1991), however in their case, the variance between days was more significant than that from morning to afternoon. A consequence of these results is that in order to record a representative response for a given subject with either stimulus, it would be more beneficial to record several responses in each session, than fewer responses spread over a period of days. The analysis of variance for the amplitude data varies according to which magnetometer or environment was studied, and so these results will be discussed separately in the following sections.

In order to establish if any correlations exist between the latencies and amplitudes of each component, these values were plotted, and regression lines fitted. Plots of the various comparisons are shown in figures 5.424 and 5.425. Significant positive correlations were found between the amplitudes ($p<0.001$) and latencies ($p<0.001$) for all components. The CIIm/CIIIm peak amplitudes (figure 5.425B) produce the closest linear correlation of all combinations. Interestingly, with the exception of one low amplitude response, in all 322 comparisons, the amplitude of the CIIIm peak is equal to or smaller than that of the preceding CIIm. This could indicate a link between the activity of the two peaks which, when combined with the similarities in topographic behaviour (chapter 6), could suggest a mutual generator. An origin from separate sources, showing a similar processing event but with close functional association, appears less likely. This could support the VEP pattern onset findings of Ossenblok and Spekreijse (1991). They used a similar check and field size to that used here, but analysed their topographic results by first defining the response according to its principal components, and then using source localisation to determine its origin. They concluded that the CI-CII-CIII period could be attributed to the temporal overlap of two equivalent dipolar sources. The first dominated the CI peak and the initial stages of the CII, while the second was active during the CII and then dominated the CIII. This might also provide evidence for a common origin between the magnetic and electrically recorded onset waveform peaks.

Figure 5.426 shows the latency/amplitude scatter plot for all of the full field averaged data, for each component within this section. Both latency and amplitude measures are more variable for the CIIIm peak than those of the

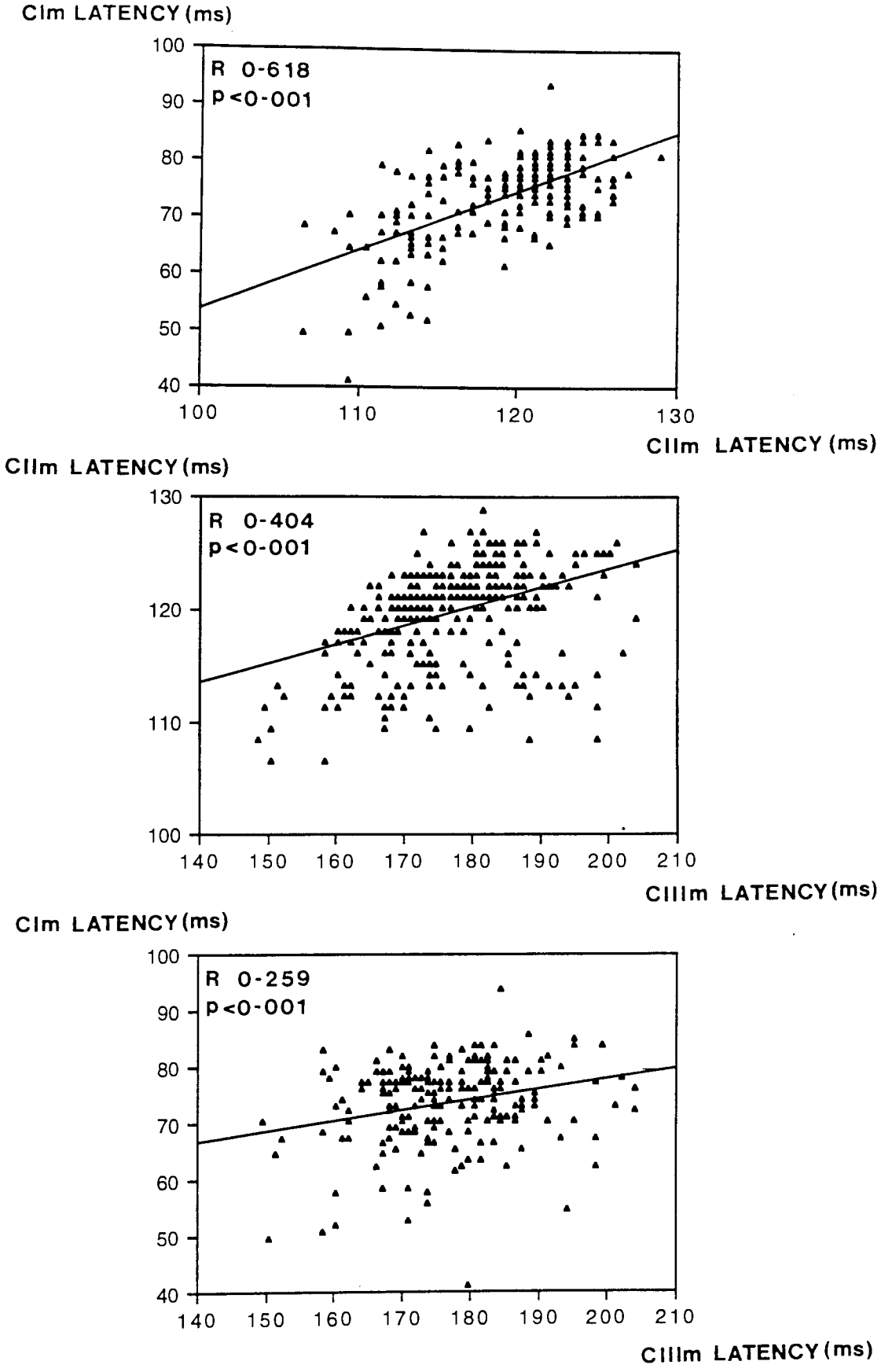

Figure 5.424 - Comparisons between the latencies of the three most prominant waveform peaks following pattern onset, for 250 averaged responses of subject CD. Regression lines are fitted to the data in each case, R indicating the goodness of fit and P its statistical significance.

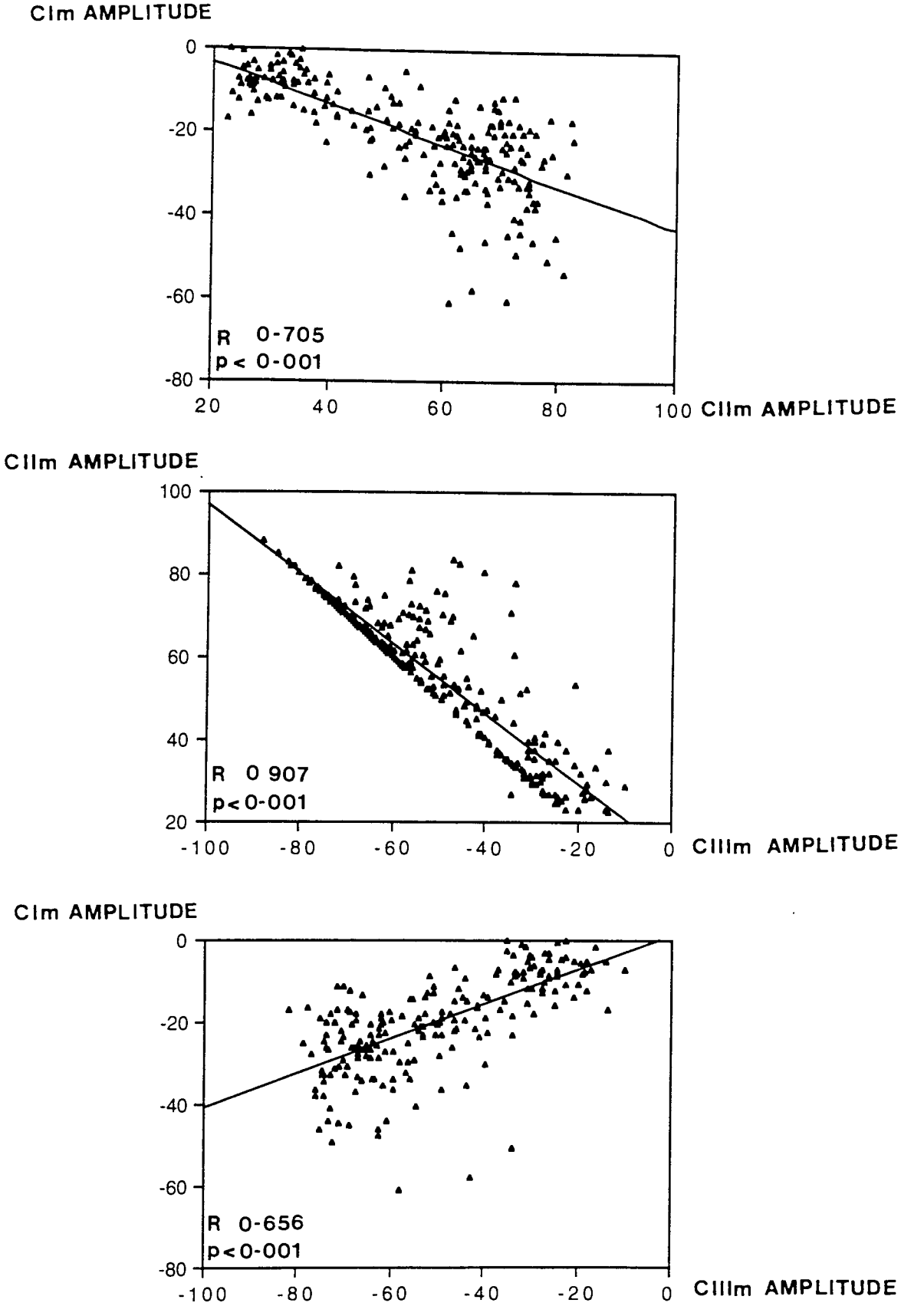

Figure 5.425 - Comparisons between the amplitudes of the three most prominant waveform peaks following pattern onset, for 250 averaged responses of subject CD. Regression lines are fitted to the data in each case. R indicating the goodness of fit and P its statistical significance.

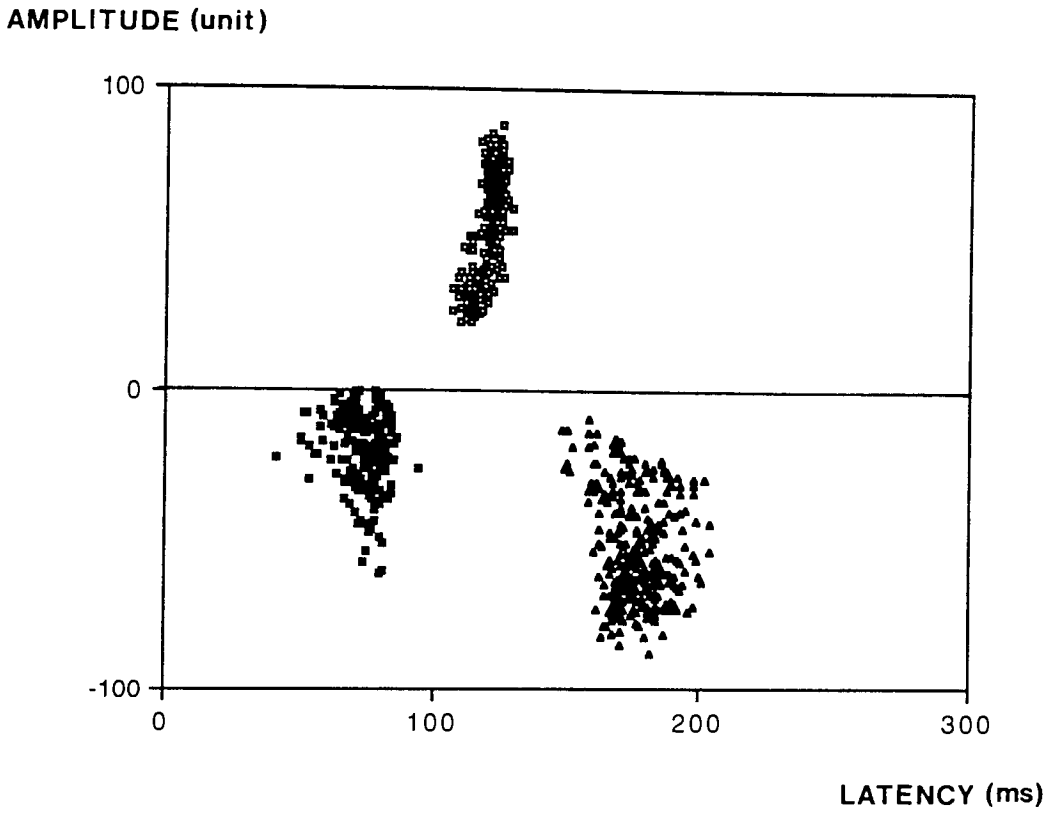

Figure 5.426 - Latency verses amplitude scatter plots for the three most prominant waveform peaks of subject CD following pattern onset. The data from 250 averaged responses recorded in three different levels of environmental shielding.

CIIm. Although the cluster size of the CIm appears to fall between those of the CIIm and CIIIm, its smaller sample size makes comparisons deceptive. Direct comparisons cannot be drawn with the unaveraged data of figure 5.332, due to differences in the amplitude scales. Also, the data depicted in figure 5.332 was recorded in a shielded environment, while the averaged data of figure 5.426 came from shielded and unshielded environments, therefore greater latency and amplitude variability is likely for the data of figure 5.426.

5.43 - TOPOGRAPHIC STABILITY.

Figure 5.431 shows the topographic distributions of the three major peaks, following full field pattern onset, for subject SC. Recordings were made on 26/5/90, 27/5/90, 9/3/91 and 3/10/91. Although variation in the location and shape of the field maxima is apparent, there are gross similarities in the positions of the inward and outward flowing field between occasions, for each of the three peaks. This is dispite variations resulting from the accuracy of marking the scalp, probe positioning (Hari et al 1988) and environmental noise fluctuations. Figure 5.432 shows the mean and standard deviation distribution for each peak of figure 5.431, the range of values being less than those seen with intersubject full field topographic comparisons (figures 6.8, 6.82 and 6.83). Over the four occasions, the standard deviation for the latency of each peak are ±5.19, ±5.19 and ±3.56ms while the average standard deviation for amplitude is 7.39, 6.99 and 5.21 per recording location respectively. Similar levels of topographic consistency have been reported by Harding et al (1991) for the two pattern reversal VEMR distributions, separated by two months, and by Stok (1986) for the pattern onset VEMR distributions separated by 17 months.

5.44 - EQUIPMENT SPECIFICITY.

The labelling of the two magnetometer systems as A and B (table 5.422), is equivalent to that used by Armstrong et al (1991). System B produced a CIm, CIIm and CIIIm latency which was on average 10.40, 8.23 and 3.61ms later than that of system A respectively. With the exception of the CIIIm peak therefore, this delay compares well to the 9.98ms delay seen for the pattern reversal P100m component (Armstrong et al 1991). System B also produced greater

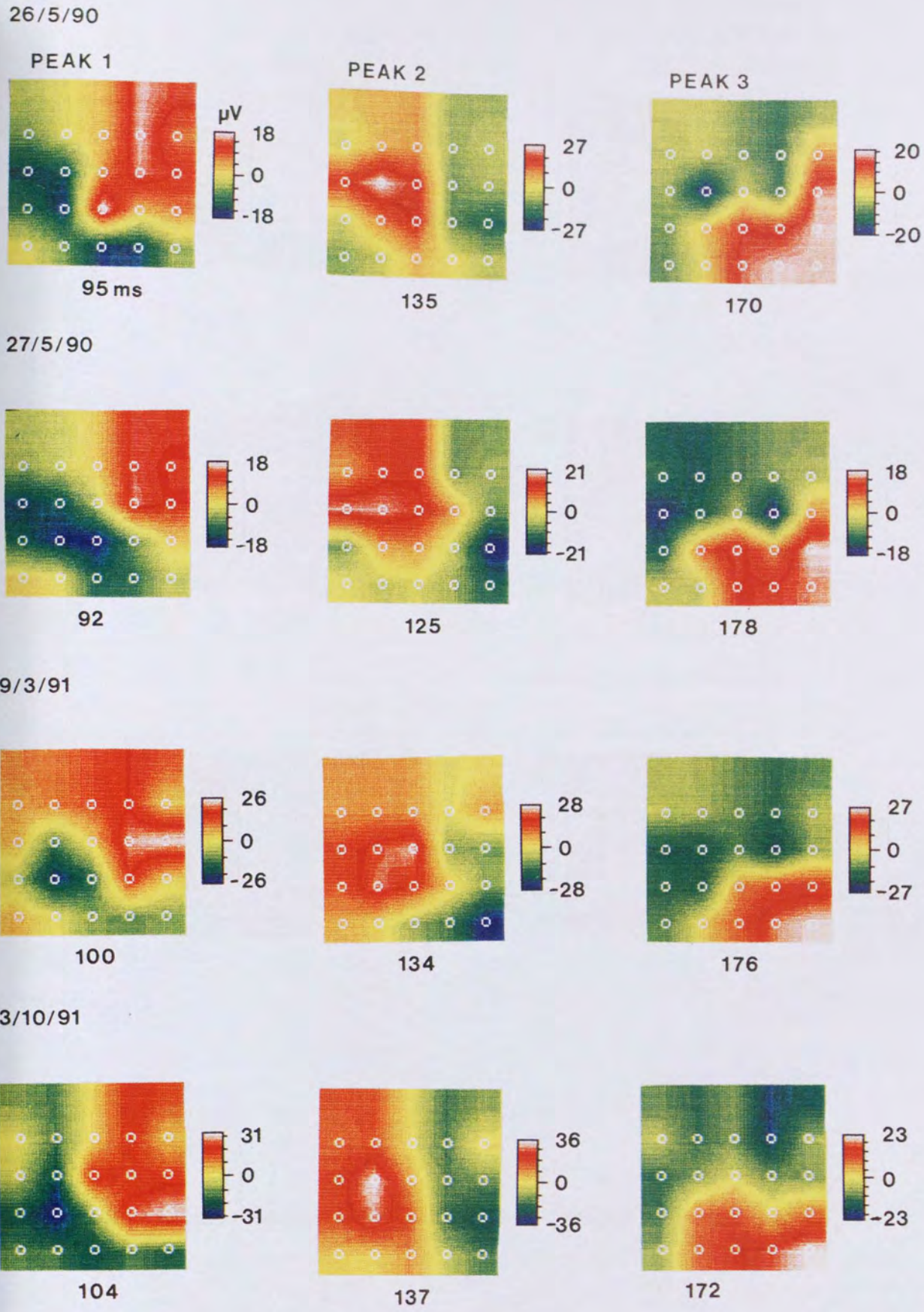

Figure 5.431 - Topographies of the three onset waveform peaks of subject SC, recorded on 26/5/90, 27/5/90, 9/3/91 and 3/10/91 respectively.

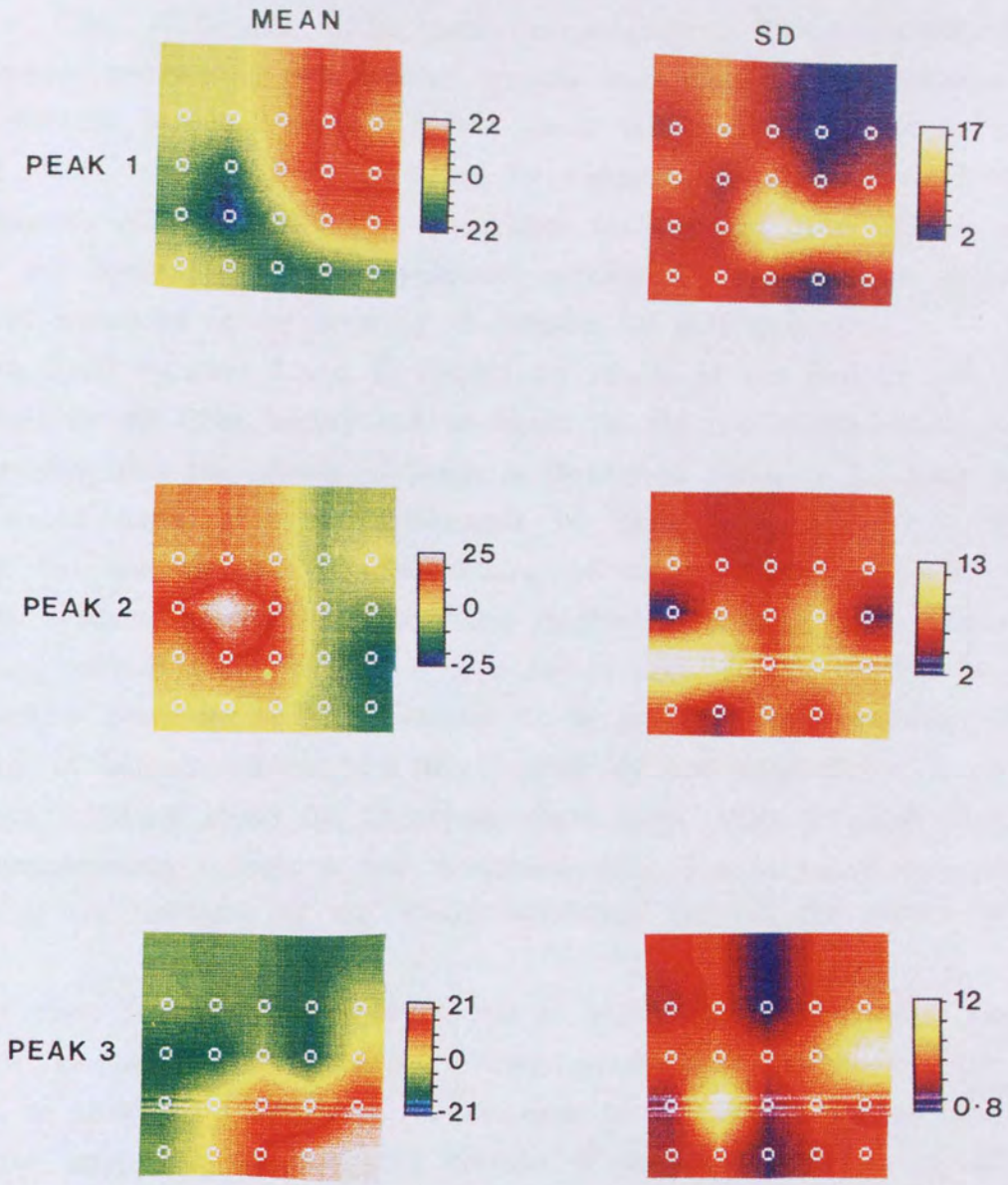

Figure 5.432 - Mean and standard deviation topographies for each peak of the data presented in figure 5.431.

amplitudes than those of A, showing an increase of 11.37, 25.61 and 35.70 units, for the CIm, CIIm and CIIIm peaks respectively. These differences are considerable considering two similar systems were used. By exchanging the filters between the two systems, it was found that they could account for the latency delay. This can be explained by variations in the tolerance of filter performance, which is known to vary more for analogue than digital systems (Skuse and Burke 1990). The amplitude variation is most likely to occur as a result of variations in the accuracy of balance for each system.

Table 5.423 columns I and II, display the results of the analysis of variance (ANOVA) on the CIIm latency and amplitude for the two magnetometer systems. It is evident that the latency variation is partitioned similarly for each system. This would imply that the differences in filter tolerance affect absolute latency but not variability. Partitioning of the amplitude variance differs between systems, system A shows most amplitude variation from morning to afternoon, while that of system B is from day to day. As the absolute amplitude also differs between the two systems, it is possible that variations in the accuracy of balance affects both their sensitivity and variability.

Figure 5.52A&B shows the latency/amplitude scatter plots for each component with magnetometer systems A and B respectively. The increased amplitudes of system B are indicated by the greater separation between the cluster of each peak.

This study indicates that if MEG data is to be transferred between different research groups, then calibration figures would also be needed for each system, to allow for comparisons. Conversions of this type would be less easily made for amplitudes than latencies because of the added problem of increased variability.

5.5 - SHIELDING EFFECTS.

The recording protocol used for the comparison between the two magnetometer systems was also used to study the effects of recording in three environments of different levels of shielding. Figure 5.51 shows the magnetic field attenuation (the ratio between the field strength of a source applied external to the room (Be) and that recorded internally (Bi)), for various signal frequencies. The trace labelled 1-SHELL refers to the eddy current shielding alone, while the 2-SHELL includes mu-metal shielding. The principles behind

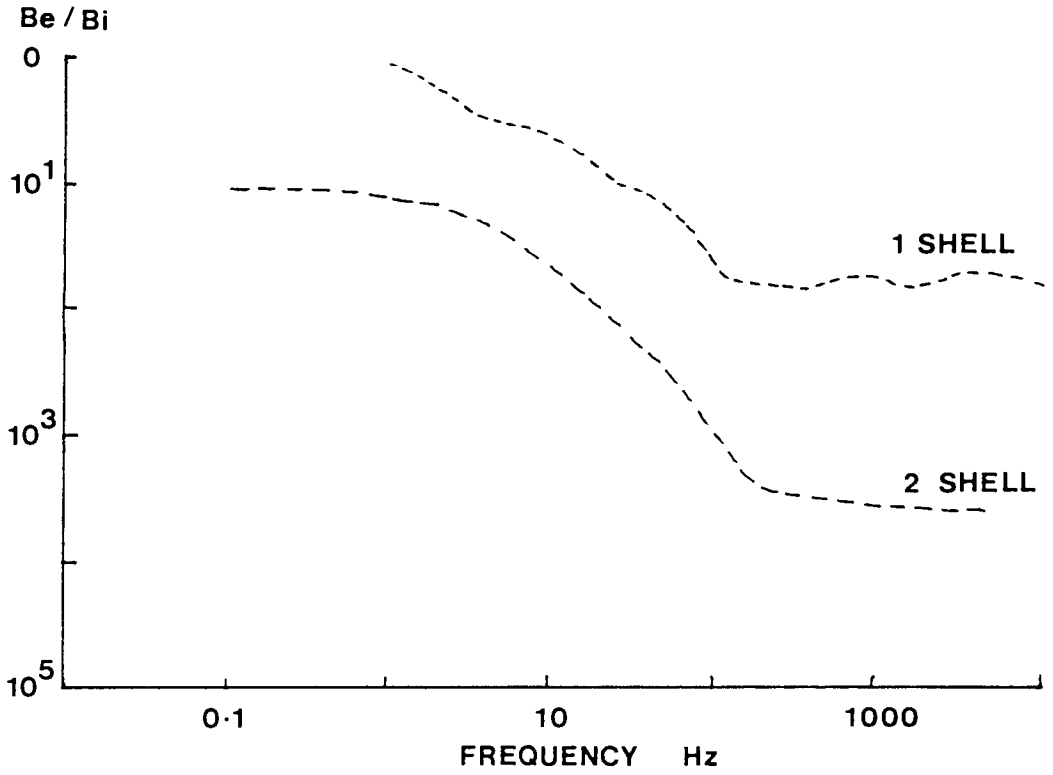

Figure 5.51 - Shielding effects of a room fitted with eddy current shielding (1 shell), and an eddy current/mu-metal shielded room (2 shell). Be/Bi indicates the magnetic field attenuation of a field applied externally to the room (Be), to that recorded within the room (Bi).

shielding and the effects of various shielding materials was discussed in chapter 1. It is apparent from figure 5.51 that the signal attenuation with the aluminium eddy current shield is frequency dependant, (Duret and Karp 1983), showing attenuation approximately proportional to the signal frequency from 1 to 100Hz. Mu-metal improves the attenuation throughout the frequency range, including frequencies below 1Hz. An attenuation of external noise of approximately 10 and 100,000 times is produced for frequencies below 10Hz and 1,000Hz for the double shielded condition. It is apparent from the values in table 5.422 II, III and IV, that as environmental shielding is introduced and increased, the mean latencies of all components remain relatively stable, while the amplitudes increase. There is also a progressive decrease in the standard deviation of all values, which shows that some of the variation between responses must be due to environmental noise. The greatest reduction in variation is achieved in the transition between the unshielded and single shielded environment, with a smaller improvement for the double shielding. The additional improvement in response stability obtained by introducing mu-metal shielding can be attributed both to an increase in noise attenuation and an extension of the frequency of attenuation below 1Hz. This would imply that the progressive increase of shielding provides diminishing returns. Hence, as the effects of environmental noise are reduced, other noise sources, such as those from the subject and equipment, have an increasingly dominant effect on response variability, until a minimum level of variation is attained.

Results from the analysis of variance, table 5.423, show that increasing the level of shielding does not affect the partitioning of variance for the latencies, although absolute levels of variance decrease. Changes do occur for amplitudes however, with most variation occurring between days in the unshielded environment, between runs with the single shielding and between mornings and afternoons with the double shielding. This implies that a study of this type would have to be performed after each change in the shielding characteristics of the room to evaluate the best recording approach.

The effect of shielding on the latency and amplitude variability of each peak is shown graphically by the latency/amplitude scatter plots of figure 5.52B and 5.53A&B. Figure 5.52B shows the data for the unshielded responses with magnetometer B, 5.53A is recorded with the same system in the single shielded room, while 5.53B is with the double shield. Increasing shielding clearly

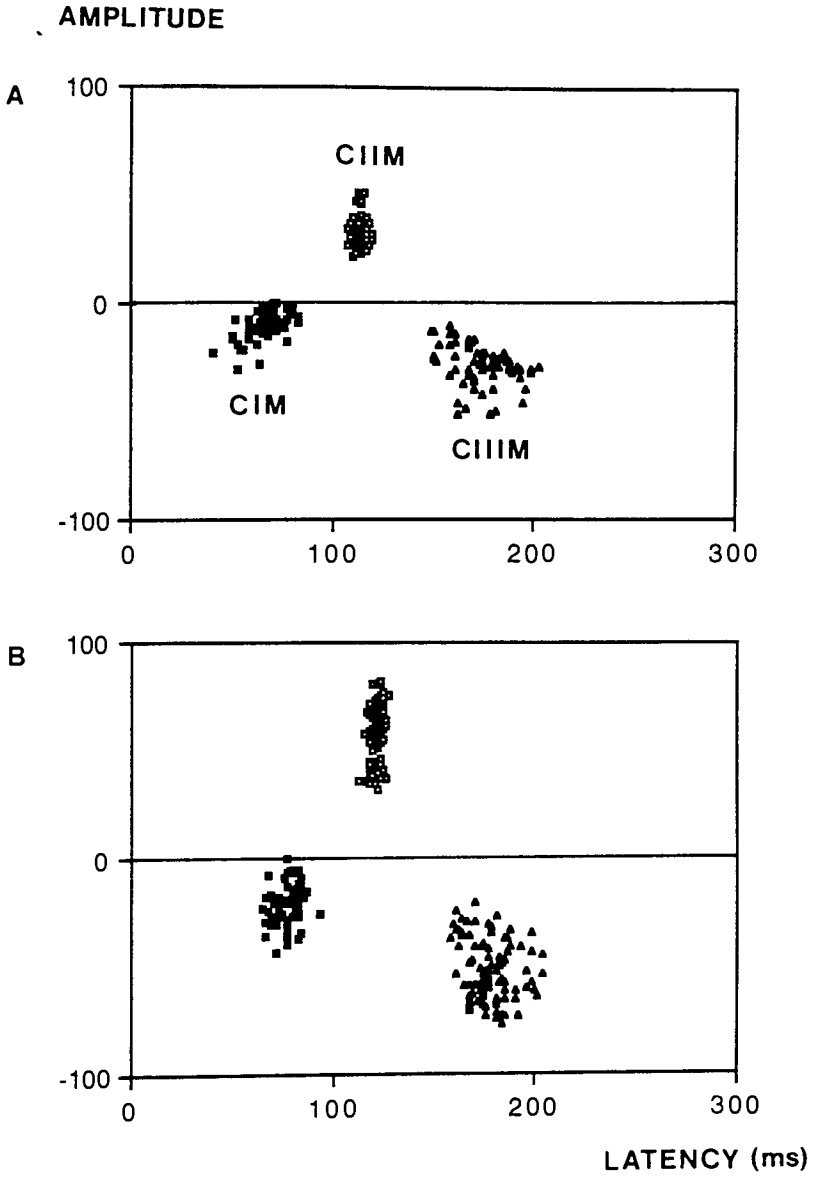

Figure 5.52 - Latency versus amplitude scatter plots for the three most dominant waveform peaks following pattern onset. The averaged responses of subject CD are shown, made with two different magnetometer systems, (**A** and **B**), in an unshielded environment.

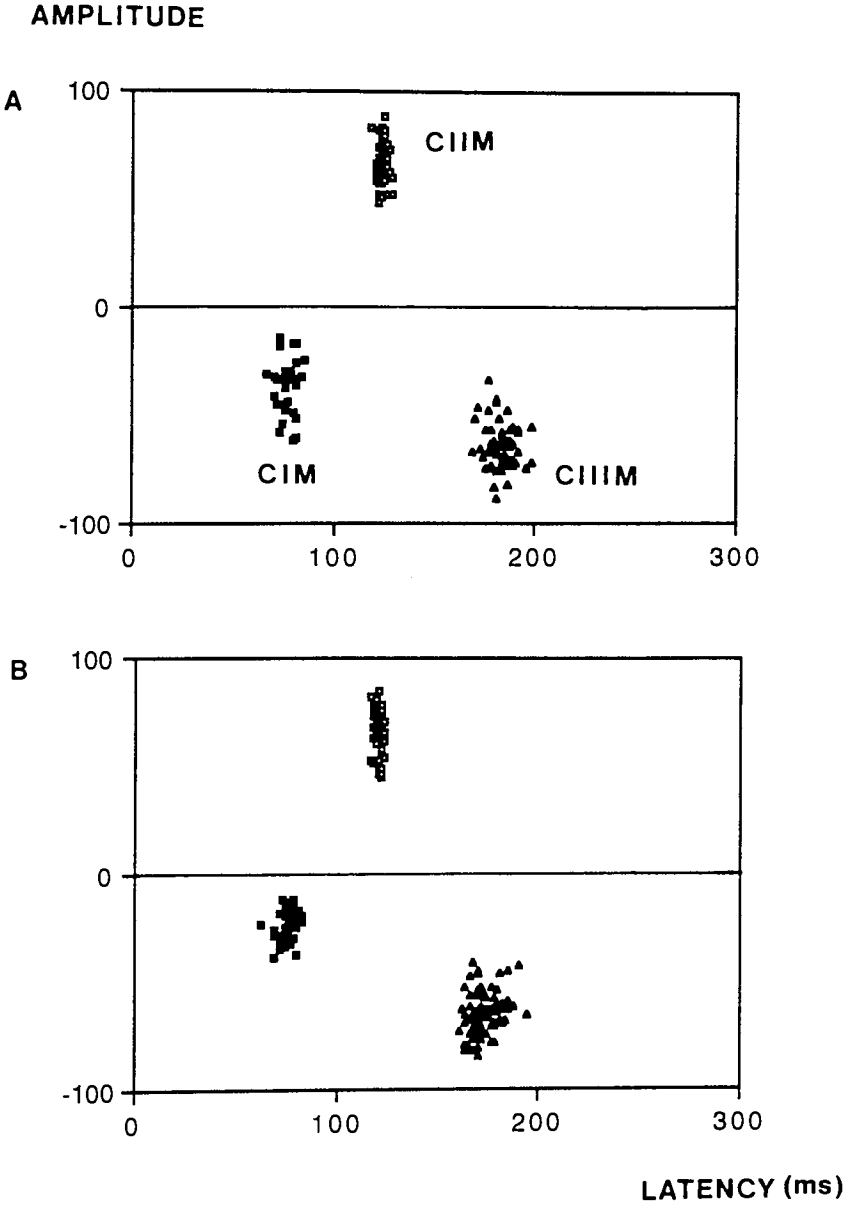

Figure 5.53 - Latency versus amplitude scatter plots for the three most dominant waveform peaks following pattern onset. The averaged responses of subject CD are shown, made magnetometer system B, in an eddy current shielded room (**A**), and an eddy current/mu-metal shielded room (**B**).

reduces variation. In addition, the separation between each component cluster increases with increasing shielding, reflecting the increases in absolute amplitude at each stage.

5.61 - INTERSUBJECT VARIABILITY.

Latency variation between subjects has been studied extensively for the VEP to flash (Kooi and Bagchi 1964, Werre and Smith 1964, Ciganek 1969, Buchsbaum et al 1974, Dustman et al 1977, Reilly et al 1977, Wright et al 1985, Harding and Wright 1986), pattern reversal (Stockard et al 1979, Snyder et al 1981, Cohn et al 1985, Wright et al 1985, Harding and Wright 1986, Stoltz et al 1988), flashed pattern (Cohn et al 1985) and pattern onset stimuli (Spekreijse et al 1973, Jeffreys 1977, Wright et al 1985, Harding and Wright 1986). Far fewer VEMR studies of this type have been reported (Harding et al 1991, Armstrong et al 1991), and these have been limited to pattern reversal and flash stimuli. Studies of this type are important clinically to establish the 'baseline' of normality in a given population, so allowing abnormal responses to be detected.

Further examinations have been made into the factors which could influence intersubject variation. These include the effects of age, sex, handedness, time of day and cardiac cycle (Shagass 1972). The method of stimulus presentation also has to be taken into consideration, as television based stimuli have been shown to increase intertrial variability, absolute latency and latency variation in comparison with optical systems (Stockard et al 1979).

5.62 - METHODS.

Most studies have measured the responses of at least ten subjects within each decade of life. In the present study, twenty subjects were investigated, ten in each of the 10 to 19 and 20 to 29 year age groups, with each group equally represented by males and females. As mentioned previously, a right half field stimulus of 38'x27' checks and 65% contrast was used due to its predictable intersubject topographic distribution (See section 6.3). Repeat recordings were taken until three similar responses were obtained, from which average latencies and amplitudes of each peak were calculated. In all cases, no more than three responses were required in total.

5.63 - RESULTS AND IMPLICATIONS.

Table 5.631 shows the latency, amplitude and standard deviation figures for each component, and for each decade of life. The CIm peaks were not consistent enough to identify with confidence, and so have been omitted from further analysis. No significant latency or amplitude differences exist between the age groups for any component. Although Harding et al (1986) and Wright et al (1985) reported that a pattern onset VEP waveform of normal morphology could not be obtained from the 10 to 19 year age group, this was not the case with the VEMR. Wright et al (1985) presented onset latencies for each VEP peak, to three check sizes and six age decades. Comparisons cannot be drawn with the VEMR responses however as different stimuli were used.

Comparison with the data from table 5.422 II suggests that the levels of inter- and intrasubject variation are similar for both the amplitude and latency of most components. It is apparent however that the absolute latency and amplitude values for the intrasubject study are greater than those seen between subjects. This might result from the difference in field size used in the two studies (full and half field), or it may be that the subject tested in the earlier experiment falls into the upper region of the normal latency and amplitude variation. No statistically significant differences were found between the responses of males and females for any component, with the subjects arranged in decade groups, or taken as a whole.

Past VEP studies have reported an increase in latency for all stimuli with increasing age (Kooi and Bagchi 1964, Wright et al 1985), while others have found no effect (Cohn et al 1985). Lueders et al (1980) reported an increased flash latency only in those subjects above the age of 50 years. For comparisons between the sexes, no differences were reported for the pattern reversal (Hammond et al 1987, Cohn et al 1985), or flashed pattern VEP latencies (Cohn et al 1985). Stokard et al (1979) and Snyder et al (1981) however did find shorter pattern reversal latencies in females.

Several reports have been published to suggest why age and sex might affect the VEP. Increases in latency with age have been attributed to demyelination of the optic nerve or tracts (Lueders et al 1980); reductions in retinal illumination due to decreases in pupil diameter (Wright et al 1985, Wright and Drasdo 1985); decreases in nerve conduction velocity and loss of central

TABLE 5.631 - Effects of age on the latency and amplitude of the CIm, CIIm, CIIIm and offset waveform peaks. The data for five males and five females is included in each decade.

AGE GROUP 10 TO 19.

	CIIm	CIIIm	OFFSET
LATENCY (ms)	107.29	155.44	148.61
	±4.43	±8.16	±22.79
AMPLITUDE (μV)	+33.03	-32.90	+32.90
	±17.34	±20.00	±20.00

AGE GROUP 19 TO 29.

	CIIm	CIIIm	OFFSET
LATENCY (ms)	103.67	150.65	142.38
	±7.22	±10.60	±8.02
AMPLITUDE (μV)	+27.52	-21.57	+30.53
	±15.58	±14.87	±12.92

neurones (Shagass 1972). Shagass (1972) also proposed that the increased amplitude seen with age could result from a shift in the natural excitatory/inhibitory processing of the brain towards excitation.

As regards the effect of sex, shorter latencies in females have been attributed to shorter visual pathways (Lueders et al 1980), although this explanation has been dismissed by Shagass (1972). Variations in gonadotrophic hormones (Buchsbaum et al 1974) and skull thickness (Dustman and Beck 1969) have also been dismissed.

Before the pattern onset VEMR could be considered for possible clinical applications, a more extensive age study would have to be performed to assess the extent of normal variation. The work of Armstrong et al (1991) for the pattern reversal VEMR has shown greater intersubject variability, especially in the elderly, than the corresponding VEP. This was attributed to the effects of noise, non optimal scalp recording locations, sensitivity to lack of attention or poor fixation and variation resulting from the examination of more select group of neurones. Increased variability of this type might not preclude the use of such a technique for clinical applications however. A high degree of intrinsic variation is only a problem if it obscures the abnormal response. The increased sensitivity of the VEMR to normal variation may be accompanied by an increased sensitivity to pathology, and possibly to conditions which cannot at present be distinguished by the VEP.

5.71 - EFFECTS OF CONTOUR CLARITY, (BLUR).

Components CII and CIII of the pattern onset VEP are known to be sensitive to the clarity of stimulus elements (James and Jeffreys 1975, Jeffreys 1977, Spekreijse et al 1977, Ermolaev and Kleinman 1983). The CI is thought to be less sensitive to such parameters, being instead contrast specific (James and Jeffreys 1975). The stability of the CI peak with blur is such that it does not disappear from the waveform until the checkerboard is blurred to the point of leaving only a uniformly illuminated field (Jeffreys 1977). Defocusing has been shown to increase the latency of the VEP pattern reversal P100 component, the extent of which increases with decreasing check size (McCormack and Marg 1973, Sokol and Moskowitz 1981, Tan et al 1984, Harding and Wright 1986, Bobak et al 1987). It has also been shown to cause a reduction in amplitude (Millodot and Riggs 1970, May and Cullen 1979, Snyder et al 1981,

Lovasik and Ahmedbhai 1985). Amplitude reductions of this type have also been recorded for the pattern onset VEP (Lovasik et al 1985). The mechanisms by which blurring of the stimulus affects response latency and amplitude have been considered by several authors, however the exact mechanism responsible is unclear. Harter and White (1968) dismissed the effects of accommodation, pupil size and the size of the image on the retina, in favour of a process of cellular lateral inhibition, which allows for the enhancement of neural activity on either side of the contour. Kulikowski (1977) attributed latency delay to the reduction in stimulus contrast. Sokol and Moskowitz (1981) examined the effects of blur on the separate component frequencies of the checkerboard, concluding that blurring of the fundamental spatial frequencies resulted in latency increases. Later, Bobak et al (1987) suggested that the higher harmonic frequencies also have an effect. The effect which contour sharpness has on the pattern onset VEMR is unclear, as there have been no reported studies.

5.72 - METHODS.

Single point recordings were made on four subjects to a full field stimulus. A full field was used to prevent errors in fixation which might occur with more focal stimuli, especially when blurred. A scalp recording position of maximal CIIm outward flowing field was chosen for each subject, as determined by prior topographic mapping. Two check sizes were used, 38'x27' and 19'x13' at a contrast of 65%. Recordings were made with ten dipotres of blur, from +5D to -5D. Three averaged responses for each condition were recorded until a consistent response was achieved. In each case, the initial recordings were made without blurring to check the accuracy of probe positioning, and following this recordings were made using a set sequence of lenses. The sequence was initially chosen at random but was then repeated throughout the experiment to maintain consistency. The lens surrounds and trial frame used were made of aluminium or plastic to prevent stimulus artifacts. Non cycloplegic conditions were used throughout.

The latency and amplitude data from each peak, for each check size and subject were plotted as a function of blur. Where a response could not be obtained after three repeat runs, data for that dioptre of blur was excluded.

In order to observe the effect refractive error has on topographic distribution, the full, left and right half field maps were recorded on subject AS with and without correction for a refractive error of 6/60.

5.73 - RESULTS AND IMPLICATIONS.

Figure 5.731 and 5.732 show the effects of blur on the onset VEMR waveforms of subject SC to 38'x27' checks and subject AS to 19'x13' checks respectively. In each case, the large positive peak within the first 200ms corresponds to the CIIm. It can be seen that with the larger check size (figure 5.731), the latency of the CIIm and CIIIm become progressively later with increasing positive or negative lens strength, while their amplitudes decrease. The CIm also seems to behave in a similar manner, however trends are less clear due to poor waveform morphology. With the smaller check size (figure 5.732), a similar trend is seen, although delays occur more rapidly, with no clear peaks apparent above ±3 dioptres.

Figures 5.733, 5.734, 5.735, 5.736, 5.737 and 5.738 show the effects of blur on the latency and amplitude of each component for each subject. The values of R provided for each graph relate to the goodness of fit of the polynomial curve to the data points, while the P value shows the level of statistical significance of that fit. Where the values of a particular distribution failed to reach significance at $p<0.05$, the graph was marked NS. In all cases, the data is best described by a second order polynomial. Of those which exhibit significant fits ($p<0.05$ to $p<0.001$), the majority show a 'U' shaped distribution with the point of inflection corresponding with a mean dioptre of -0.78, (absolute range from +1.5D to -3.5D). In all cases, latency is lengthened, and amplitude reduced with increasing blur. The mean value of -0.78D suggests that none of the subjects have a particularly significant refractive error, as the point of inflection should lie at the position of optimal refraction (Sokol and Moskowitz 1981). This principle has been applied in the use of the VEP as a means of computerised refraction (McCormack and Marg 1973) who were able to obtain an accuracy of ±2.5 dioptres of blur.

Several of the distributions show an asymmetric 'U' shape, consistent with accommodation occurring with negative lenses. This could be explained by the non cycloplegic state of the subjects (Sokol and Moskowitz 1981). Having said that, McCormak and Marg (1973) and Bobak et al (1987) reported that the

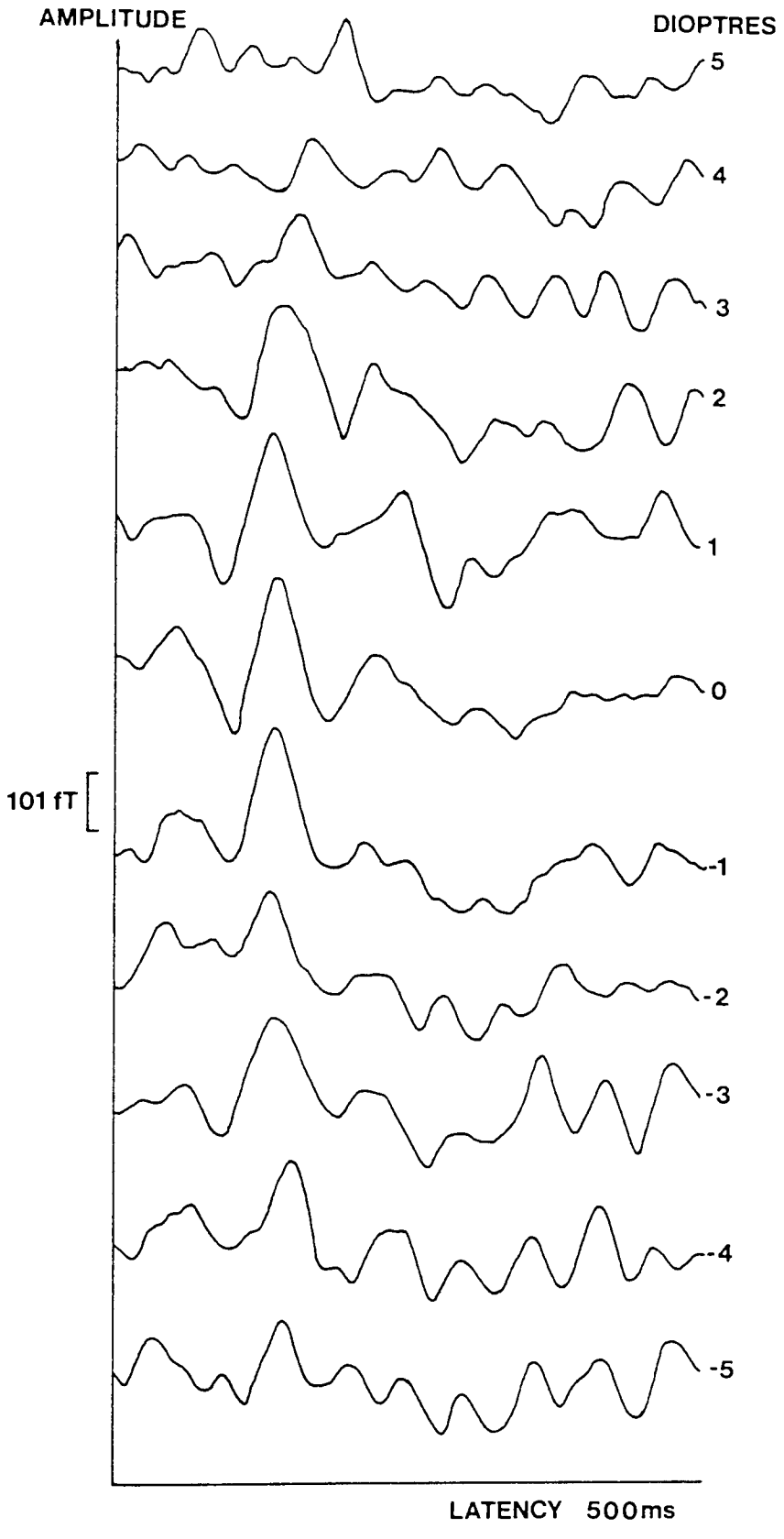

Figure 5.731 - Effects of optical blur (±5 dioptres) on the onset response waveforms of subject SC to a check size of 38' x 27'.

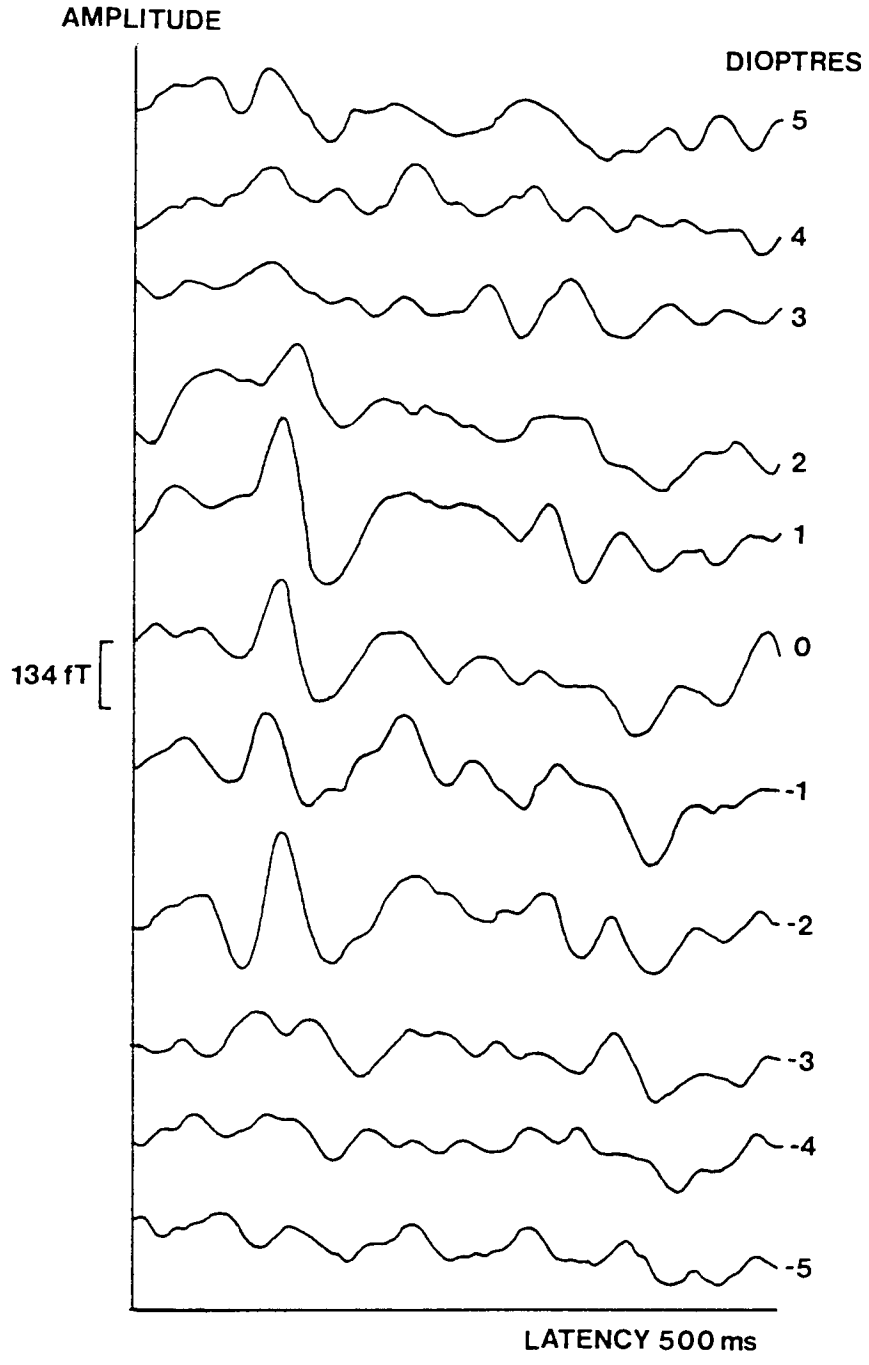

Figure 5.732 - Effects of optical blur (±5 dioptres) on the onset response waveforms of subject AS to a check size of 19' x 13'.

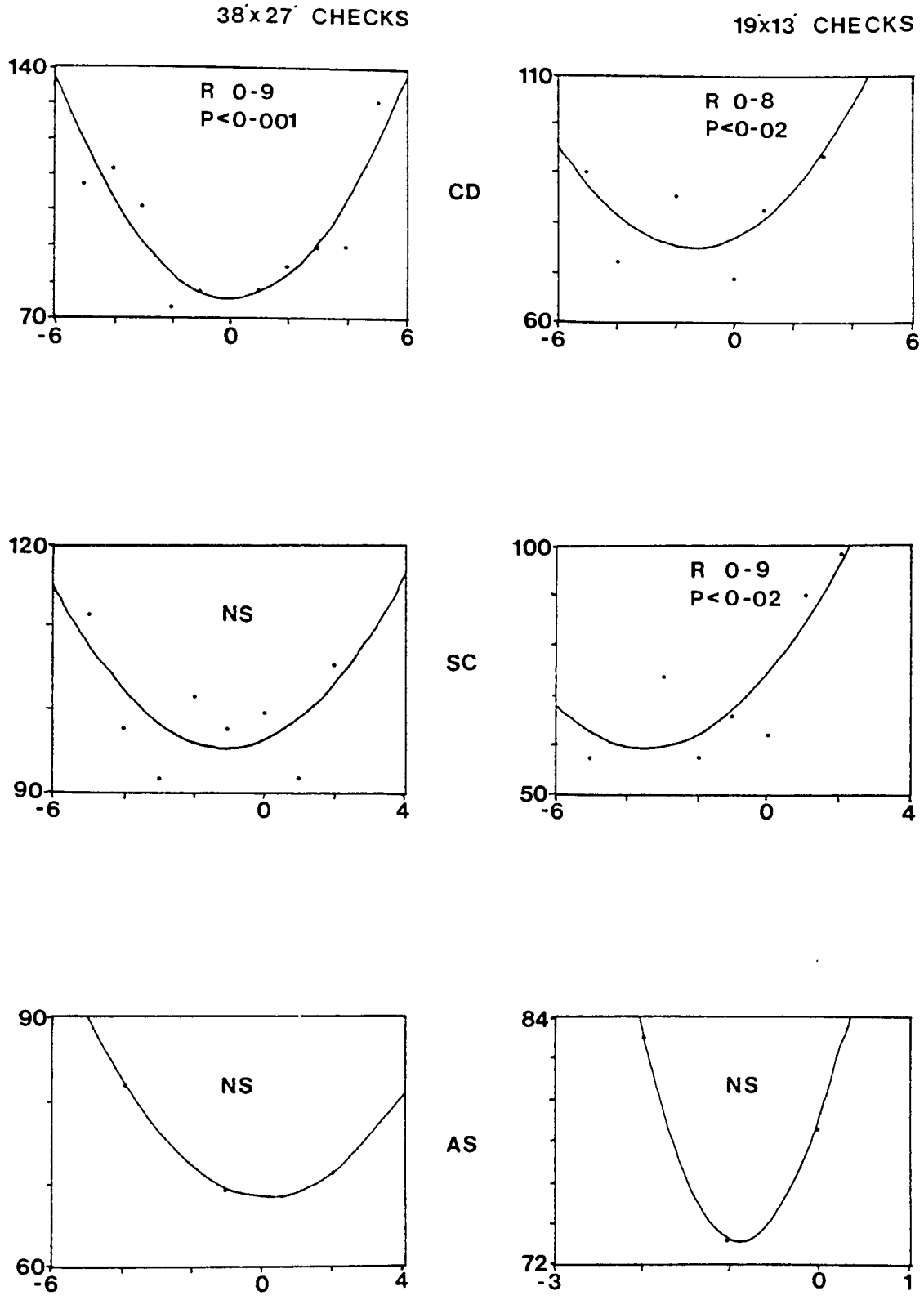

Figure 5.733 - Effects of optical blur (±5 dioptres) on the latency of the CIm component of subjects CD, SC and AS to checks of 38' x 27' and 19' x 13'. Second order polynomials are fitted to each data set, R and P values showing the goodness of fit and statistical significance in each case. NS - not significant. In each case, refractive error (dioptres) is shown along the horizontal axis, while latency (ms) is shown vertically.

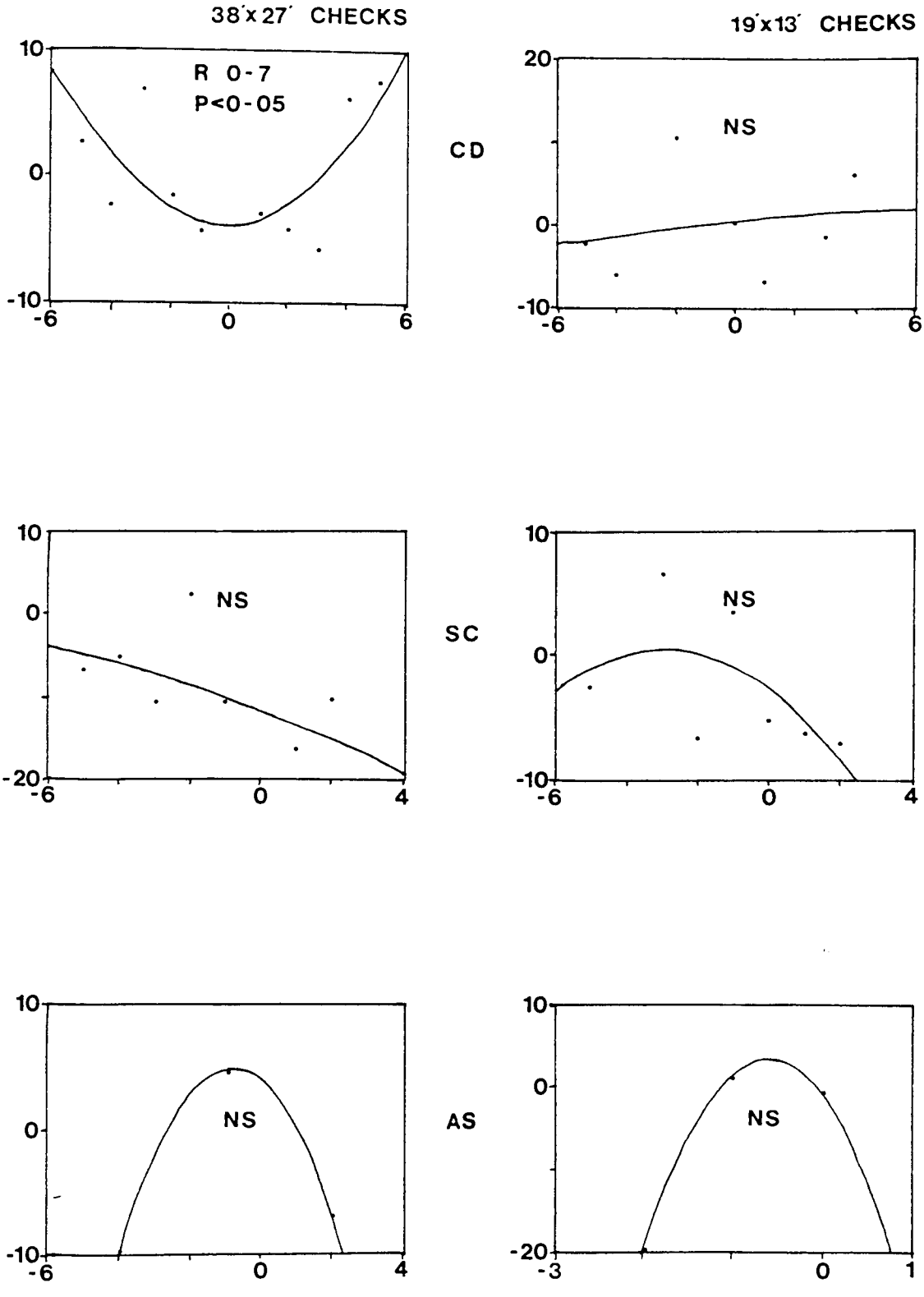

Figure 5.734 - Effects of optical blur (±5 dioptres) on the amplitude of the CIm component of subjects CD, SC and AS to checks of 38' x 27' and 19' x 13'. Second order polynomials are fitted to each data set, R and P values showing the goodness of fit and statistical significance in each case. NS - not significant. In each case, refractive error (dioptres) is shown along the horizontal axis, while amplitude (μV) is shown vertically.

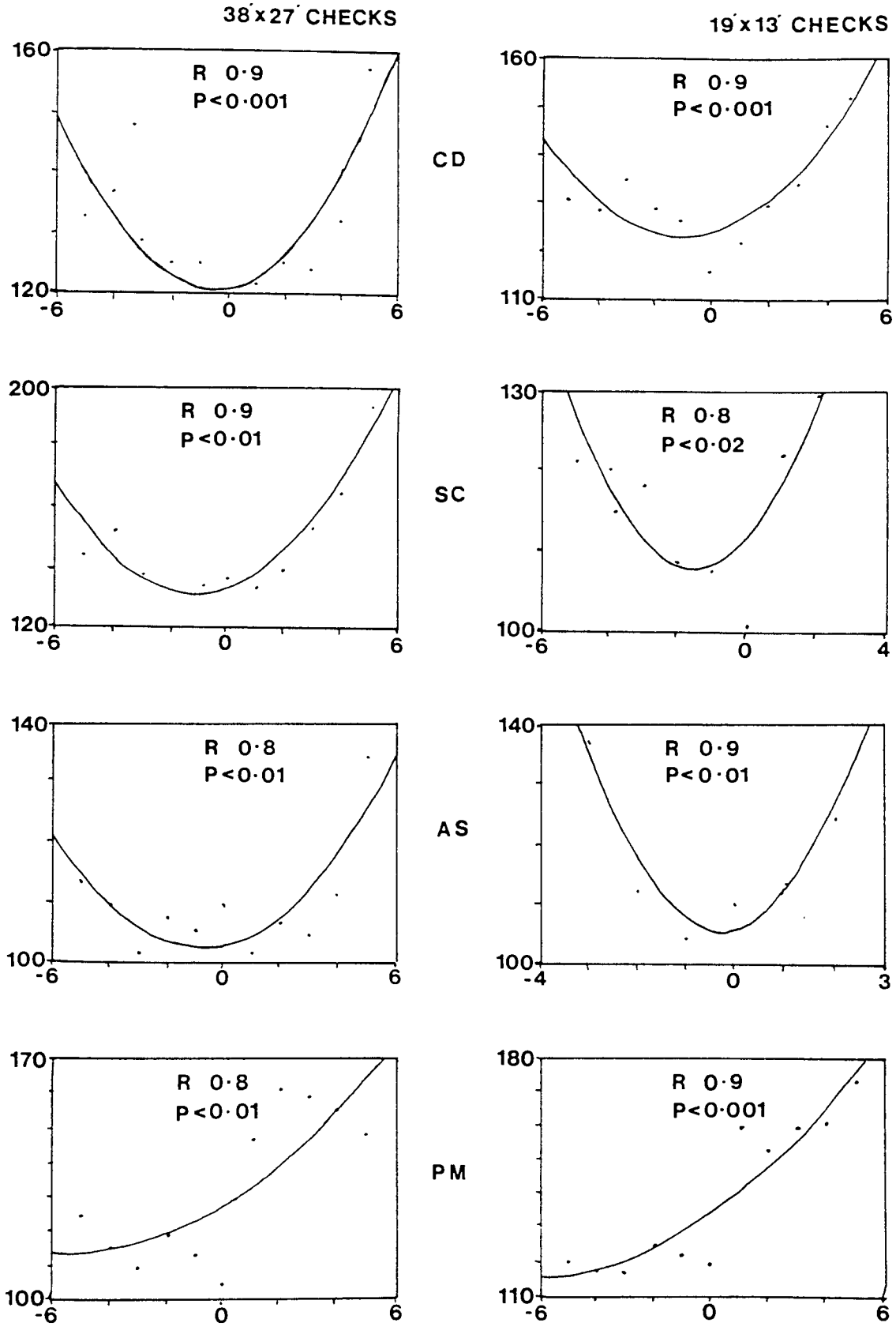

Figure 5.735 - Effects of optical blur (±5 dioptres) on the latency of the CIIm component of subjects CD, SC, AS and PM to checks of 38' x 27' and 19' x 13'. Second order polynomials are fitted to each data set, R and P values showing the goodness of fit and statistical significance in each case. NS - not significant. In each case, refractive error (dioptres) is shown along the horizontal axis, while latency (ms) is shown vertically.

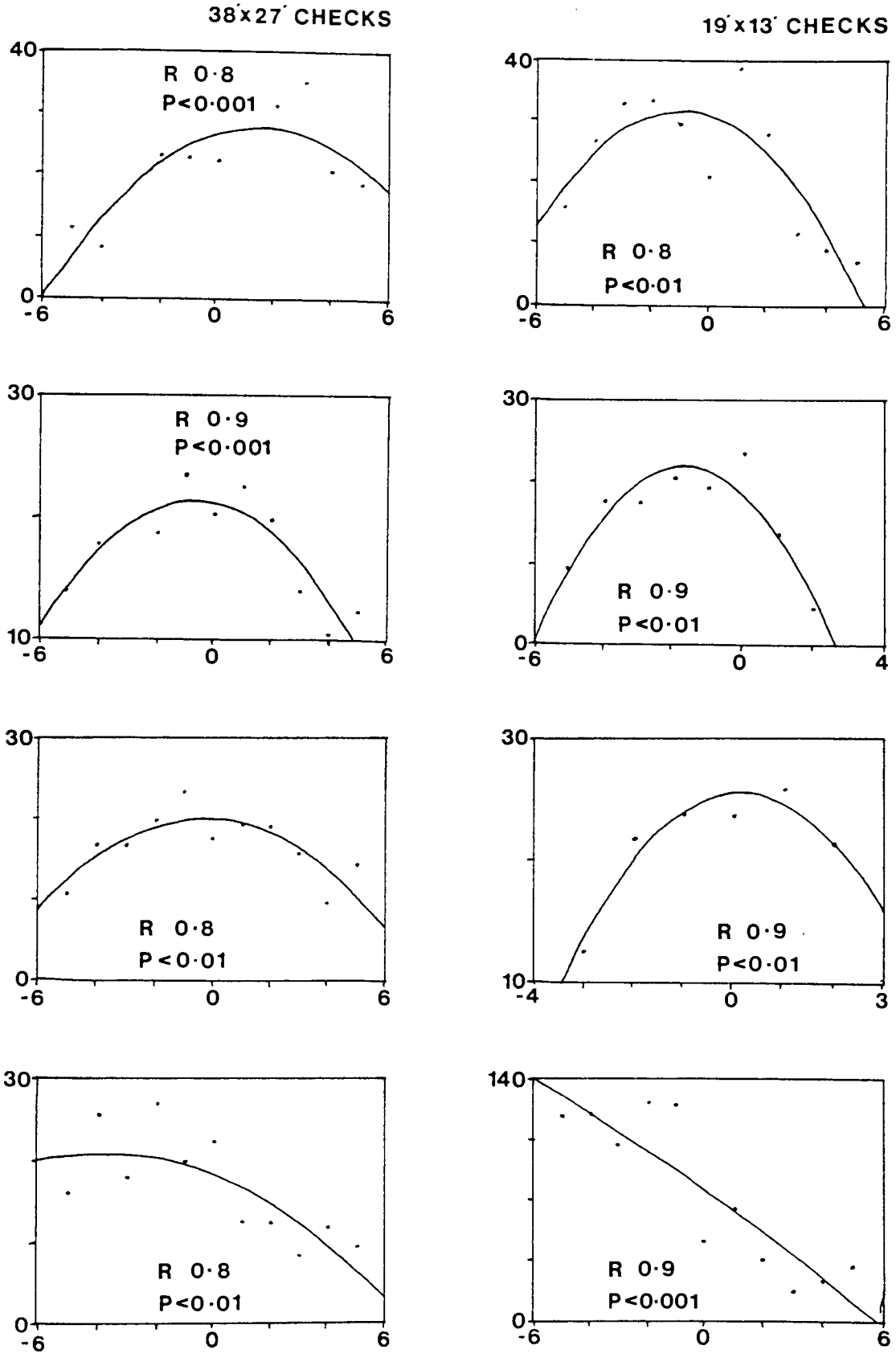

Figure 5.736 - Effects of optical blur (±5 dioptres) on the amplitude of the CIIm component of subjects CD, SC, AS and PM to checks of 38' x 27' and 19' x 13'. Second order polynomials are fitted to each data set, R and P values showing the goodness of fit and statistical significance in each case. NS - not significant. In each case, refractive error (dioptres) is shown along the horizontal axis, while amplitude (μV) is shown vertically.

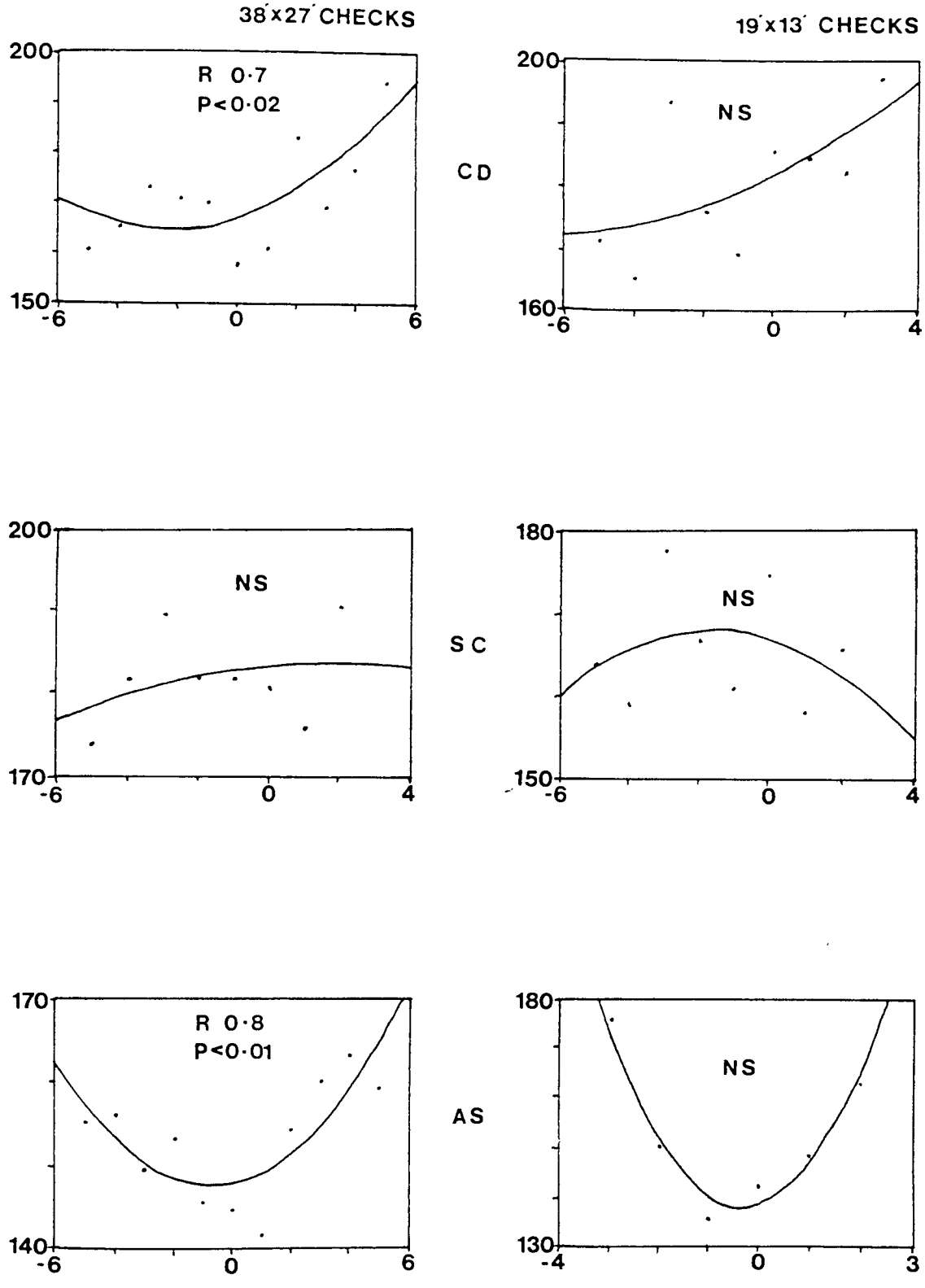

Figure 5.737 - Effects of optical blur (±5 dioptres) on the latency of the CIIIm component of subjects CD, SC and AS to checks of 38' x 27' and 19' x 13'. Second order polynomials are fitted to each data set, R and P values showing the goodness of fit and statistical significance in each case. NS - not significant. In each case, refractive error (dioptres) is shown along the horizontal axis, while latency (ms) is shown vertically.

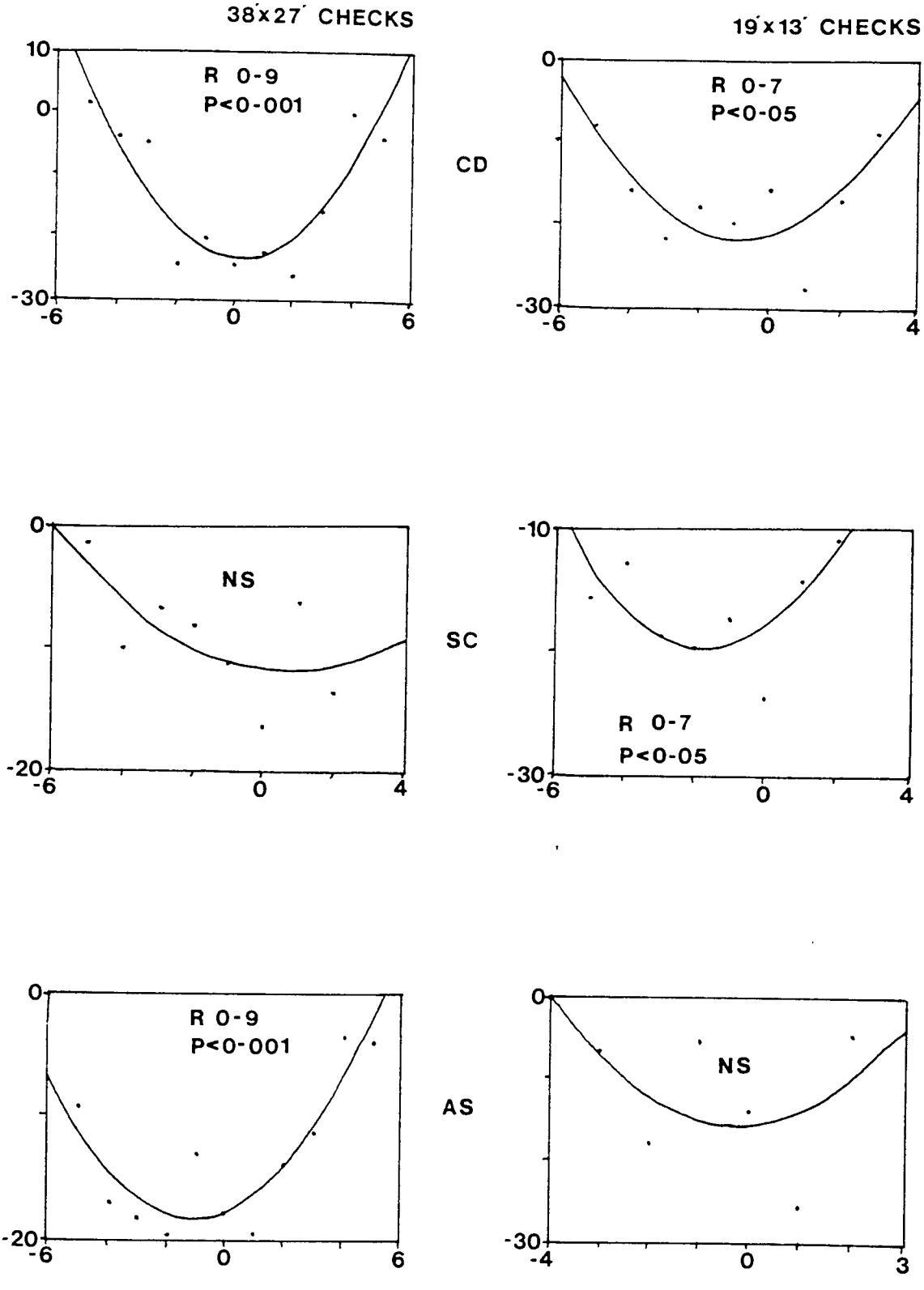

Figure 5.738 - Effects of optical blur (±5 dioptres) on the amplitude of the CIIIm component of subjects CD, SC and AS to checks of 38' x 27' and 19' x 13'. Second order polynomials are fitted to each data set, R and P values showing the goodness of fit and statistical significance in each case. NS - not significant. In each case, refractive error (dioptres) is shown along the horizontal axis, while amplitude (μV) is shown vertically.

VEP latency is less affected by negative blur than positive with or without cycloplegia, depending on the subject.

As mentioned previously, for most subjects, the increase in latency and decrease in amplitude with blur is more severe for the smaller check size. This is consistent with the observations for the pattern onset VEP (Jeffreys 1977, Spekreijse et al 1977, Harding and Wright 1986) and for the flashed pattern VEP (Harter and White 1968). Such behaviour would be consistent with a contour spectific mechanism for the generators of the CIIm and CIIIm sources (Spekreijse et al 1973).

The work of Harding and Wright (1986) on the effects of blur on the pattern onset and reversal VEP, indicate that the latency of the onset CII component is more sensitive to blur than that of the reversal P100. Their results showed that for 14' checks, under cycloplegic conditions, ±5 dipotres of blur resulted in a latency delay of 72ms for the CII and 27.4ms for the P100. For the CIIm to 19'x13' checks, +5 dioptres of blur produce an average latency delay of 45.9ms (maximum = 53.7ms), with -5 dioptres giving a mean delay of 12.04ms (maximum 20.5ms). 38'x27' checks cause a mean delay of 40.4ms (maximum 56.6ms) and 16.36ms (maximum 33.69ms) for +5 and -5 dioptres of blur respectively. This would suggest that the onset VEMR is less sensitive to refractive error than the VEP, possibly indicating a difference between the CIIm and CIIIm components with regards contour specificity. Alternatively, differences in intrinsic variability between the two techniques could act to mask the effects of alterations in stimulus parameters.

Figure 5.739 shows the CIIm topography of subject AS to each of the three field types, with and without correction for a visual acuity of 6/60. Also shown are the standard deviation (SD) and coefficient of variance (CV) distributions (See section 4.3), calculated for each field type, by comparing the responses before and after optical correction. Following refraction, amplitude increases by a factor of between two and three, while latencies decrease for the half fields, but increase slightly for the full field. For the full field response, an area of inward and outward flowing field is present to the right and left of the midline respectively, both before and after refraction. Blur produces a spreading of the field maxima, particularly the outward flowing field, as shown in by the SD and CV topographies. Similarities can also be seen for the half field responses recorded before and after refraction, with blur again producing a more diffuse distribution. Additional field areas appear following

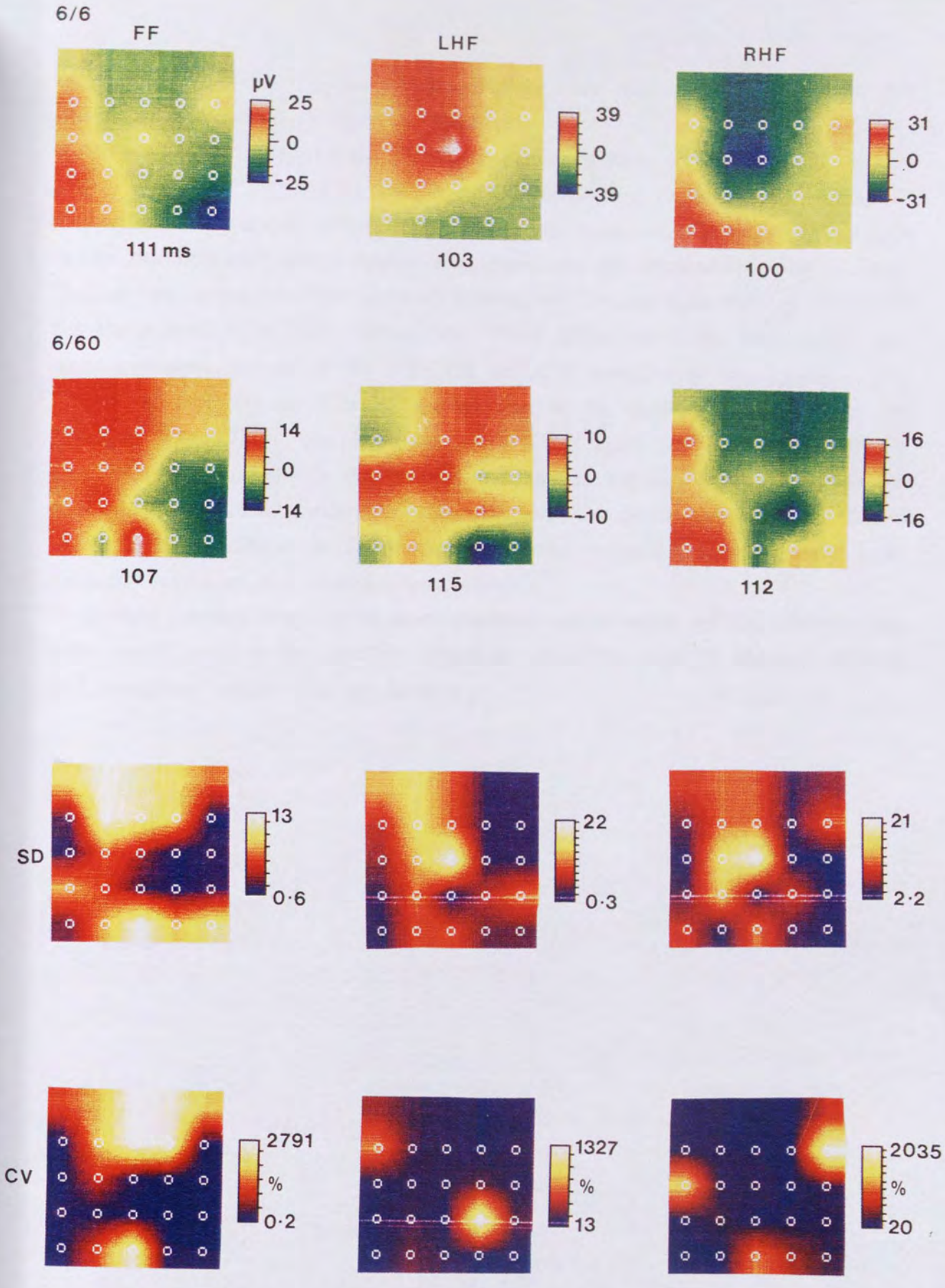

Figure 5.739 - CIIm topography of subject AS to a full field (FF), left (LHF) and right half field (RHF) stimulus, recorded before and after optical correction for a refractive error of 6/60. Below is shown the standard deviation (SD) and coefficient of variance (CV) distributions for the comparison of the topographies recorded before and after optical correction.

blurring, as identified by the CV distributions, and these might result from the effects of a reduction in signal to noise ratio.

This study shows that both the latency and amplitude of the onset CIIm and CIIIm peaks are affected by the degree of defocusing of the pattern stimulus. The effects with small checks are greater than those with large, to the extent where the response can disappear altogether with ±3 dioptres of blur. These findings are consistent with those of Jeffreys (1977) and Spekreijse et al (1977) for the pattern onset VEP. Hence, the VEMR CIIm and CIIIm components may have analogous sources to the VEP CII and CIII components respectively. The effects of blur on the CIm is unclear due to its unreliable presence in the averaged waveform. The waveforms shown in figure 5.731 suggest that the CIm latency and amplitude may behave in a similar way to that of the CIIm and CIIIm. If true, this would be inconsistent with an origin analogous to that of the VEP CI (Jeffreys 1977), however its poor definition in the majority of subjects precludes any definite conclusions.

If this stimulus were to be used clinically, or to study normal distributions, care would have to be taken to minimise refractive error if absolute latency and amplitude values were of interest.

CHAPTER 6

TOPOGRAPHY OF THE FULL AND HALF FIELD RESPONSE.

The process by which the location of the stimulus field on the retina influences the area of occipital cortex stimulated was discussed in chapter 3. These projections have been simplified into the cruciform model (Jeffreys and Axford 1972 a), and although it does not take into account any inter- and intrasubject variation in brain morphology, it has proved to be useful when applied to the VEP and VEMR data of previous authors. The VEP to full and hemifield stimulation, using a pattern reversal and/or onset stimulus has been mentioned by several authors previously (Estevez and Spekreijse 1974, Shagass et al 1976, Lesevre and Joseph 1979, Skrandies et al 1980). Pattern reversal stimuli presented full field have proved beneficial for the localisation of pre-chiasmal lesions, while half fields are better suited for post-chiasmal lesions (Blumhardt 1987).

The objectives of most VEMR studies have been to localise component generators (Richer et al 1983, Kouijzer et al 1985, Stok 1986, Spekreijse 1991 and Ahlfors 1992). To achieve this, half or smaller octant field stimuli have been employed, so as to activate specific neuronal populations, with no reference made to the effects of full field stimulation. These studies have also used small subject numbers, usually between two and four, possibly due to the recording protocols which are required to improve signal to noise ratios and increase the statistical accuracy of the dipole fitting algorithms. These requirements include dense arrays of mapping positions and large numbers of averages per point, (Romani and Leoni 1984, Hari et al 1988), both of which are time consuming using a single channel magnetometer.

The VEMR to a sinusoidal grating stimulus has been studied to full field presentation (Brenner et al 1981, Aine et al 1990). The checkerboard onset has been studied to half field (Stok et al 1985, Kouijzer et al 1985, Stok 1986), and to quadrant fields (Ahlfors et al 1992); while the flashed checkerboard pattern has also been studied half field (Richer et al 1982, Stok 1986). Of these studies, the stimulus parameters used by Stok (1986) are the closest to those used in the present study. However, in his study observations were made on two subjects only for right half field stimulation and four to the left half field.

Richer et al (1982) produced a more extensive study, with four subjects to left and right half field stimulation. However, the flashed pattern used differed from a true pattern onset stimulus as it is thought to elicit a pattern onset, offset and flash response simultaneously (Jeffreys 1977, Stok 1986). Neither of these authors compared the topography of full and half field response on a large number of subjects. In addition, little information is available about the behaviour of the pattern offset VEMR in the literature (Stok 1986).

The aim of this study was to characterise the topographic behaviour of the VEMR to a pattern onset/offset stimulus, presented both full and half field. It was hoped that this might offer an insight into the way in which the stimuli are processed and go some way to assessing the suitability of such stimulus fields for possible clinical applications.

As the study was concerned with comparative, intersubject topographic distributions, and not in the localisation of underlying sources, twenty recording positions over the occipital scalp were used, as opposed to the 40+ locations used by authors such as Stok (1986) and Aine et al (1990). While such an array would theoretically reduce the accuracy of localisation techniques (Romani and Leoni 1984), the savings made in recording time allowed more subjects to be recorded. In addition, the use of localisation algorithms which compute the locations of underlying sources by comparisons to simple dipolar distributions would be of limited practical value for these data, as full and half field stimuli are likely to activate multiple sources within the occipital cortex (Okada 1983).

6.1 - METHODS.

Full and half field stimuli subtended an angle of 7°20'x5°43' and 3°40'x5°43' respectively to the eye. In all cases, a check size of 38'x27' was used at a contrast of 65%.

The full, left and right half field topographies were recorded in the same five subjects so as to allow comparisons to be drawn between the fields, the subjects and the similarities between the recorded full field responses and those produced by the arithmetic summation of the half fields. In order to assess the stability of the full and half field topography in a larger population, the number of subjects recorded to full and right half field stimuli was increased

to ten. A total of fifteen different subjects were therefore recorded to full and/or half field stimulation.

Twenty recording positions over the occipital scalp were used for mapping, the array of which is shown in chapter 4, with fifty responses averaged for each point.

Where group average maps are presented, the topographic distribution at the peak latency for each subject were combined arithmetically to produce mean and standard deviation distributions, not mean waveform distributions.

Source localisation was performed on data for the right half field response of subject CD. This was recorded using 42 probe positions, the array for which is shown in chapter 4. Two localisation algorithms were employed:-

1. A single dipole in a sphere (Janday et al 1989).
2. A distributed source approach using 42 constrained current dipoles in a sphere (Bedford 1992).

This latter method was also used to analyse the mean subject full, right and left half field CIIm distributions, and the mean right half field CIIm, CIIIm and offset topographies.

6.2 - FULL AND HALF FIELD WAVEFORM MORPHOLOGY.

Waveform peak identification was discussed in chapter 5, along with a description of the general averaged and unaveraged waveform morphologies.

Of the twenty waveforms recorded as mapping input for each stimulus, several showed large amplitude peaks with a 'classical' morphology. These corresponded to positions of high signal to noise ratio. As the recording positions moved increasingly further away from the field maxima, the decrease in signal strength was reflected in the poor amplitude and morphology of each peak. As peak identification was performed by visual inspection of the waveforms, each of the twenty mapping waveforms were printed on a uniform amplitude scale, to allow the choice of mapping latency to be weighted towards waveforms showing high signal to noise conditions.

Figure 5.421 (chapter 5) shows an example of an averaged waveform with each peak marked. Inter- and intrasubject variations from such morphology were evident, with some subjects showing a late peak following that of the CIIIm, with a similar amplitude but opposite polarity. Peak identification was more complex with full field stimulation than it was for half fields, as many

individuals displayed an early peak which was comparatively large and well formed, even though it was smaller than the later peaks. As will be discussed later, the full field peak topographies of many subjects suggested that this earlier peak might describe the activity of the CIIm sources more accurately than any of the later, dominant peaks.

With right half field stimulation, the majority of subjects showed a dominant second peak, however two subjects showed a larger third peak. These two subjects, marked on table 6.22A by (* and **), both showed a complex waveform morphology, in which there appeared an extra peak at approximately 110ms.

Although offset waveform peaks were regularly seen for all subjects, those produced by left half field stimulation tended to be less well defined than those for the full or right half field.

The latencies and amplitudes for each peak of the onset and offset response are given for full field (table 6.21A and B), right half field (table 6.22A and B) and left half field stimulation (table 6.23A and B). In each case, prominent peaks are labelled either I, II or III depending upon their relative positions on the waveform. This was achieved by visual inspection alone, without reference to their respective topographic distributions. The highlighted figure in each case indicates the most dominant peak.

Figure 6.21 shows the twenty waveforms used as mapping input for the right half field response of subject GB. The numbers printed next to each waveform correspond to the scalp recording locations detailed in chapter 4. The three latencies mapped are marked on the waveforms, the values of which are shown at the bottom of the figure. The general waveform morphologies are similar to those published by Kouijzer et al (1985), Stok (1986) and Ahlfors et al (1992) for the onset/offset VEMR.

6.31 - RIGHT HALF FIELD TOPOGRAPHIES.

The group mean CIm topography shown in figure 6.311A is complex and of low amplitude. This is consistent with the poor definition of the waveform peaks, suggesting a poor signal to noise ratio. The distribution of the most dominant waveform peak (the CIIm), in figure 6.311B, shows predominant activity over the hemisphere contralateral to that of the stimulus field. The area of outward flowing field seen ipsilaterally for the mean CIIm topography

TABLE 6.21 A - Latencies (LAT.) and amplitudes (AMP.) of the full field onset waveform peaks from ten normal subjects, together with the group means and standard deviations. Highlighted figures indicate the peaks which appear to dominate the waveform.

PEAKS		I		II		III	
SUBJECT		LAT. (ms)	AMP. (±unit)	LAT. (ms)	AMP. (±unit)	LAT. (ms)	AMP. (±unit)
	CD	70.31	16.0	**111.33**	**43.5**	156.25	33.9
	SC	91.80	18.4	**125.00**	**20.8**	177.73	18.3
	RAA	94.73	14.6	**129.88**	**23.6**	171.88	22.9
	AS	80.08	10.6	**111.33**	**25.0**	158.20	17.2
	JoG	66.41	8.3	**111.33**	**28.1**	181.64	27.0
	JaG	85.94	21.9	**111.33**	**24.3**	181.64	34.1
	PG	76.17	10.6	**115.23**	**33.4**	153.32	33.9
	MD	68.36	9.8	103.52	18.2	**162.11**	**18.5**
	PM	73.24	10.6	**125.00**	**28.7**	166.99	25.7
	EW	65.43	14.0	**92.77**	**20.3**	123.05	33.9
	x	77.25	13.48	113.67	26.59	163.28	26.54
	SD	±10.55	±4.32	±10.97	±7.45	±17.53	±7.10
	CV (%)	13.66	32.43	9.65	28.02	10.74	26.75
	n	10	10	10	10	10	10

TABLE 6.21 B - Latencies and amplitudes of the full field offset waveform peaks for eight subject, with the group mean and standard deviation.

SUBJECT	LAT. (ms)	AMP. (±unit)	SUBJECT	LAT. (ms)	AMP. (±unit)
SC	152.54	21.3	CD	160.35	20.9
RAA	149.61	19.9	AS	140.82	21.9
EW	142.77	27.8	PM	144.73	36.2
PG	144.73	35.0	MD	144.73	16.0
JoG	---.--	--.-	JaG	---.--	--.-
	x	147.54ms	24.88units		
	SD	±6.38	±7.37		
	CV	4.32%	29.62%		
	n	8	8		

TABLE 6.22 A - Latencies (LAT.) and amplitudes (AMP.) of the right half field onset waveform peaks for ten subjects, together with the graoup means and standard deviations. Highlighted figures indicate the peaks which appear to dominate the waveform.

PEAKS	I		II		III	
SUBJECT	LAT. (ms)	AMP. (±unit)	LAT. (ms)	AMP. (±unit)	LAT. (ms)	AMP. (±unit)
CD	77.15	10.2	**116.23**	**20.8**	153.32	16.9
SC	65.43	8.7	**109.38**	**17.2**	147.46	22.9
RAA	79.10	15.3	**113.28**	**32.8**	165.04	25.0
AS	63.48	17.1	**99.61**	**31.4**	146.48	24.4
PB	71.29	21.7	**108.40**	**45.8**	144.53	45.5
GB	57.62	20.0	**103.52**	**63.7**	152.34	63.6
EW	83.98	17.2	**111.33**	**29.5**	14.063	26.4
JB *	66.41	11.2	99.61	26.4	**152.34**	**45.8**
NE	71.29	14.4	**101.56**	**32.7**	145.51	24.4
GR **	67.38	12.4	101.56	31.3	**169.92**	**35.5**
x	70.31	14.82	106.45	33.16	151.76	33.04
SD	±7.95	±4.26	±6.04	±13.19	±9.25	±14.45
CV (%)	11.31	28.74	5.67	39.78	6.10	43.73
n	10	10	10	10	10	10

* An extra peak is seen at 120.12ms ±27.2units.
* * An extra peak is seen at 132.81ms ±21.8units.

TABLE 6.22 B - Latencies and amplitudes of the right half field offset waveform peaks for ten subjects with the group mean and standard deviation.

SUBJECT	LAT. (ms)	AMP. (±unit)	SUBJECT	LAT. (ms)	AMP. (±unit)
SC	153.52	11.2	CD	143.75	21.2
RAA	158.40	21.9	AS	141.80	28.4
EW	145.70	35.7	PB	152.54	33.6
GB	145.70	52.1	NE	143.75	32.6
JB	142.77	17.6	GR	136.91	34.0
x	146.48ms	28.83units			
SD	±6.43	+±1.53			
CV	4.39%	40.00%			
n	10	10			

TABLE 6.23 A - Latencies (LAT.) and amplitudes (AMP.) of the left half field onset waveform peaks of five subjects with the group means and standard deviations. Highlighted figures indicate the peaks which appear to dominate the waveform.

PEAKS		I		II		III	
SUBJECT		LAT. (ms)	AMP. (±unit)	LAT. (ms)	AMP. (±unit)	LAT. (ms)	AMP. (±unit)
	CD	82.03	12.9	**117.19**	**25.4**	157.23	23.6
	SC	57.62	7.9	**96.68**	**23.6**	143.55	23.4
	RAA	70.31	10.7	**103.52**	**27.1**	143.55	21.8
	AS	70.31	16.0	**102.54**	**38.6**	145.51	31.6
	EW	68.36	12.6	**94.73**	**27.2**	139.65	34.9
	x	69.73	12.02	102.93	28.38	145.90	27.06
	SD	±8.67	±2.99	±8.81	±5.90	±6.68	±5.81
	CV (%)	12.43	24.88	8.56	20.79	4.58	21.47
	n	5	5	5	5	5	5

TABLE 6.23 B - Latencies and amplitudes of the left half field offset waveform peaks for five subjects.

SUBJECT	LAT. (ms)	AMP. (±unit)	SUBJECT	LAT. (ms)	AMP. (±unit)
SC	167.19	15.6	CD	160.35	23.2
RAA	154.49	27.0	AS	137.89	29.1
EW	142.77	34.4			
x	152.54ms	25.86units			
SD	±12.14	±7.02			
CV	7.96%	27.15%			
n	5	5			

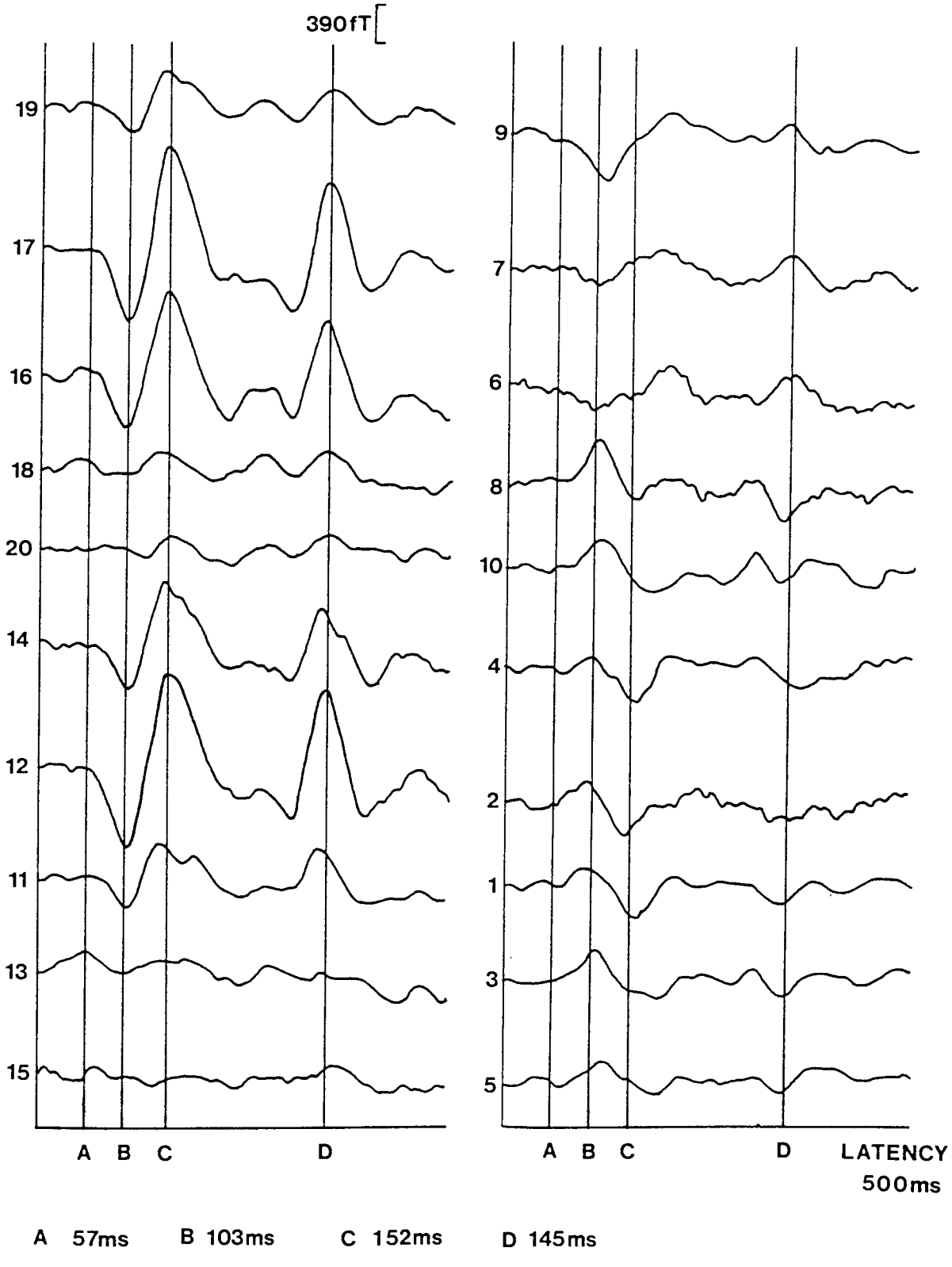

Figure 6.21 - Twenty waveforms used as mapping input for the right half field response of subject GB. The numbers to the left of each waveform correspond to the scalp position from which they were recorded (see figure 7.34). The latencies of the CIm, CIIm and CIIIm peaks are given.

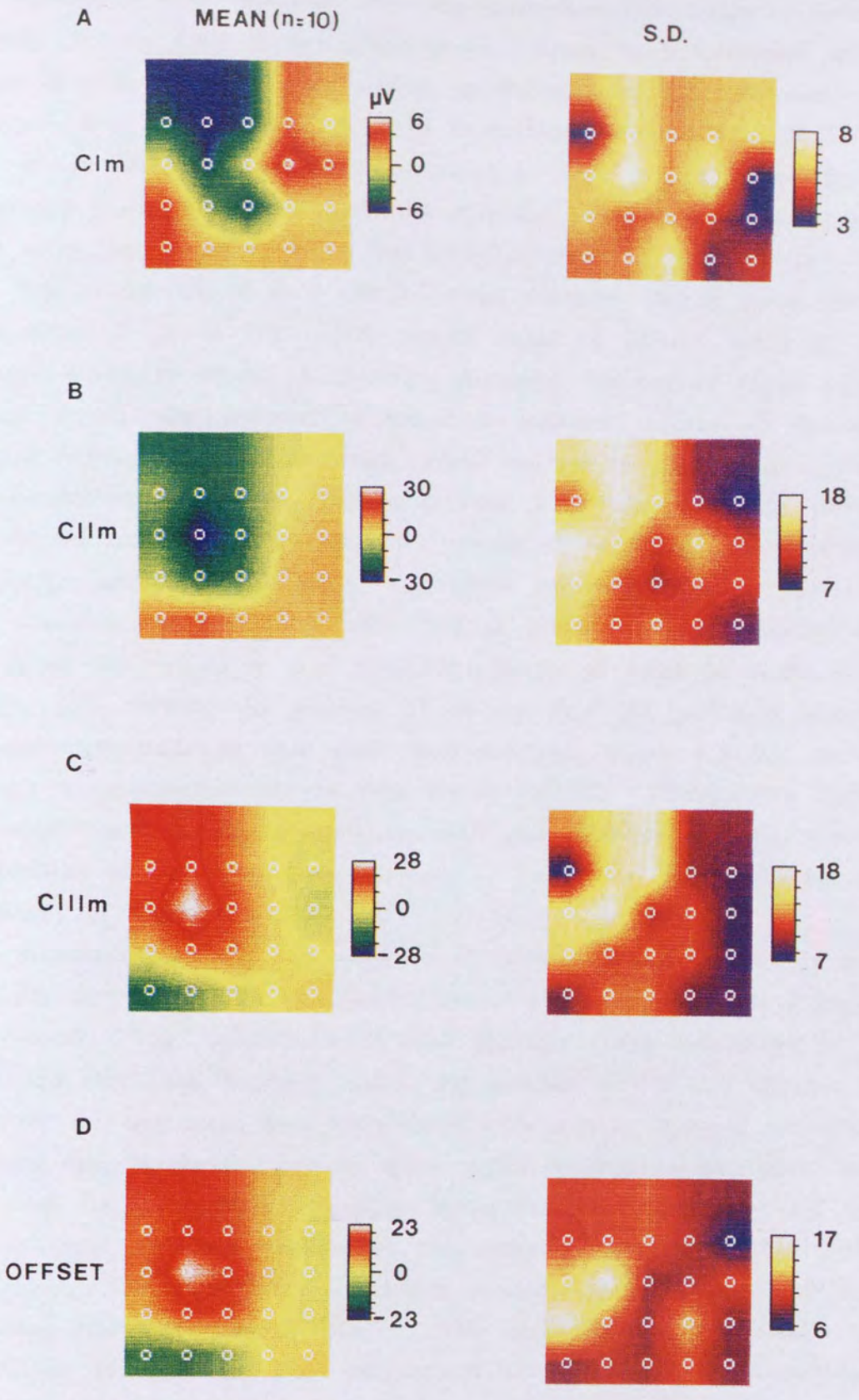

Figure 6.311 - Mean and standard deviation topographies for the CIm, CIIm, CIIIm and offset right half field responses of ten subjects.

was considered less important than the contralateral hemispheric fields, and so was excluded from further consideration. Hence, such ipsilateral activity is absent in 30% of the subjects studied, as indicated by the high coefficient of variance value of figure 6.312G. For contralateral activity, although the lower area of positive field is small compared to that of the upper negativity, recordings made with more extensive mapping grids showed that the lower field areas tend to occur below the array of recording positions (see chapter 8). The localisation of such sources would therefore require recordings to be made below the inion line. Such studies would be difficult using the present protocol, owing to subject discomfort. Assuming the activity of an equivalent current dipole, the location of transition between regions of inward and outward flowing field (yellow areas), would indicate the activity of a source in the contralateral hemisphere, centred between 1 to 3cm above the inion, and 3cm to the left of the midline, with current flowing horizontally away from the medial surface of the brain. Individual variations from the group mean were found in many subjects, with 40% of subjects showing rotation of the field areas with respect to each other, an example of which is shown in figure 6.312A; 70% showing the presence of activity over the ipsilateral hemisphere, of lower amplitude to that seen contralaterally, figure 6.312B; and some showing a combination of the two, figure 6.312C. Disregarding ipsilateral hemispheric activity, the greatest variation seen between subjects appears in the position of the upper field maxima, as shown by the standard deviation topography of figure 6.311B.

As mentioned previously, the responses of subjects JB and GR gave a complex waveform morphology with two small peaks at a latency where the CIIm would be expected. The topographies of each of these peaks are shown in figure 6.313, and similarities within a subject and between subjects are apparent. The earlier of the two peaks have distributions analogous to those of the CIIm for the eight other subjects, hence an upper region of negative and lower positive field over the contralateral hemisphere, while the latter show an extra area of positive field at lower regions of the mapping grid, over the ipsilateral hemisphere. The mean CIIIm distribution, (figure 6.311C), is similar to that of the CIIm, except of reversed polarity. The amplitudes and distributions of the CIIm/CIIIm standard deviation topographies are also similar, suggesting that each component varies in a similar manner between subjects. Variations from the CIIIm mean between individuals were similar to those recorded for the

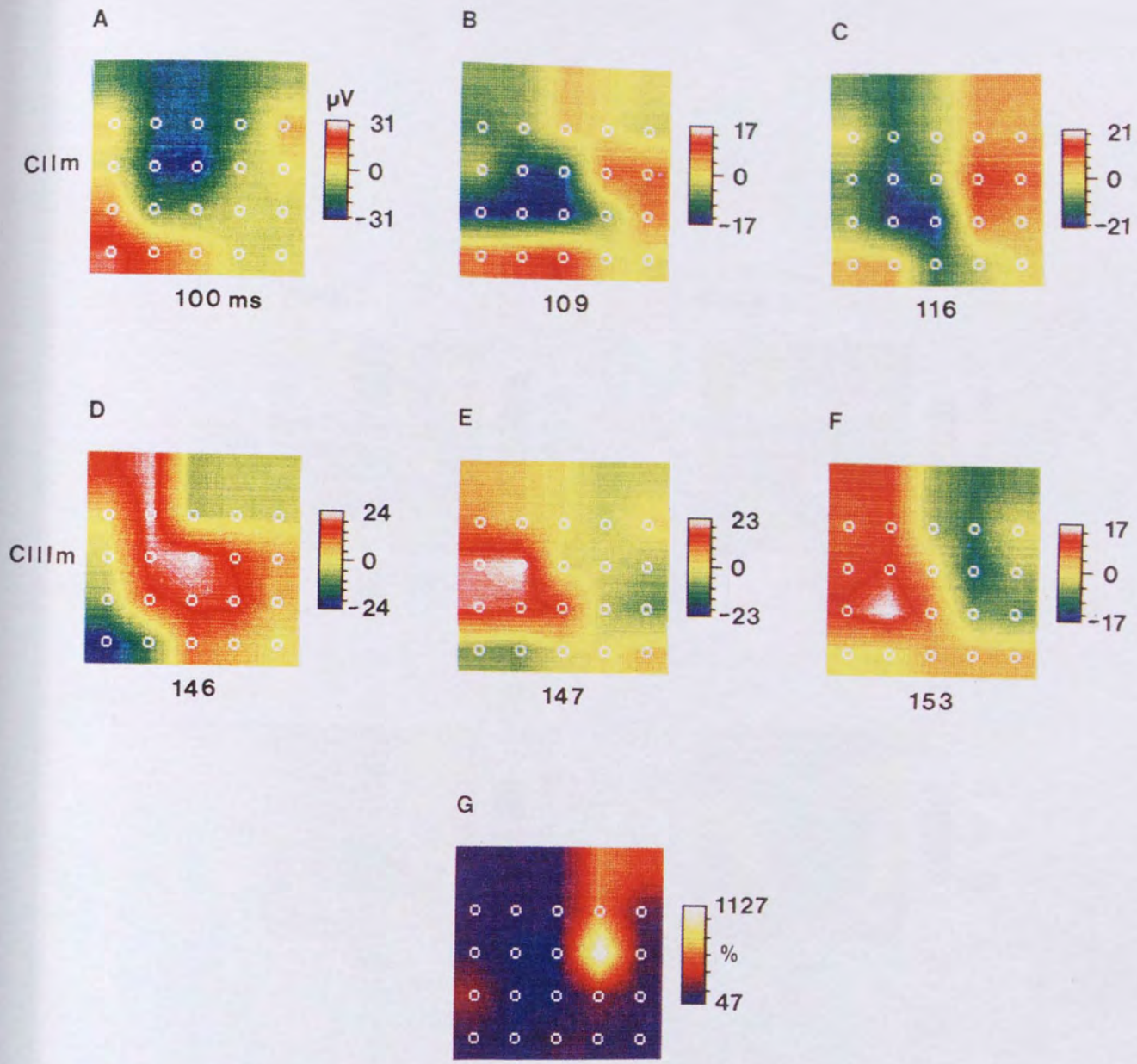

Figure 6.312 - Right half field topographies from six individuals illustrating possible intersubject variation in the CIIm and CIIIm responses (A to F). Figure G shows the coefficient of variance (CV) distribution calculated from the mean and standard deviation CIIm right half field topographies of figure 6.311.

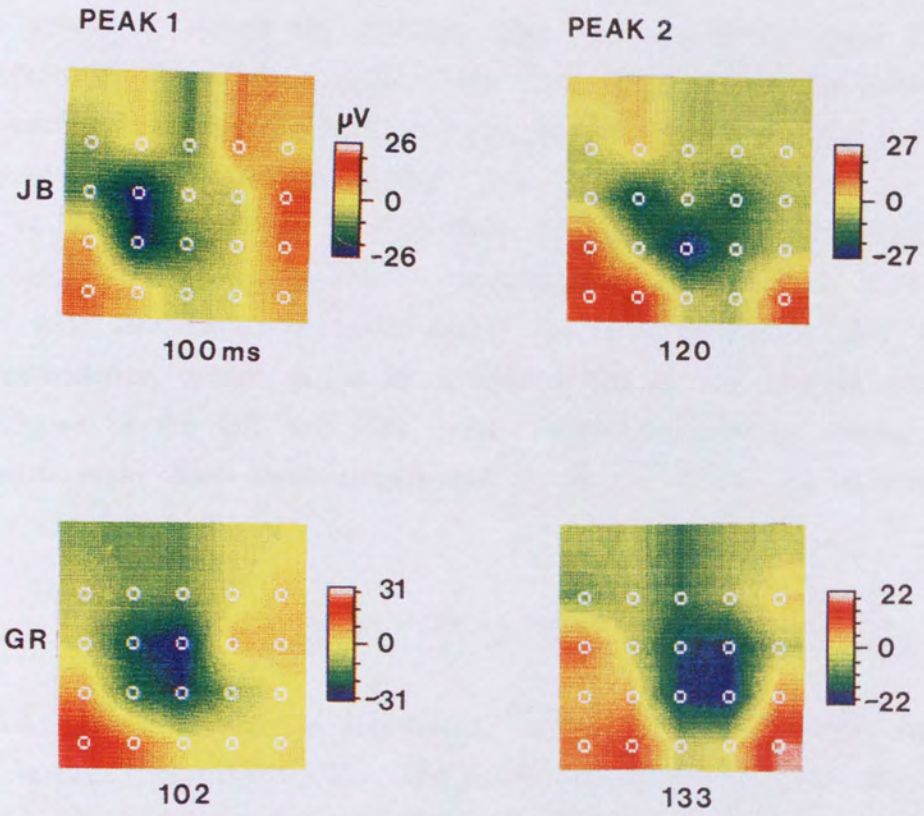

Figure 6.313 - Right half field topographies of subjects JB and GR.

CIIm (figures 6.312D, E and F). The mean offset topography (figure 6.311D) is similar to that of the CIIIm, while the offset SD map indicates less variation, especially over the regions of contralateral positivity.

6.32 - LEFT HALF FIELD TOPOGRAPHIES.

The mean topographies to left half field stimulation exhibit a low amplitude, diffuse CIm distribution with no consistent pattern (figure 6.321A). The CIIm mean (figure 6.321B), shows a predominant response over the contralateral hemisphere spreading across the midline, with current flowing away from the medial surface of the brain. The CIIIm and offset mean distributions are similar to each other (figure 6.321C and D), and of grossly similar topography, but of opposite polarity to that of the CIIm. The area of transition between regions of inward and outward flowing field is displaced by approximately 2cm anteriorly for both CIIIm and offset topographies, compared to that of the CIIm. The field maxima of all peaks appear less focal than those seen for right half field stimulation, which might be accounted for by the smaller number of subjects included in the left half field mean. Ipsilateral activity similar to that observed with right half field stimulation is absent when the stimulus was presented to the left half field.

6.4 - SOURCE LOCALISATION.

Figure 6.41 shows the source localisation results for the 42 point, right half field, CIIm response of subject CD. The results of the single dipole in a sphere model (Janday et al 1989), (figure 6.41A), suggests that the source of the CIIm lies close to the midline of the brain, with current flowing towards the lateral surface of the left hemisphere, at a depth of approximately 2cm. The values marked on each axis correspond to the co-ordinates of the recording positions in cm relative to the inion (marked + at position 0,0). This result is similar to the origin of the pattern reversal, P100m half field response, (Slaven et al 1991), except with a 180° degree rotation in current flow. This would be consistent with activity in or arround the medial and/or calcarine fissures of the contralateral hemisphere (Harding et al 1991).

Figure 6.41B shows a distributed source analysis (Bedford 1992) of the same data. The size of each arrow is proportional to the signal strength, and their

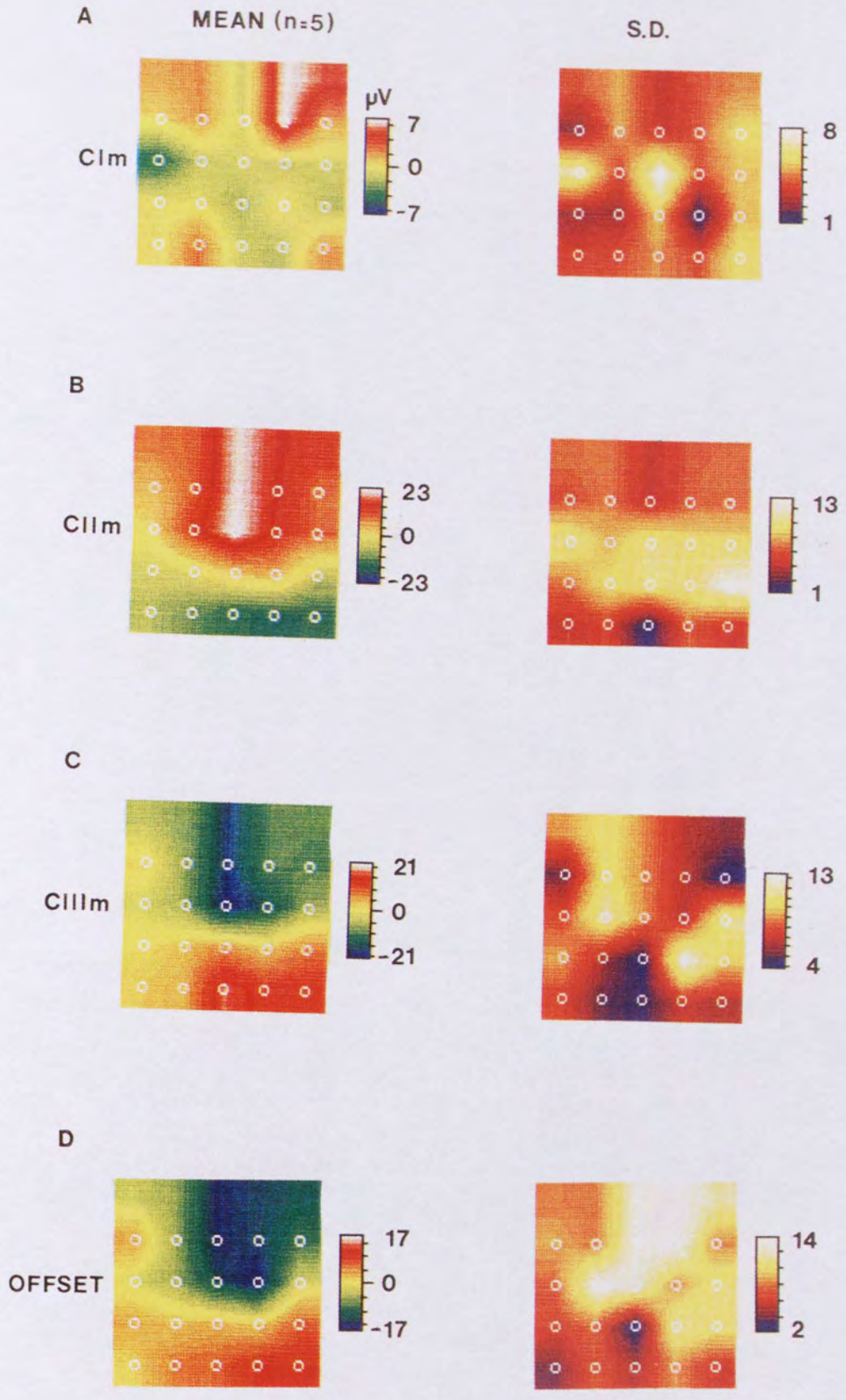

Figure 6.321 - Mean and standard deviation topographic distributions for the CIm, CIIm, CIIIm and offset left half field components of five subjects.

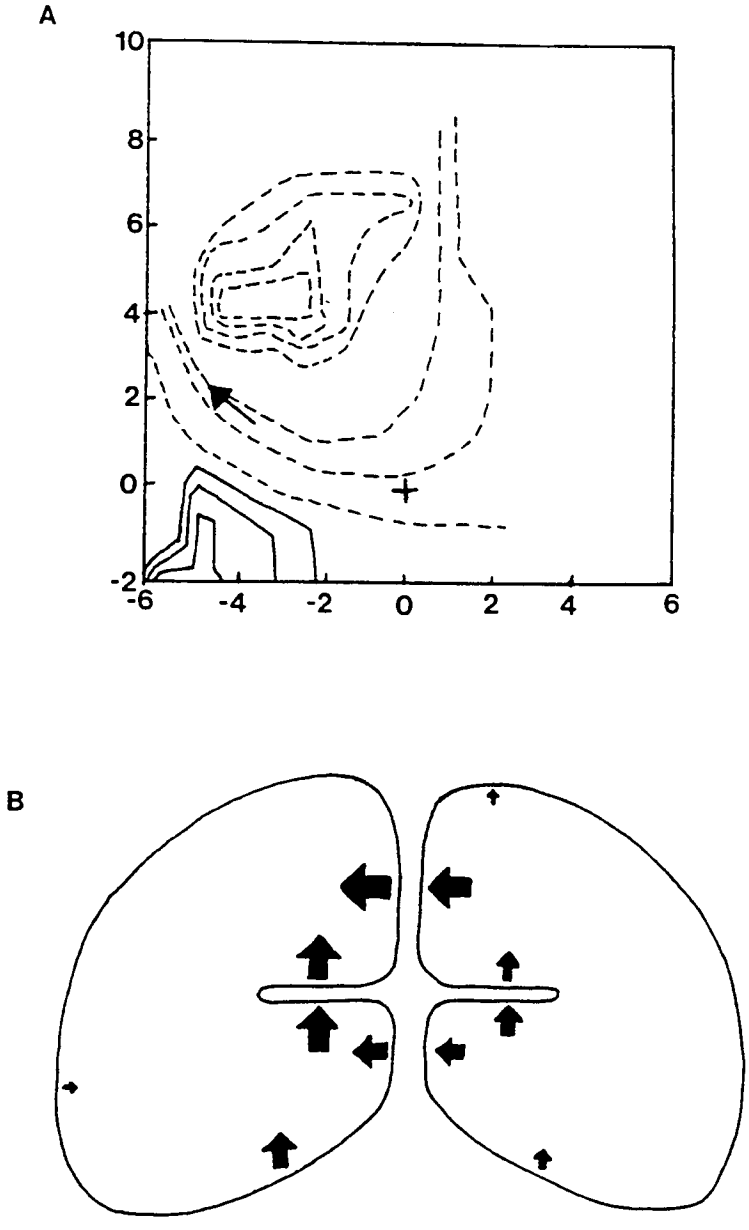

Figure 6.41 - Source localization of the right half field CIIm response of subject CD using a single dipole in a sphere (**A**) and a distributed source approach (**B**). In **A**, the inion corresponds to position 0,0 (+), while inward and outward flowing field areas are represented by solid and dashed lines respectively. In **B**, the occipital lobes are represented as if viewed from the rear, with a horizontally orietated calcarine fissure in each. The arrows indicate the direction of current flow in dipolar source sheets, their size indicating comparative source strength.

orientation indicates the direction of current flow. A predominantly contralateral response is again suggested, but in this case inferences can be made about the relative positions, strengths and orientations of the possible contributory sources. These assumptions are based on an 'average brain', whose anatomical and functional properties may bear no relation to those of subject CD. More appropriate analysis would therefore require greater tailoring of the model to the individual, by the inclusion of MRI data. Hence, the strong ipsilateral activity seen in the analysis might indicate activity in both hemispheres, or it could be due to a difference in the lateral midline position for the cortical hemispheres of subject CD, relative to that assumed by the model.

Figure 6.42 shows a distributed source analysis of the full, left and right half field mean CIIm topographies discussed in sections 6.31, 6.32 and 6.8. The half field responses are again dominated by activity in the contralateral hemisphere. Unlike the result of figure 6.41B, the influence of the ipsilateral hemisphere is greatly reduced, particularly for left half field stimulation. This might be attributed to the effects of modelling, since the inclusion of data from several individuals incorporated as an average, could increase the validity of using an 'average brain' model. A number of anomalies are evident with the results of this technique, all of which would have to be rectified before analysis of the data could be performed with any confidence. For example, the routine did not attribute any source activity to the data resulting from full field stimulation (figure 6.42FF), although the corresponding topographic distribution (mean distribution of figure 6.82) clearly shows the presence of activity over each hemisphere. Unpredictable current source orientations are apparent for the lower calcarine fissure sources of figure 6.42 (RHF) and the left hemispheric longitudinal fissure sources of figure 6.42 (LHF). This might be accounted for by differences between the cortical morphology of the subjects, and that assumed by the model. For example, the longitudinal fissure may be displaced laterally with respect to the midline, while the calcarine fissure can be displaced in the anterior/posterior plane. The angle which the calcarine fissure makes with respect to the scalp can also vary, as discussed in chapter 10. If so, the model would require MRI data for each individual under examination, with consequent reductions in the methods potential application. Finally, the presence of sources in unpredictable locations (eg the sources on the outer

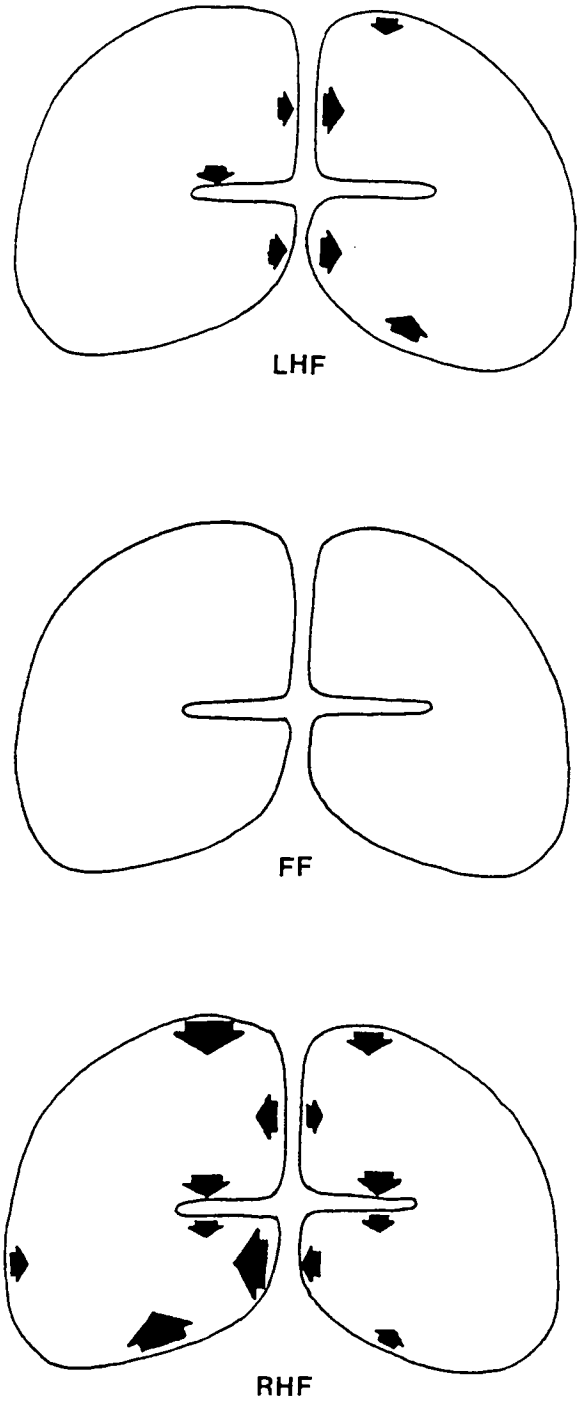

Figure 6.42 - Distributed source analysis of the mean subject full (n = 10), left (n = 5) and right (n = 10) half field, CIIm topographic distributions. In each case, arrows are used to show the presence of a dipolar source with their direction indicating the direction of current flow, and their size indicating the relative amplitude.

lobe surfaces of figure 6.42LHF) and of unpredictable strengths (eg the lower hemispheric dominance of figure 6.42RHF), could not be considered physiologically important until the possibility of an erroneous origin from within the analysis routine had been excluded.

Figure 6.43 shows the distributed source analysis of the mean right half field CIIm, CIIIm and offset topographies (see section 6.31). The most significant implications of this data is not so much in the positions of the generators for each component, but the similarities between components. It is apparent that the activity assumed for the CIIIm and offset components are similar, and these are in turn similar to that of the CIIm, except with a reversal of current flow. This would be consistent with an analogous cortical origin for each component, but of differing functional processing. The use of localisation routines for comparative analysis such as this is useful since differences between the model and the individual are less important. Hence, the technique is used to provide an objective comparison between two, or a number of images, instead of trying to resolve a complex pattern into its constituent parts.

6.5 - CORTICAL ORIGINS OF THE ONSET VEMR COMPONENTS.

Many previous studies have been concerned with the localisation of onset component generators within the visual cortex for the VEP (Jeffreys and Axford 1972 a and b, Jeffreys 1977, Lesevre and Joseph 1979, Darcey et al 1980, Drasdo 1980, Kriss and Halliday 1980, Lesevre 1982, Srebro 1985, Butler et al 1987, Edwards and Drasdo 1987, Maier et al 1987, Ossenblok and Spekreijse 1991) and the VEMR (Richer et al 1983, Kouijzer et al 1985, Stok 1986, Harding et al 1991, Ahlfors et al 1992). Their conclusions have been contradictory however, and the actual origins remain debatable. Possible reasons for the disagreements include differences in stimulus parameters; the limited resolution of the recording techniques compared with the small intracortical separations; and the large inter- and intrasubject variations in brain morphology. More accurate predictions might be attainable with the combination of MEG data to focal field stimuli, and MRI scanning. Problems might still occur however, since the small number of sources activated by focal stimuli could reduce signal to noise conditions and consequently increase variability. Such a study has been performed by Aine et al (1990), using a

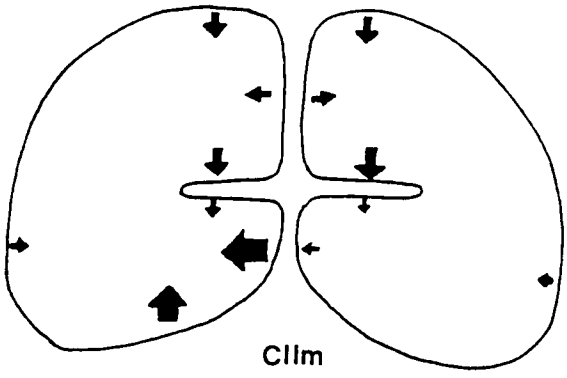

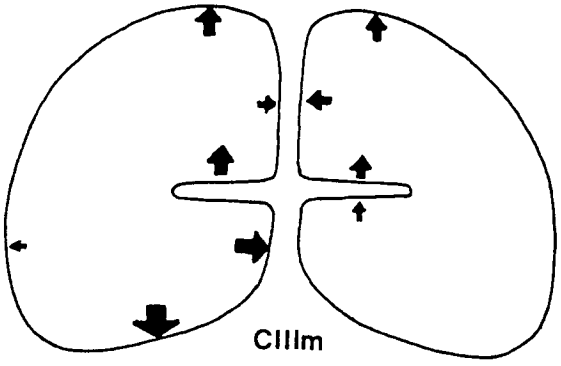

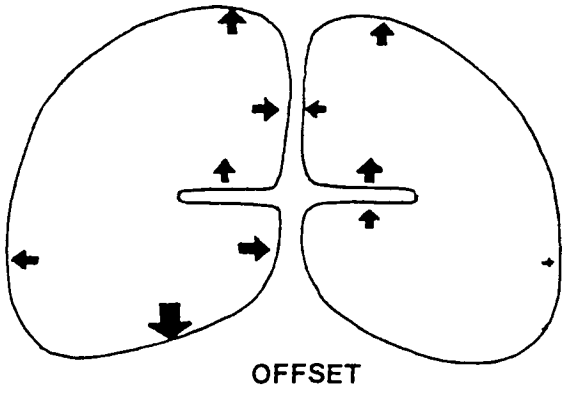

Figure 6.43 - Distributed source analysis of the mean right half field CIIm, CIIIm and offset topographies (n = 10) (See figure 6.311).

sinusoidal onset grating presented quarter and full field. Their conclusions were limited to a source origin near the calcarine fissure at 90 ms, and one in extrastriate cortex at 110ms. The full field data presented for their second subject was said to show an overlap of upper field areas of each hemispheric response. Consequently, the localisation algorithm produced a dipole in the right hemisphere oriented horizontally away from the medial surface, while that of the left was oriented almost vertically downwards. Although this solution provides a good fit for the data, it is difficult to reconcile the orientation of the left hemispheric dipole with reference to cortical morphology. Such an acute orientation is not seen in any of the half field data recorded in the present study. An alternative explanation for this distribution could be that the lower field maxima of the left hemispheric response emerges below the level of the mapping array. If this were the case, it provides a good example of why great care must be taken in the interpretation of data produced by extensive stimuli such as full fields.

The complex, low amplitude topographic distributions of the CIm components observed in this study, are consistent with the poor definition of the waveform peaks. Both observations could arise if the CIm generators displayed intermittent firing, or excessive latency variation between successive responses, (see chapter 5). Alternatively, the signal strength may be weak due to radial source orientation, as has been found for the VEP CI component (Ossenblok and Spekreijse 1991).

The left and right half field CIIm distributions are similar to those of Stok (1986) and Richer et al (1983) for the pattern onset and flashed pattern VEMR respectively. The CIIIm distributions are also similar to the M180 of Richer et al (1983). The half field CIIm and CIIIm peaks give rise to mean distributions over the contralateral hemisphere, centred between 1 and 3cm above the inion, approximately 3cm to the side of the midline, and at a depth below the scalp of approximately 2.5cm. The depth estimate is calculated by $d/\sqrt{2}$, where d is the distance between the field maxima (Kaufman and Williamson 1982). Source localisation of the 42 point, right half field response of subject CD gave a depth estimate of 2cm below the scalp. This is consistent with the half field VEMR findings of Kouijzer et al (1985) who estimated the position of all onset generators to lie 2.4cm below the scalp, at a position equivalent to O_2. These results differ from those of the flashed pattern VEMR data of Richer et al (1983) however, who located the M120 source at a depth of 1.25cm while the

M180 was 1cm deep for the right half field and 2cm for left half field stimulation. These results seem too superficial, considering the scalp to cortex separation.

The mean and standard deviation topographies for the CIIm and CIIIm peaks are similar, suggesting origins in analogous cortical regions, or from different, closely adjacent areas. The reversed field polarity seen for the two could arise from an opposing current flow in similar neural populations, or similar processing in regions of cortex oriented 180° with respect to each other. Opposing current flow such as this has been associated with excitatory versus inhibitory processing events, for the two components of the pattern reversal response (Jeffreys and Smith 1979). The VEMR is assumed to represent post synaptic graded potentials originating in the apical dendrites of pyramidal cells (Okada 1982). The CIIm could therefore represent the flow of current down the dendrites towards the cell body, as would result from an excitatory afferent. Likewise, the CIIIm could represent the inhibitory post synaptic potential, whose current flow is predominantly away from the soma (Okada 1982). The CIIm/CIIIm amplitude correlations presented for the averaged single point data (see chapter 5) are also consistent with analogous source generators.

Similarities between the VEP CII and CIII topographies have been reported by Spekreijse et al (1977), whilst similar neural mechanisms (Lesevre and Joseph 1979) and behaviour to changes in stimulus parameters (James and Jeffreys 1975) have also been shown. Disagreements with a common origin have come from Jeffreys and Axford (1972 a), who suggested that although both CII and CIII generators were from extrastriate cortex, their origins were not identical. A separate cellular origin has also been proposed for the flashed pattern M120 and M180 (Richer et al 1983).

The mean offset topographic distributions are similar to those of the corresponding CIIIm, again suggesting the possibility of analogous cortical origins. Such similarities have not been observed previously. The VEMR data of Kouijzer et al (1985) showed a 1.5cm difference in position between the onset and offset generators, interpreted as evidence of each having different origins within the visual cortex. VEP studies have also shown different properties for the offset and CII/CIII peaks (Spekreijse et al 1977), with the onset response said to be sensitive to the transient and sustained properties of

the stimulus, while the offset is mainly sensitive to the transient components (Vassilev et al 1983).

Several observations from this study suggest that the onset and offset VEMR components are more likely to originate from sources within the calcarine and longitudinal fissures, than from the lateral surface of the occipital lobes. Firstly, the half field mean and individual topographies show equivalent sources close to the midline of the scalp. Secondly, the dipole localisation results and depth estimates are similar to those published by Harding et al (1991) for the pattern reversal VEMR, itself thought to originate from the medial surfaces of the calcarine fissure. Thirdly, the topographic distributions of the VEMR to full, half and quarter field stimulation (see chapter 9), together with their response to changes in check, field and scotoma sizes (see chapter 8 and 9), could largely be explicable by sources organised as in the cruciform model. Finally, the intersubject half field response stability, is consistent with an origin from cortical regions of minimal morphological variation. The area of striate cortex posterior to the calcarine fissure has been shown to be highly variable between subjects, both in its morphology, the occurrence of the lateral calcarine fissure and the extent of projection onto the occipital pole (Polyak 1952, Butler et al 1987). Although the extrastriate cortex on the lateral surface of the occipital lobes is said to be relatively stable morphologically, (Butler et al 1987), its fissure pattern is still less stable than that of the calcarine area (see chapter 10). Sources here would also tend to give rise to scalp distributions lateral with respect to the midline, of shallow depth and predominantly radially oriented.

If the VEMR onset sources are assumed to originate from striate cortex within the calcarine fissure therefore, the CIIm component could be analogous to the CII VEP component of Darcey et al (1980), Maier et al (1987) and Van Dijk and Spekreijse (1990). A non analogous origin would be suggested however if the results of Jeffreys and Axford (1972 a and b), Lesevre and Joseph (1979), Kriss and Halliday (1980), Butler et al (1987) and Drasdo and Edwards (1989) were considered, as each concluded that the CII was extrastriate. A link between the onset VEP and VEMR components has been proposed by Richer et al (1983), who observed similarities between the flashed pattern VEMR M120 and VEP N120 components.

The findings of this study also differ from the previous VEP studies, since although several authors concluded that the CII is striate in origin, all say that

CI, CII and CIII activity do not originate from the same cortical regions. These apparent discrepancies could be explained if the onset stimulus were to activate striate sources within the calcarine fissure, and striate and/or extrastriate polar sources simultaneously. In such a situation, the VEP would primarily detect those sources at the pole, due to their radial orientation, while the VEMR would be most sensitive to the tangential sources of the fissure. The two techniques could therefore be detecting differing aspects of the same processing events.

6.6 - IMPLICATIONS FOR CLINICAL RECORDING.

The mean half field topographic distributions indicate that if such stimuli were to be used on previously unrecorded subjects, then a single recording position, 6cm above the inion, on the midline or 3cm to the left, would fall over the area of maximum inward or outward flowing field, for the right and left half field stimulus respectively. This might not be the case if different stimulus parameters were chosen. The use of such a recording approach would be particularly useful when using a single channel magnetometer, as it would reduce unproductive recording time by allowing for the quick identification of a position of high signal to noise ratio. This recording strategy was employed for the single point intersubject variation study of chapter 5, and a response of high amplitude was obtained with a single probe positioning for all of the twenty subjects.

6.7 - SUMMATION OF THE PEAK HALF FIELD RESPONSES WITH RESPECT TO THOSE OF THE FULL FIELD.

Figure 6.7 shows the topographic distributions produced by the arithmetic summation of the left and right half field CIIm topographies, for each subject (column 1). Column 2 shows the recorded full field topographies, corresponding to the latency of the most prominent waveform peak, while those of column 3 relate to a waveform peak preceding that of column 2. The summated half field topographies resemble those of the recorded full field dominant peak for subjects CD and AS only (figure 6.7 columns 1 and 2). For subjects RAA, EW and SC, the summated topographies show greater similarities with the earlier full field peak than with the later dominant peak (columns 1

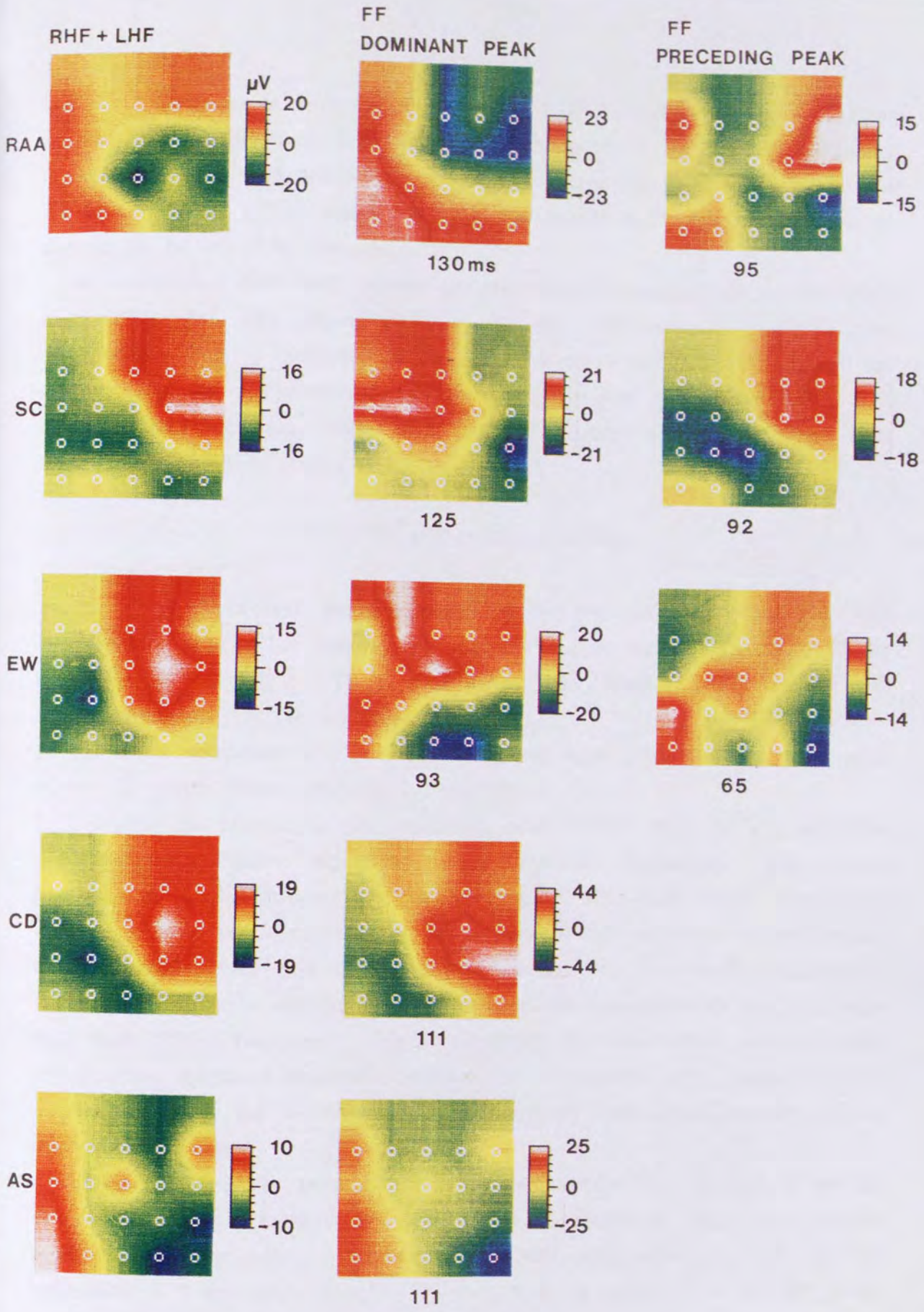

Figure 6.7 - Comparison between the summated right and left half field CIIm topographies, (RHF + LHF) and those of the recorded full field (FF) CIIm for subjects RAA , SC, EW, CD and AS. For each subject, the summated half field CIIm distribution is shown in the left hand column. The second column shows the topographic distribution of the most prominant waveform peak within the first 140ms following full field (FF) onset. The third column shows the topography of a smaller waveform peak for subjects RAA, SC and EW, at a latency preceding that shown in the second column.

and 3). Comparisons between the summated half field topographies and those of the most prominent full field response produce an average standard deviation of 9.17, 8.23 and 8.5 per recording location for subjects RAA, SC and EW respectively, while comparison with the earlier full field peak gives an average SD of only 5.16, 3.26 and 6.35.

The intrasubject half field latency and amplitude differences cannot be solely responsible for the unpredictability of the dominant full field peak distribution. This is illustrated by the responses of subject AS, who showed the closest CIIm full and summated half field match (figure 6., average SD = 3.19 per recording location), while exhibiting the largest disparity in half field latency and amplitude (tables 6.22A and 6.23A).

6.8 - FULL FIELD STIMULATION.

The disparity between the prominence of the full field waveform peak and the predictability of its topographic distribution, in certain subjects, will be considered in chapter 7. There are two methods therefore by which the full field components can be identified:-

1. The CIIm component can be attributed to the most prominent waveform peak within the first 130ms following stimulus onset.
2. It can be marked as the waveform peak which produces a predictable topographic distribution, regardless of its waveform dominance. The criteria adopted for the identification of a 'predictable' full field CIIm topographic distribution was one explicable by the activity of an equivalent current source in each hemisphere, with current flowing away from the medial surface of the brain. Hence, a distribution equivalent to the summation of left and right half field CIIm responses. Variation from this was often present, with distributions displaced anteriorly, posteriorly or laterally with respect to the mapping array, or due to the presence of additional field areas, possibly due to the effects of noise.

Figures 6.81 and 6.82 show the CIIm full field distributions for each of the ten subjects studied, marked by waveform prominence and topographic appearance respectively. Although the CIIm amplitude of 60% of the individuals is lower when identified by method 2, as compared to method 1, the resulting mean distribution is of equal amplitude, but lower standard deviation (figures 6.81 and 6.82). Hence, intersubject similarities in topographic

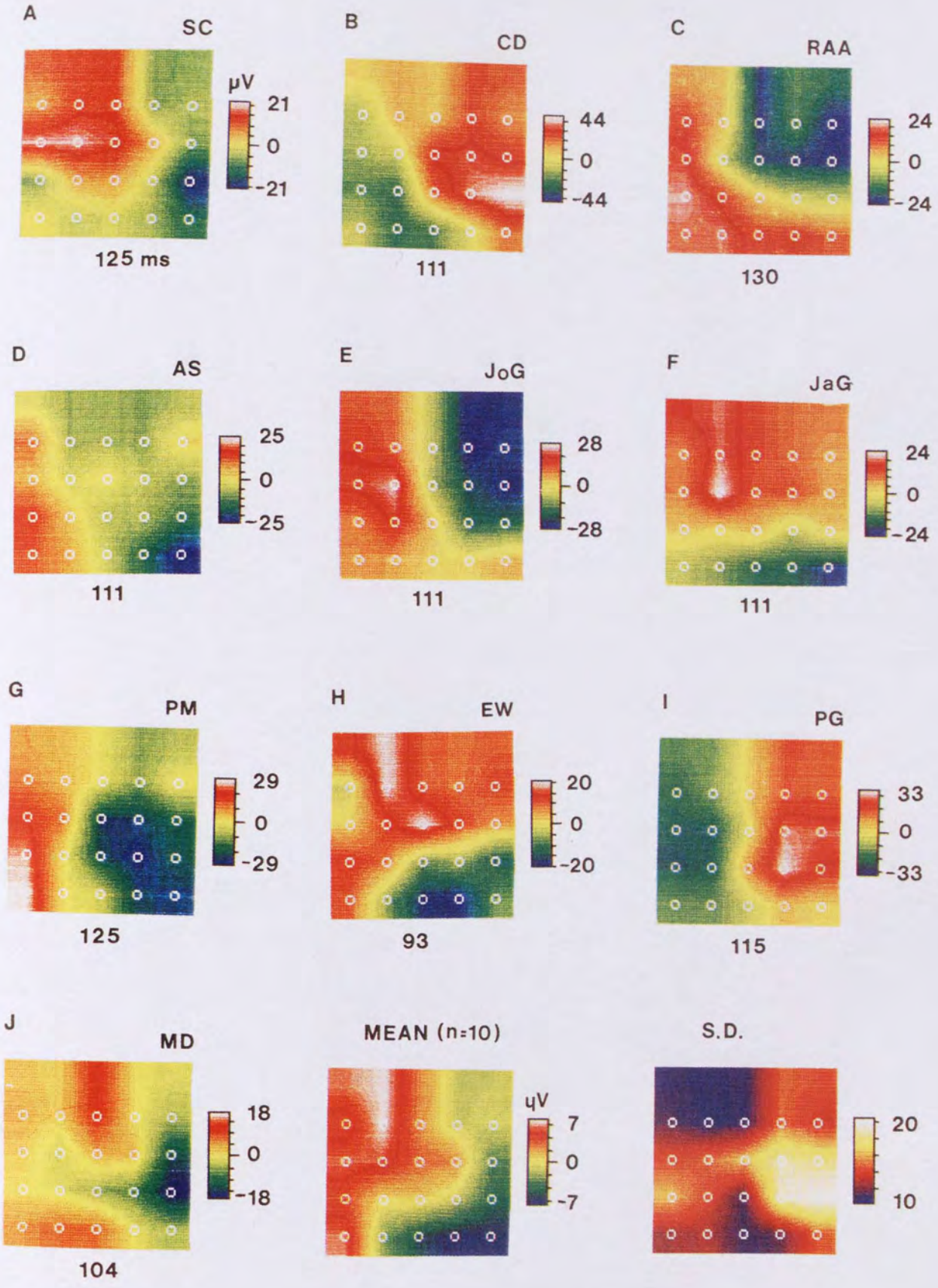

Figure 6.81 - Full field topographies of ten subjects as identified by the prominance of the waveform peak within the first 180ms following pattern onset. Also shown is the mean and standard deviation of the ten topographies.

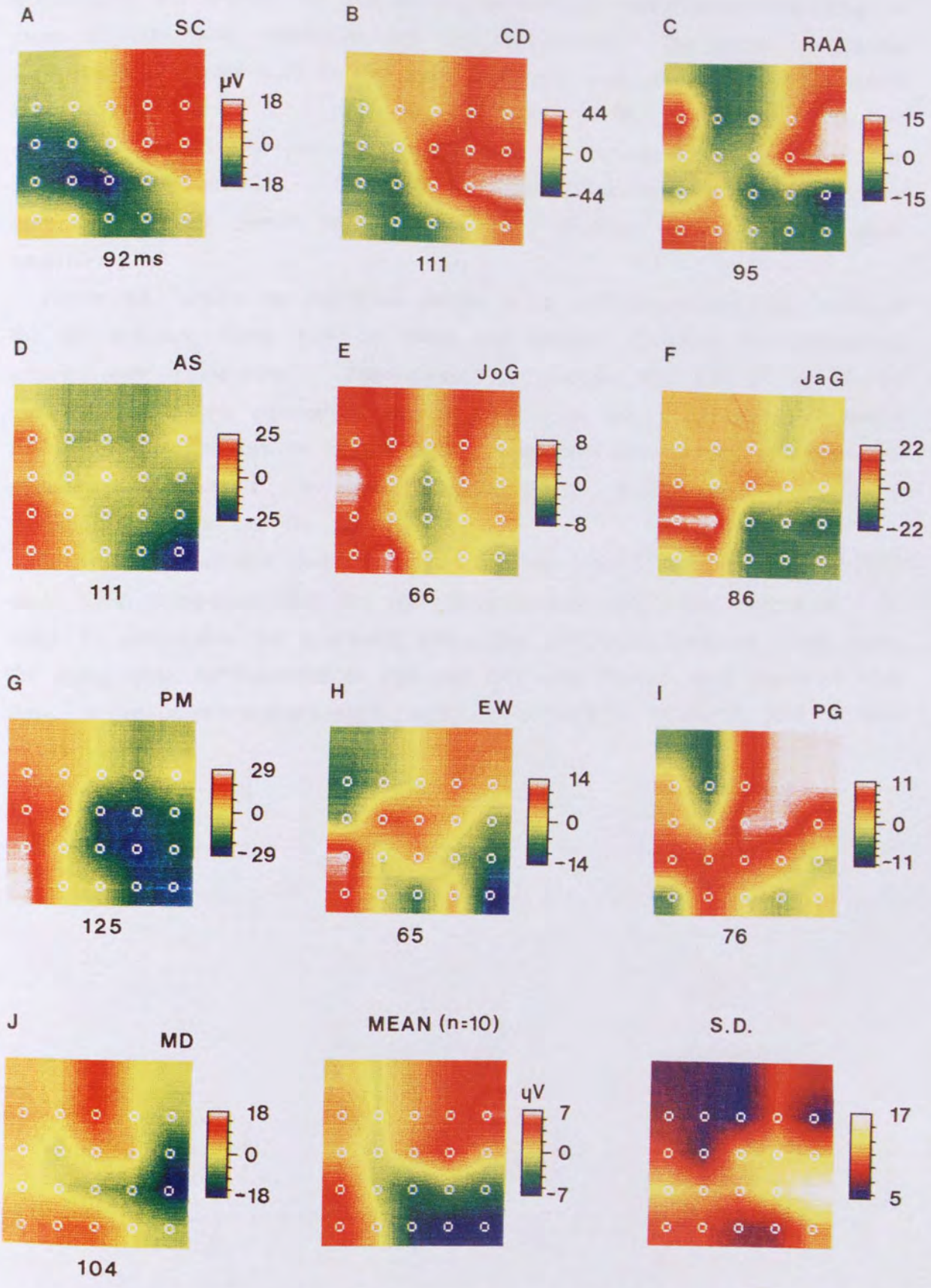

Figure 6.82 - Full field topographies of ten subjects, identified by the waveform peak within the first 180ms following pattern onset, which produced a predictable CIIm topography. Also shown is the mean and standard deviation of the ten topographies.

distribution are greater for the second method of identification, resulting in more efficient field summation and less cancellation. The mean topographic distribution of figure 6.82 is also more explicable with regards the CIIm model than that of figure 6.81. Hence, the fields of the right hemisphere are consistent with an equivalent current dipole, 4 to 5cm above the inion and 3cm lateral of the midline. The left hemispheric activity is less explicable however, with a lower region of outward flowing field, but no upper negativity.

Figure 6.83 shows the individual subject offset field topographies for eight of the ten subjects, along with the mean and standard deviation distributions to which they contribute. The mean topographic distribution would be consistent with an equivalent current source in each hemisphere, oriented towards the medial surface of the brain. The amplitude of this distribution is greater than that of the onset response (figure 6.82), suggesting greater intersubject similarities for the offset.

It would appear that problems occur for peak identification of the full field onset CIIm component, but not for offset or half field onset responses. In order to investigate the processes underlying the onset response more fully, the topographic developments to full and half field stimuli were observed with time, using chronotopographical mapping techniques (Lesevre and Joseph 1979).

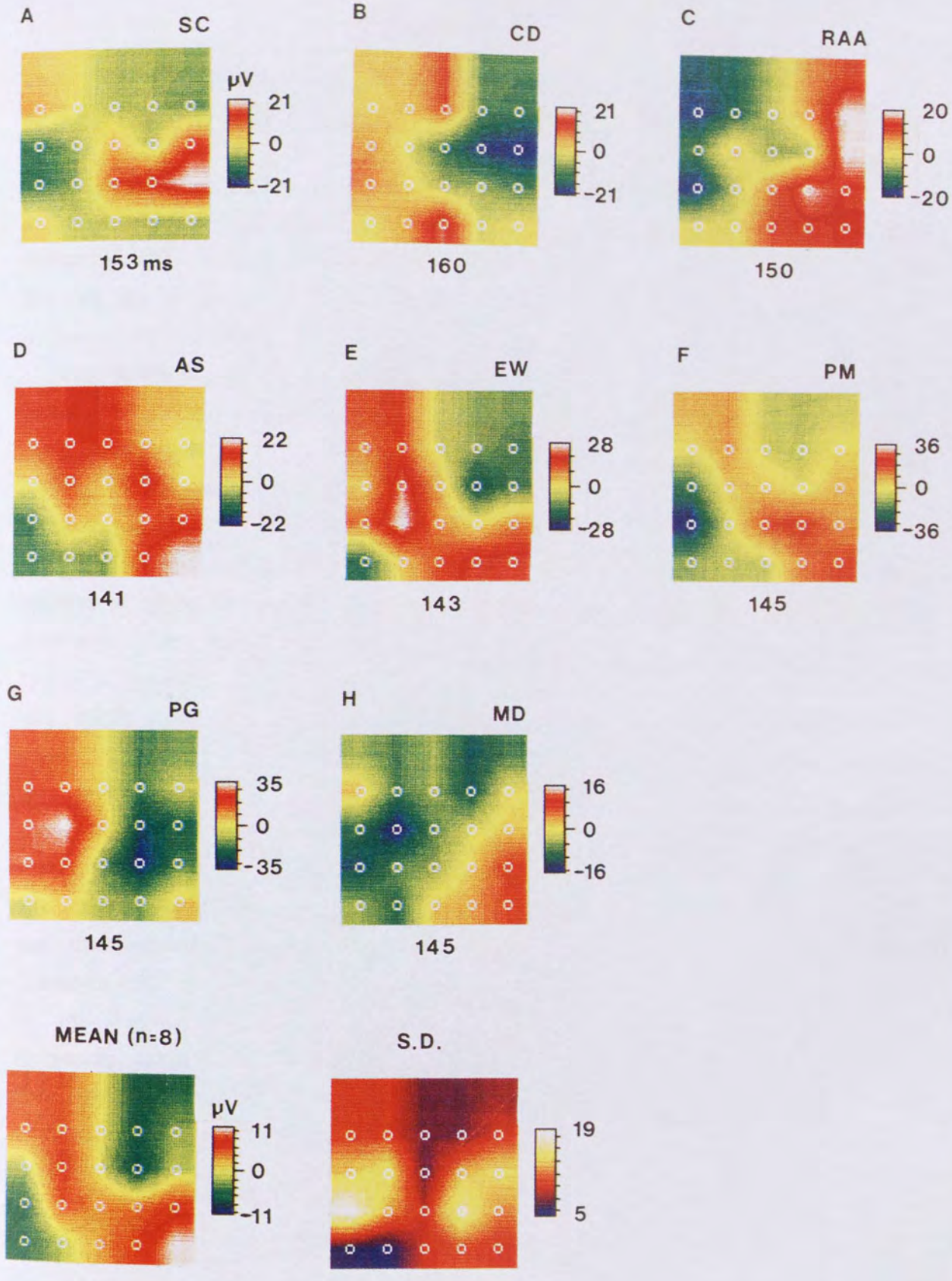

Figure 6.83 - Full field offset component topographies of eight subjects, together with the mean and standard deviation.

CHAPTER 7

CHRONOTOPOGRAPHIC DEVELOPMENT OF THE PATTERN ONSET VEMR. IMPLICATIONS FOR WAVEFORM PEAK IDENTIFICATION.

The objective of this chapter is to study the topographic changes of the VEMR fields over the occipital scalp, which occur within the first few milliseconds following the onset of a full and half field stimulus. It is hoped that this may provide an insight into the problems of full field response interpretation, and a better understanding of the response origins.

The problem of relying solely upon the latency and amplitude of waveform peaks for identification, without regard for their underlying components, has been mentioned for the VEP studies using pattern onset/offset (Jeffreys and Smith 1979, Ossenblok and Spekreijse 1991), and flashed pattern stimuli (Jeffreys et al 1977, Darcey et al 1980). No such problems have been reported for the VEMR. Aine et al (1990) described how the position of the VEMR equivalent dipole source to an onset grating appeared to move with time. Although they attributed this to the possible asynchronous activation of spatially separable sources, they did not extend their discussion to the effects this might have upon waveform peak identification. Stok (1986) presented his onset half field VEMR data in the form of sequential topographies, however they were used only to determine the movement of equivalent dipoles with time, and not to draw any comparisons between stimulus field types. The spatio-temporal organisation of the VEP has been used to compare the upper and lower hemispheric responses with a pattern reversal stimulus (Lehman and Skrandies 1977, Lehman et al 1979); for the comparison of stimulus types (Skrandies et al 1980); and to identify the number of VEP components present in the pattern reversal (Lehman and Skrandies 1980) and flashed pattern responses (Darcey et al 1980). Extensive chronotopographical studies have also been performed by Lesevre and Joseph (1979) and Lesevre (1982), to determine the number and location of underlying VEP cortical generators, to onset and reversal stimuli, presented at various retinal locations.

7.1 - METHODS.

Full and half field topographies were studied at regular latency intervals following pattern onset, for subjects CD, RAA, SC, AS and EW. A detailed sampling interval of 5ms was used for the data of subject RAA and a 10ms interval was used for the remaining subjects. In order to allow both topographic and amplitude variation to be viewed simultaneously, a fixed amplitude scale was used for all maps within a given series.

Mean full field distributions were obtained by calculating the arithmetic mean of the two constituent half field topographies at the same latency, the resulting data being used as mapping input.

The time sequences of recorded full and half field maps were examined for periods of stable topographic distribution. These were determined subjectively, by visual inspection, and objectively by the analysis method described by Lehman and Skrandies (1980). Hence, "to provide a numerical assessment of the similarities between successive field maps", (Lehman and Skrandies 1980), the topographies from each latency epoch for a given data set, were scaled to the same amplitude range. The standard deviation between equivalent recording positions of adjacent maps were then calculated. The sum of these standard deviations for successive pairs of maps were plotted as a function of post stimulus time. In the resulting graph, periods of highly variable topography appeared as peaks, while troughs depicted relative stability. A similar approach has also been used by Darcey et al (1980), for an objective analysis of the time course produced by the flashed pattern VEP.

7.2 - CHRONOTOPOGRAPHICAL DEVELOPMENT.

Chronotopography of the half fields were similar for all subjects. For the first 80 to 90ms following pattern onset, a complex, low amplitude topography was seen. Between 90 and 130ms, a strong contralateral response developed, the CIIm, consistent with a current flowing away from the medial surface of the brain. The positions of the field maxima remained relatively stationary for most subjects, while a few showed a rotation of the upper field towards the midline in the latter stages. The waveform peaks corresponded to the latencies at which one or more field areas showed maximal amplitude.

For subjects CD and SC, the field areas of opposite polarity reached maximum amplitude at slightly different latencies. Although such variation could reflect the effects of noise, it might also represent a shift in emphasis between two or more of the sources contributing to the half field response (Aine et al 1989).

A period of rapid topographic change followed the CIIm activity, the form of which differed for right and left half field stimulation. With the right half field, all subjects with the exception of AS, showed activity over each hemisphere (figure 7.21 map 18). This was consistent with a current flow towards the medial surface of the brain, as seen with a full field CIIIm response. With left half field stimulation, only subject SC showed activity of this type. In all other instances, the transitional topographies were too complex to interpret. Similar differences between left and right half field stimulation were mentioned in chapter 6, as 60% of subjects displayed some ipsilateral activity, during the peak right half field CIIm response.

Between 130 and 165ms, a strong contralateral response developed, the CIIIm, being of similar topography to that of the preceding CIIm, but of opposite polarity. This distribution remained stable for an average of 50ms, the latency of the waveform peak again corresponding to the maximum amplitude of one or more field extrema.

Figure 7.21 shows the topographic time course of subject RAA, to right half field stimulation, calculated using spline interpolation. The series of maps start in the upper left hand corner of the figure, at 60ms post stimulus, and move from left to right, and top to bottom in 5ms increments. The periods of stable distribution are indicated by those maps which have positive or negative signs marking their field maxima. During the period of stable CIIIm, there appears to be a rotation of the underlying current source from one which points towards the midline and downward (maps 24 to 26), to one which points slightly upward (maps 29 to 33). This would be consistent with a change in dominance from the upper to the lower hemispheric sources.

Figure 7.22 shows the results of a Lehmann and Skrandies (1980) type representation of the data set from figure 7.21. The sections marked A and B correspond to the periods of stable CIIm and CIIIm distribution, determined visually from figure 7.21. It can be seen that the subjective and objective analysis agree fairly closely. The change in orientation of the CIIIm sources

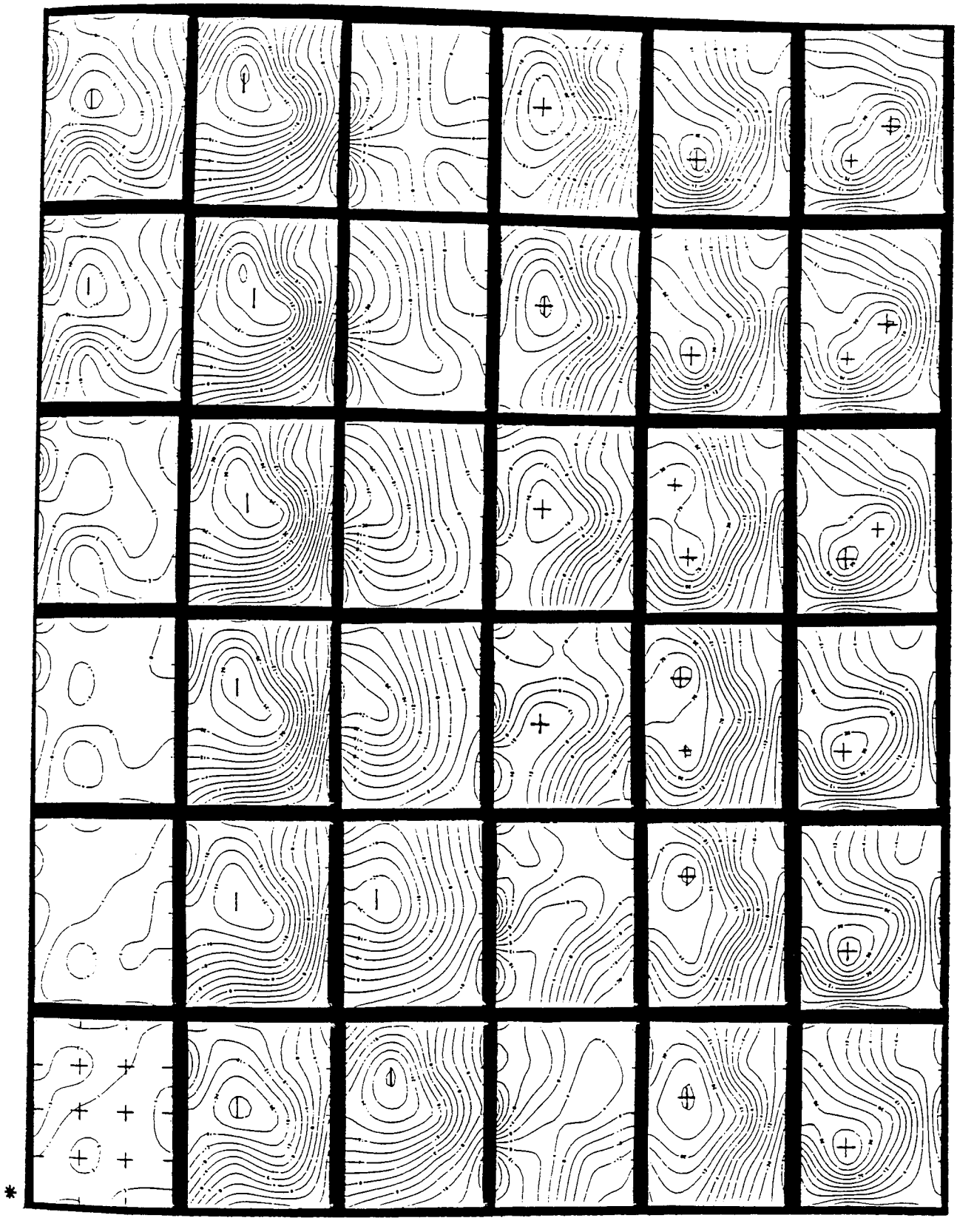

Figure 7.21 - Topographic development of the right half field response of subject RAA. This figure should be viewed horizontally, with the topographic map marked (*) in the upper left hand corner. The series begins in the upper left hand corner at 60ms poststimulus (*) and moves from left to right and top to bottom in 5ms increments. The positions of each recording location (+) are shown on the first map of the sequence. Throughout the sequence, the polarity of the field maxima are marked either + or - for outward and inward flowing fields respectively.

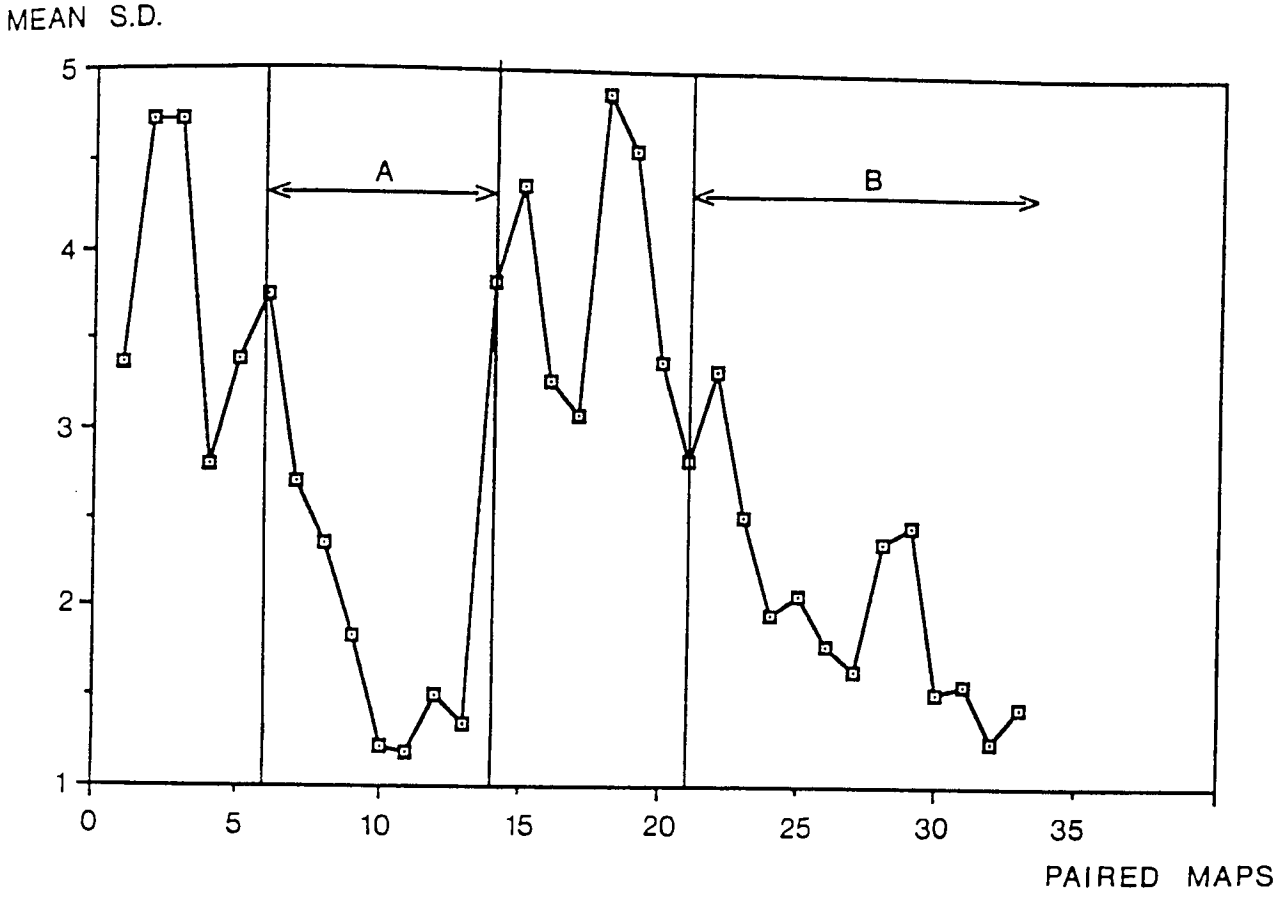

Figure 7.22 - A Lehman and Skrandies (1980) type analysis of the data set from figure 7.21 to objectively determine periods of stable topographic distribution. Troughs in the graph correspond to relative topographic stability between sucessive time intervals, while peaks indicate rapid change. Sections A and B correspond to periods of stable CIIm and CIIIm topography respectively, as determined by visual inspection of figure 7.21. Values along the horizontal axis indicate the pair of maps under comparison, hence 5 = the comparison between maps 5 (80ms) and 6 (85ms).

mentioned previously is also apparent in figure 7.22, appearing as a small peak during the period marked B.

Figure 7.23 shows a summary of the stable responses for each subject. Three fields are depicted in each case, the right half field, followed by the left half field and the full field. For the half field responses, the earlier bar indicates the time when a stable CIIm topography is present, while the later bar provides the same information for the CIIIm, (bar length is proportional to response duration). The short lines indicate the latencies of waveform peaks. The bar shown for the full field stimulus represents the presence of a 'classical' CIIm full field topography, hence, activity over each hemisphere with a current flow directed away from the medial surface of the brain in each case. The long vertical lines crossing all three stimulus bars indicate the latencies of the full field waveform peaks, the values of which are marked below. The highlighted latency corresponds to the most prominent full field peak.

It is apparent from figure 7.23 that the half field responses of all subjects display two periods of stable activity. As already mentioned, these are of similar topography but opposite polarity, corresponding to the CIIm and CIIIm peaks. Opposing field activity of this type has also been mentioned by Stok (1986) for the onset VEMR and Lehman and Skrandies (1980) for the pattern reversal VEP. Richer et al (1983) showed that the flashed pattern VEMR produced two components of opposite polarity, the M120 and M180, however they observed that the distances separating the maxima were larger for the M180, which also showed greater intersubject distribution variability.

With the exception of the right half field response of subject EW, the period of stable CIIIm activity is the same, or longer than that of the preceding CIIm. Large duration differences are evident between the CIIm and CIIIm for subjects CD and RAA, the reason for which is unclear. It is also evident that for all subjects, with the exception of AS, the stable periods of each half field are asynchronous.

7.3 - IMPLICATIONS FOR COMPONENT IDENTIFICATION.

At any instant following pattern onset, the full field topography is similar to the arithmetic summation of the two half field responses at that latency. An example of this is provided in figure 7.31 for the full and summated half field

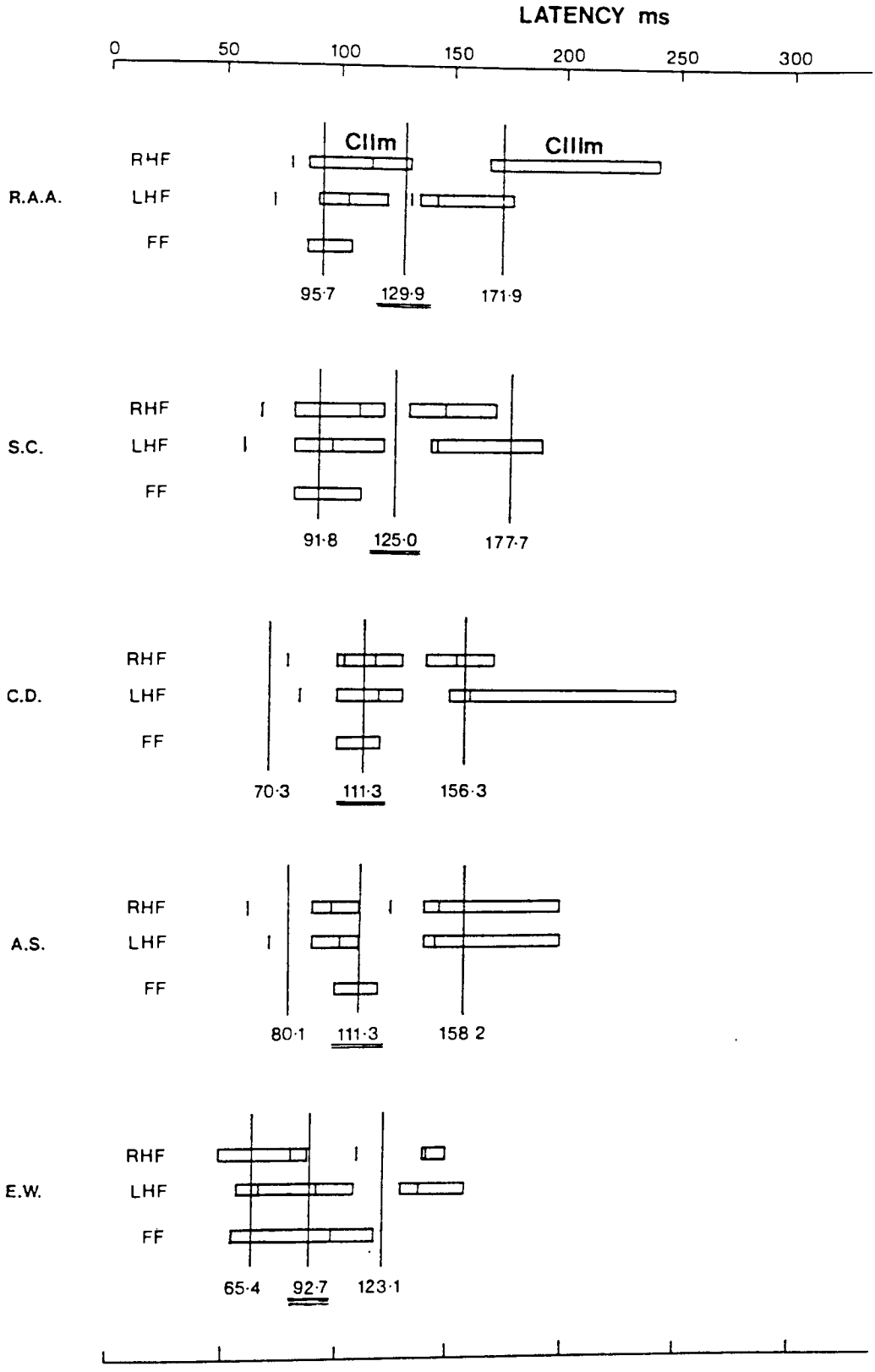

Figure 7.23 - Illustration of the stable periods of topography for subjects RAA, SC, CD, AS and EW. In each case, the responses to right (RHF), left (LHF) and full field (FF) stimulation are shown. The length of the earlier and later bars, in each case, represent the duration of stable CIIm and CIIIm topography respectively. Small vertical lines indicate the latencies of half field waveform peaks, while the longer lines show full field peak latencies. The latency of each full field peak is given below each line, the most prominant being underlined.

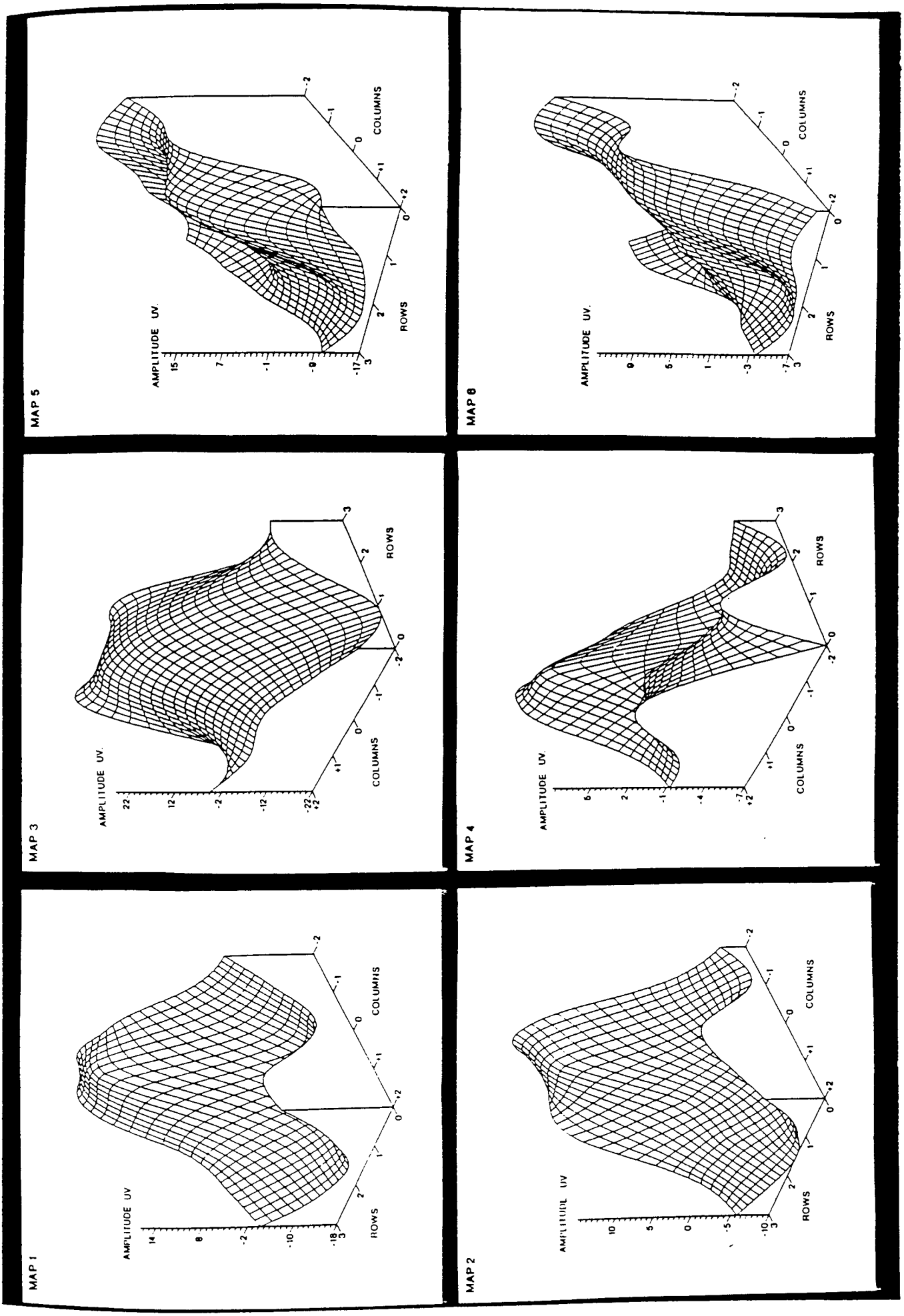

Figure 7.31 - Surface relief maps for the recorded full field (maps 1, 2 and 3) and summated half fields (2, 4 and 6) of subject SC at latencies of 91, 125 and 177ms respectively. Peaks and troughs represent outward and inward flowing magnetic fields respectively.

topographies of subject SC. For ease of comparison, the data is displayed in the form of stimulus relief maps, with peaks and troughs representing outward and inward flowing fields respectively. Maps 1, 2 and 3 correspond to the recorded full field peaks at latencies of 91, 125 and 177ms respectively. Maps 2, 4 and 6 represent the arithmetic summation of the half field responses, also at these latencies (ie they show mean topographies, not the topographies calculated from mean waveforms). The amplitude of the full field peak at 125ms (map 3), is dominant. Comparisons between full field topographies and those of the summated half fields are also illustrated by the chronotopographic data of figure 7.32. The average standard deviation values between full and summated field topographies, at successive latencies, are 5.17, 5.29, 4.78, 4.09, 4.01, 4.21, 4.43 and 4.05 per recording location respectively. Hence, full and summated half field responses produce no more variation than that observed for repeated topographic recording (See section 5.43). Similar observations have been made for the VEP response. Jeffreys and Axford (1972 a) described an additive relationship between the electrical CII half field and constituent quadrant distributions to a flashed pattern stimulus; while a similar relationship has been reported for the full and half field waveform components and topographies for pattern onset (Ossenblok and Spekreijse 1991), and pattern reversal responses (Blumhardt and Halliday 1979).

If the full field topography is produced by a summation of the constituent half fields, it would seem likely that the topographic predictability of its waveform peaks would depend largely upon how the stable periods of half field CIIm activity overlap temporally. The data from figure 7.23 supports this hypothesis, since all subjects display a predictable full field CIIm distribution during such periods (See also figure 6.82). It is also apparent however, that the maximum full field waveform peak only coincides with this period in three of the five subjects, (CD, EW and AS), the rest showing a later dominant peak (See also figure 6.81). Examination of the half field distributions at these later latencies, revealed greater mutual similarities in the position of their field areas, than seen earlier. Although the amplitudes of these constituent half field responses may be lower than those at preceding latencies, the mutual similarities in field pattern results in a more efficient summation, so producing maximal augmentation with minimal cancellation. Hence, a dominant full field waveform peak results, with an unpredictable latency and topography. An example of this is provided by the chronotopographical

Figure 7.32 - Following page - Chronotopographical sequences of the full field (**FF**), right half field (**RHF**), left half field (**LHF**) and summated half field (**LHF & RHF**) responses of subject RAA. Each sequence begins at 95ms poststimulus and progresses from left to right in 5ms increments. The topography corresponding to the latency of the most prominant full field waveform peak is labelled **B**, while topography **A** arises from a smaller, preceeding peak (See figure 7.33).

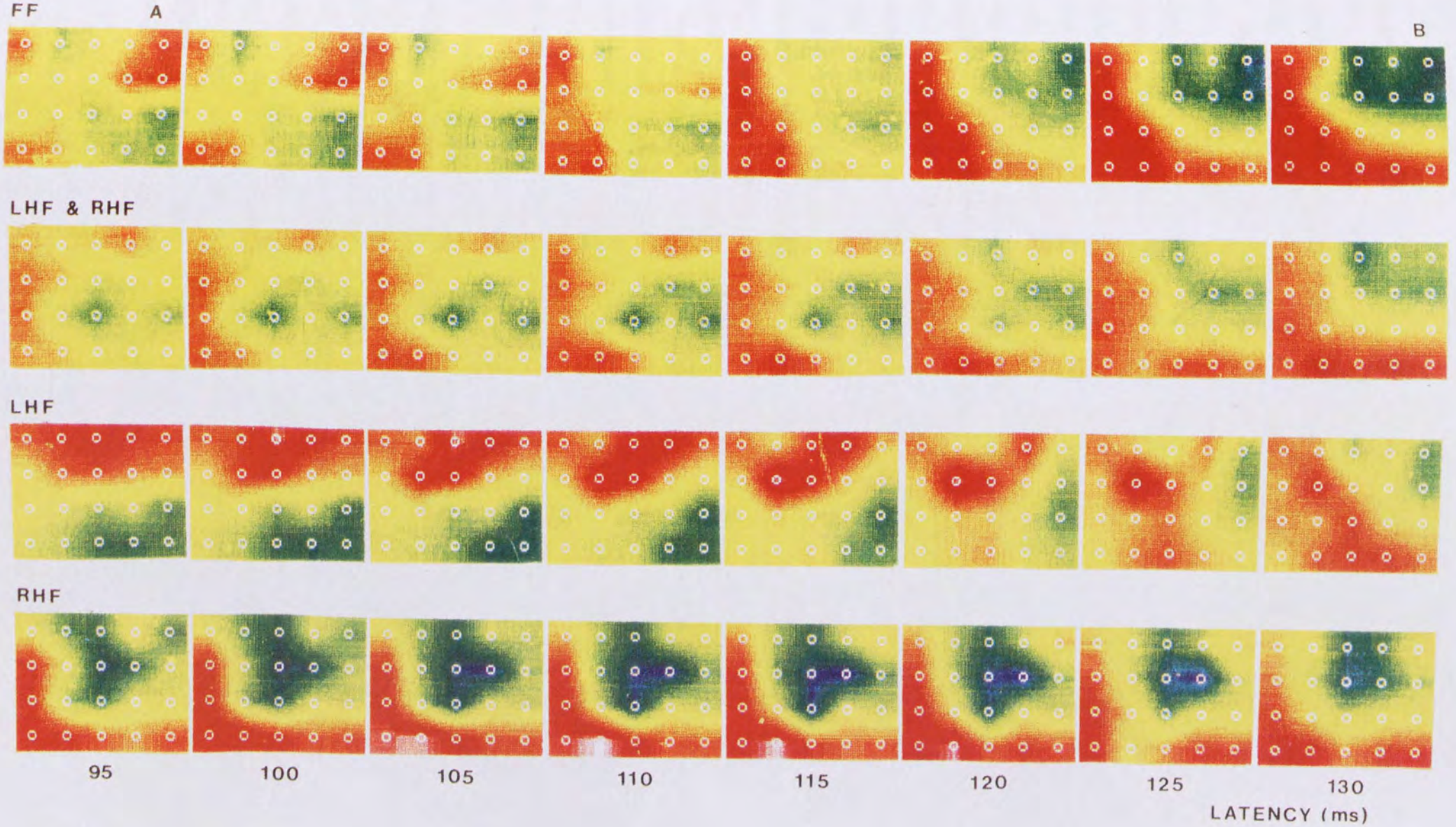
FF
A
B
LHF & RHF
LHF
RHF
95
100
105
110
115
120
125
130
LATENCY (ms)

sequences presented in figure 7.32. The figure shows the recorded full field (FF), right half field (RHF) and left half field (LHF) responses of subject RAA, together with the arithmetic summation of the two half field responses (LHF & RHF). The sequence covers the period from 95 to 130ms post stimulus, from left to right across the page, in 5 ms increments. All maps are displayed using the same amplitude scale. For each half field, a contralateral response of strong amplitude, with predictable CIIm topography, is apparent between 95 and 110ms. For the corresponding full field however, the topography of maximal amplitude occurs at 130ms (B), with an unexpected distribution regarding the CIIm (See section 6.8). This latency corresponds to that of the dominant full field waveform peak (figure 7.33). The half field topographies at 130ms each show lower amplitudes than those at earlier latencies, however the relative similarity in their distribution results in the most efficient summation. A more predictable full field CIIm topography is apparent at 95ms (A), corresponding to the CIIm activity of each half field. The inefficiency of half field summation at this latency however results in a full field waveform peak of low amplitude and prominence (figure 7.33). The average standard deviation between the left and right half field topographies is 14.66 and 8.72 per recording location, for latencies of 95 and 130ms respectively. Hence, greater topographic similarities are present at the later latency.

For subject SC, the latency of the later full field peak corresponds to the transitional period of activity, occurring between the CIIm and CIIIm components of each half field (figure 7.23). For subjects RAA and EW, the CIIm activity of one hemisphere coincides with that of the transitional activity for the other (figure 7.23). Only subjects CD and AS show a dominant full field peak which coincides with the CIIm activity of each half field (figure 7.23).

It is also insufficient to rely upon the polarity of a waveform peak as an indicator of its identity. Figure 7.34 shows three full field waveforms from subjects CD and SC, the numbers beside each corresponding to the scalp recording position from which they were obtained. The dominant waveform peak of subject CD occurs at 111ms post stimulus, (Line A), and its topographic distribution is shown below, (A). Solid lines represent magnetic fields flowing out of the scalp, while hatched lines show inward flowing field. This distribution could be explained by the upper field maxima of an equivalent current source in each hemisphere, with current flowing away from the medial surface of the cortex, consistent with the CIIm full field response. For

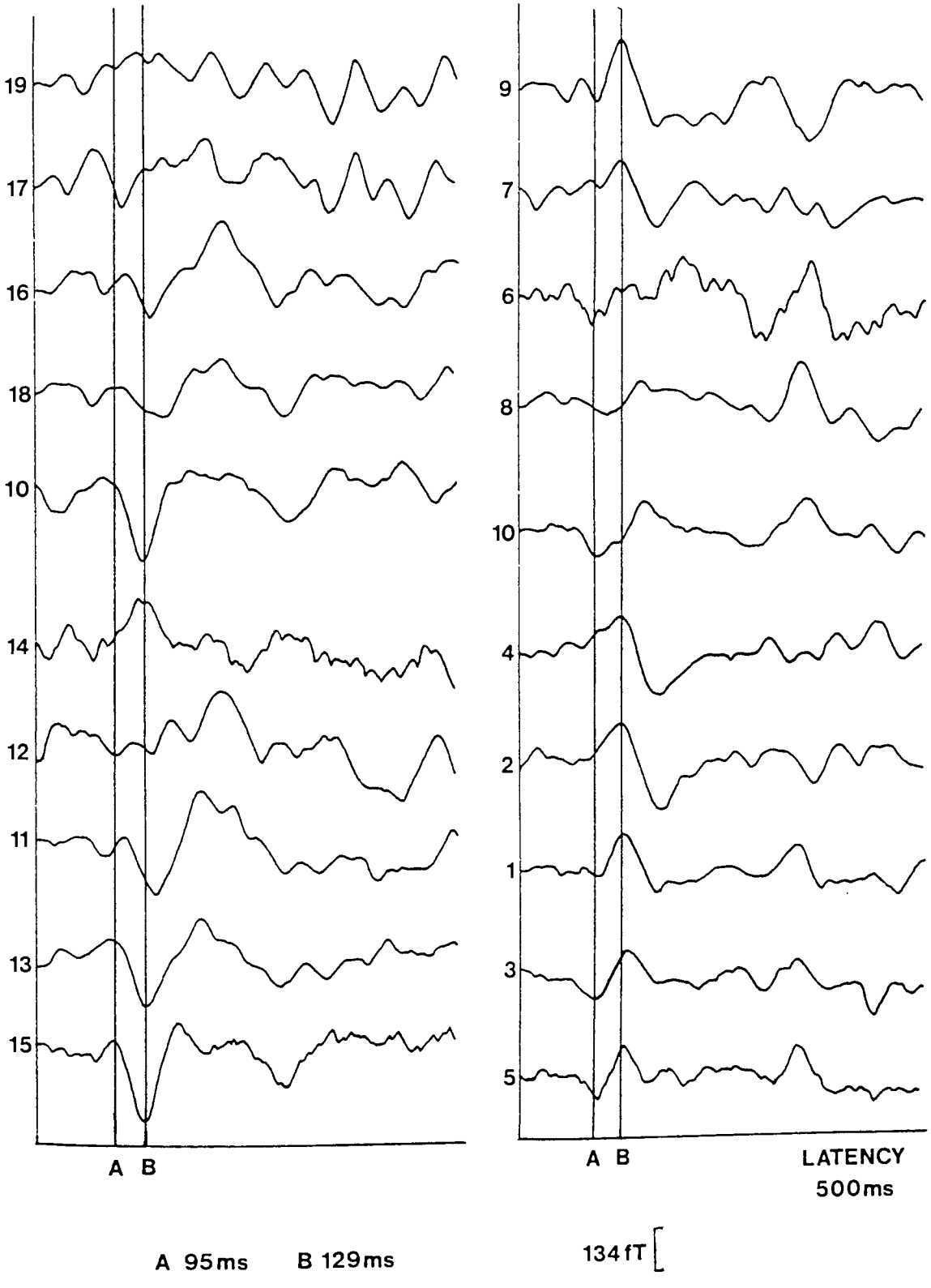

Figure 7.33 - Twenty full field waveforms of subject RAA, used as mapping input for the chronotopographic analysis of figure 7.32. The waveform peaks labelled A and B correspond to the topographies, A and B of figure 7.32. The numbers next to each waveform correspond to the scalp location from which they were recorded (See figure 7.34).

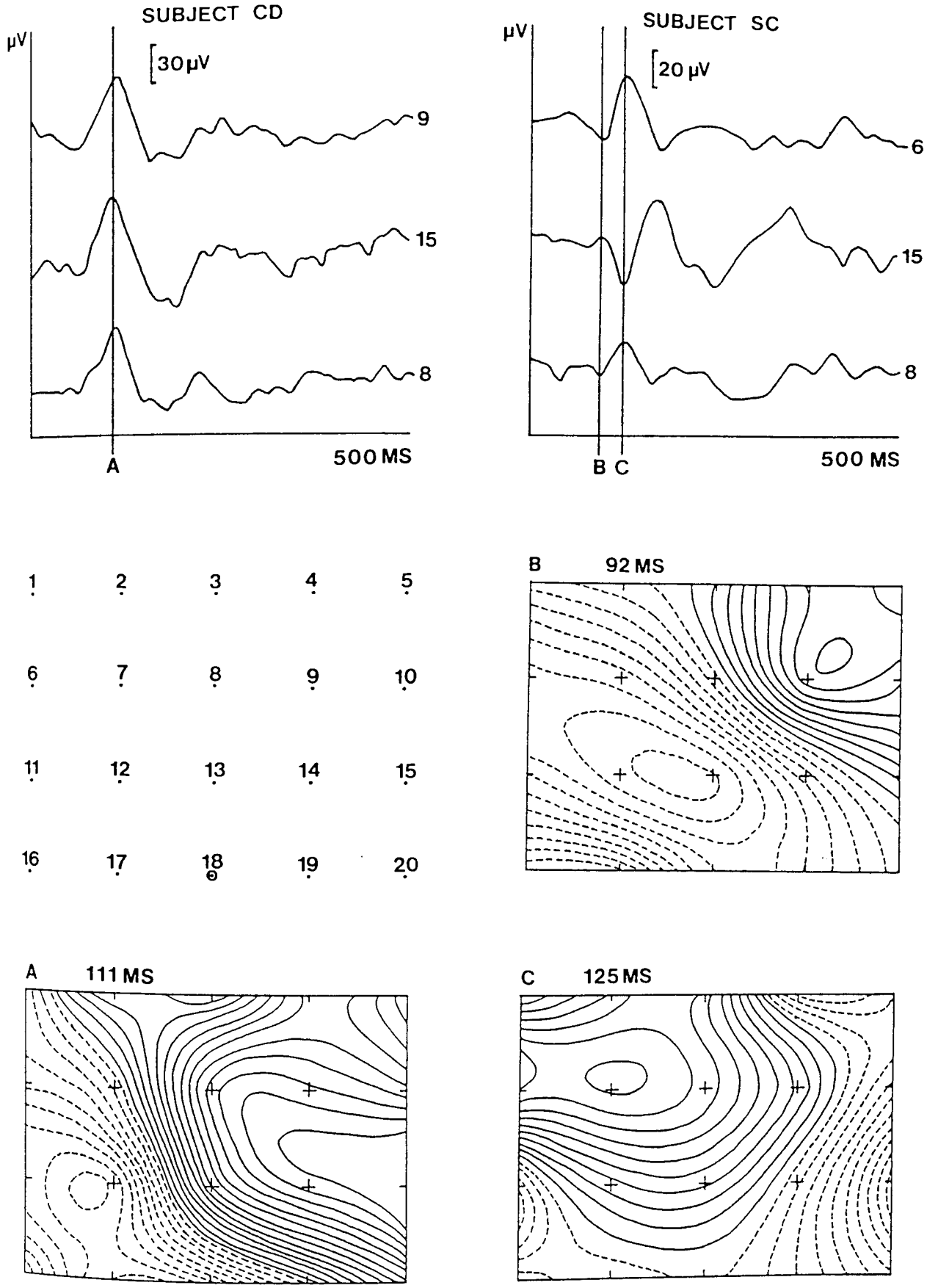

Figure 7.34 - Full field responses of subjects CD and SC. Upper panel shows three waveforms from each subject with the recording location indicated by the number next to each. Below is the mapping matrix used throughout this thesis (left), positions 18, 12 and 14 corresponding to the inion, O1 and O2 respectively from the international 10/20 electrode placement system. Also shown are the topographic distributions for the latencies indicated on the corresponding waveforms above. Areas of outward and inward flowing field are represented as solid and dashed lines respectively.

subject SC, the most prominent waveform peak occurs at 125ms (C), producing an unpredictable topography (C). The topographic distribution of the earlier (92 ms), but smaller waveform peak, does however produce a predictable topography (B). If the waveforms from recording location 15 are compared, the error in CIIm identification for subject SC would be apparent by the polarity reversal of the dominant peak between the two subjects. At recording position 8 however, no such indications are given, as the dominant peaks of each subject are of the same polarity. The large number of field maxima produced by full field stimuli, combined with the intersubject variations in their positions, makes it impossible to predict a scalp position of known field polarity, without prior knowledge of the individuals topography. Such a problem has also been identified for the VEP (Parker et al 1982).

The latency of the dominant full field waveform peak therefore depends upon the temporal overlap of CIIm activity from each hemisphere, and the relative efficiency of summation at each successive latency. As these interactions cannot be predicted from the half or full field waveforms alone, great care must be taken in attributing the activity of any component to a specific peak. Ideally, the topographic distributions of each full field peak would be required for reference, however this would seriously restrict its use with a single channel magnetometer.

7.4 - WIDER IMPLICATIONS OF COMPONENT INTERACTIONS.

The same arguments as those proposed above could also be applicable to half field topographies, as they are formed by the summation of two quarter fields; and to quarter fields, being the combination of two octants. This does not appear to be the case however, since the dominant half field waveform peak within the first 130ms post stimulus produced a predictable topography in all subjects (See figures 6.311 and 6.321). Hence, the CIIm response of each constituent quarter field must produce a summated topography which is of greater amplitude than those at subsequent latencies. This stability may occur due to the smaller number of active sources, with fewer scalp field maxima to interact.

Although the topography of the dominant half field waveform peak was relatively stable between subjects, evidence of asynchronous quarter field summation can be inferred from some of the data presented. A number of

individuals showed a half field equivalent current source which was either tilted upwards or downwards from the horizontal (figure 6.312, chapter 6). A horizontal source would be expected if both quarter field responses summated equally. An upward tilt would not be surprising, as this would suggest the dominance of the upper hemispheric sources, which for any angle of the calcarine fissure greater than 90° with respect to the scalp would be closer to the probe than sources on the lower surfaces of the calcarine and medial fissures, and hence of larger amplitude (Harding et al 1991). The downward tilt is more difficult to explain in terms of amplitude differences alone, unless time course variations were also having some effect. A further suggestion of an asynchronous quarter field interaction is shown by the CIIIm right half field data of subject RAA, figure 7.21. The change in orientation of the underlying current source from a downward to an upward tilt could be expected if the two quarter field CIIIm activities were not synchronised. Hence, the response originating in the upper quarter of the brain may begin and end before that of the lower hemisphere. During the period when both sources are active simultaneously, the upper field areas of each can be seen combined in a relatively broad field distribution. The inference that variations in surface field topography occur due to changes in the relative activity of current sources of fixed cortical location is similar to that proposed by Aine et al (1990). The theoretical computer simulations of Kaufman et al (1991) also demonstrated how such interactions could give the impression of a rotating equivalent current dipole. A second possibility is that the apparent movement results from a progressive change in dominance between the activity of dipolar sources in different cortical regions. This was suggested by Stok (1986) to explain his half field onset VEMR results. Although either situation would be possible, the former seems more likely physiologically, considering the half field stimulus is likely to project to each cortical region simultaneously. Topographic analysis might be complicated by activity on the dorsal and ventral convexities of the occipital lobes. Source activity on the dorsal surface of the brain should be magnetically silent, due to the radial orientation. Hence, the outer convexity of the upper hemisphere follows the interior boundary of the skull. Sources on the ventral surface would have a tangential component however, since this region of cortex is angled away from the scalp. The contributions from such sources is difficult to predict however since they are likely to produce field activity low on the scalp

relative to the mapping array used here, and the morphology of these cortical regions varies between individuals (Polyak 1957).

Problems caused by interactions of overlapping component activity have also been proposed by the work of Jeffreys and Smith (1979), for the pattern onset VEP to upper and lower hemifield stimulation. They concluded that the intra- and intersubject variations in peak latency could be attributed to the significant temporal overlap of the CI and CII components. In addition, they concluded that there is no consistent relationship between the amplitudes and latencies of the waveform peaks and those of their underlying components. Hence, no sound physiological basis could be made for any measurement made solely on waveform peaks, without regard for their relative component contributions. Parker et al (1982), found problems in waveform interpretation for the full field onset VEP response to sinusoidal gratings, when using a single electrode placement. This was attributed to the unpredictable changes in scalp topography with variations in stimulus parameters, suggesting that multichannel recording would be required for accurate peak identification. Ossenblok and Spekreijse (1991) studied the pattern onset VEP to similar stimulus parameters as those used here. They concluded that caution should be used when assigning the activity of a particular source to a given VEP onset waveform peak, due to the overlapping activity of spatially and temporally separate sources.

The findings of this study differ subtly from those of the VEP (Jeffreys and Smith 1979, Parker et al 1982), since instead of problems due to the temporal overlap of different components (ie the CI, CII and CIII), these are caused by the temporal overlap of analogous peaks (ie the CII alone), from differing cortical regions. The problem with the full field onset VEMR would still be present therefore, even if the stimulus was carefully tailored to selectively activate only one of the onset components.

Although the CI component, or its magnetic equivalent (CIm), is not seen in the averaged VEMR waveform, possibly due to a predominantly radial orientation, (Ossenblok and Spekreijse 1991), the argument proposed by Jeffreys and Smith (1979) might also be applicable, confounding the problem of identification. The CIm would only be truly radial in a perfectly spherical conductor, which is not likely in the human brain, and so its activity could influence that of other components. If the CIm and CIIm sources were active in closely adjacent cortical regions, their activity would interact to produce a

tilted resultant field. If the CIm activity varied temporally, in a similar manner to the CIIm, then variations in such a tilt would become unpredictable.

Similar problems of overlapping activity from different cortical regions, and waveform peak anomalies, might also explain the VEP and VEMR findings of other authors. Stok (1986), studied the half field pattern onset VEMR and observed that while the equivalent dipoles of some subjects were oriented horizontally across the scalp, others were angled more vertically. He also described how the orientation of the equivalent dipoles of some subjects appeared to rotate prior to polarity reversal. Blumhardt and Halliday (1979), studying the pattern reversal VEP, noted that in some healthy individuals, one half field response arose only from the lower quadrant field, while the other half field was evenly distributed between the two. Although these authors attributed their findings purely to variations in cortical morphology, they could also be explained by asynchronous quarter field activity. To test this hypothesis, the topographies preceding and proceeding their peak distributions would have to be examined for the presence of a more predictable topography, of lower amplitude.

Harding et al (1991), presented topographic data for the pattern reversal VEMR to full and half field stimulation, to three check sizes. Although the stimulus parameters are not comparable with those of this study, the topographic distributions of the major reversal component, the P100m, are similar to those of the CIIm, except of reverse field polarity. Summation of the half field P100m responses produced a topographic distribution similar to that of the recorded full field, with 70' checks, but not with smaller check sizes. This discrepancy was attributed to a different cortical origin for each half field stimulus, compared to that of the full field. Another possible explanation could be due to an alteration in the efficiency of half field summations as check size decreased. Such a change has been observed for the onset VEMR (see chapter 8).

7.5 - CLINICAL CONSIDERATIONS.

The ability to overcome the problems associated with full field VEMR stimuli would be beneficial for possible clinical implementation. The full field stimulus provides an easily fixated target (Onofrj et al 1982), while offering the potential for maximal stimulation for the visual system. The first clinical

application of the full field VEP was proposed by Halliday et al (1972) for the diagnosis of optic neuritis. Subsequently, authors have found applications in the detection of prechiasmal abnormalities resulting from a wide range of diseases (See Blumhardt 1987). Unfortunately, clinical studies using the pattern onset stimulus are few, since the pattern reversal stimulus has become prevalent, possibly due to its greater waveform consistency (Blumhardt 1987).

Several authors have since questioned the validity of using full field stimuli, in preference to the half field, for the detection of certain types of lesion, (Blumhardt 1987, Blumhardt and Halliday 1979, Haimovic and Pedley 1982 I and II). Although the use of half field stimuli is preferred for the detection of chiasmal and post chiasmal abnormalities, it is not without its problems. Blumhardt et al (1982), reported that for defects which were quadrantic or smaller, the half field response suffered from the same variability problems as those of the full field. Onofrj et al (1982) mentioned problems in lateralisation for hemifield stimulation, which they attributed to fixation problems as a result of random scanning of the visual field, and head movements due to respiration and fatigue.

In many routine clinical investigations into the integrity of the optic nerves, the monocular full field stimulus may be useful. Only when unusual distributions arise is it necessary to make further examinations with half field stimuli. Flanagan and Harding (1988), mentioned that the normal population do not demonstrate more than 20% interhemispheric asymmetry in P100 amplitude for full field stimulation, with 50% asymmetry a reliable upper limit of abnormality when comparing amplitudes from electrodes at least 20% lateral to each side of the midline.

Blumhardt and Halliday (1979) and Onofrj et al (1982) recommended the use of the full field stimuli as a preliminary screening test when extensive field defects were present, and if the VEP proved normal, hemifield stimuli should then be applied.

Although binocular stimulation was used throughout this experiment, similar findings might be expected with the more clinically useful monocular stimulus. This is supported by the findings of Jeffreys and Axford (1972 b), who observed that the monocular and binocular half field VEP distributions were very similar for both the CI and CII components.

The use of full field onset stimuli for any clinical VEMR applications, with few channel recording, would require the careful choice of stimulus

parameters to obtain a dominant full field peak of predictable topography. Following this, normative data studies would be required to determine if the intersubject variations produced by such parameters were sufficiently small to be clinically applicable.

7.6 - ASYMMETRIC HALF FIELD PROCESSING.

Many studies of the pattern VEP have described asymmetric half field potential distributions (Halliday et al 1972, Blumhardt and Halliday 1979, Lesevre and Joseph 1979, Blumhardt et al 1982, Onofrj et al 1982). These refer to asymmetries in the amplitude and distribution of ipsilateral and contralateral potential areas. Lateralisation of this type occurs naturally, due to the orientation of the current generators with respect to the surface electrodes (Barrett et al 1976). As the magnetometer detects magnetic fields oriented at 90° to their electrical equivalents (Stok 1986), the distribution of the half field VEMR is confined to the contralateral hemisphere to that of the stimulus field, so removing such asymmetries (Brenner et al 1981, Richer et al 1983, Kouijzer et al 1985, Stok 1986). However, the half field pattern reversal VEMR data of Harding et al (1991), displayed distinct activity over each hemisphere, for both left and right half field stimulation. This was attributed to the effects of poor subject fixation. The left half field VEMR results of this study showed a predominantly contralateral distribution. The weak ipsilateral activity seen in 70% of subjects to right half field stimulation suggests that both hemispheres were active. The ipsilateral activity was generally consistent with a current source orientation in an opposing direction to that seen contralaterally. This differs from the findings of Harding et al (1991), which were less predictable.

Explanations for this ipsilateral activity can be separated into two categories. Firstly, problems with the stimulus and recording protocols, resulting in the stimulation of retinal areas which project to each hemisphere; or secondly, the interhemispheric transfer of information via neural pathways. Problems with the recording protocols seem unlikely, since they should affect both half fields. Harding et al (1991) considered subject fixation a problem, while Onofrj et al (1982) suggested that random scanning of the stimulus field was responsible for the lack of lateralization of the half field VEP. To test the accuracy and stability of fixation in a number of subjects, an 'eye-mark'

camera was used. This provides a view of the stimulus field, with the position of gaze of each eye superimposed, allowing for the continuous monitoring of eye position. Variation in fixation was minimal during the recording period. Head movements with respect to the stimulus field due to fatigue, could also allow stimulation across the vertical meridian of the retina (Onofrj et al 1982). Rotation of the monitor to match head movements, or screening off the central 1° of the stimulus field (see chapter 9), as proposed by Blumhardt and Halliday (1979), had little effect on field distribution.

The work of Leventhal et al (1988) on primates has demonstrated the presence of a 0.5° width band of nasal retina near the fovea, which contains ganglion cells that project to the ipsilateral LGB and presumably to the ipsilateral cortex. Such bilateral cortical representation has also been suggested in man, by the pattern reversal VEP studies of Victor et al (1991). This seems unlikely to be responsible for the findings of this study, since similar responses would be expected for both right and left half field stimulation. Also, the right half field ipsilateral activity is still evident, even following occlusion of the central 5° of the retina (see chapter 9).

Another possibility is the passage of information across the corpus callosum. Such a transfer could also be responsible for the activity seen in each hemisphere during the CIIm to CIIIm transition period of many right half field responses (figure 7.32). If this were the case, it would suggest a preference for movement from the left to the right hemisphere. Callosal transfer has been disregarded as an explanation for the VEP half field asymmetries (Blumhardt and Halliday 1979), however as mentioned previously, such asymmetrical distributions can be explained by the orientation of the underlying current source. An alternative explanation to callosal transfer is not so apparent for the VEMR.

As well as differences in the presence of hemispheric activity with half field stimulation, there is also evidence of hemispheric variation in the duration of processing (figure 7.23). For the three female subjects (AS, SC and EW), the duration of the stable CIIm/CIIIm distribution varies by only 0 to 4 ms between hemispheres. For the two males however (RAA and CD), interhemispheric variations of 20 and 28 ms are evident. The hemisphere displaying the longest duration differs between subjects, and no correlation exists between hemispheric differences and handedness or eye dominance. A response of longer duration could indicate more detailed, or less efficient processing

within a hemisphere. The greater asynchrony for the two males might reflect a gender difference in functional specialisation (Rizzolatti and Buchtel 1977), or in the variation of occipital lobe morphology (Bear et al 1986). Vella et al (1972) observed larger amplitudes for right than left hemispheric responses to a half field pattern onset VEP. They attributed this to the specialised involvement of the right hemisphere in the analysis of spatial information. Subsequent work by Shagass et al (1976) however, found no such asynchrony. If the CIIm/CIIIm peaks are assumed to represent the early processing of form, as with the VEP CII and CIII (Smith and Jeffreys 1978), then the results of this study would confirm interhemispheric processing differences, although specialisation cannot be attributed to a particular hemisphere. Hemispheric specialisation has been studied previously for the VEP, a good review of which is provided by Sinelli and Mecacci (1990). Although asymmetric behaviour has been correlated with handedness and eye dominance, field sizes larger than 6° had to be used to see any effect (Spinelli and Mecacci 1990). The potential sensitivity of the MEG to activity of localised neuronal populations might allow such hemispheric processing specialisation to be observed more readily than is the case for the VEP. Carefully controlled, large scale studies would be required to test such a hypothesis.

The data analysis used in this chapter has revealed how the topographic predictability of waveform peaks are influenced by the interactions of their constituent generators. If the pattern onset VEMR is influenced in a similar manner to that of the reversal, the findings of Harding et al (1991) suggests that such interactions may differ with changes in check size. To test this hypothesis further, the onset response was studied full and half field, to varying stimulus parameters.

CHAPTER 8

STIMULUS PARAMETERS.

Numerous studies have been made into the effects into varying stimulus parameters on the VEP, e.g. spatial frequency, field size and contrast level. Care has to be taken when comparing the results of such studies since recording protocols often vary, as do the methods of stimulus presentation, either pattern reversal, onset/offset or flashed pattern. Comparisons between the responses to bar grating and checkerboards also differ, due to differences in their fourier composition (DeValois et al 1979) (see chapter 2). However, an understanding of the effects of such variables is important as it provides an insight into the mechanisms of visual processing, while also allowing for the development of optimal stimuli for clinical application.

8.11 - EFFECT OF VARYING CHECK SIZE.

The effects of altering spatial frequency on the onset of a grating stimulus has been studied psychophysiologically using reaction time as a measure of performance (Breitmeyer 1975, Musselwhite and Jeffreys 1985) and electrophysiologically using the VEP (Parker et al 1982, Musselwhite and Jeffreys 1985). The checkerboard onset stimulus has also been studied electrophysiologically (Harding and Wright 1986, Beers et al 1992). Fewer studies of the VEMR have been reported. Okada et al (1982), studied the effect of spatial frequency on a reversing bar grating, while Williamson et al (1978) and Kaufman and Williamson (1980) studied reversing and flickering gratings respectively. Similarities have been drawn between the results of the psychophysical and electrophysiological methods, with reaction times being equivalent to VEP latency with the addition of a constant value, representing processing and motor times (Williamson et al 1978). Musselwhite and Jeffreys (1985) however, reported differences between the two techniques when studying the behaviour of the CI onset component to changes in spatial frequency. Several physiological properties of the visual system have to be taken into consideration when interpreting changes in response latency, amplitude and topography to differing stimulus parameters. Firstly, due to the centre surround antagonistic arrangement of retinal ganglion cells (see

chapter 3), for any retinal eccentricity, the optimum evoked response is likely to be obtained by a check size which stimulates the majority of excitatory and the minimum of inhibitory field areas. Hence, decreasing spatial frequency results in the optimal stimulation of progressively more peripheral retina (Harter 1970). Such a relationship between check size and the average retinal receptive field has been made by several authors, with optimal check sizes of between 7.5' and 30' proposed for the central 0.5° of retina, and between 30' and 1° in the periphery (Eason et al 1970, Harter 1970, Regan and Richards 1971, Wright 1983, Lueders et al 1980, Bodis-Wollner et al 1990). Secondly, the cortical magnification factor varies with retinal eccentricity (Meridith and Celesia 1982). Hence, as eccentricity increases, there is a corresponding increase in the area of retina required to stimulate a given volume of striate cortex, with consequent effects on response amplitude. Thirdly, the activity of parallel processing channels (see chapter 3), has effects on response latency and amplitude. As retinal eccentricity increases, M cell concentration increases more rapidly than that of the P cell, with a corresponding increase in mean dendritic tree size; a trend which is said to parallel the variation seen in the spatial frequency response function with eccentricity (Kaplan et al 1991). Hence, stimuli of decreasing spatial frequency might be expected to stimulate areas of retina positioned more peripherally, and the increasing contribution from the faster M cell pathway could result in an overall reduction in response latency. Finally, it is known that foveal retina projects to sources at the occipital pole, while increasing eccentricity results in the stimulation of more anterior sources along the medial surface of the occipital lobe (Jeffreys and Axford 1972 a). Depending upon the angle of the calcarine fissure with respect to the scalp, sources at the pole should be predominantly radial, and therefore magnetically 'quieter' than the tangential sources within the fissure (Harding et al 1991). It is also known that the portion of striate cortex at the posterior regions of the calcarine fissure shows greater interindividual morphology variation than that anteriorly (Polyak 1957). When interpreting the topographic distribution to a stimulus of given check and field size, it is therefore important to determine approximately which portion of the occipital cortex is being stimulated. Estimates of the amount of retina expressed as striate cortex on the lateral surfaces of the occipital lobes varies between authors. Blumhardt et al (1978) and Van Dijk and Spekreijse (1990) suggested that the central 8° and 4° respectively were projected

laterally, while lower estimates of between 1° and 2° have been proposed by Jeffreys and Axford (1972 a), Spekreijse et al (1977) and Spekreijse (1991). Such differences could be due to the subjective methods of VEP interpretation on which they are based, or to a small, non-representative sample size. If the extent of striate cortex is measured anatomically, using the presence of the white line of Gennari as an indicator (Polyak 1957) (see chapter 10), then large inter- and intrasubject variation is apparent. In some subjects, striate cortex does not extend as far as the occipital pole, while in others it can extend for several millimetres onto the lateral surfaces.

The aim of this section is to examine the effect of varying stimulus check size on the VEMR to an onset stimulus; to observe retinotopic projection and any changes in waveform peak predictability.

8.12 - METHODS.

The topographic distribution of four subjects, (CD, SC, AS and RAA), were recorded to four check sizes (77'x57', 38'x27', 19'x13' and 9'x6'), to a full field stimulus of 7°20'x5°43', at a contrast of 65%. The responses of subject CD were also recorded to the four check sizes with two different quarter field sizes, as will be described in chapter 9.

8.13 - WAVEFORM MORPHOLOGY.

In general, the waveforms display larger peaks of clearer morphology with the two smaller check sizes (figure 8.141), consistent with the electrophysiological findings for the foveal and parafoveal receptive field size (Harter 1970). The 77'x57' checks produced a triphasic waveform within the first 180ms, with greater noise contamination than that seen with the smaller check responses. Although the smaller checks produced less noisy waveform morphologies, they did appear more complex, with many subjects showing four peaks (figure 8.141). This could be explained by the electrophysiological findings of Drasdo (1980), who reported that increases in spatial frequency resulted in multiple waveform peaks. He attributed this to the movement of the CI peak across that of the CII, with the resultant creation of an additional waveform peak, the C0. If an analogous process were responsible for the

VEMR findings of this study, it could suggest a common relationship between VEP and VEMR components.

The check size which produced the sharpest offset waveform peak differed between subjects, with the poorest response in all subjects obtained with the largest check. The onset and offset responses obtained with the 77'x57' check size were consistent with the VEP onset findings of Spekreijse et al (1977), who noted that with check sizes in the order of 40 to 80 minutes of arc, onset responses became 'sluggish', while offset amplitudes were markedly reduced.

8.14 - COMPONENT IDENTIFICATION.

As discussed in chapter 7, a full field stimulus of 38'x27' checks produced an anomalous response in a significant percentage of subjects. In such cases, the most dominant waveform peak did not produce a predictable full field topographic distribution, which instead occurred at an earlier latency. As will be discussed in this, and the following section, the ability to attribute waveform peaks to specific activity varies according to which check and field sizes were employed. Hence, for each combination of stimulus parameters, waveform peaks can be identified according to their waveform morphology, or topographic distribution.

Figure 8.141A and B show the waveforms of subject SC to the four check sizes, with the CIIm peaks identified by peak morphology and topographic distribution respectively. It is apparent that the two different methods produce opposite latency trends with decreasing check size, the peak morphology suggesting a decrease in latency, while the peaks of similar topography showed a latency increase. Considering the anatomical structure and functional properties of the visual system, the trends shown by the latter method of peak identification are most easily explicable. A relatively stable topographic distribution with decreasing check size might also be expected, as it would suggest that the positions and interactions of the contributory sources do not change greatly (Parker et al 1982).

Of the four subjects studied, CD and AS showed a predictable CIIm topography for the most dominant waveform peak, to all check sizes. Subject RAA showed a predictable topography only with the smallest check size. Subject SC showed a gradual shift in prominence between a later peak of unpredictable

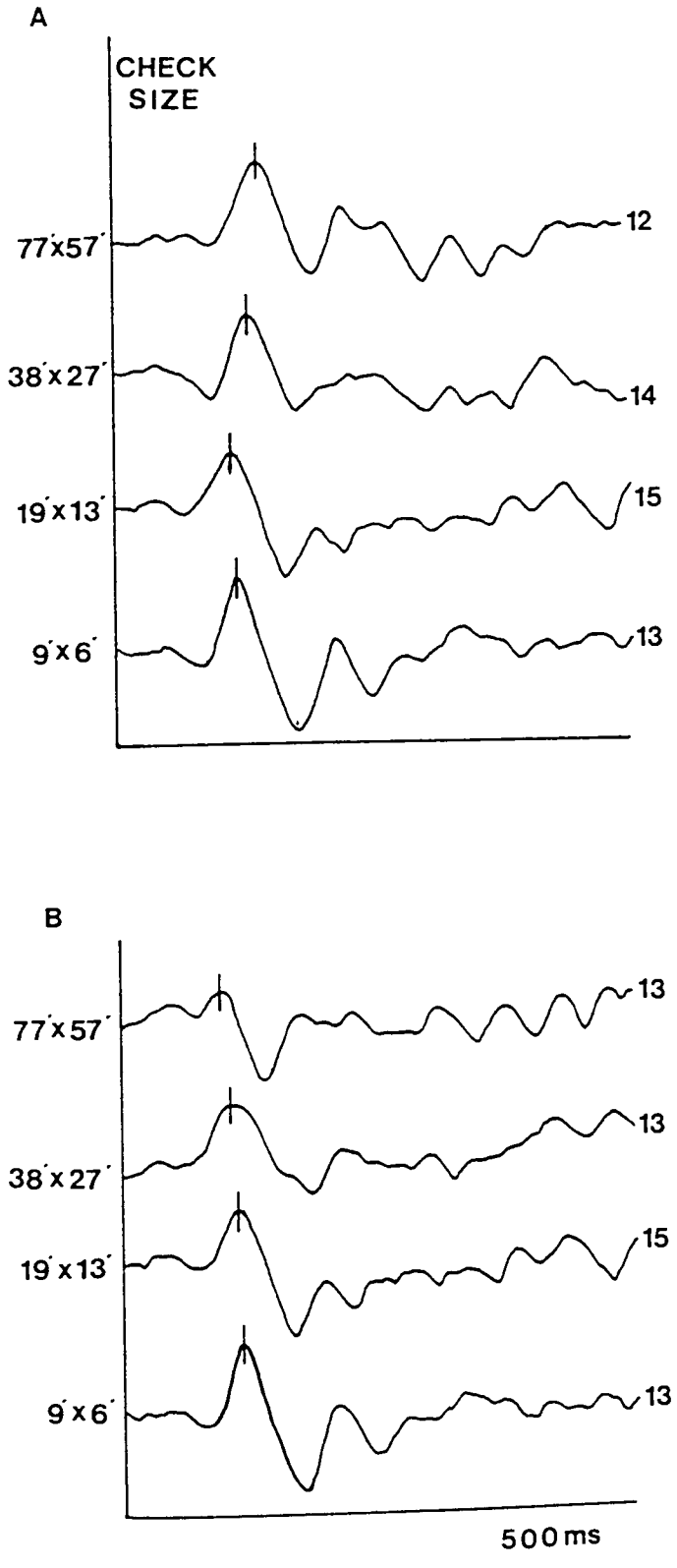

Figure 8.141 - A selection of full field waveforms of subject SC recorded to four different check sizes. The CIIm peak for each check size has been identified either as the most prominant peak following pattern onset (**A**), or the peak which produces a consistant topographic distribution regardless of its waveform prominance (**B**).

topography to an earlier one of more predictable distribution, the transfer occurring below a check size of 19'x13'.

These results suggest that if a full field stimulus were to be used with single point recording, the largest waveform peak within the first 180 ms could only be identified with any confidence as the CIIm, with check sizes below 19'x13'. For larger check sizes, the topographic distribution of each peak would have to be considered when identifying components, an obvious disadvantage when using a single channel magnetometer. Variation to this might occur with larger field sizes, due to the increased stimulation of peripheral retina, and the corresponding increase in receptive field size. Problems with identifying full field waveform peaks with single channel recording has also been mentioned by Parker et al (1982) for the VEP to the onset of a sinusoidal grating as spatial frequency increased. This was attributed to changes in the interactions between foveal and parafoveal source projections, and they recommended the use of multichannel recording to aid identification. Direct comparisons are difficult to draw between results obtained to checkerboard and bar grating stimuli, due to differences in their fundamental fourier composition (see section 2.4). An increase in spatial frequency of a check or bar pattern would still however increase the pattern content of each.

From here on, peaks referred to as the CIIm are those identified primarily by the predictability of their topographic distributions (See section 6.8, point 2).

8.15 - LATENCY AND AMPLITUDE TRENDS WITH ALTERATIONS IN CHECK SIZE.

The mean latency and amplitude of the CIIm, CIIIm and offset peaks were calculated from the responses of the four subjects, and plotted against check size. The CIm peaks did not prove consistent enough to identify and so were excluded from further analysis. Figures 8.151 and 8.152 shows the effect of check size on mean amplitude and latency respectively. In all cases, a second order polynomial curve was fitted to the data, the value of R indicating its goodness of fit.

The small number of check sizes depicted for each component limits the accuracy of any conclusions drawn from them, however it is still possible to suggest general trends. The amplitude data for all components shows an almost linear decrease as check size increases, the maximum amplitude occurring with the 6' check. The trends of the CIIm and CIIIm components are

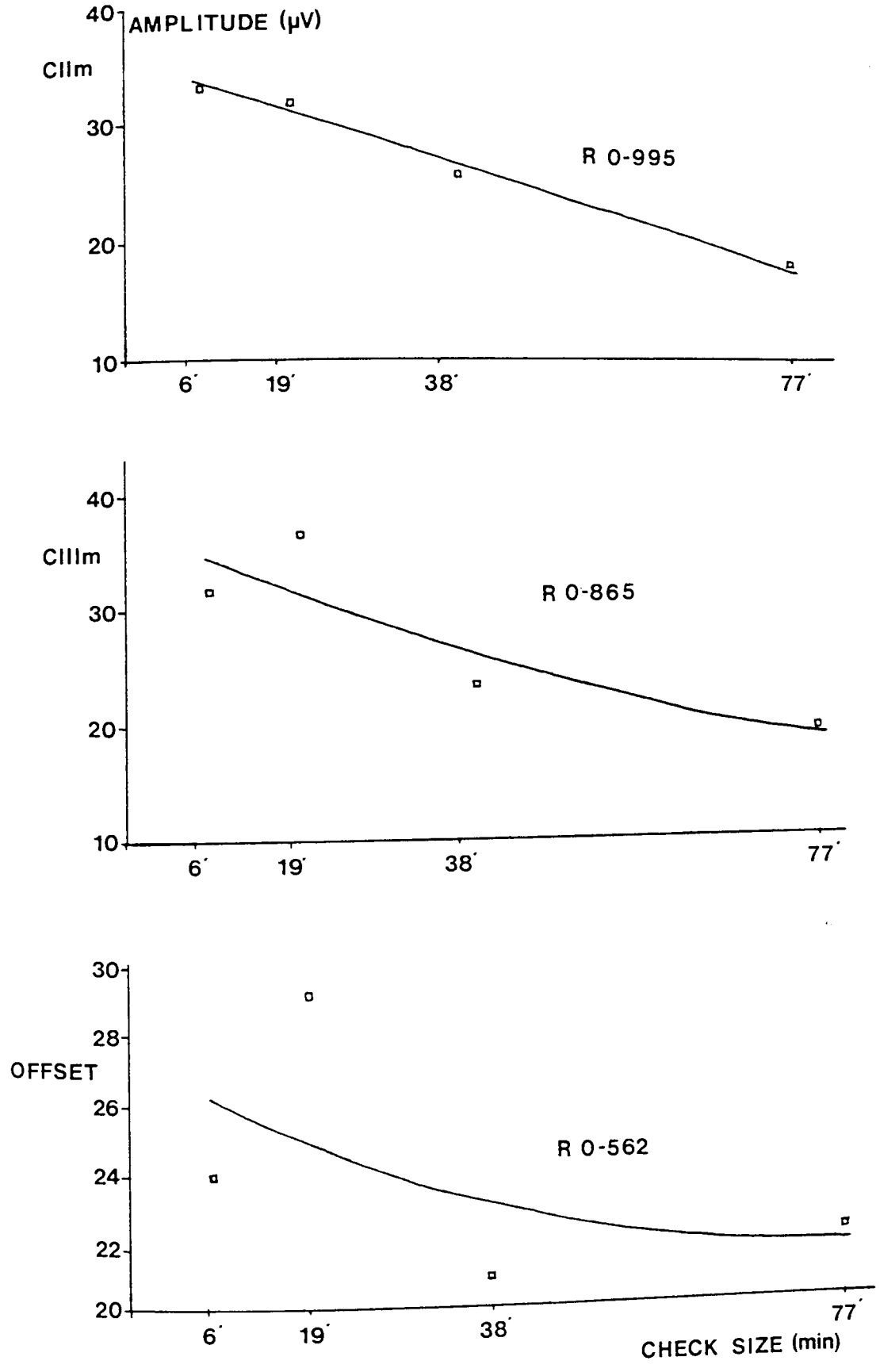

Figure 8.151 - Effect of varying check size on the mean CIIm, CIIIm and offset peak amplitudes for subjects CD, RAA, AS and SC. In each case a second order polynomial is fitted to the data, its goodness of fit indicated by R.

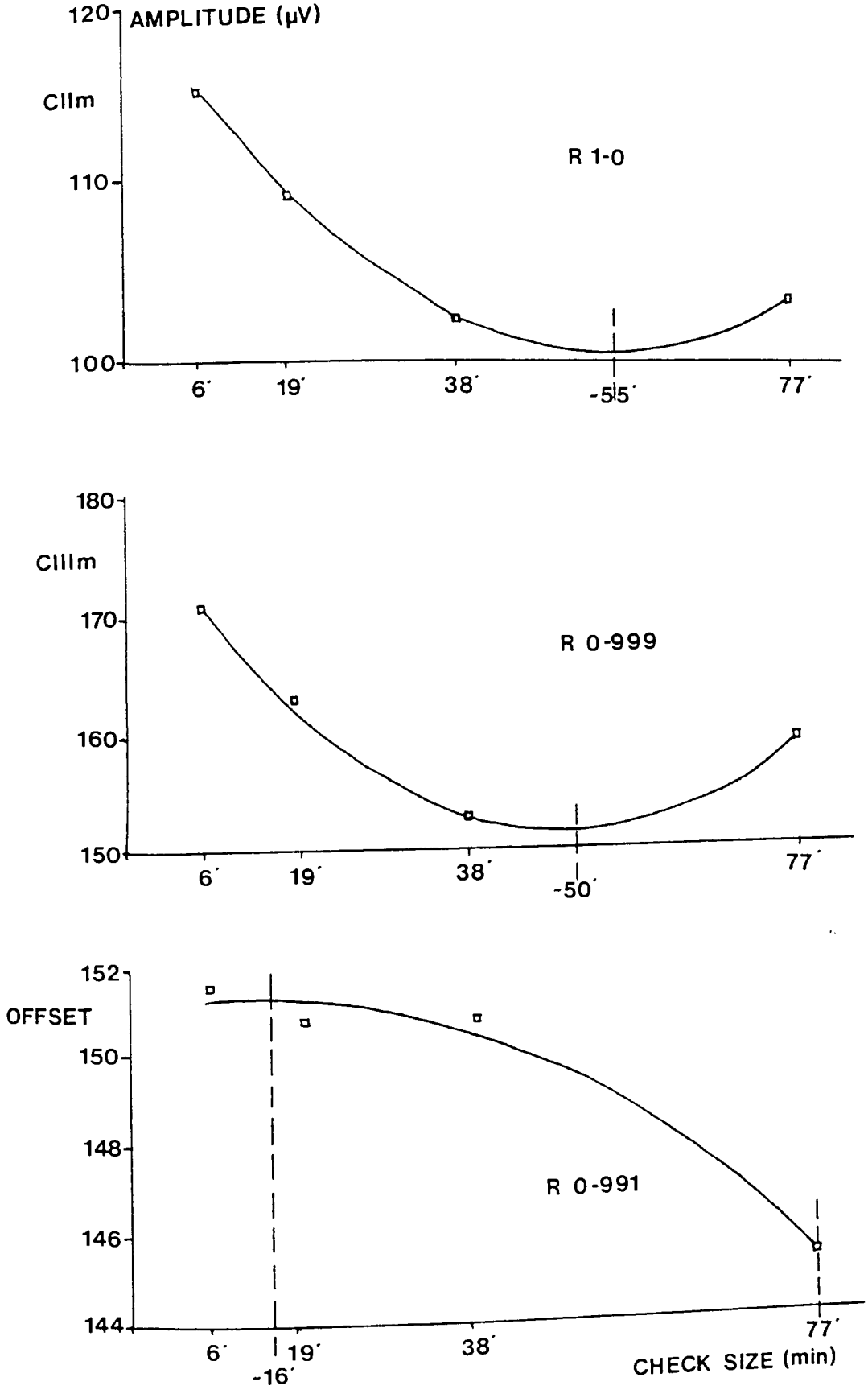

Figure 8.152 - Effect of varying check size on the mean CIIm, CIIIm and offset peak latencies for subjects CD, RAA, AS and SC. In each case a second order polynomial is fitted to the data, its goodness of fit indicated by R.

almost identical, while that of the offset shows a smaller amplitude decrease. The decrease in the goodness of fit values with each successive component would be consistent with an increase in variability with the longer latency components, possibly reflecting the effects of additional levels of neural processing. A peak response with 6' checks is consistent with the onset VEP findings of Drasdo (1980), who showed 3' to 4.5' checks to be optimal foveal stimuli. The VEP studies mentioned previously also showed that check sizes between 7.5' and 30' produced optimal responses for centrally fixated, 5° fields.

The decrease in amplitude seen with increasing check size could be explained by the optimal stimulation of progressively more peripheral retina, with a corresponding decrease in cortical activation due to the changes in cortical magnification. Ristanovic and Hajdukovic (1981) attributed the amplitude increases seen with smaller checks to both an increase in the number of contrast borders and the change in retinal receptive field size properties. The similarity between the onset and offset amplitude behaviour seen in this study differs from the VEP checkerboard findings of Torok et al (1992) who showed that the onset amplitude was check size specific, while the offset behaviour was less so. The effects of spatial frequency on latency and amplitude measures is also dependent upon the contrast levels adopted (Spekreijse et al 1973). Hence, the use of patterns of fixed contrast but varying spatial frequency produces similar VEP latency and amplitude trends as those described above. With contrast levels adjusted to a fixed multiple above threshold for each spatial frequency however, changes in spatial frequency have been shown to produce constant VEP latencies and amplitudes.

The linear amplitude versus check size relationship also differs from the findings of previous VEP studies. Drasdo (1980) and Spekreijse (1991), using a checkerboard onset stimulus and Eason et al (1970) and Ristanovic and Hajdukovic (1981) using a flashed checkerboard, all reported an inverted U shaped distribution for amplitude against check size. A sharper, inverted asymmetric U shaped distribution was found by Ristanovic and Hajdukovic (1981) with a flashed bar grating, differing from that of the checkerboard. A curvilinear relationship could explain the data in figure 8.151, producing the largest CIIm and offset amplitude response with the 19' check size. Regardless of the curve used to fit the data, both a 6' and 19' check size would fall within the predicted range of optimal foveal receptive field sizes.

Once more, these results are probably dependent on field size, as a larger field would increase the percentage of larger receptive field sizes present, thereby increasing the stimulatory capacity of the larger checks. As the magnetometer is preferentially sensitive to tangentially oriented sources (Okada et al 1987), the large amplitude responses seen with the 6' check suggests that a significant proportion of central retina must project to the medial surface of the occipital lobe, as opposed to the lateral pole surface. This assumes that the onset VEMR originates from sources within the calcarine fissure, as opposed to fissures within the lateral surfaces of the occipital lobes. This was suggested by the intersubject stability of the half field topographies (see chapter 6), and their similarity to those of the pattern reversal VEMR (Harding et al 1991). An increase in amplitude with decreased check size could also be explained by changes in the depth of each source below the scalp. This assumes that smaller checks stimulate areas of cortex closer to the occipital pole (Meredith and Celesia 1982), and that signal amplitude decreases as a function of $1/D^3$, where D is equal to the depth of the sources below the pick up coil (Wikswo 1983, Kaufman et al 1991).

The effects of check size on mean latency (figure 8.152) shows a similar trend for the CIIm and CIIIm components, which differs from that of the offset. The similarity between the CIIm and CIIIm behaviour is consistent with the amplitude trends of figure 8.151, as well as the unaveraged and averaged sequential responses presented in chapter 5. The differences between onset and offset responses would not be expected from the half field topographic study of chapter 6 however, as both onset and offset responses appeared to have analogous origins, from the same or similar cortical sources. Differences between the onset and offset amplitude trends with altering spatial frequency have been described for the VEP, the offset being likened more to the pattern reversal response (Torok et al 1992), however no reference to latency was made. If the onset and offset VEMR components do arise from equivalent cortical sources, then the latency variation might reflect differences in processing time at various stages along the visual pathways. For both onset components, a curvilinear decrease in latency of between 15 and 20ms was seen as check size increased from 6' to approximately 50'. As discussed previously, it is accepted that larger check sizes optimally stimulate larger retinal receptive fields, whose size increases with retinal eccentricity (Harter 1970). Possible explanations for the latency delays seen with smaller checks

are more varied however. Williamson et al (1978) and Okada (1982), both suggested that patterns of higher spatial frequency are subject to larger conduction and processing times. Parker and Salzen (1977), Williamson et al (1978) and Vassilev and Strashimirov (1979) have all suggested that decreasing spatial frequency could cause a shift in emphasis from the stimulation of the transient, Y cell system, to the sustained X system, which show fast and slow conduction velocities respectively. Parker and Salzen (1977) also proposed that the delay might occur within the transient system alone, reflecting increasing integration time, or it could just be a product of the retinal axon sizes of each receptive field, (the axons of the central retina being of smaller diameter and slower conduction velocity than those of the periphery). Alternatively both Drasdo (1980) and Parker et al (1982) have proposed that latency delays with increasing spatial frequency could reflect the change in emphasis between components from separate cortical origins. Drasdo (1980) proposed that the CI component detects transient activity, being deeper within the cortex than the source of the more superficial, sustained activity sensitive CII. At higher spatial frequencies, the sustained activity would begin before that of the transient, causing the CI peak to move across that of the CII.

The increase in latency as check size increases above 55' might indicate that this is the largest receptive field size within the 7x5° field, and therefore larger checks produce sub optimal stimulation. Alternatively, the increase could represent an increase in synaptic activity, processing time, or the transfer of signals to different cortical areas. An increase in onset response latency has also been reported by Spekreijse (1977), for check size increases between 40 and 80'.

The offset trend differs from that of the onset, showing a curvilinear decrease in latency of approximately 6ms, with a maximum latency for 6 to 19' checks, and a minimum at 77'. Since the amplitude variation behaved similarly for all components, the latency differences are unlikely to be caused by receptive field effects, but most likely reflect visual processing differences.

8.16 - THE EFFECT OF CHECK SIZE ON TOPOGRAPHIC DISTRIBUTION.

Topographic distributions for each subject and check size are shown in figures 8.161, 8.162 (CIIm); 8.163, 8.164 (CIIIm); and 8.165 and 8.166 (Offset) respectively, for the onset and offset responses. For all subjects, the CIm peak

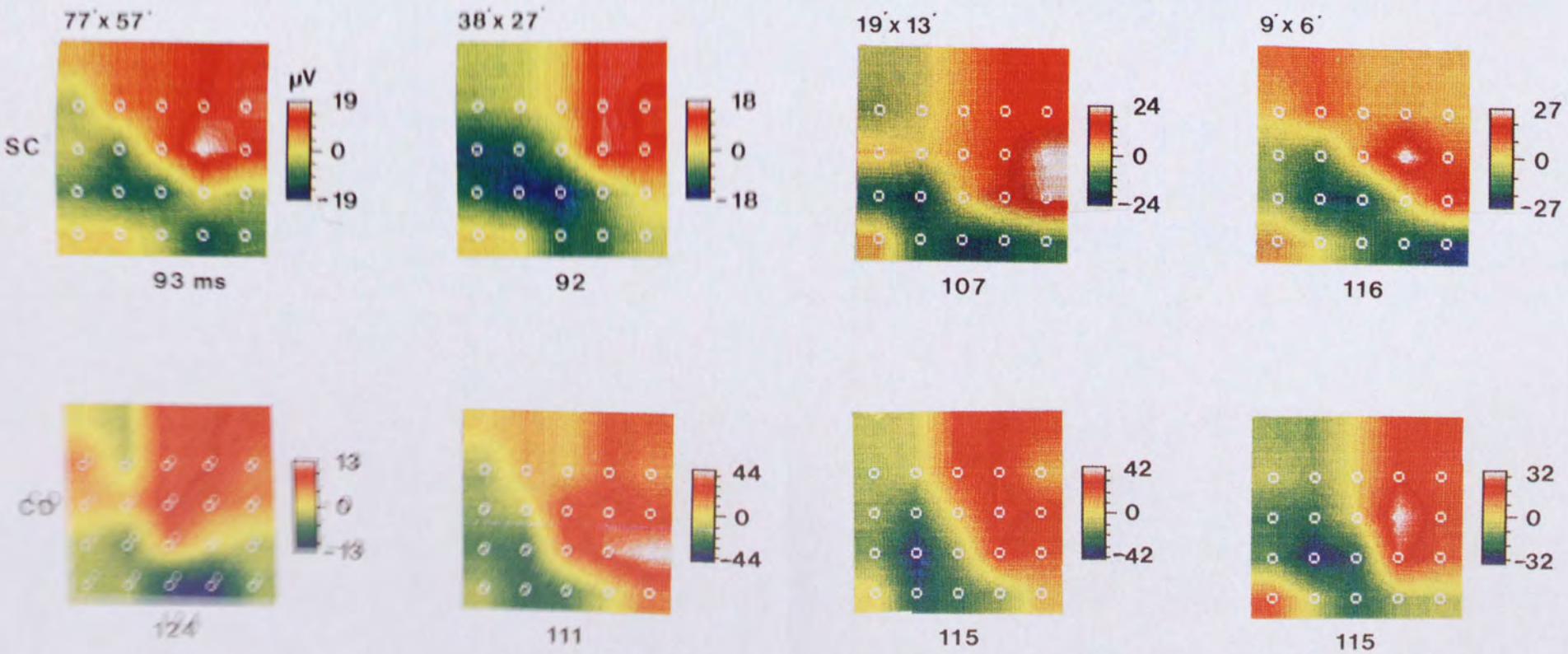

Figure 8.161 - Effect of varying check size on the full field CIIm topography of subjects SC and CD.

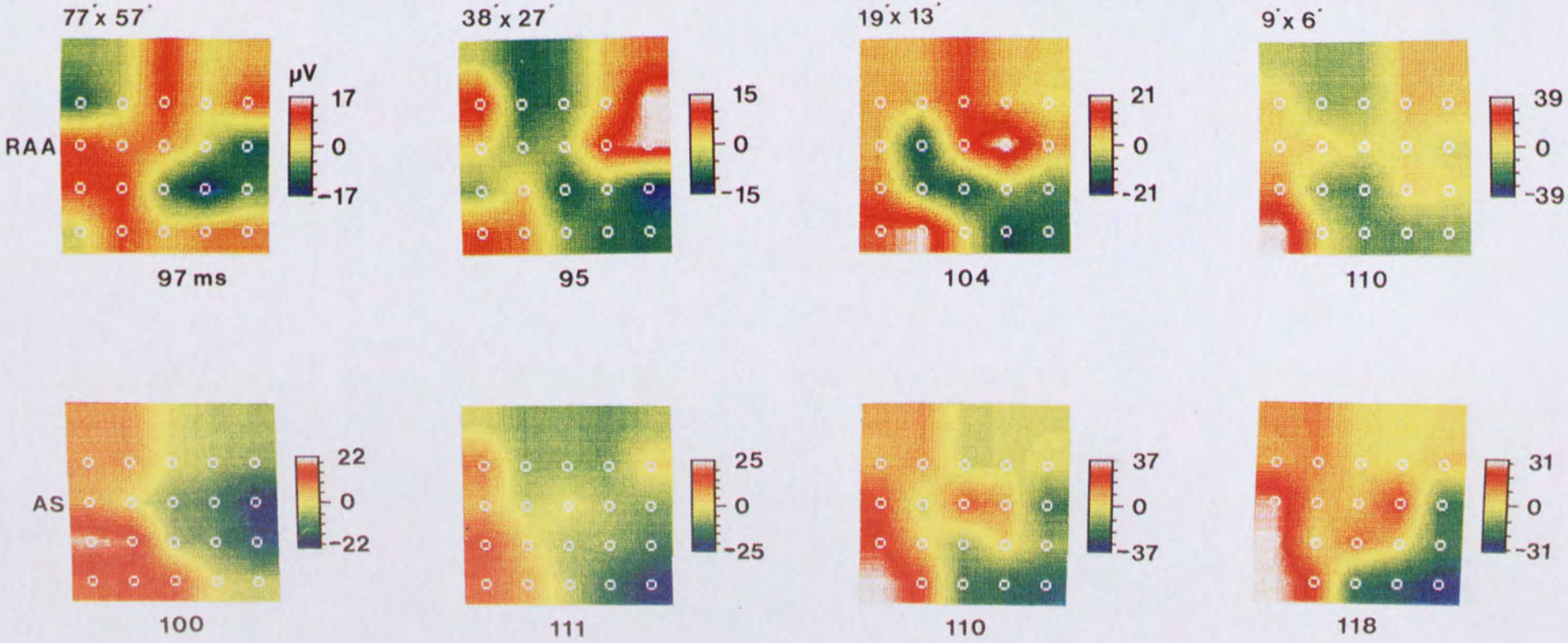

Figure 8.162 - Effect of varying check size on the full field CIIm topography of subjects RAA and AS.

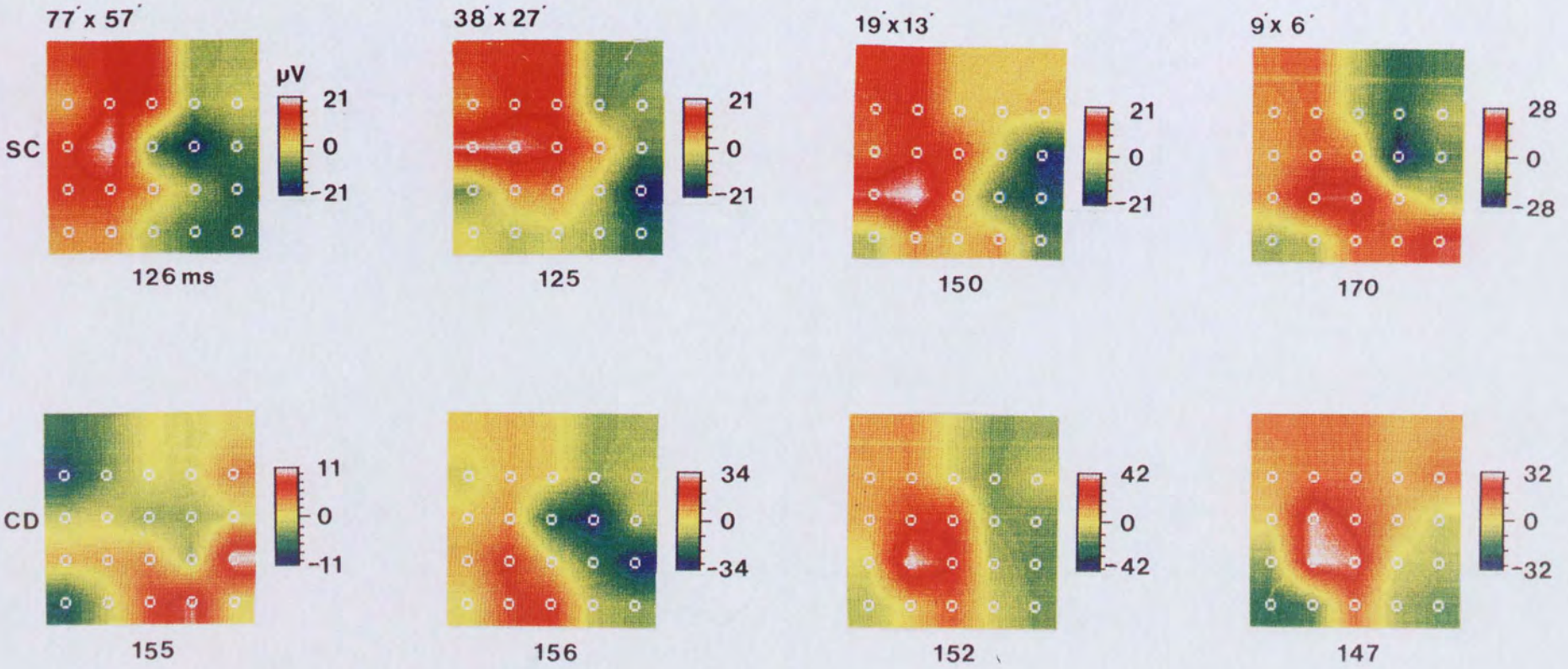

Figure 8.163- Effect of varying check size on the full field CIIIm topography of subjects SC and CD.

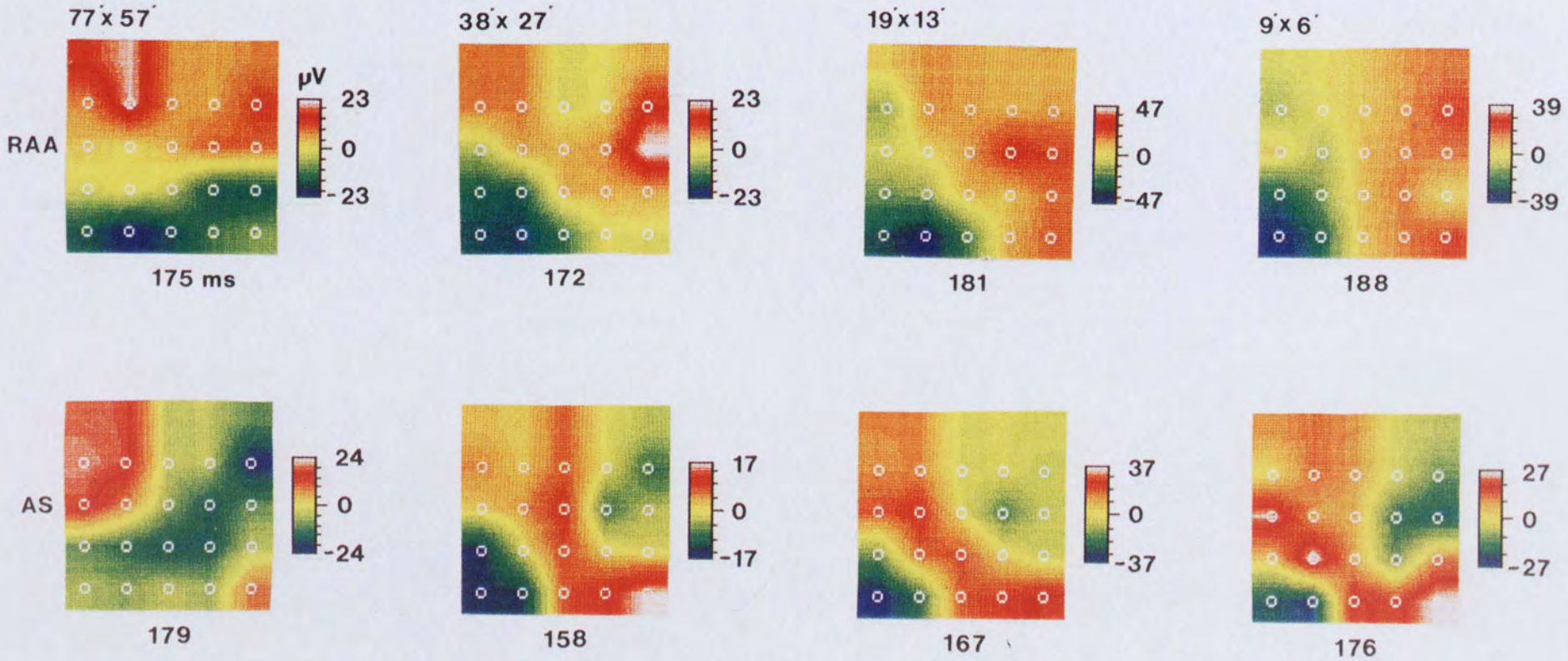

Figure 8.164- Effect of varying check size on the full field CIIIm topography of subjects RAA and AS.

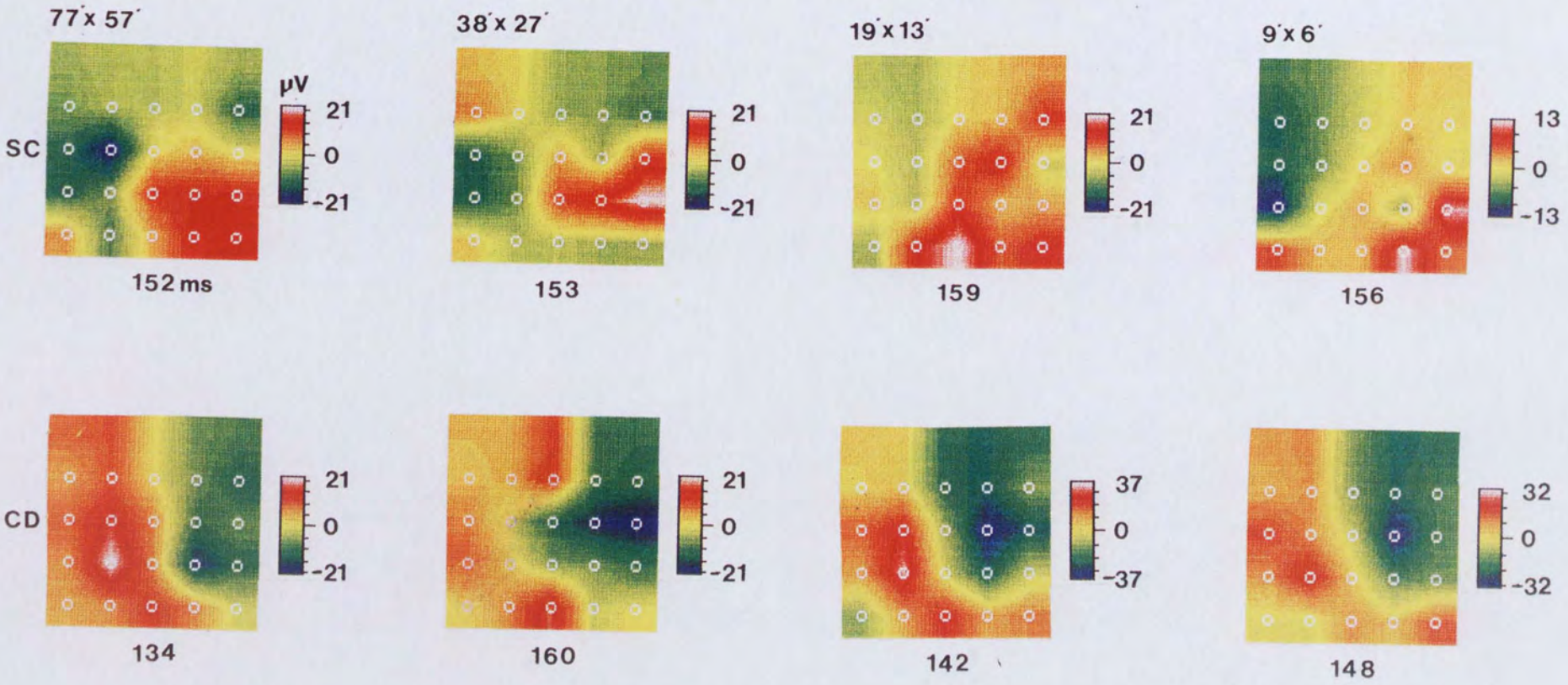

Figure 8.165 - Effect of varying check size on the full field offset topography of subjects SC and CD.

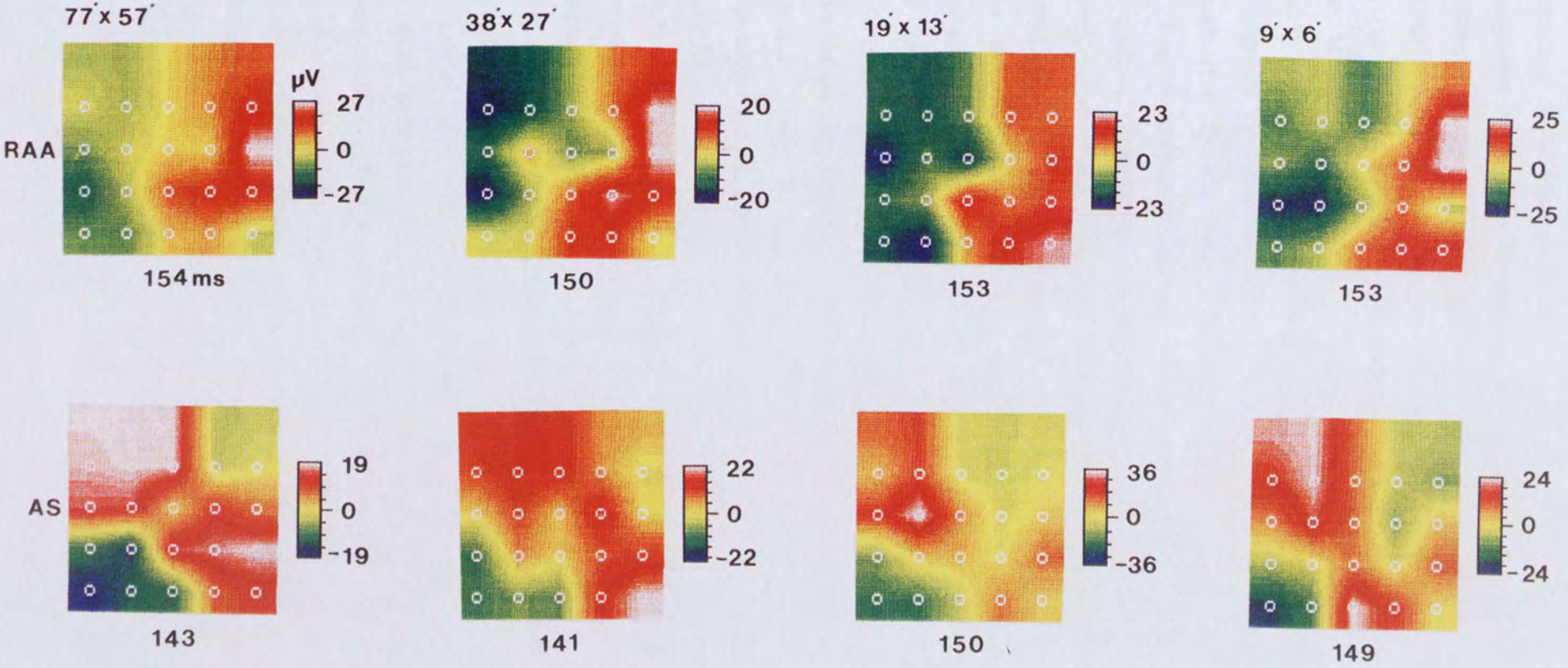

Figure 8.166 - Effect of varying check size on the full field offset topography of subjects RAA and AS.

was not stable enough to be marked with any degree of confidence, and so it has been omitted from further study.

It was proposed in chapter 6 that the behaviour of the CIIm component could largely be described by the activity of sources within the calcarine and medial fissures, organised as in the cruciform model (Jeffreys and Axford 1972 a), with a current flow away from the surface of the pia. It is accepted that increases in the size of stimulus elements causes the optimal stimulation of more eccentric regions of the retina (Meridith and Celesia 1982) and that such stimulation results in the activation of striate cortex progressively further down the calcarine fissure away from the occipital pole (Jeffreys and Axford 1972 a). For a calcarine fissure oriented normal to the scalp therefore, increasing spatial frequency would presumably produce topographies of similar overall distribution, except showing a decreasing separation between the field maxima as sources become more shallow. The MRI studies of Steinmetz et al (1989) however has shown large intersubject variation in the angle and shape of calcarine fissures. For a steeply angled fissure, decreasing check size would presumably produce a topography which showed a progressive anterior to posterior movement of the sources down the scalp, with less variation in depth. Depending upon fissure angle, trends between the two extremes could be expected, and in the case more complex angles, a mixture of positional and depth changes would be possible. Hence, it would be advantageous for interpretation, to combine the results of such topographic studies with the MRI data of the subjects involved.

The CIIm distribution of subject SC (figure 8.161) recorded to 77'x57' checks could be explained by the activity of a dipolar source in the right hemisphere, approximately 3cm above the inion and 3cm to the right, with current flow oriented away from the medial surface of the brain. A source of similar orientation could also be inferred by the field pattern over the left hemisphere, with reference to the right half field mean topography of figure 6.311. Interpretation of the left hemispheric activity with varying check size is complicated however, by the presence of multiple field areas. These fields might occur due to the effects of noise, and so further analysis will be limited to right hemispheric activity alone. As check size decreases, the region of positive field over the right hemisphere appears less diffuse, and this coupled with the increase in amplitude would be consistent with progressively shallower source activity. The position of the underlying source, as indicated

by the region of zero net field (yellow areas) also moves in an anterior to posterior direction with decreasing check size (total displacement of approximately 3cm), consistent with an origin in a calcarine fissure angled away from the perpendicular with respect to the scalp. The VEP onset findings of Parker et al (1982) also showed that the cortical origin did not alter appreciably with changing spatial frequency, as the topographical distributions remained unaltered. Unlike the half field responses presented earlier (chapter 6), the CIIIm distributions of subject SC (figure 8.163) differ from those of the corresponding CIIm, especially for the two largest check sizes. The two smaller checks give distributions which could be explained by sources in the same cortical areas as those of the CIIm, except with a current flow in the opposite direction (ie towards the surface of the pia). With the largest check size response, only one prominent field area is present to either side of the midline. If a similar cortical process to that of the CIIm is assumed, then this distribution would indicate that the sources are sufficiently deep and/or posterior on the scalp, so that the lower field maxima occur below the level of the mapping array. This would in turn suggest that either the CIIm/CIIIm source similarity does not extend to larger check sizes, or that the CIIIm component topography is more susceptible to the effects of noise. The latter is probable if one considers how the amplitude goodness of fit values shown earlier (figure 8.151) decreased with increasing component latency. Unlike the onset responses, the offset topographies of subject SC (figure 8.165) cannot all be explained by sources arranged in the cruciform model. The only response showing a predictable topography is that over the right hemisphere with 77'x57' checks, the remaining responses showing diffuse, complex field patterns. The right half field topographies presented earlier, (figure 6.311) showed a close relationship between CIIIm and offset components, therefore the differences seen here are difficult to explain. It is possible that the offset response is affected more by noise than the CIIIm, and that this is exacerbated by the large number of sources active with full field stimulation. Alternatively, the onset and offset properties could differ with changes in spatial frequency, as has been suggested for the VEP, which would mean that the earlier half field similarities were anomalous. This latter possibility seems unlikely considering the large number of subjects in which the half field similarities were found.

With subject CD, a predictable CIIm topography is seen with 9'x6' checks (figure 8.161), suggesting a current source in the left hemisphere, 1 cm above the inion and 4cm to the left of the midline, with current flowing away from the medial surface of the brain and upwards. A horizontally oriented source is seen in the right hemisphere, 2 to 3cm above the inion and 3cm to the right of the midline. As check size increases, the topographies become increasingly diffuse, with the lower field maxima appearing to be displaced below the level of the mapping array for the left hemisphere. With the largest check size, a clear dipolar pattern is seen only over the right hemisphere. The position of zero magnetic field over the right hemisphere remains relatively stable as check size increases, consistent with activity within a calcarine fissure angled perpendicular to the scalp. The largest check response is unusual since only the right hemisphere contributes to the topography. The half field response of this subject (chapter 6) showed that the right hemisphere was active even when the left hemisphere only was stimulated, and that with left and right hemispheric stimulation, the right produced the largest amplitude response. Such a full field distribution might therefore be expected if the amplitude of the right hemispheric response is sufficiently larger than that of the left to dominate the summation. Both the CIIIm (figure 8.163) and offset topographies (figure 8.165) are grossly similar to those of the corresponding CIIm, except with a reversal of field polarity, for all but the largest check size.

Interpretation of the CIIm topographies of subject RAA (figure 8.162) is complicated by the presence of multiple field areas, particularly with the two largest check sizes. With 19'x13' checks, a dipolar source could be inferred from activity over the right hemisphere, 4cm above the inion and 3cm to the right of the midline, with current flowing horizontally away from the medial surface of the brain. Assuming that the area of positive field in the lower right corner of the 77'x57' check topography represents the effects of noise, then the region of zero magnetic field would suggest that the right hemispheric source becomes more posterior over the scalp as check size decreases. Hence, the underlying current dipole is positioned 8, 5, 4 and 3cm above the inion for 77'x57', 38'x27', 19'x13' and 9'x6' checks respectively. This would be consistent with activity in a calcarine fissure angled acutely with respect to the scalp (Harding et al 1991). Activity over the left hemisphere is particularly complex for this subject, as are the CIIIm (figure 8.164) and offset (figure 8.166) field responses.

Although the full field CIIm responses of subject AS (figure 8.162) are not readily explicable by the CIIm model (See section 6.8), the 38'x27' check topography was shown to be explicable by the summation of the left and right half field CIIm responses (figure 6.7). Hence, the upper field areas from each hemispheric source both occurred over the midline of the scalp, resulting in mutual cancellation. As check size decreases below 38'x27', (figure 8.162) an area of positive field appears over the midline, spreading to the right, possibly resulting from a rotation of the underlying right hemispheric source.

The CIIIm and offset topographies (figure 8.164 and 8.166) show more predictable distributions, with suggestions of a horizontal current source in each hemisphere oriented towards the medial surface of the brain. As check size is reduced, the areas of positive and negative field for both CIIIm and offset responses remain relatively stable. The region of zero magnetic field for the left hemispheric CIIIm response (figure 8.164) shows a slight posterior displacement with smaller checks (the 9'x6' check response being between 2 and 3cm lower than that of the 77'x57' check), possibly due to activity in a calcarine fissure angled away from the perpendicular. The differences between the CIIm and CIIIm topographic trends could be used to argue against a common source origin, or alternatively, they could represent differences in half field interactions for the two components.

In conclusion, topographic interpretation is complicated for most subjects by the presence of multiple field activity, possibly caused by noise, or the interaction of activity from each hemisphere. Many subjects show less complex field distributions over the right hemisphere, which is surprising since the half field CIIm responses presented earlier produced greater amplitudes with left than right hemispheric activation (figures 6.311 and 6.321). Where inferences about underlying source activity can be made, most are consistent with CIIm activity within the longitudinal and/or calcarine fissures of the brain. If this were the case, then the responses seen with a check size of 9'x6' indicates that, although such a stimulus should predominantly activate radially oriented sources at the occipital pole, a sufficient area of tangentially oriented cortex on the medial surface must also be active. A striate origin for the VEMR CIIm is consistent with the VEP CII onset findings of Maier et al (1987) and Van Dijk and Spekreijse (1989), although others have proposed an extrastriate origin (Jeffreys and Axford 1972 a and b, James and Jeffreys 1975, Lesevre and Joseph 1979).

8.21 - THE EFFECT OF VARIATIONS IN FIELD SIZE.

The effects of altering the size and retinal position of stimulus fields on the VEP have been reported for both pattern reversal (Meredith and Celesia 1982) and pattern onset stimulation (Rietveld et al 1967, Jeffreys and Axford 1972 a and b, Barber and Galloway 1981, Lesevre and Joseph 1979). The pattern VEP response has been shown to originate predominantly from the central 3 to 4° of the visual field (Rietveld et al 1967, Blumhardt et al 1978) or the central 5 to 10° (Leuders et al 1980), which projects to sources at the occipital pole. Stimulation of more eccentric retinal locations (beyond 7 to 10°) is said to have little or no additional effect on response amplitude (Meredith and Celesia 1982, Lueders et al 1980). With onset/offset stimulation, the onset response is said to predominate from foveal stimulation (Spekreijse et al 1973), with the central 1° contributing most to the CII and CIII components (Jeffreys and Axford 1972 a and b, Spekreijse 1977), while the CI arises from stimulation outside the central 1° (Jeffreys and Axford 1972 a and b, Lesevre and Joseph 1979, Spekreijse et al 1977). The offset VEP is maximal with stimulation away from the centre of vision, by approximately 30 to 90 minutes of arc (Spekreijse 1973). The predominance of foveal stimulation in the VEP response is explicable by the projection of retinal fibres from this region to sources at the occipital pole, whose radial orientation is optimal for electrophysiological recordings.

As the VEMR is primarily sensitive to tangentially oriented sources (Okada et al 1987), such as those within the walls of fissures, an optimal response is more likely to arise from the stimulation of peripheral, rather than foveal retinal regions. This makes the assumption that the fovea projects to radially oriented sources at the pole, while the periphery projects to tangential sources in a calcarine fissure oriented perpendicular with respect to the scalp (Harding et al 1991). If the onset response originates from sources within the calcarine fissure, as has been proposed previously (chapter 6), then detectable sources of tangential orientation should occur by the stimulation of retinal regions outside the fovea. It must be remembered however, that since signal strength decreases as a function of $1/D^3$, where D is equal to the depth of the source below the pick up coil (Wikswo 1982), the evoked amplitude is also likely to decline with increasing eccentricity. The VEMR amplitude is therefore a

balance between source orientation and depth. The use of the large field sizes required for extrafoveal stimulation is also advantageous for a number of reasons. Greater patient co-operation is required to fixate small field areas (Ghilardi et al 1990); the signal to noise ratio increases with larger fields (Ossenblok and Spekreijse 1991); and fissure sources show less intersubject morphology variation than those at the pole, which varies in shape, extent of striate cortex and the presence of a lateral calcarine sulcus (Kaplan et al 1991, Ghilardi et al 1990).

8.22 - METHODS.

Full and right half field topographies were recorded on subject SC to four field sizes (14°40'x11°32', 7°20'x5°43', 3°30'x2°43' and 1°45'x1°22') full field, and (7°20'x11°32', 3°40'x5°43', 1°45'x2°43' and 52'x1°22') half field, and two check sizes (38'x27' and 19'x13'). In all cases, a contrast level of 65% was employed. Subject SC was chosen to examine if the shift in peak dominance seen with alterations in check size for this subject also occurred with altering field size. The full field responses of subject CD were recorded to fields of 7°20'x5°43' and 1°45'x5°43', to a check size of 19'x13'. Lower left quarter field topographies were also recorded on subject CD to two field sizes, however the results of this will be covered in chapter 9.

Figure 8.221 shows a scale diagram of the retinal regions stimulated by each of the full fields used. The retina can be divided into a number of concentric regions, according to their morphological structure (see chapter 3). The sizes of each zone have been obtained from morphological studies of retinal structure, as published in Adlers Physiology of the Eye (1987). Discrepancies in the sizes of these regions are evident in the literature; Ghilardi (1990) and Lesevre and Joseph (1979) used 1°30' and 5° as foveal and macular field stimuli respectively; while Harter (1970), Drasdo (1980), Ristanovic and Hajdukovic (1981) and Bodis-Wollner et al (1990) used foveal fields of 1°30', 2°30', 4° and 4°30' respectively. None of these authors defined the criteria by which they decided upon the size of a foveal stimulus, however the study of Rietveld et al (1967) did differentiate between the different foveal regions shown in figure 8.221.

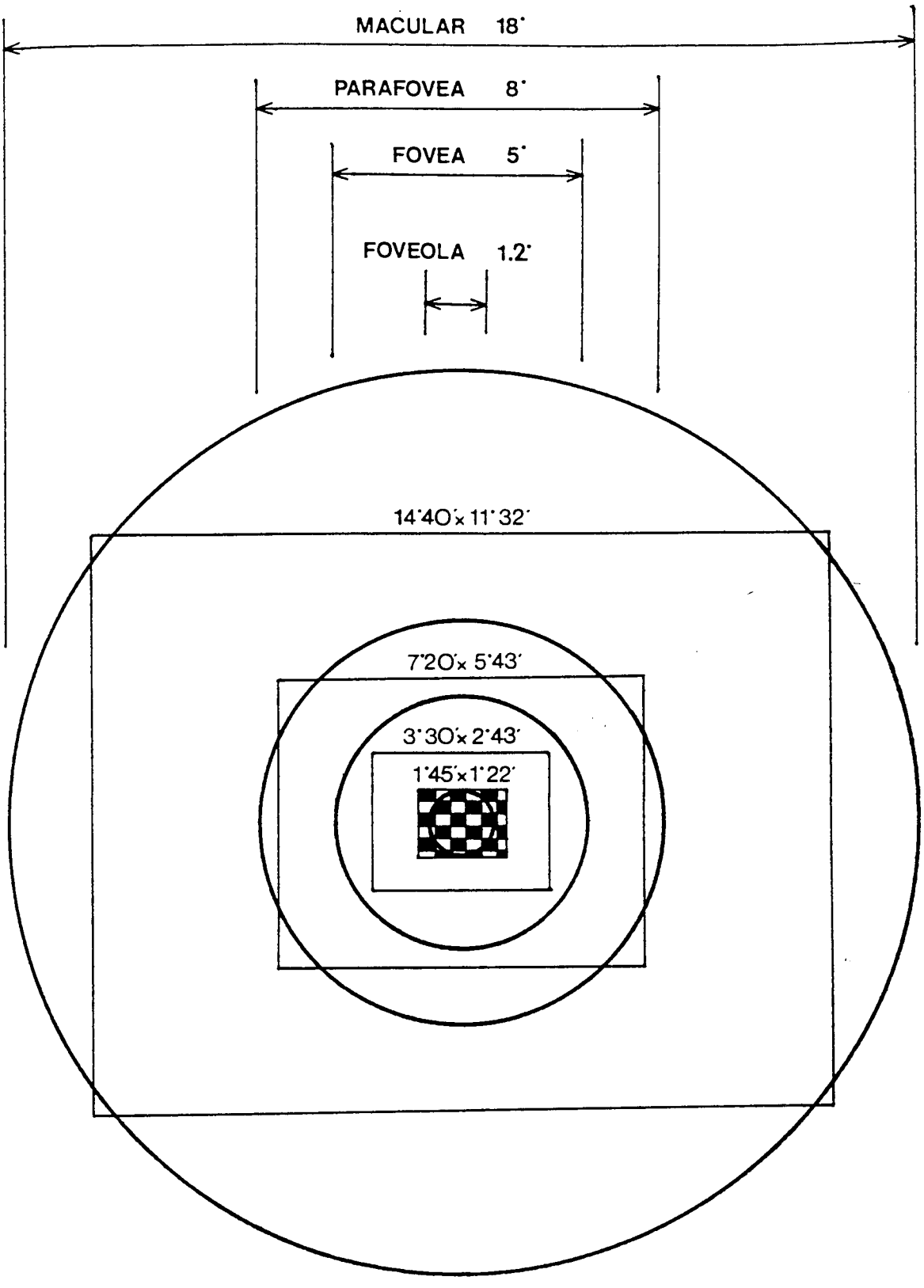

Figure 8.221 - Representation of the retinal regions onto which each of the full field stimuli used here project. The sizes of the retinal regions were obtained from Adlers physiology of the eye (1987).

8.23 - THE EFFECT OF FIELD SIZE ON LATENCY AND AMPLITUDE.

Figure 8.231 shows latency versus field size plots for the full field onset components to 38'X27' and 19'X13' checks, and the offset peak to 38'x27' checks, presented full and right half field.

A latency decrease of approximately 5ms occurs with decreasing field size for the full field peaks with 19'x13' and 38'x27' checks, however no trends are apparent with half field stimuli. A latency decrease has also been described for the VEP onset CI component as stimulation moves from peripheral to foveal retina (Barber and Galloway 1981), although Bodis-Wollner et al (1990) reported no latency trends. Although no consistent amplitude changes are apparent for the VEMR data, previous authors have shown trends for the VEP to pattern onset, reversal and flash stimuli. Ermolaev and Kleinman (1984) showed that the onset CII amplitude was maximal with foveal stimulation; Lueders et al (1980) showed an increase in the flash P2 amplitude with stimulation up to approximately 10°; and Bodis-Wollner et al (1990) showed that the pattern reversal N70 and P100 amplitudes did not increase with stimulation beyond the central 6°. As mentioned previously, the VEP amplitude peak for foveal stimulation can be explained by cortical source orientation and cortical magnification. Such comparisons are less easily made for the VEMR however since amplitude is dependent upon both source orientation and depth.

Figure 8.232 shows the prominent waveform peak of subject SC recorded full field to each check and field size. Each peak is marked either CIIm or CIIIm by reference to topographic distribution, and it is evident how confusion in peak identification could arise. The response to all stimuli shows a shift in prominence from an early peak (at approximately 100ms), to a later peak (approximately 140ms) as field size decreases below 7°20'x5°43' and 3°40'x5°43' for full and half field stimulation respectively. Since the topography of the 100ms peak could be explained by the activity of sources organised as with the CIIm for all stimulus conditions, this change in peak prominence could be similar to that seen with changes in check size. However, the trends seen with altering field size and check size appear contradictory. Hence, the waveform peak which produces a predictable CIIm topography becomes dominant as field size increases (ie with stimulation of sources further from the occipital pole, along the medial surfaces of the lobes), and as check size decreases (ie as the cortical sources optimally stimulated move towards the occipital pole) (Jeffreys

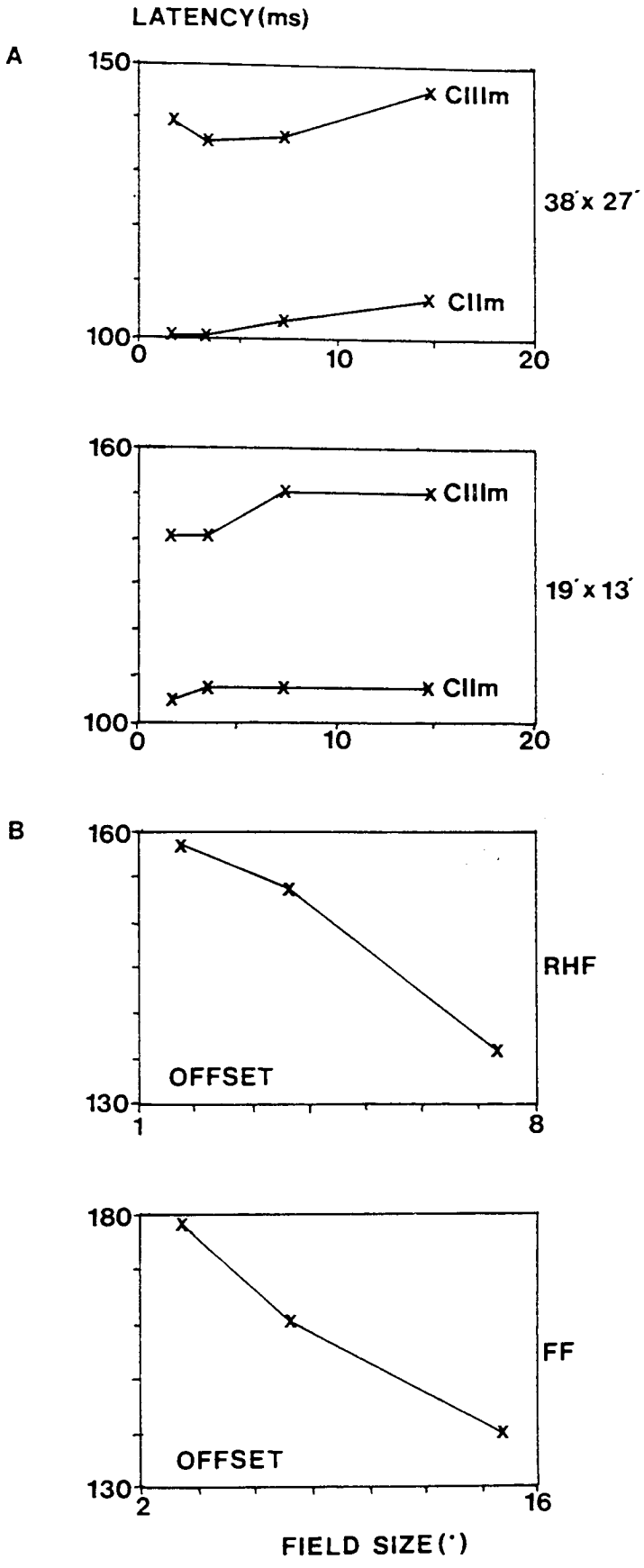

Figure 8.231 - The effect of varying field size on the latency of the full field CIIm and CIIIm peaks to check sizes of 38'x27' and 19'x13' (**A**), and the offset peak latency to 38'x27' checks presented full and right half field (**B**).

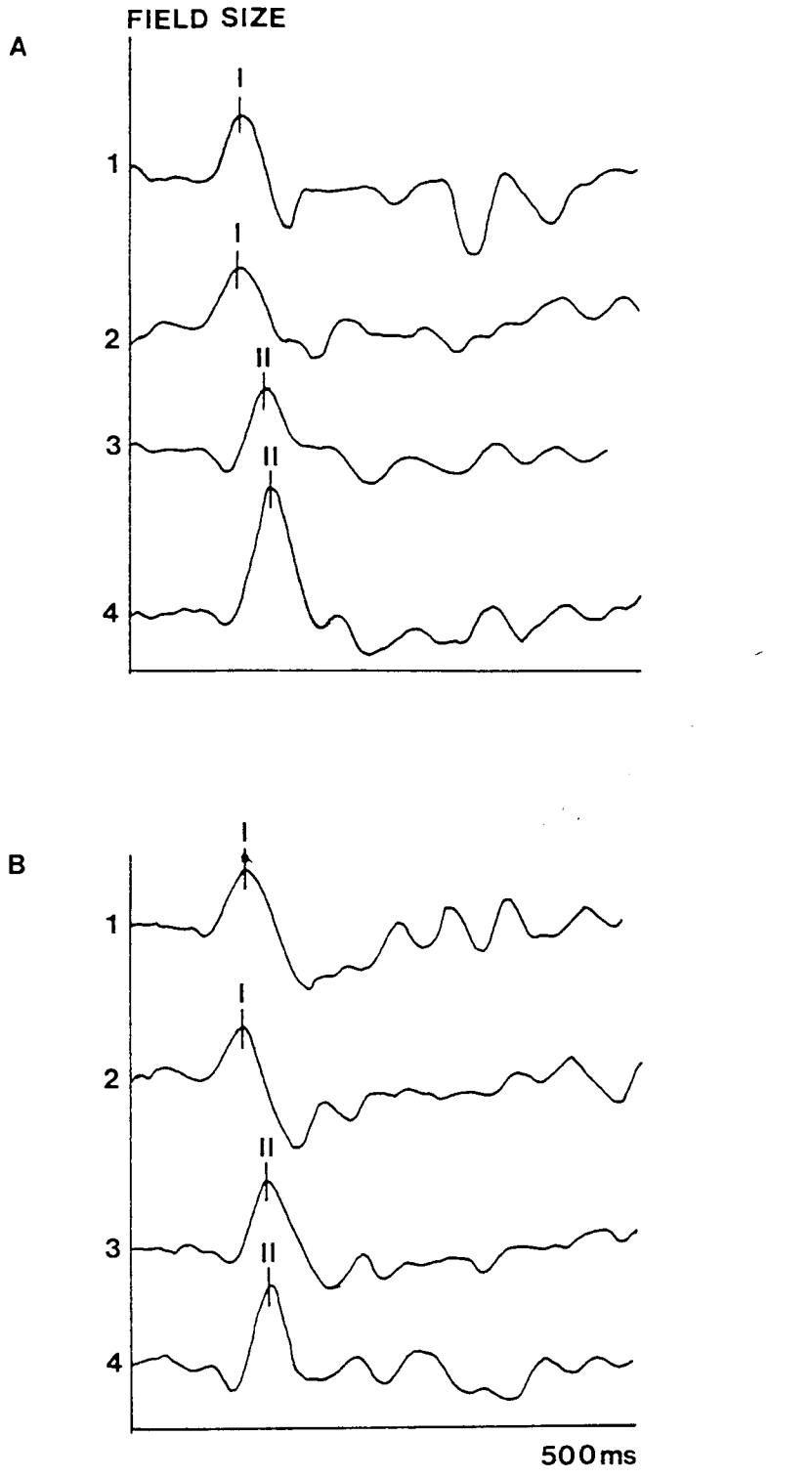

Figure 8.232 - A selection of full field waveforms of subject SC, recorded with check sizes of 38'x27' (**A**) and 19'x13' (**B**), to four different field sizes. The most prominant peak is identified as either CIIm (I) or CIIIm (II), by reference to the topographic distributions of each. This illustrates the need for topographic information when identifying waveform peaks

and Axford 1972 a). These apparent differences could be explained by consideration of the volume of cortex stimulated by each stimulus. For a fixed field size, a decrease in check size would progressively stimulate more foveal regions of the retina, resulting in an increased volume of cortex stimulated due to a cortical magnification effect (Meredith and Celesia 1982). By contrast, with a fixed check size, increasing the size of the stimulus would allow progressively more peripheral retina to be stimulated, and even if the check size used was not ideal for all of the retinal receptive fields present, the amount of cortex stimulated should still increase. With reference to chapter 6, it would appear that a predictable full field distribution must occur when the number of cortical sources contributing to the summated half field response are increased. Presumably, the larger source number could help to 'cancel out' the effects of any variation between the constituent field responses which contribute to the summation.

The similarity between the effects of check and field size on the topographic predictability of the dominant waveform peak was further tested by examining full field responses of subject CD, to fields of 7°20'x5°43' and 1°45'x1°22'. This subject displayed a dominant waveform peak of CIIm topography regardless of changes in check or field size, which again suggests that the two parameters might affect the VEMR in a similar manor. If the magnetometer were to be used for single point recording with a full field stimulus, the largest waveform peak within the first 200ms could only be assumed to represent activity of CIIm sources if small check sizes (below 19'x13'), and/or large field sizes (at or above 7°20'x5°43') were used.

The effect of field size on the offset response showed a number of differences to that of the onset. For both full and half field stimulation with 19'x13' checks, an offset peak could not be marked with any confidence for any field size. Vassilev et al (1983) also showed that VEP offset peaks could not be obtained with small check sizes. With 38'x27' checks, no peaks were evident with the smallest fields (1°45'x1°22' full field and 52'x1°22' half field). These findings would be consistent with the poorer signal to noise ratios obtained with more local stimuli (Ossenblok and Spekreijse 1991), and the effects of cortical magnification. With 38'x27' checks, the latency of the offset peaks increased progressively as field size decreased, showing a total increase of 38.09ms and 22.46ms for full and half fields respectively (figure 8.231B). This again differs from onset stimulation, as latencies decreased in that case with

smaller fields, the magnitude of latency change being 4 to 7 times smaller for the onset. The latency trend of the offset response is more easily explicable relative to the anatomy of the visual system, than that of the onset, considering the transmission velocities of the retinal fibres at differing eccentricities (chapter 3).

8.24 - THE EFFECT OF FIELD SIZE ON TOPOGRAPHIC DISTRIBUTION.

The topographic distribution for the CIIm, CIIIm and offset components are shown for full (8.241 and 8.242) and half (8.243 and 8.244) field stimuli, to each check size. As mentioned previously, no offset peaks were apparent with 19'x13' checks. The CIIm distribution for the 7°20'x5°43' response to 19'x13' checks (figure 8.242A) could be explained by the activity of an equivalent current source in each hemisphere, with current flow directed away from the medial surface of the brain. Interpretation of the larger field response is less clear, since a positive field area is present in the upper left hand corner of the mapping array, while that seen previously in the lower left corner is absent. With the two smaller fields, a single area of magnetic field appears to each side of the midline, which could occur if the sources mentioned previously were located more posteriorly, resulting in field areas which arise below the level of the mapping array. Alternatively, it could suggest the activity of an equivalent current source oriented vertically over the midline, with current flowing down the scalp for the CIIm and upwards for the CIIIm. This latter explanation might occur if the fields below 3°40'x2°43' predominantly stimulated sources at the pole, and the angle of the calcarine fissure were sufficiently steep to give polar sources a significant tangential component (Harding et al 1991). The problem with this latter explanation however, is that the source orientations would suggest that the direction of current flow varied between sources at the pole and those within the fissure. Hence, for the CIIm, current would flow away from the pia surface for sources within the fissure and towards it at the pole. An opposite polarity of neuronal current flow such as this has been proposed by Butler et al (1987) for foveal and extrafoveal VEP activity with stimuli of equal spatial frequency. To resolve this problem, the 1°45'x1°22' stimulus response was re-recorded using a more extensive mapping array of 35 locations (chapter 4). Both the CIIm and CIIIm topographies (figure 8.242B) could be explained by the activity of an

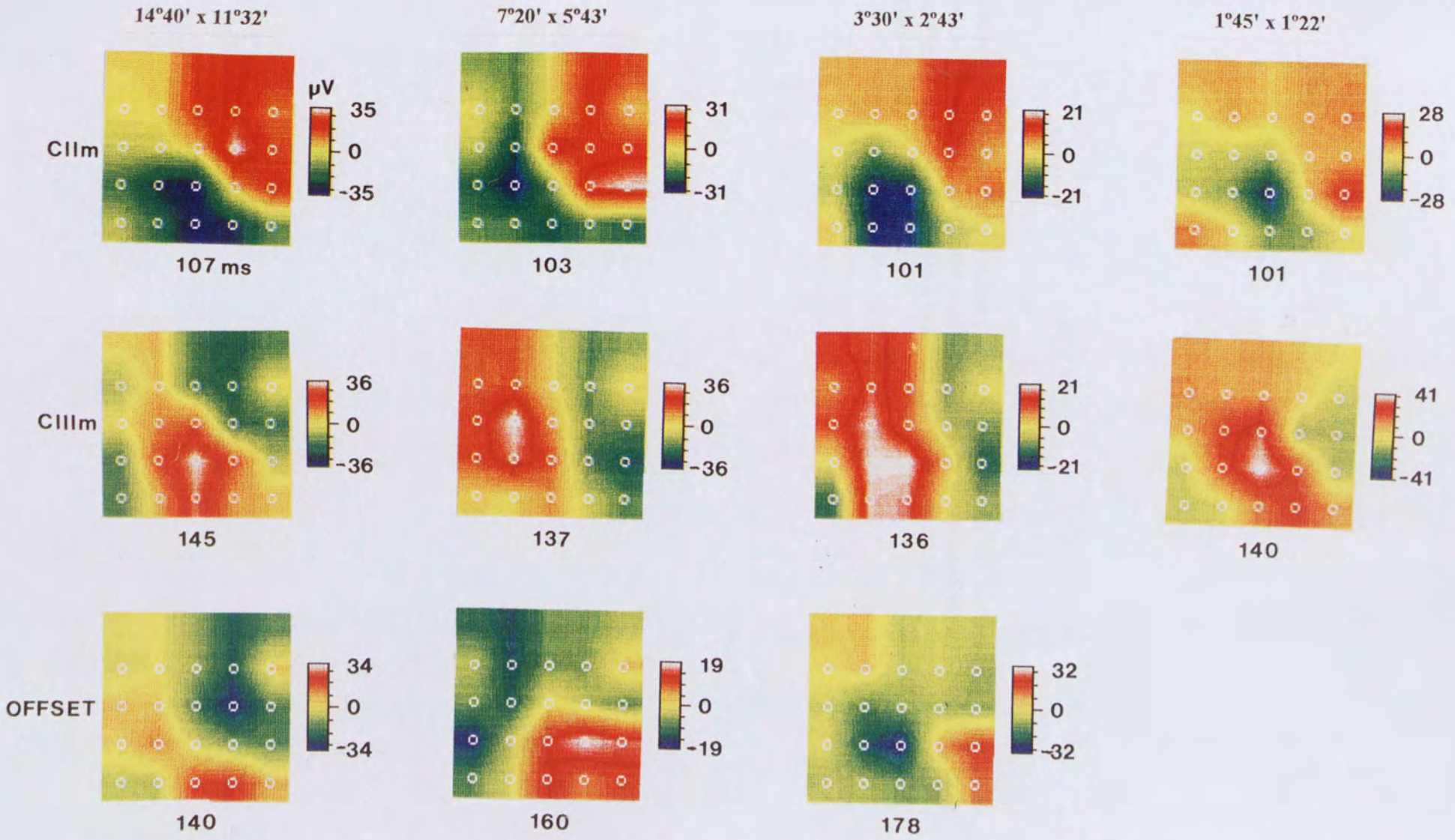

Figure 8.241 - Effect of varying field size on the full field CIIm, CIIIm and offset topographies of subject SC to a 38'x27' check size.

Figure 8.242 - Following Page - Effect of varying field size on the full field CIIm and CIIIm topographies of subject SC to a 19'x13' check size (**A**). Also shown is the full field CIIm and CIIIm topographies of subject SC, recorded to a check size of 19'x13' and field size of 1°45'x1°22', over a 35 point mapping array (**B**).

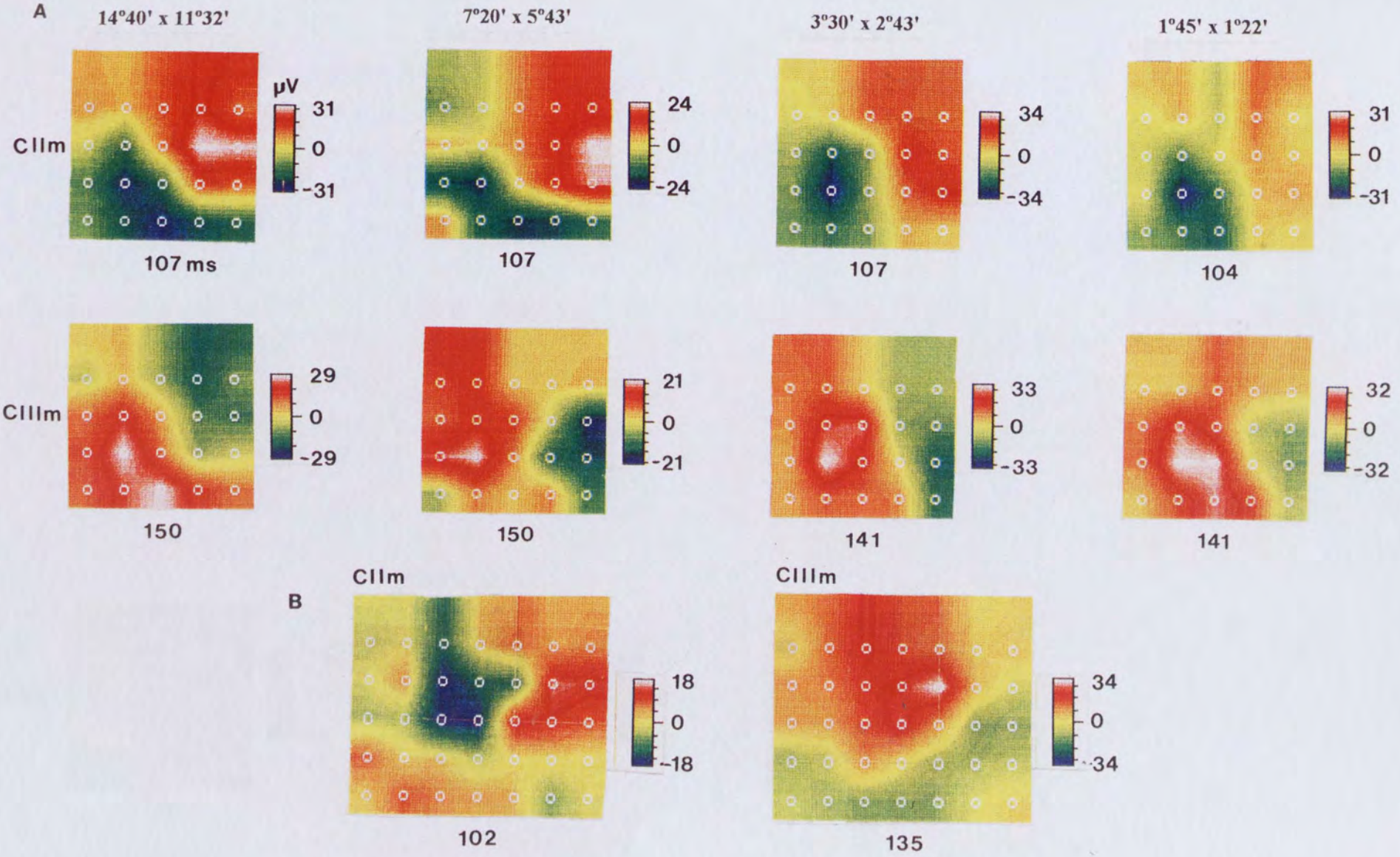
A
14°40' x 11°32'
7°20' x 5°43'
3°30' x 2°43'
1°45' x 1°22'
CIIm
CIIIm
μV
31
0
-31
24
0
-24
34
0
-34
31
0
-31
29
0
-29
21
0
-21
33
0
-33
32
0
-32
107 ms
107
107
104
150
150
141
141
B
CIIm
CIIIm
18
0
-18
34
0
-34
102
135

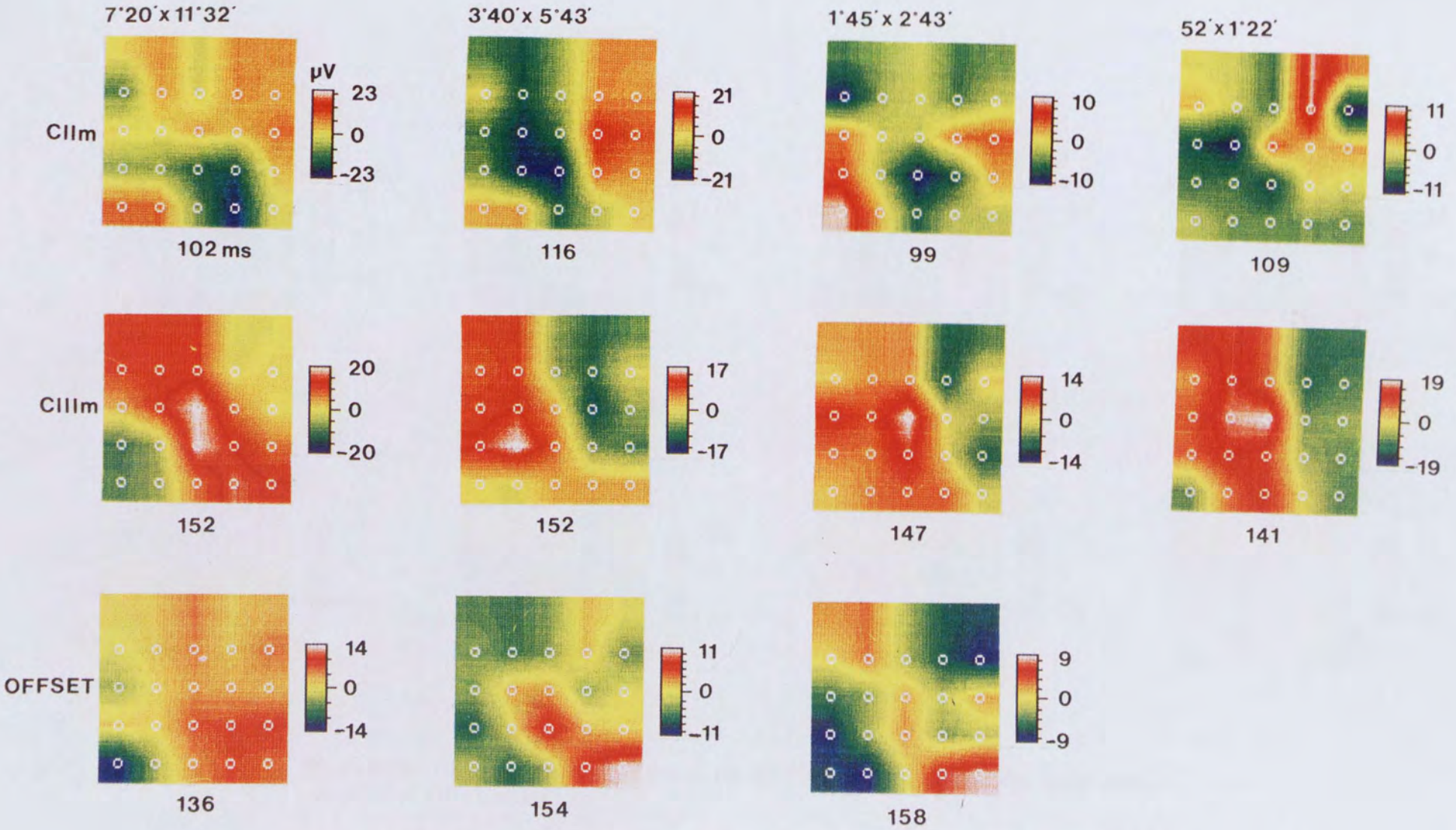

Figure 8.243 - Effect of varying field size on the right half field CIIm, CIIIm and offset topographies of subject SC to a 38'x27' check size.

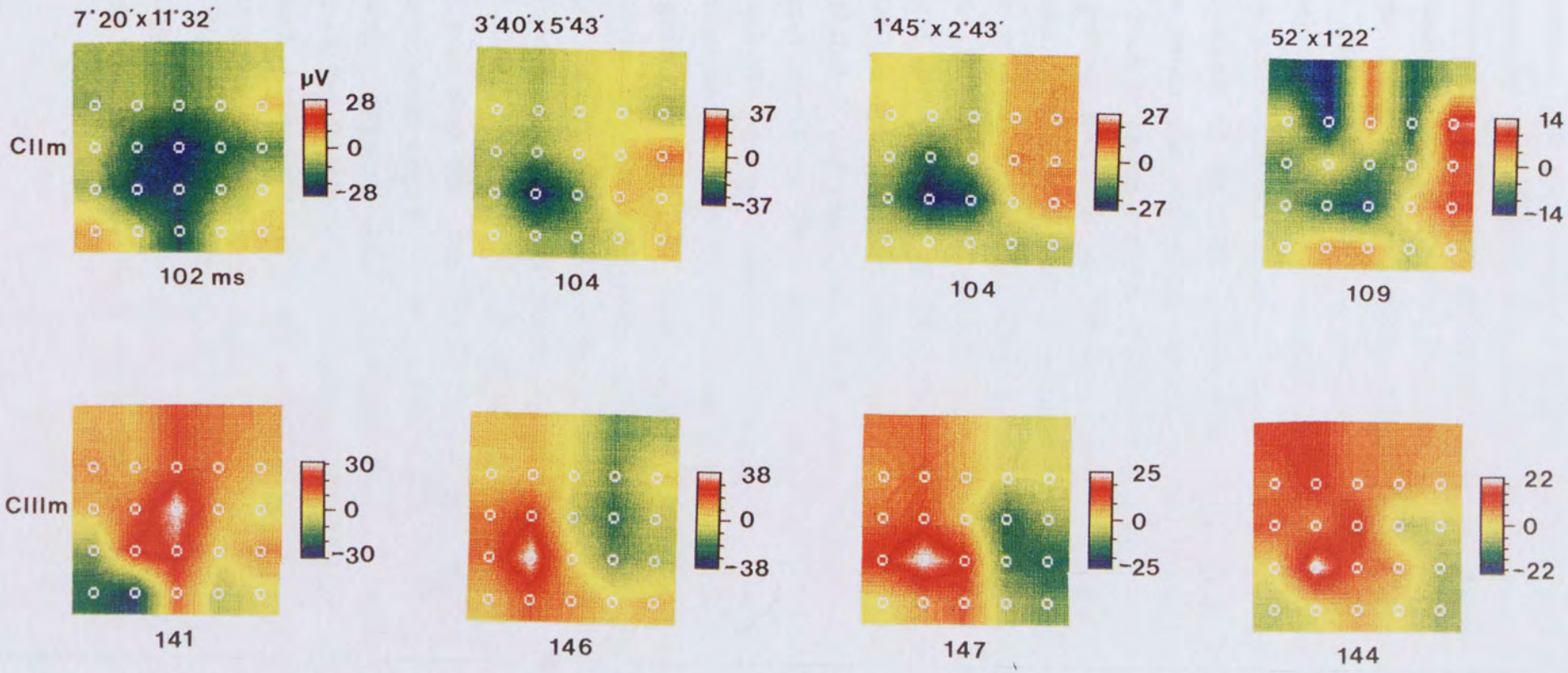

Figure 8.244 - Effect of varying field size on the right half field CIIm and CIIIm topographies of subject SC to a 19'x13' check size.

equivalent current source in each hemisphere, therefore it would appear that reducing stimulus field size results in a slight anterior to posterior movement of the sources, by approximately 2cm. Such a movement would be consistent with the progressive stimulation of central retina at smaller field sizes, and the corresponding shift in cortical projection to cortical sources nearer the occipital pole, along an acutely angled calcarine fissure (Harding et al 1991). This would also suggest that field sizes as small as 1°45'x1°22', must have sufficient representation on the medial surface of the occipital lobe, to produce tangentially oriented sources. Lesevre and Joseph (1979) also noted a posterior movement of the VEP CII and CIII onset sources with smaller field sizes, to the extent that with foveal stimulation, the response peaked below the level of the inion in certain subjects. Maclin et al (1982) studied the VEMR to a sinusoidal grating presented at different retinal eccentricities using semi-circular annuli, and showed that increasing eccentricity caused an increase in the depth of sources which remained at the same scalp positions. Such a finding could be attributed to the stimulation of sources along a calcarine fissure oriented perpendicularly to the scalp. The use of annuli is preferential for monitoring changes in source depth, as the contributions from the central retina are excluded with increasing field size. Problems with such stimuli include a poor signal to noise ratio, resulting from a reduction in cortical stimulation and the increased difficulty of maintaining stable fixation.

Full field stimulation with 38'x27' checks (figure 8.241) produces CIIm and CIIIm of gross similarity to those with 19'x13' checks (figure 8.242), particularly over the right hemisphere. The position of zero magnetic field for the right hemispheric CIIm activity does not alter appreciably with decreasing field size, unlike the results for 19'x13' checks. This could be explained if stimulation with 19'x13' checks activated cortical regions nearer the occipital pole than that with 38'x27' checks, and the calcarine fissure was angled acutely with respect to the scalp. The behaviour of the offset component with changes in field size (figure 8.241) is difficult to interpret. Hence, although the 14°40'x11°32' field topography is explicable by a current source in each hemisphere, of larger amplitude to the right, smaller field responses are more complex.

The half field topographies of figure 8.243 and 8.244, show differences in behaviour to the two check sizes, not apparent with full field stimulation. For 38'x27' checks (figure 8.243), the CIIm distribution for the two largest field

sizes are consistent with a current source in the left hemisphere, 1 to 2cm above the inion, rotated clockwise from the horizontal. The largest field response is complicated by the presence of additional field areas in the upper left hand corner of the distribution, possibly attributable to the effects of noise. The presence of field areas over the ipsilateral hemisphere were discussed more fully in section 6.31. With the two smaller field sizes, the distributions become more complex, of lower amplitude and diffuse, possibly reflecting a reduction in signal to noise ratio. The CIIIm distributions differ from those of the CIIm, such that a consistent field pattern is apparent over the left hemisphere for all field sizes. The robust nature of the CIIIm with changes in field size was also shown in section 8.23, as its waveform peak became dominant over that of the CIIm with smaller field sizes. The offset topographies also become increasingly complex and diffuse as field size decreases, but with no apparent trends.

The CIIm and CIIIm half field distributions with 19'x13' checks (figure 8.244) have more focal field maxima, which are less affected by reductions in field size than those seen with 38'x27' checks. With the exception of the 7°20'x5°43' field response, the contralateral hemispheric activity displays a single field area, consistent with a source low on the scalp relative to the mapping array (as discussed for the full field response of figure 8.242B). As field size decreases, the topographic distributions remain relatively consistent down to 1°45'x2°43' for the CIIm and 52'x1°22' for the CIIIm. Figure 8.245 shows a representation of the half field stimuli used, onto which annuli have been superimposed to represent the retinal regions in which optimal stimulation could occur for each check size. The size of these regions has been arrived at by assumptions made from the VEP work of Eason et al (1970), Harter (1970), Regan and Richards (1971) and Bodis-Wollner (1990). Although simplistic, the changes in the retinal area stimulated depicted in figure 8.245, and the cortical projections which would follow, can explain the half field findings of figures 8.243 and 8.244. Hence, the majority of the 19'x13' check annulus appears in all four field sizes, and a relatively consistent topographic distribution is seen for each. As the 38'x27' check annulus falls around the periphery of that of the 19'x13' check, its presence is predominantly seen for the two larger field sizes, and it is these which produce a predictable topography with respect to the mean right half field data of section 6.31.

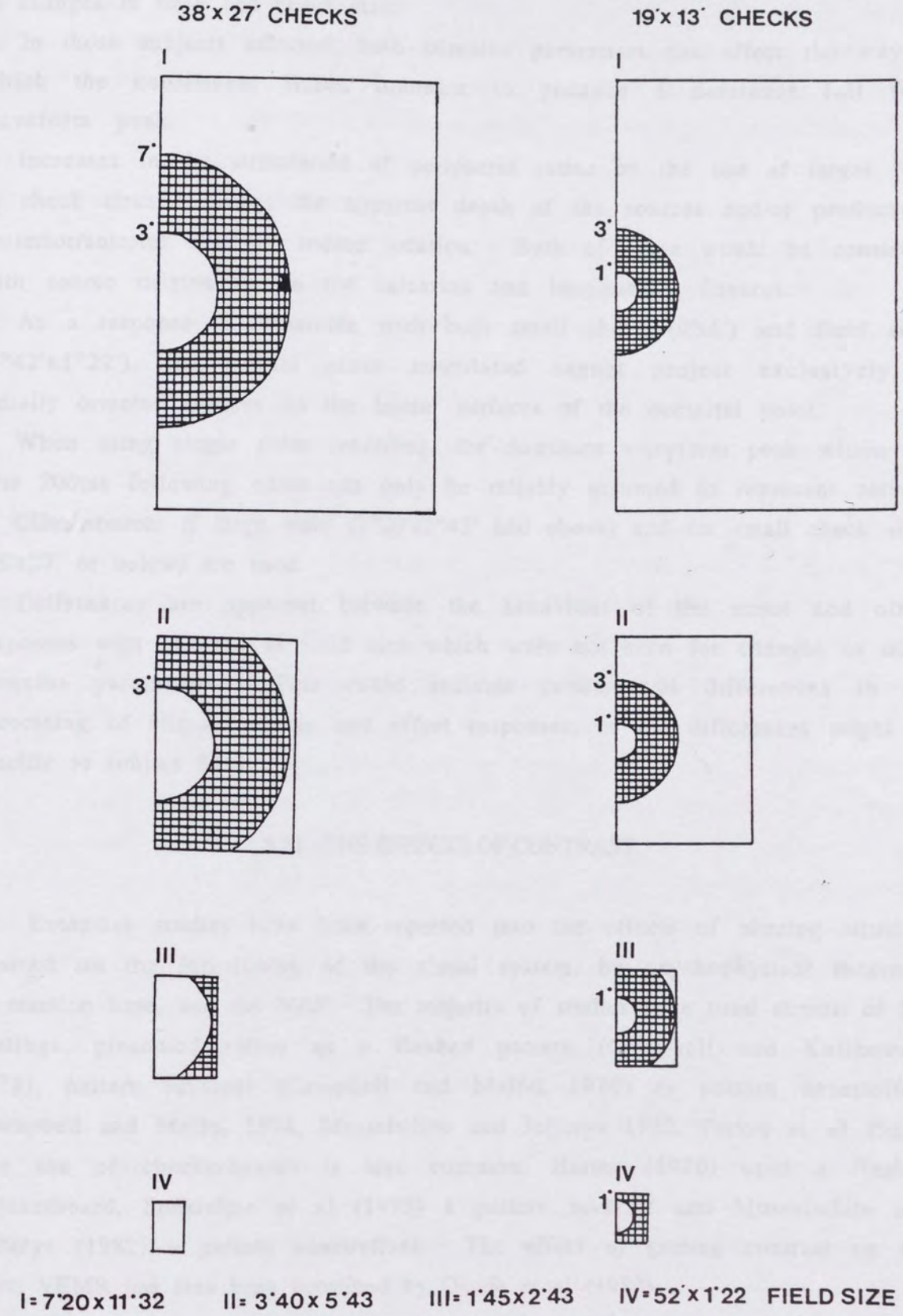

Figure 8.245 - Proposed model for the area of retina optimally stimulated (shaded area) for each half field size (rectangular area) with 38'x27' and 19'x13' checks.

In conclusion, a number of similarities are evident for the VEMR behaviour to changes in field and check size.

1. In those subjects affected, both stimulus parameters can affect the way in which the constituent fields summate to produce a dominant full field waveform peak.
2. Increases in the stimulation of peripheral retina by the use of larger field or check sizes increases the apparent depth of the sources and/or produces a posterior/anterior shift in source location. Both of these would be consistent with source origins within the calcarine and longitudinal fissures.
3. As a response is detectable with both small check (9'x6') and field sizes (1°42'x1°22'), the retinal areas stimulated cannot project exclusively to radially oriented sources on the lateral surfaces of the occipital poles.
4. When using single point recording, the dominant waveform peak within the first 200ms following onset can only be reliably assumed to represent activity of CIIm sources if large field (7°20'x5°43' and above) and /or small check sizes (38'x27' or below) are used.
5. Differences are apparent between the behaviour of the onset and offset responses with changes in field size which were not seen for changes in other stimulus parameters. This could indicate fundamental differences in the processing of stimulus onset and offset responses, or the differences might be specific to subject SC.

8.31 - THE EFFECTS OF CONTRAST.

Extensive studies have been reported into the effects of altering stimulus contrast on the functioning of the visual system, by psychophysical measures of reaction time, and the VEP. The majority of studies have used stimuli of bar gratings, presented either as a flashed pattern (Campbell and Kulikowski 1972), pattern reversal (Campbell and Maffei 1970) or pattern onset/offset (Campbell and Maffei 1974, Musselwhite and Jeffreys 1982, Parker et al 1982). The use of checkerboards is less common, Harter (1970) used a flashed checkerboard, Spekreijse et al (1973) a pattern reversal and Musselwhite and Jeffreys (1982) a pattern onset/offset. The effect of grating contrast on the onset VEMR has also been described by Okada et al (1982).

As the sensitivity of the visual system to stimuli of various spatial frequencies is also affected by their contrast (Spekreijse et al 1973, Campbell and Maffei

1974), the majority of psychophysical studies have been concerned with the determination of contrast sensitivity functions. Since these provide a measure of the contrast at which a stimulus pattern is just visible, the contrast levels studied tend to be very low. By recording the VEP to larger, suprathreshold contrast levels, and extrapolating the resulting data to zero, as a function of log contrast, similar threshold values have been obtained for each technique (Spekreijse et al 1973, Musselwhite and Jeffreys 1982).

The purpose of this study is to observe how the contrast levels available on a commercial TV stimulator affect the VEMR. As the contrasts used are much greater than those at threshold, the results are unlikely to be directly comparable with those of previous studies.

8.32 - METHODS.

Four subjects were studied topographically (CD, RAA, SC and AS), to a full field stimulus of 7°20'x5°43', with checks of 38'x27'. Three contrast levels were available, 15.38%, 65.97% and 93.25%, or 0.15, 0.66 and 0.93 respectively, using the equation :- contrast = (Lmax-Lmin)/(Lmax+Lmin) (Parker et al 1982). The largest contrast levels used in the studies mentioned previously ranged from 0.3 and 1.0, with 1.0 corresponding to a contrast level of 100%.

As will be discussed more fully later, the stimulus used here was contaminated by a luminance imbalance between the on and offset screens, especially at high contrast. Although such imbalance is common with TV monitor systems (Yoshii et al 1991), its effects must be kept in mind. The luminance of the onset screen was 0.04, 7.84 and 63.48% greater than that of the offset grey screen for contrasts of 15.38, 65.97 and 93.25% respectively. These represent absolute increases of 0.03, 5.82 and 47.14 Cd/m^2.

8.33 - WAVEFORM MORPHOLOGY AND COMPONENT IDENTIFICATION.

Three peaks were produced within the first 200ms following stimulus onset, figure 5.421. As contrast increased, the waveform morphology became less noisy and peaks were evident at more recording locations, consistent with an increased signal to noise ratio. Changes in the topographic distribution of the most dominant waveform peak, as discussed in chapter 7, also occurred with changing contrast, however a consistent pattern was not seen between all

subjects. Subject RAA showed a later peak dominant at all contrasts; subjects CD and SC showed a shift in dominance to the earlier peak of more predictable topography as contrast rose above 65.97% and 93.25% respectively, while AS showed a shift from a predictable to unpredictable peak above 65.97%.

A CIIm peak dominance with high contrasts might be expected due to an increase in signal strength, however this cannot be applied to all subjects. As with the previous sections therefore, peak identification is made with reference to the topographies of each waveform peak.

8.34 - THE EFFECT OF CONTRAST ON AMPLITUDE.

Figure 8.341 shows the effects of contrast on the mean amplitude for the CIIm, CIIIm and offset peaks. All three show an increase in amplitude with increasing contrast, the rate of change of both CIIm and CIIIm being greater than that of the offset. A linear increase in amplitude with the log of contrast has been shown for both the VEP (Campbell and Maffei 1970 and 1974, Campbell and Kulikowski 1972, Parker et al 1982), and the VEMR (Okada et al 1982). A relationship has also been proposed between the VEP amplitude and the subjective stimulus contrast level reported by the subject (Harter 1970). The VEMR data of this study differs from the VEP and VEMR findings of previous authors with regard to amplitude saturation. Pattern reversal and onset components have been shown to saturate at contrast levels as low as 10 to 20% (Spekreijse et al 1973, Okada et al 1982), depending upon stimulus conditions such as the type, size and clarity of the pattern elements (Spekreijse et al 1973, Jeffreys 1977). Luminance imbalance might contribute to/or account for the non saturation seen here, since luminance is known to influence the saturation point (Spekreijse et al 1973), and luminance saturation behaviour differs from that of contrast saturation. Yoshii et al (1991) also found that by progressively increasing onset luminance with respect to that of the offset, onset and offset amplitudes increased and decreased respectively. This could explain the increased onset amplitudes of this study, which continue up to high contrast levels, and possibly the shallower offset trend. However, Parker et al (1982) found no evidence of saturation, while Jeffreys (1977) stated that saturation amplitude of the CII and CIII components are more dependent on the structural details of the pattern than on its contrast and luminance levels. The triphasic VEP waveform

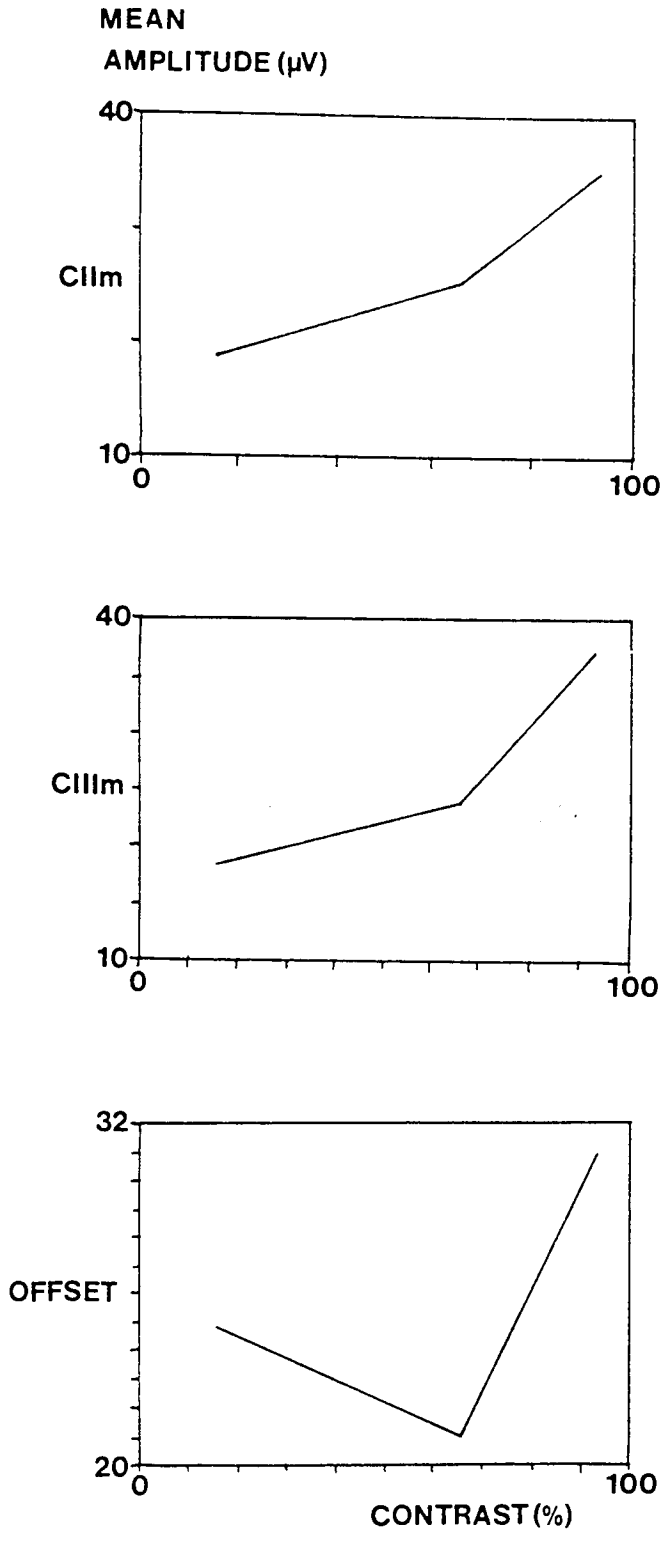

Figure 8.341 - Effects of varying contrast level on the mean amplitude of the CIIm, CIIIm and offset peaks for subjects CD, RAA, AS and SC.

produced by pattern onset stimulation has different stimulus related properties for each of the peaks. The CI has been shown to be related to stimulus contrast, while the CII and CIII are more contour specific, their amplitude affected by contrast according to its effects upon the subjective impression of contour clarity. If the VEMR CIIm and CIIIm components have analogous cortical origins to those of the VEP CII and CIII therefore, the lack of VEMR amplitude saturation could reflect their contour specific properties.

Stimulus duration is also known to affect onset amplitude, since the CI and CII components obey Blochs law, whereby amplitude is related to the product of contrast and duration (Spekreijse et al 1973, Jeffreys 1977). Musselwhite and Jeffreys (1982) have shown a linear relationship between amplitude and log (contrast x duration), however the extent to which this applies to the data shown here is unclear, since the contrast/duration reciprocity should not occur for stimulus duration's above 70 ms.

8.35 - THE EFFECT OF CONTRAST ON LATENCY.

The onset latency has been shown to decrease with increasing contrast for the VEP (Parker et al 1982, Musselwhite and Jeffreys 1982) and VEMR (Okada et al 1982), with the CI and CII components showing a linear decrease with the log of contrast (Musselwhite and Jeffreys 1982). Unlike the amplitude behaviour described previously, latency trends do not obey Blochs law, as they appear uninfluenced by stimulus duration (Musselwhite and Jeffreys 1982). Regan (1989) suggested that this difference might be accounted for by the suprathreshold contrast levels used in VEP studies, being so much greater than those used psychophysically.

Figure 8.351 shows the mean latency versus contrast plots for the CIIm, CIIIm and offset peaks, taken from the four subjects. As data is only presented for three contrast levels in each case, it is unreasonable to draw too many conclusions from the trends. However there does appear to be differences between the three components. As contrast increases, the CIIm latency decreases linearly, that of the CIIIm would best be described by a U shaped second order polynomial, while that of the offset rises then flattens or falls slightly. A difference between the onset and offset trends would be consistent with the previous amplitude findings, however the CIIm/CIIIm difference is less expected. Such variation could be erroneous, due either to the small

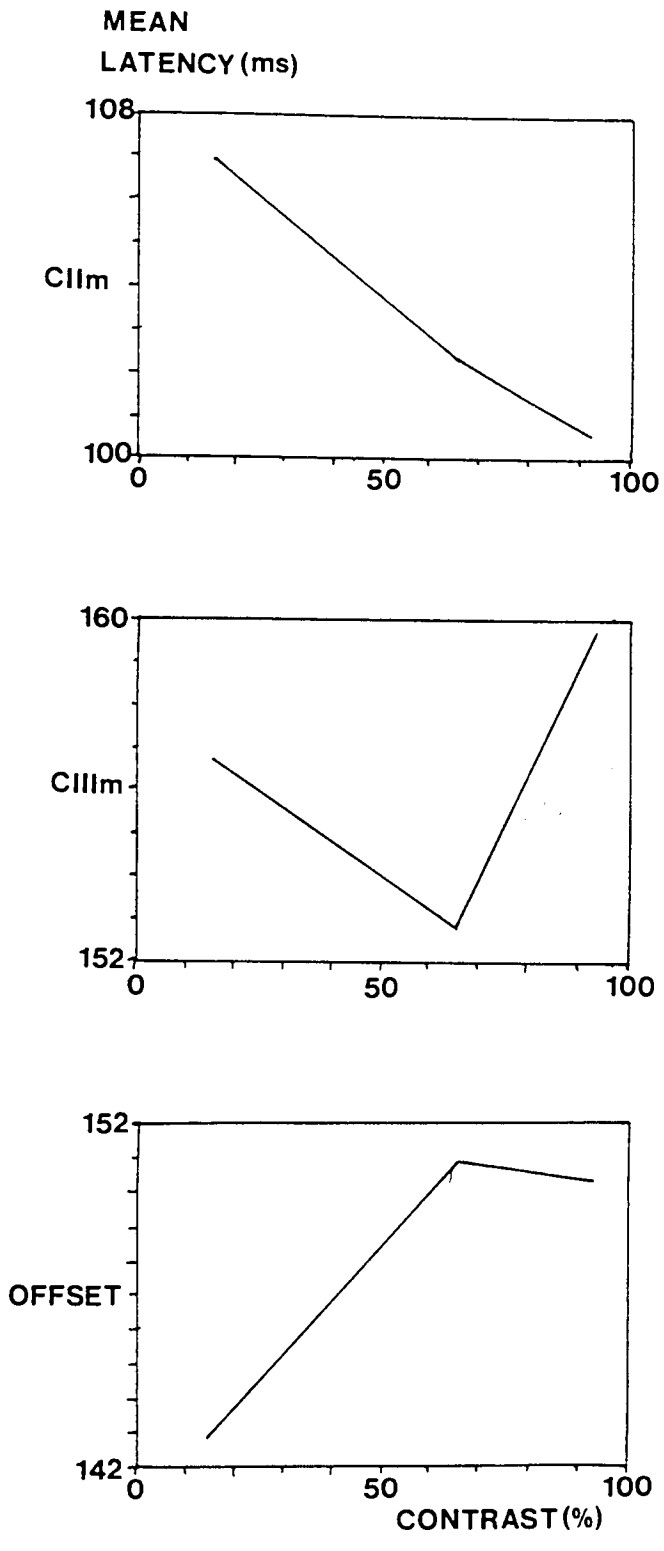

Figure 8.351 - Effects of varying contrast level on the mean latency of the CIIm, CIIIm and offset peaks for subjects CD, RAA, AS and SC.

sample size, or possibly variation in peak latency due to the unpredictable half field summation with later components at high contrast. Alternatively, it might be showing genuine differences in processing behaviour. This could only be resolved by undertaking a more extensive study, incorporating more subjects and contrast levels.

8.36 - THE EFFECT OF CONTRAST ON TOPOGRAPHY.

To my knowledge, no studies have been reported previously into the effects of altering contrast on topographic distribution. Figures 8.361 and 8.362 show the topographies of the CIIm and CIIIm peaks respectively, to the four subjects and three contrast levels. The distribution of the mid contrast level to all subjects have been described previously in chapter 6. Pattern offset produced topographic distributions of poor quality, and so these were excluded from further analysis. Table 8.363 shows the average standard deviation (SD) values per recording location, for the CIIm (A) and CIIIm (B) data of figures 8.361 and 8.362 respectively. Comparisons are made between responses recorded with contrasts of 15 and 65%, and those between 65 and 93%. The values marked correspond to pairs of topographies showing fewer differences (lower SD) than those obtained with intertrial repeatability (See section 5.43, CIIm SD limit = 7.39, CIIIm SD limit = 5.21). While all subjects show differences between topographies recorded at each contrast level, the SD figures indicate that increasing contrast from 15 to 65% produces no more CIIm variation than that seen for intertrial variation. The CIIm responses of subject SC are also relatively consistent between contrasts of 65 and 93% (figure 8.361 and table 8.363A). Although topographic similarities are evident between the larger contrast CIIm responses of subject CD (figure 8.361), the corresponding SD value is high, reflecting differences in maxima position, field spread and absolute amplitude variation. The CIIIm responses of figure 8.362 show less consistent topographic distributions with increasing contrast than those of the CIIm. The distributions of subject RAA vary less than intertrial variation (table 8.363), while CD and AS both produce similar high contrast topographies but with high SD values.

This study indicates that although topographic variation occurs with increasing stimulus contrast, gross similarities are still evident for the CIIm distributions of many subjects, but with fewer CIIIm. The poor quality of the

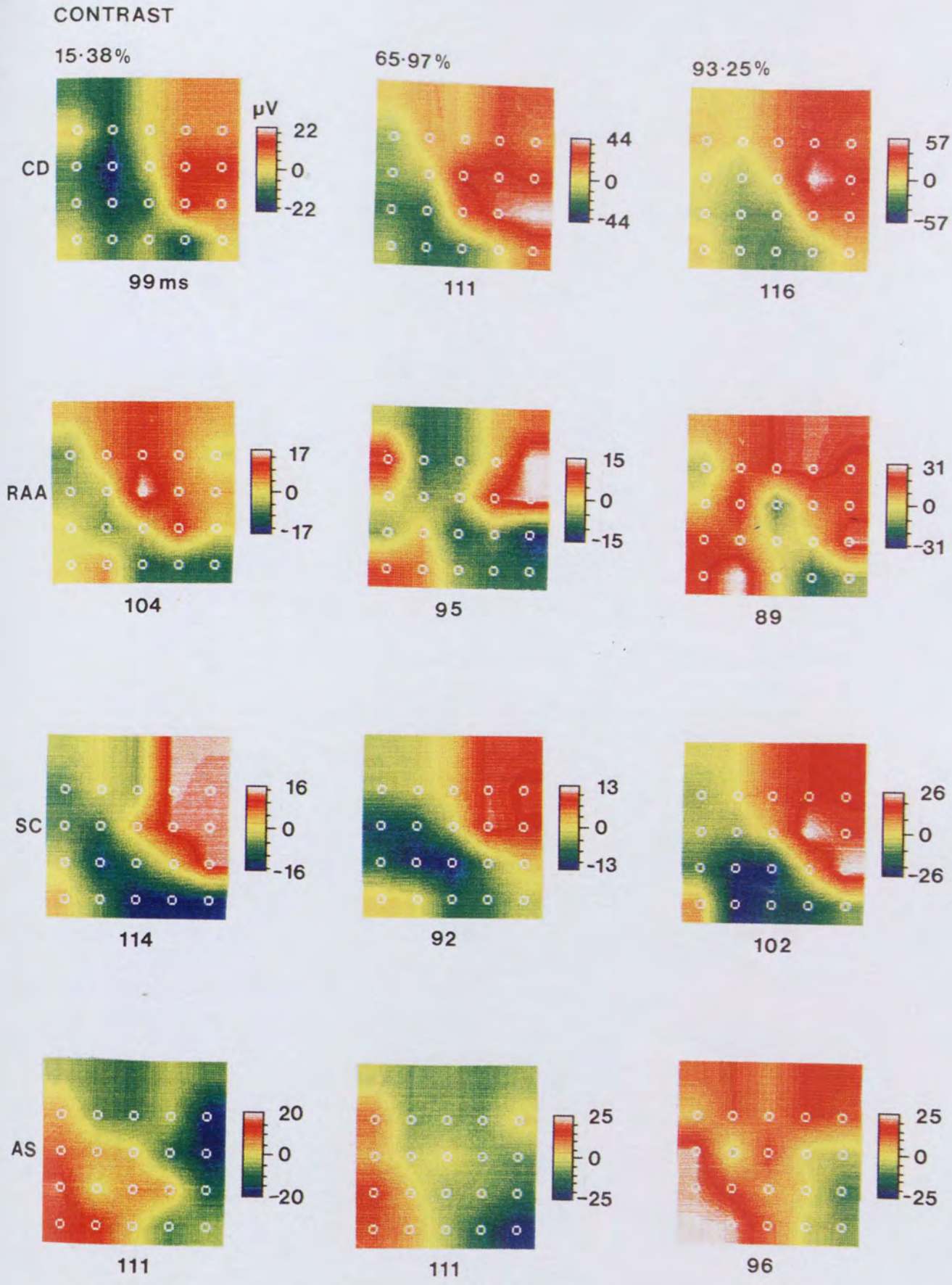

Figure 8.361 - Effects of varying contrast level on the CIIm peak topography for subjects CD, RAA, SC and AS.

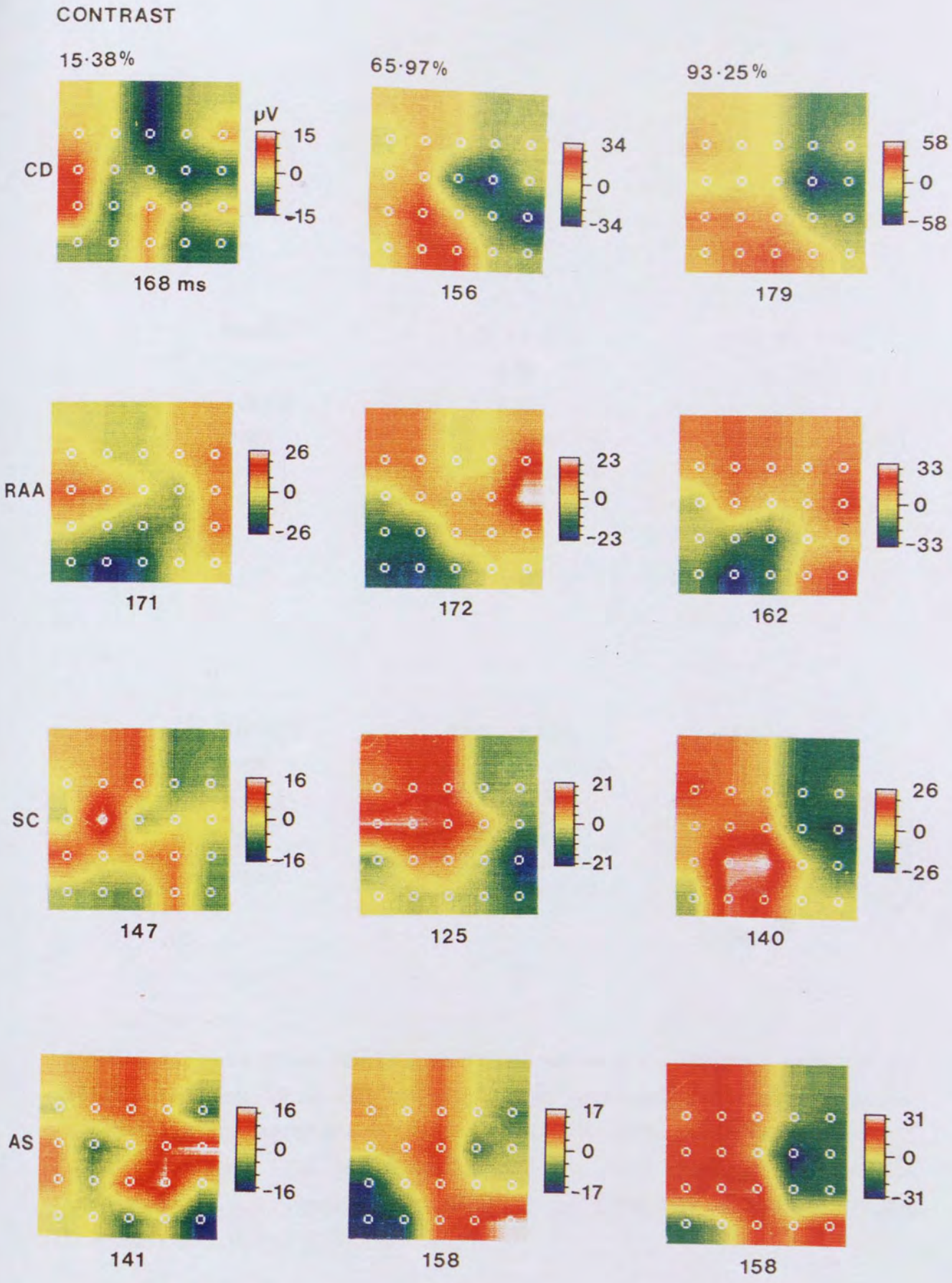

Figure 8.362 - Effects of varying contrast level on the CIIIm peak topography for subjects CD, RAA, SC and AS.

A.

CIIm

SUBJECT	15% v's 65%	65% v's 93%
CD	6.36 *	10.41
RAA	6.63 *	10.06
SC	3.88 *	5.88 *
AS	4.28 *	8.21

B.

CIIIm

SUBJECT	15% v's 65%	65% v's 93%
CD	8.34	5.73
RAA	4.97 *	5.11 *
SC	5.70	8.02
AS	7.19	9.31

TABLE 8.363 - Average standard deviation values (per recording location) for the CIIm (A) and CIIIm (B) topographies of each subject. Comparisons are made between the distributions recorded to 15 and 65% and those between 65 and 93% contrast. The values marked (*) are those showing less variation than that found with intertrial repeatability of the CIIm (SD = 7.39) and CIIIm (SD = 5.21) (See section 5.43).

offset data might suggest a different processing mechanism for onset and offset responses. The clinical importance of being able to adjust stimulus contrast has been mentioned by Bodis-Wollner et al (1990) who said that the absence of an adequate VEP response at 45% contrast, with the presence of one at 85 to 90% in the same subject, gives a strong suggestion of visual abnormality. Bodis-Wollner et al (1990) also showed that low contrast levels were better suited for comparing responses to different levels of illumination, as contrast sensitivity is stable over a wide range of photopic conditions (6 to 600 Cd/m^2). If this were also found to be the case for the VEMR, its application would prove a compromise between photopic range and signal to noise ratio.

CHAPTER 9.

FOCAL FIELD STIMULI.

In previous chapters, the behaviour of the pattern onset VEMR was investigated using full and half field stimulation. Such stimuli were chosen because they provided easily fixated targets whose large retinal size maximised cortical activation. The stimulation of multiple sources, and the complex interactions with result can cause problems in determining the sites of cortical origin. The aim of this chapter is to examine the response of the visual system to focal stimuli, e.g. quarter fields, octants and full and half fields with central scotomas. Such stimuli should reduce the number of active sources and hence provide a clearer indication of visual processing.

9.11 - QUARTER FIELD STIMULATION.

Many authors have employed quarter or quadrant field stimuli in studies of the checkerboard VEP to pattern reversal (Michael and Halliday 1971, Blumhardt and Halliday 1979, Lesevre and Joseph 1979, Haimovic and Pedley 1982), flashed pattern (Jeffreys and Axford 1972 a and b, Jeffreys 1977) and pattern onset stimulation (Lesevre and Joseph 1979, Lesevre 1982, Butler et al 1987, Van Dijk and Spekreijse 1990, Ossenblok and Spekreijse 1991). The onset of sinusoidal gratings were studied by Parker et al (1982). The VEMR to quarter field stimulation has also been studied for checkerboard reversal (Janday et al 1989, Ioannides et al 1989) and the onset of sinusoidal gratings (Aine et al 1989, Aine et al 1990). All of these studies attempted to determine the cortical origins of each component by observing changes in surface field polarity over the scalp, with stimulation of the different quarter fields and/or the use of source localisation techniques. Each author interpreted their results with reference to the cruciform model of striate cortex, as described by Jeffreys and Axford (1972 a) (chapter 2). Using such approaches, a striate origin has been proposed for the CI onset component (Jeffreys and Axford 1972 a, Darcey et al 1980, Parker et al 1982, Butler et al 1987), while an extrastriate origin has been proposed for the CII (Jeffreys and Axford 1972 a) and the CI (Lesevre and Joseph 1979). VEMR data in agreement with the

cruciform model has also been reported by Maclin et al (1983), Aine et al (1990), Kaufman et al (1991) and Ahlfors et al (1992).

Other authors have encountered problems with response interpretation in relation to the cruciform model. Ossenblok and Spekreijse (1991) did not observe any polarity reversals for the quadrant responses to the VEP pattern onset CI and CII components seen by previous authors. This was attributed to source origins in extrastriate cortex. Kaufman and Williamson (1987) also found lateral shifts of the pattern onset VEMR to quadrant stimuli inconsistent with the cruciform model. Michael and Halliday (1971) and Lesevre and Joseph (1979) studying the VEP pattern reversal and onset responses respectively both observed polarity reversals for upper and lower field stimuli, the displacement of which was considered too great to originate from sources on opposite sides of the calcarine fissure. Both groups explained their findings by the activity of sources in area 19, on the lateral surfaces of the occipital lobes, with lower field stimuli projecting to sources on the upper convexity and upper fields to the underside of the occipital lobes. Ahlfors et al (1992) and Srebro (1985), studying the pattern onset VEMR and VEP responses respectively found that peripheral stimuli elicited responses more superior on the scalp than those from the fovea, with little difference in apparent depth. This was attributed either to the activity of multiple sources (Ahlfors et al 1992) or to the stimulation of sources along a calcarine fissure angled acutely with respect to the scalp. This latter explanation has also been proposed by Maier et al (1987) and Ono et al (1990). Butler et al (1987) found an added problem with the model when using foveal stimuli to an onset checkerboard VEP. Although peripheral fields produced responses for the CI component consistent with a striate origin, foveal stimulation gave a surface positive response, instead of the surface negative predicted. Similar findings have also been made by Lesevre and Joseph (1980) and Lesevre (1982). Explanations for this anomaly include opposing micropotentials for foveal and extrafoveal striate cortex, or the physiological variation in cortex orientation caused by the presence of the lateral calcarine sulcus, whose appearance and shape varies between individuals (Butler et al 1987). The latter of these seems likely, since Parker et al (1982) also suggested that the cruciform model needed improving for use with stimuli of high spatial frequency, which project predominantly to the occipital pole.

9.12 - SOURCE MODEL ASSUMED.

The majority of the full and half field results discussed in previous chapters were explicable by sources originating within the walls of the longitudinal fissure, with current flow directed away from the pia surface for the CIIm and towards it for the CIIIm and offset components. An origin on the lateral lobe surfaces was doubted, since the large degree of intersubject morphological variation of these regions (Polyak 1957), combined with the predominantly radial source orientation, would be inconsistent with the results obtained. A striate or extrastriate origin cannot easily be inferred from this however, as both areas are known to extend down the medial walls of the longitudinal fissure. A possible indication of a striate origin was provided by the rotation of the half field maxima seen in several subjects (chapter 6), and also illustrated by the chronotopographical analysis of the right half field CIIIm component of subject RAA (figure 7.21). Such a rotation would be consistent with intersubject variation in the angle of the medial surfaces of the occipital lobes or, more likely, a shift in prominence between the quarter field responses contributing to the half field. The latter of these would occur if the chronotopographies of the constituent quarter field responses were asynchronous, (as shown for the full field and constituent half field responses) (chapter 7), and each quarter field represented the summation of sources oriented at 90° with respect to each other. Sources in such a configuration would be found in the striate cortex, with activity in the longitudinal and calcarine fissures summating to produce a resultant current source oriented at approximately 45° to the horizontal.

For these reasons, the quarter field responses shown in this chapter will be interpreted with respect to the cruciform model of striate cortex outlined by Jeffreys and Axford (1972 a), with two additional considerations. Firstly, since visual stimuli are likely to activate sources at the occipital pole and within the medial lobe surfaces simultaneously or consecutively, (chapter 6.5), the activity of polar sources cannot be excluded. Secondly, although polar sources would have a radial orientation for calcarine fissures running perpendicular to the scalp, many subjects show acutely angled fissures, which could result in a correspondingly tangential source component (Harding et al 1991).

Figure 9.121A shows the sources which would theoretically be activated by stimulation of the lower quadrant of the visual field. According to retinotopic

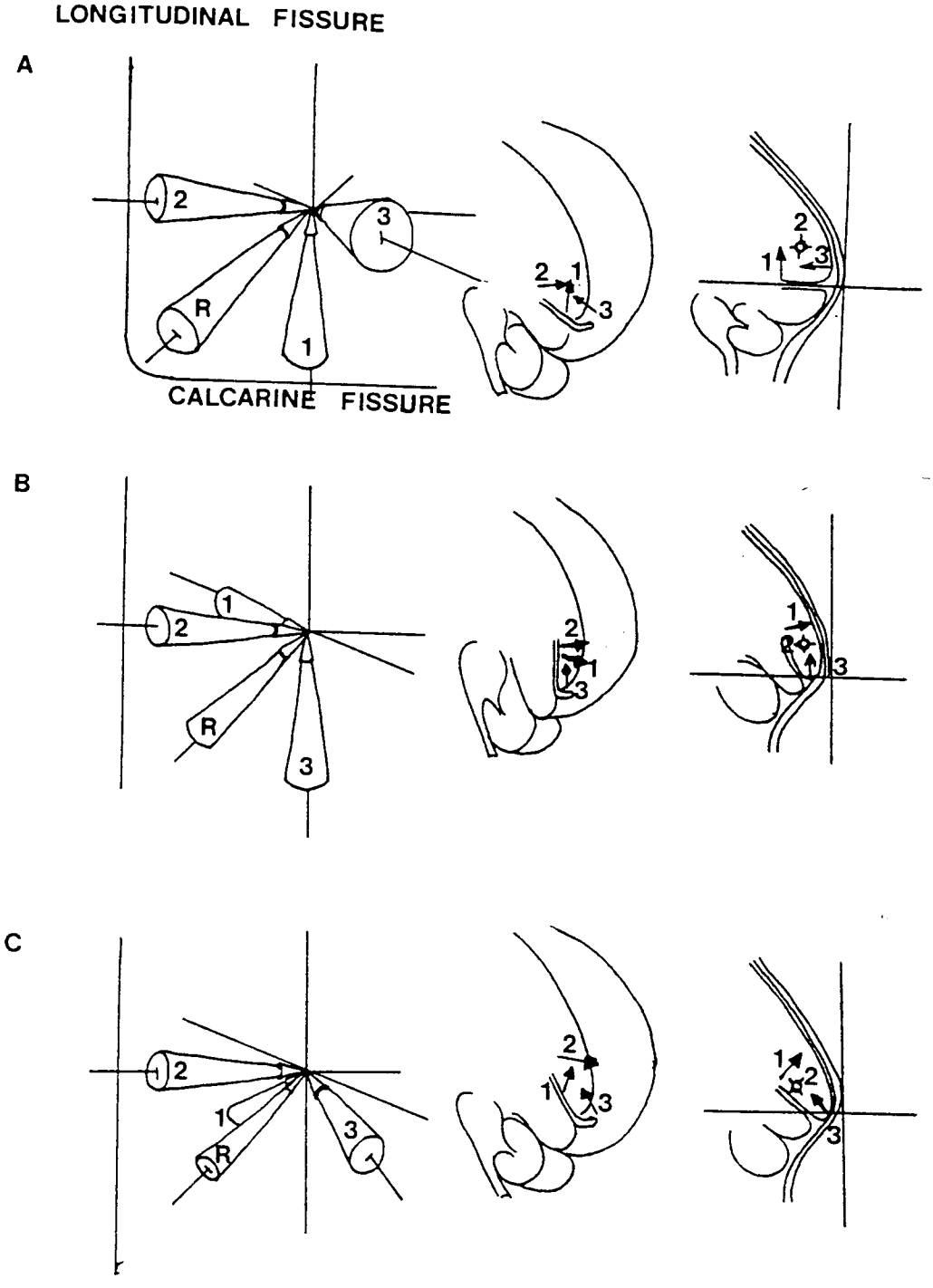

Figure 9.121 - Adaption of the cruciform model of visual cortex (Jeffreys and Axford 1972 I) to consider the effects of sources at the occipital pole (3) and variations in the angle of the calcarine fissure with respect to the scalp, 90° (**A**), 0° (**B**) and 45° (**C**). Arrows 1, 2 and 3 represent the flow of current away from the pia surface for sources within the calcarine fissure, longitudinal fissure and at the pole respectively. The direction of the resolved current source in each case is also shown.

projections (Jeffreys and Axford 1972 a), stimuli lying next to the vertical meridian of the visual field, should activate sources in the contralateral hemisphere, in the walls of the longitudinal fissure, above the calcarine fissure (2). Stimuli next to the horizontal meridian would again activate contralateral hemispheric sources, this time in the superior walls of the calcarine sulcus (1). Stimulation of peripheral retina projects to sources in posterior regions of the fissure, while central retina projects to polar sources (3). Assuming all three of these areas were active simultaneously, the resolved current source would lie at an angle of approximately 45° from the horizontal, with polar sources having no appreciable effect on orientation. A distribution of this type has been shown for the resolution of two computerised dipole sheets oriented at 90° with respect to each other (Nunez 1986, Lutkenhoner et al 1991). Activation of cortical locations more anterior to those of the pole, for example by the use of large checks or peripheral annuli, should have no effect on the orientation of the resolved source, however the maxima would become increasingly separated (Maclin et al 1983). The reduced activity of the polar sources in such a situation would alter the aspect of the resolved source in the Z plane. In the extreme case of a calcarine fissure oriented parallel to the scalp (figure 9.121B), the sources at the pole and those lining the longitudinal fissure would have a significant tangential component, while those in the calcarine fissure would be predominantly radial. Hence, the orientation of the resolved current source would depend on the relative contribution from the polar and fissure sources, from a horizontal source with activation of the fissure exclusively, to a vertical one with polar stimulation alone. In the case of a fissure angled at 45° with respect to the scalp (figure 9.121C) both fissure and polar sources would have a tangential component. The angle of the resolved source would be less than 45° to the horizontal, and alteration of the fissural versus polar contribution would result in an orientation change in the Z plane and an increased angle in the XY plane, as polar sources became dominant. In both of these latter cases (figure 9.121B and C), stimulation of progressively deeper locations along the calcarine and medial surfaces would result in an apparent posterior to anterior displacement of the scalp distributions, as shown by Ahlfors et al (1992). With stimulation of the other three quarter fields, cortical activation would appear as mirror images of the models shown in figure 9.121.

Allowing for an angular variation of the calcarine fissure of between 0 and 90° with respect to the scalp, the quarter field stimulus should produce a response in the contralateral hemisphere, more anterior over the scalp for lower than upper field stimulation; with an equivalent source oriented between 0 and 90° to the horizontal, but most likely at approximately 45°. Altering the depth of cortical projection by increasing stimulus check size, should produce an increased field maxima separation over a fixed point (Maclin et al 1983) or a posterior to anterior movement of field maxima of fixed separation (Ahlfors et al 1992).

A more accurate method of attributing activity to striate or extrastriate cortex might be possible with the combination of MEG and MRI techniques, as the resolution of the MRI is now sufficient to detect the white line of Gennari. Problems would still exist however with the MEG source localisation algorithms since the inverse problem is ill posed, having no unique solution (see chapter 2) (Lesevre 1982).

9.13 - METHODS.

The topographic distribution of subjects CD, RAA and SC were studied to a quarter field stimulus of 7°20'x5°43' at a check size of 38'x27' and contrast of 65%. Subjects were instructed to fixate a dark spot placed in the corner of the monitor for each quarter field. The responses of subject CD were also recorded to quarter field sizes of 7°20'x5°43' and 3°40'x2°51' with four check sizes, 77'x57', 38'x27', 19'x13' and 9'x6'.

9.14 - INDIVIDUAL QUARTER FIELD RESPONSES.

Figure 9.141 shows the CIIm, CIIIm and offset peak topographies of subject CD to stimulation of each of the four quarters of the visual field. Figures 9.144 and 9.145 show the upper and lower right quarter field responses of subject RAA and the upper and lower left quarter fields of subject SC respectively. In each case, the underlined latency corresponds to that of the most prominent waveform peak, and the line drawings above the topographies indicate the source orientation which would be predicted from the cruciform model.

For subject CD (figure 9.141), while the left upper field stimulus produces a dominant waveform peak whose latency is consistent with the CIIm

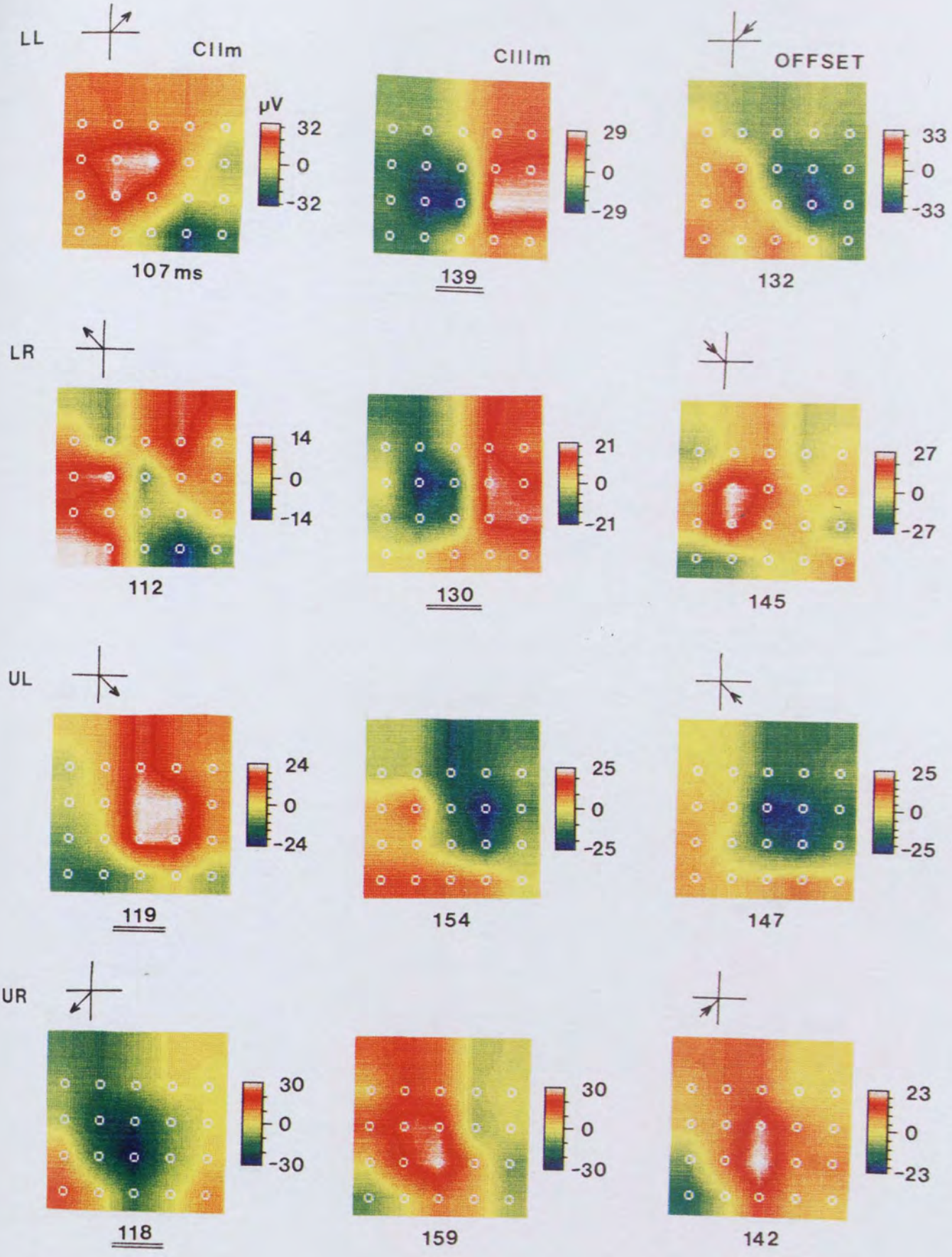

Figure 9.141 - Topographic distribution of the CIIm, CIIIm and offset peaks of subject CD to lower left (**LL**), upper left (**UL**), lower right (**LR**) and upper right (**UR**) quarter field stimulation. The line drawings shown beside selected topographies indicate the direction of current flow which would be predicted from sources organized as in the cruciform model (Jeffreys and Axford 1972 a).

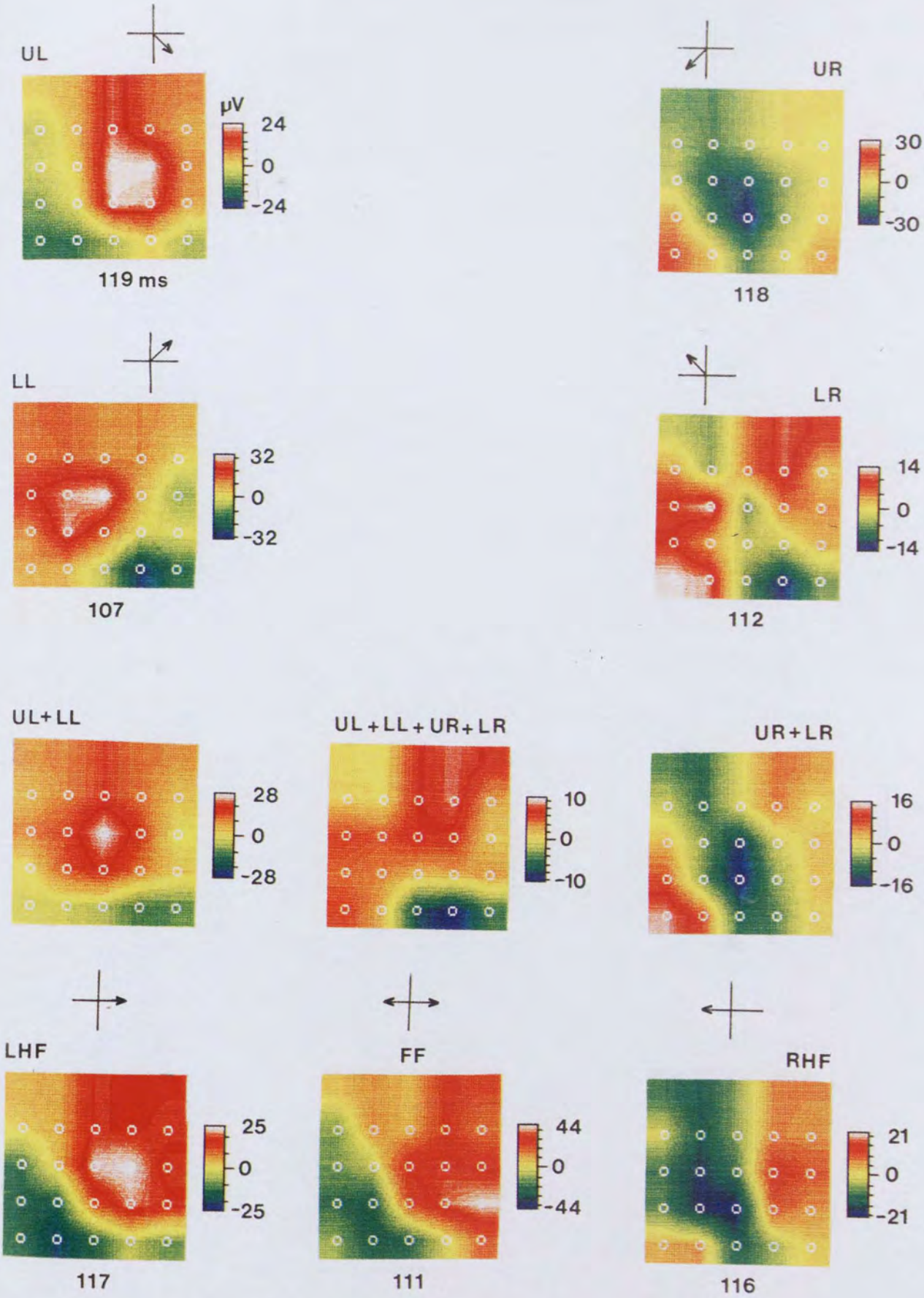

Figure 9.142 - Summation of the upper and lower left (**UL+LL**) and upper and lower right (**UR+LR**) quarter field CIIm responses of subject CD, together with the summation of all four quarter fields (**UL+LL+UR+LR**). Recorded full (**FF**), right (**RHF**) and left half field (**LHF**) CIIm topographies are included for comparison, although the effective field size of the summated responses would be larger. The line drawings shown beside selected topographies indicate the direction of current flow which would be predicted from sources organized as in the cruciform model (Jeffreys and Axford 1972 a).

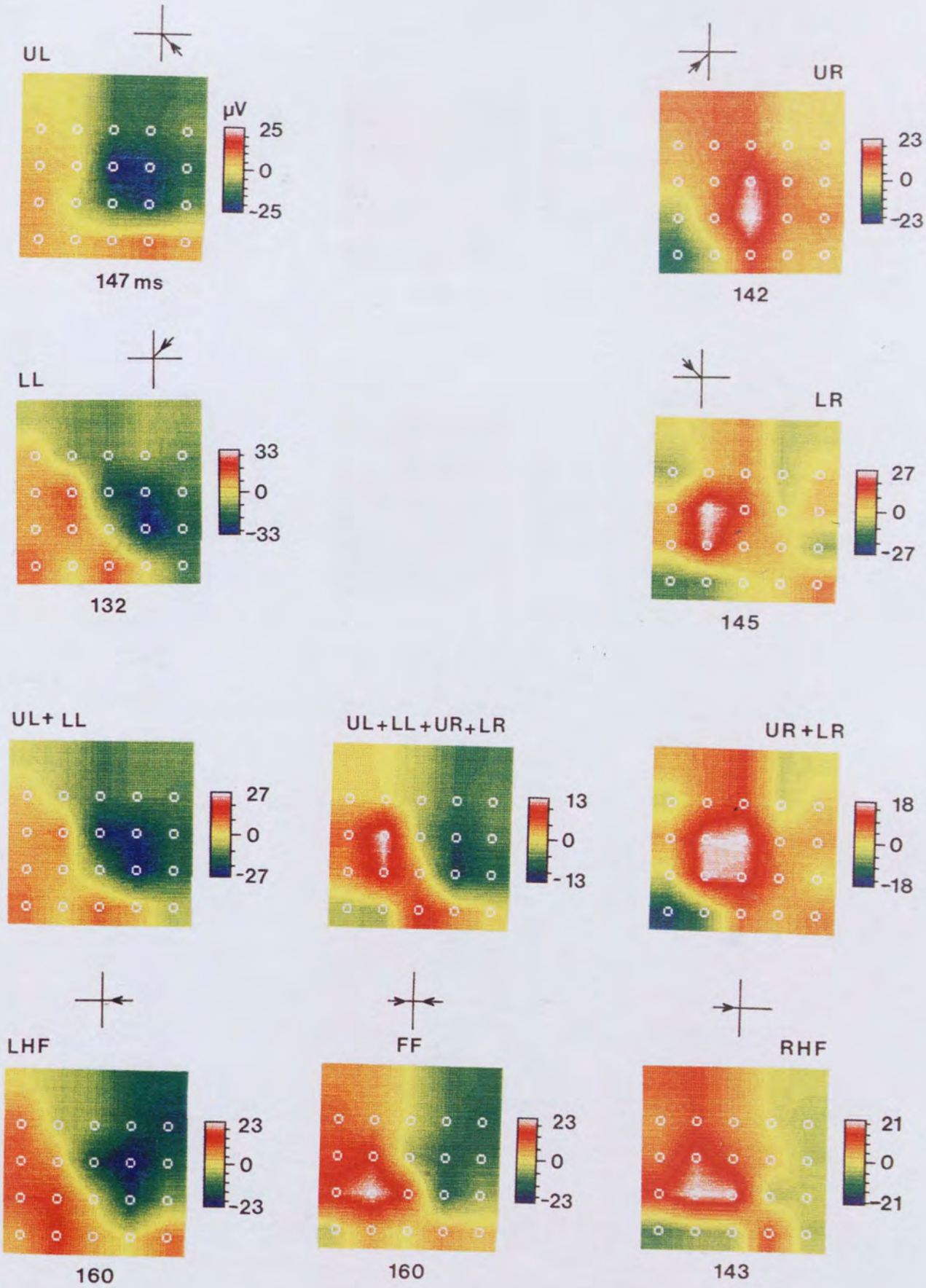

Figure 9.143 - Summation of the upper and lower left (**UL+LL**) and upper and lower right (**UR+LR**) quarter field offset responses of subject CD, together with the summation of all four quarter fields (**UL+LL+UR+LR**). Recorded full (**FF**), right (**RHF**) and half field (**LHF**) offset topographies are included for comparison, although the effective field size of the summated responses would be larger. The line drawings shown beside selected topographies indicate the direction of current flow which would be predicted from sources organized as in the cruciform model (Jeffreys and Axford 1972 a).

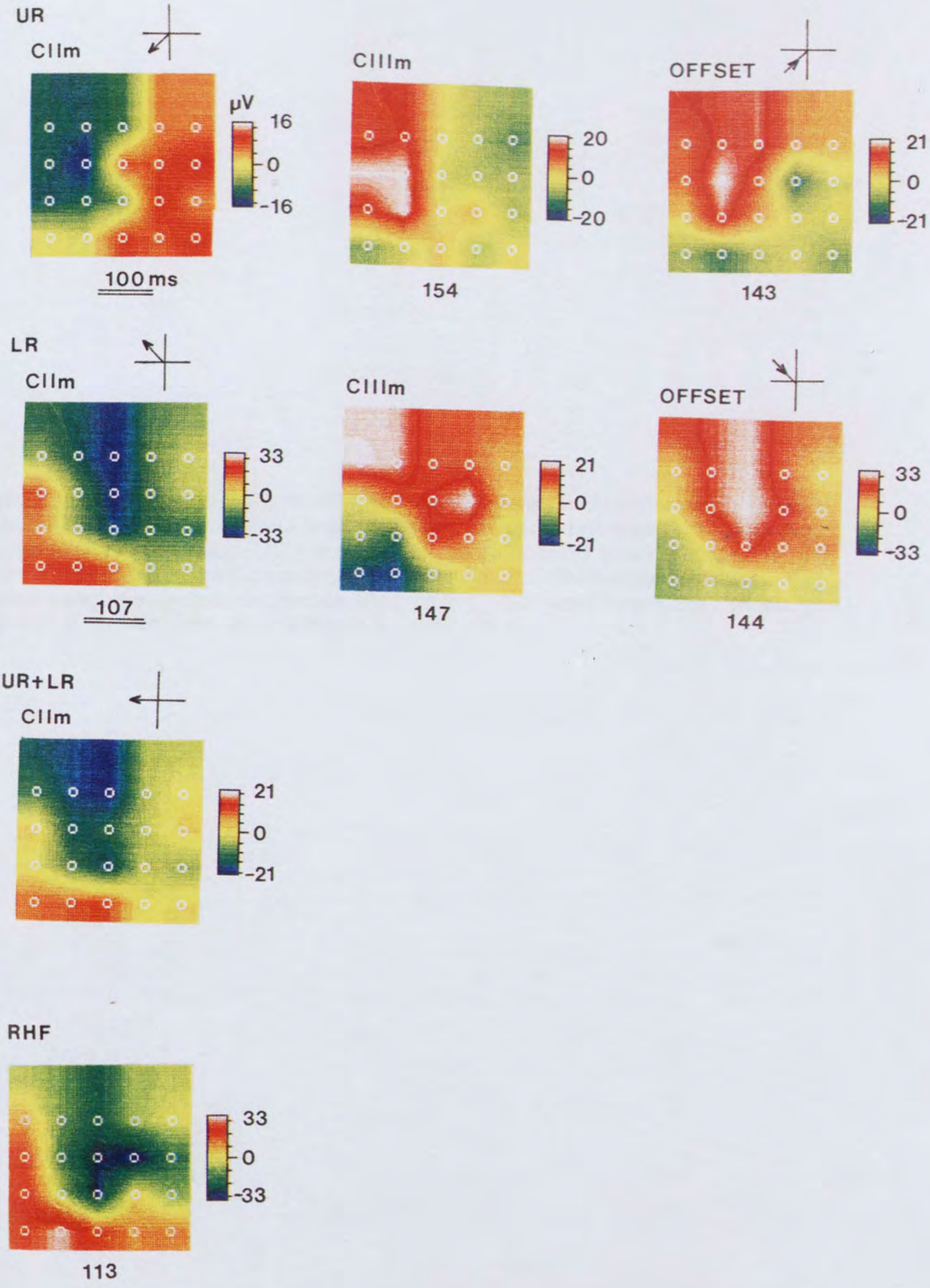

Figure 9.144 - Upper (**UR**) and lower right (**LR**) quarter field CIIm, CIIIm and offset responses of subject RAA. Also shown is the summated CIIm quarter field response (**UR+LR**) along with the recorded right half field (**RHF**) for comparison. The line drawings shown beside selected topographies indicate the direction of current flow which would be predicted from sources organized as in the cruciform model (Jeffreys and Axford 1972 a).

Figure 9.145 - Following Page - Upper (**UL**) and lower left (**LL**) quarter field CIIm, CIIIm and offset responses of subject SC. Also shown is the summated CIIm quarter field response (**UL+LL**) along with the recorded left half field (**LHF**) for comparison. The topographies of two waveform peaks are shown at a latency where the CIIm component would be expected. The line drawings shown beside selected topographies indicate the direction of current flow which would be predicted from sources organized as in the cruciform model (Jeffreys and Axford 1972 a).

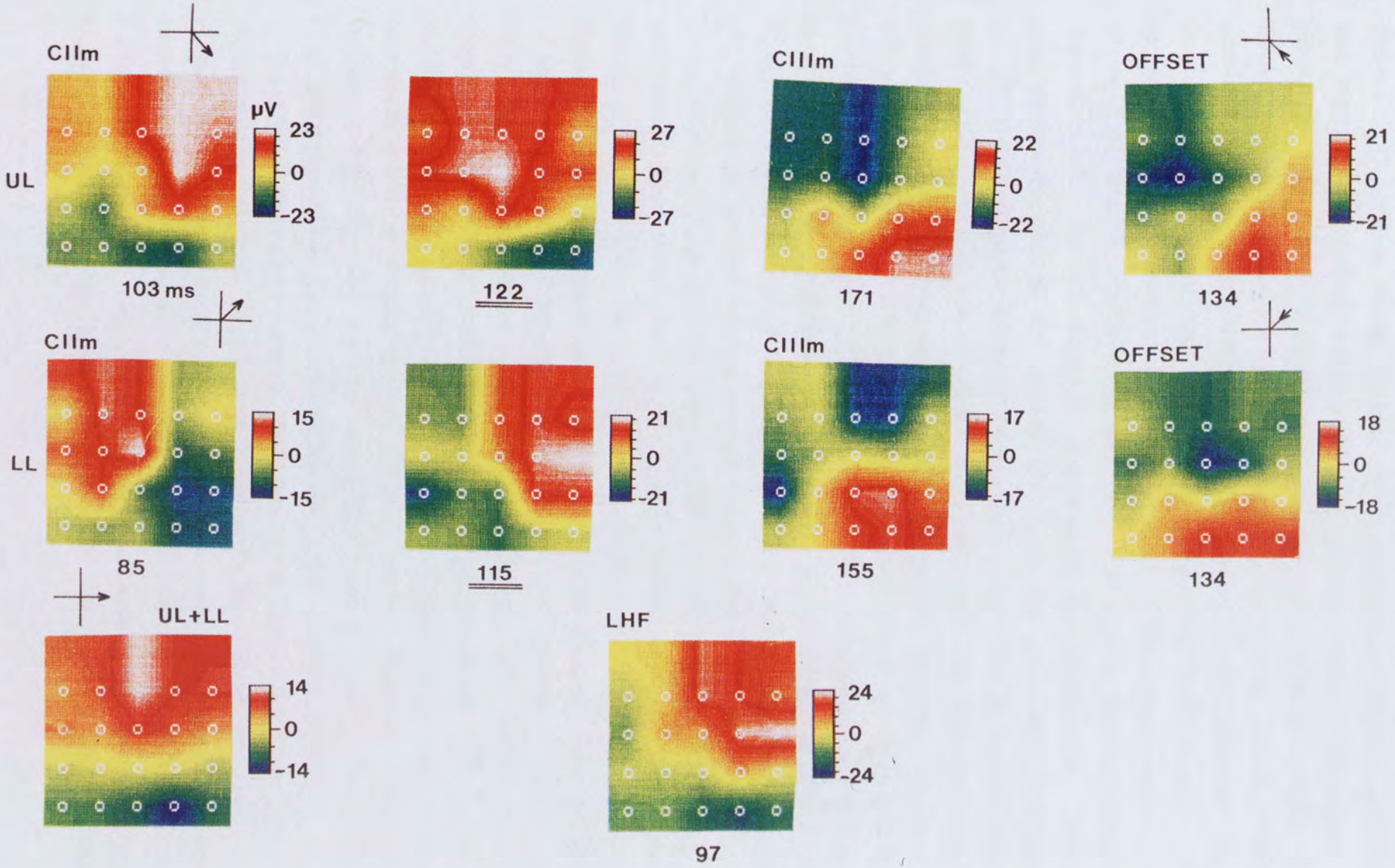
CIIm
μV
23
0
-23
UL
103 ms
27
0
-27
122
CIIIm
22
0
-22
171
OFFSET
21
0
-21
134
CIIm
15
0
-15
LL
85
21
0
-21
115
CIIIm
17
0
-17
155
OFFSET
18
0
-18
134
UL+LL
14
0
-14
LHF
24
0
-24
97

component, that produced by the lower left field stimulus is much later. Subject RAA (figure 9.144) produces a dominant peak of predictable latency and topography for both upper and lower quarter fields. The responses of subject SC (figure 9.145) appear more complex than those of subjects CD and RAA, with two clear waveform peaks evident at similar latencies corresponding to the CIIm, each being prominent at different recording locations. Of the two, the topographies of the first peak in each case are consistent with the cruciform model, while those of the second show a rotation of the field maxima, clockwise for the lower left stimulus and anticlockwise for the upper left. In each case, the second peak appears dominant. Anomalous peak dominance such as this appears similar to that seen when recording with a full field stimulus (chapter 7). Hence, this would suggest that the predictability of the quarter field waveform peaks is dependent upon the synchrony of the constituent octant field responses, and the efficiency with which they summate. The intersubject variations might be accounted for by cortical morphology and processing variation. Alterations in octant field contributions are also indicated by the multiple peaks of subject SC, as Ahlfors et al (1992) demonstrated that multiple peaks of similar latency were a sign of the activity of several asynchronous cortical sources.

For subjects CD and SC, the latency of all components except that of the offset, are shorter with lower than upper quarter fields. Subject RAA shows no trends, consistent with the findings of Ossenblok and Spekreijse (1991) who displayed equivalent latencies for upper and lower quadrant field components.

Amplitude trends are equally variable, subject CD showing no trends, subject SC giving larger amplitudes with upper field stimuli, while subject RAA shows larger amplitudes with lower fields. A larger amplitude with lower field stimuli would be expected, considering the relative depths of the cortical sources to which each field projects (Wikswo 1983). However, Blumhardt and Halliday (1979) observed that the contralateral pattern reversal VEP N105 and P135 components had larger amplitudes for upper quadrant stimuli.

The CIIm topographies of both upper and lower field stimuli for subjects SC (figure 9.145) and RAA (figure 9.144), and those for the left half field quarters of subject CD (figure 9.141), all show distributions broadly consistent with the cruciform model. The upper left quarter field response of subject CD (figure 9.141) produces field areas explicable by an underlying current source of expected orientation. The position of this source (as indicated by the region of

zero magnetic field) is however over the opposite hemisphere to that expected. This might be due to variations in probe positioning, fluctuating noise conditions, or due to the lateral position of the subjects longitudinal fissure with respect to the inion. The responses of subject SC show a more anterior scalp distribution for lower than upper field quarters, as would be expected from the model. Aine et al (1990) also demonstrated distributions consistent with the cruciform model, being close to the calcarine fissure for the 90 ms peak to lower right quadrant stimulation. The right half quarter field CIIm responses of subject CD appear complex and cannot be interpreted with regards to the cruciform model. The lower right quarter produces a topographic distribution more consistent with a full field response. Butler et al (1987) also found problems with right hand quarter fields, as the onset VEP responses to left half quadrant stimuli gave predictable dipoles oriented obliquely above and below the horizontal meridian, while no such reversals were seen for right hand quarters. Ossenblok and Spekreijse (1991) observed identical position and orientation for the CIII component between upper and lower quadrants, without any mirror symmetries. The findings of this section, combined with the problems of ipsilateral hemispheric contamination shown for right half field stimuli (chapter 6), suggest that the MEG might be detecting fundamental differences in hemispheric processing of visual information.

When comparing the topographies of the CIIm peaks with those of the corresponding CIIIm and offset for each subject, the similarities seen with full and half field stimulation (chapter 6) are not apparent with quadrant fields. This could reflect differences in the origin and/or behaviour of each component, which become apparent when the number of sources included in the summation are decreased. Alternatively, it may simply reflect the decreased signal to noise conditions resulting from reducing retinal stimulation.

With subject CD, gross similarities are evident between CIIm, CIIIm and offset peak distributions with right quarter field stimuli (figure 9.141) (CIIIm and offset topographies are of opposite field polarity to that of the CIIm). The responses from lower quadrants however showed no similarities, although it is interesting to note that although the lower right quarter field gives an unpredictable CIIm peak distribution, that of the offset is more explicable by the cruciform model. An opposite trend was observed by Jeffreys (1977), who

demonstrated that the distributions of CII and CIII components were similar, but of reversed polarity, for lower but not upper quadrant stimuli. Aine et al (1990), also noticed differences between the topographies of each peak of the lower right quadrant responses. The lower quadrant CIIIm peaks of subject CD (figure 9.141) are unusual because they show similar topographies, without mirror symmetry. Each distribution could be explained either by a vertical current source oriented down the scalp, or a dipole in each hemisphere with current flow directed away from the medial surface of the brain. The former could occur with a purely polar CIIIm response, for an acutely angled calcarine fissure, while the latter would indicate activity in each hemisphere.

For subject RAA (figure 9.144), the CIIm peak is of similar distribution, but reversed polarity to that of the CIIIm and offset peaks for lower right quarter field stimuli. With the upper right quarter however, the CIIIm and offset topographies are similar to each other, but dissimilar to the CIIm. Subject SC (figure 9.145) shows similar topographies for the CIIIm and offset peaks, which differ from those of the CIIm.

9.15 - SUMMATION OF THE QUARTER FIELDS.

Many authors have demonstrated that as the full field response can be attributed to the sum of the half field responses (Brenner et al 1981), then the summation of the quarter field responses give similar amplitude distributions (Jeffreys and Axford 1972 a and b, Jeffreys 1977), waveform shapes (Blumhardt and Halliday 1979, Ossenblok and Spekreijse 1991), topographic distribution and comparable locations for the equivalent dipole sources (Ossenblok and Spekreijse 1991) as those of the half field. It has also been demonstrated that the quarter field response itself is equal to the sum of its constituent octants for the pattern onset CI component (Jeffreys and Axford 1972 a and b, Blumhardt and Halliday 1979).

The summation of the upper and lower, left and right quarter field topographies, together with the summation of all four quarters are shown in figures 9.142 and 9.143 for the CIIm and offset components respectively of subject CD. The recorded full and half field topographies are also provided, for comparison. The two sets of data (recorded and summated), are not directly comparable, due to differences in field size. Hence, summation of the two quarter fields in each case gives an effective half field size of 7°20'x11°26'

compared to the recorded half field of 3°40'x5°43', while summation of the four quarters gives an effective full field size of 14°40'x11°26' compared to the recorded 7°20'x5°43'. It was shown however in chapter 8 that little difference in topography was observed by increasing the field size beyond 7°20'x5°43' (figure 8.241 and 8.242).

Summation of the right quarter field CIIm responses of subject CD (figure 9.142) produces a similar distribution to that of the recorded right half field (average SD value = 4.87, compared with 7.39 seen for intertrial variability). The result of left quarter field summation differs from that of the recorded half field however (average SD = 7.69), the summated field showing greater similarity with the lower quarter field topography, while the half field is similar to the upper quarter field. Dominance of the half field distribution by lower hemispheric source activity contradicts earlier descriptions about the interaction of source depths and signal strength (See chapter 8). Such behaviour might be explained however by the summation of asynchronous quarter field responses, similar to that described for the full field response (See chapter 7). Such a lower field dominance has also been demonstrated for the CI onset component (Ossenblok and Spekreijse 1991), however Blumhardt and Halliday (1979) observed that lower and upper quadrants emphasised the ipsilateral and contralateral waveform components respectively upon summation. Summation of the four CIIm quarter field responses produces a distribution consistent with the cruciform model for the right hemisphere only, while comparison with the recorded full field shows greater differences than those seen with intertrial repeatability (average SD = 13.56). Comparisons between the quarter field CIIIm summations and those of the respective half or full fields (figure 9.143) produce greater similarities than observed with the CIIm (average SD of the left quarters versus the left half field = 4.37; right quarters versus half field = 4.18 and all four quarters versus full field = 4.63). Subjects RAA (figure 9.144) and SC (figure 9.145) both shown gross similarities between their respective quarter field summated distributions and those of the recorded half fields (average SD = 4.22 for subject SC and 7.56 for subject RAA).

9.16 - THE EFFECTS OF VARYING CHECK SIZE.

The effect of altering check size on the full and half field VEMR was discussed in chapter 8, and many of the results were consistent with source origins as

described by the cruciform model. Hence, as check size decreased, some subjects showed an anterior to posterior movement of the field maxima, while others showed less diffuse maxima and/or an increase in amplitude. It was also observed that for certain subjects, larger check sizes produced a dominant waveform peak of unpredictable latency and topography, while the dominant peak obtained with smaller checks was earlier, coinciding with a predictable CIIm type topography. This behaviour was attributed to the efficiency of the half field summation, which appeared to give a more predictable result as the volume of stimulated cortex increased. The effects of altering check size are investigated here to quarter field stimuli to observe if focal stimuli give any clearer evidence of the expected retinotopic projection of the retina to the visual cortex.

Figures 9.161 and 9.162 show the effect of check size on the prominent onset and offset peak topographies of subject CD to a lower left quarter field of 7°20'x5°43' and 3°40'x2°51' respectively. As was seen with full field stimulation, the larger check quarter field responses produce a dominant waveform peak of unpredictable latency and topography regarding the CIIm, for each field size, while that of the smaller check is more predictable. It is interesting to note however that the full field responses of this subject were predictable at all check sizes (See chapter 8). If response predictability is dependant upon the efficiency of summation of constituent field areas therefore, this would suggest that a subject showing predictable half field interactions might not automatically show similar efficiency at the smaller scale, such as octant interactions. For each field size, an extra waveform peak appears with the 19'x13' check response (figure 9.161 and 9.162), coinciding with the transition from a dominant waveform peak of unpredictable, to one of predictable topography. Problems with peak identification have also been demonstrated by Parker et al (1982) who studied the onset of sinusoidal gratings of varying spatial frequencies, presented quarter and full field. They found a polarity reversal of the earlier quarter field waveform peak at position Oz when spatial frequency was increased, and concluded that for full field stimuli, erroneous peak identification could occur unless criteria were used based on latency, polarity reversal and multichannel recording. This is similar to the present data in that the CIIm peak can also be seen to change polarity with check size, depending upon which recording position is used (chapter 7).

Figure 9.161 - Following Page - Effect of altering check size on the lower left quarter field response of subject CD, to a field size of 7°20' x 5°43'. For each check size, the topography of each of the onset and offset peaks are shown, the most prominant peak being underlined. The line drawings shown beside selected topographies indicate the direction of current flow which would be predicted from sources organized as in the cruciform model (Jeffreys and Axford 1972 a).

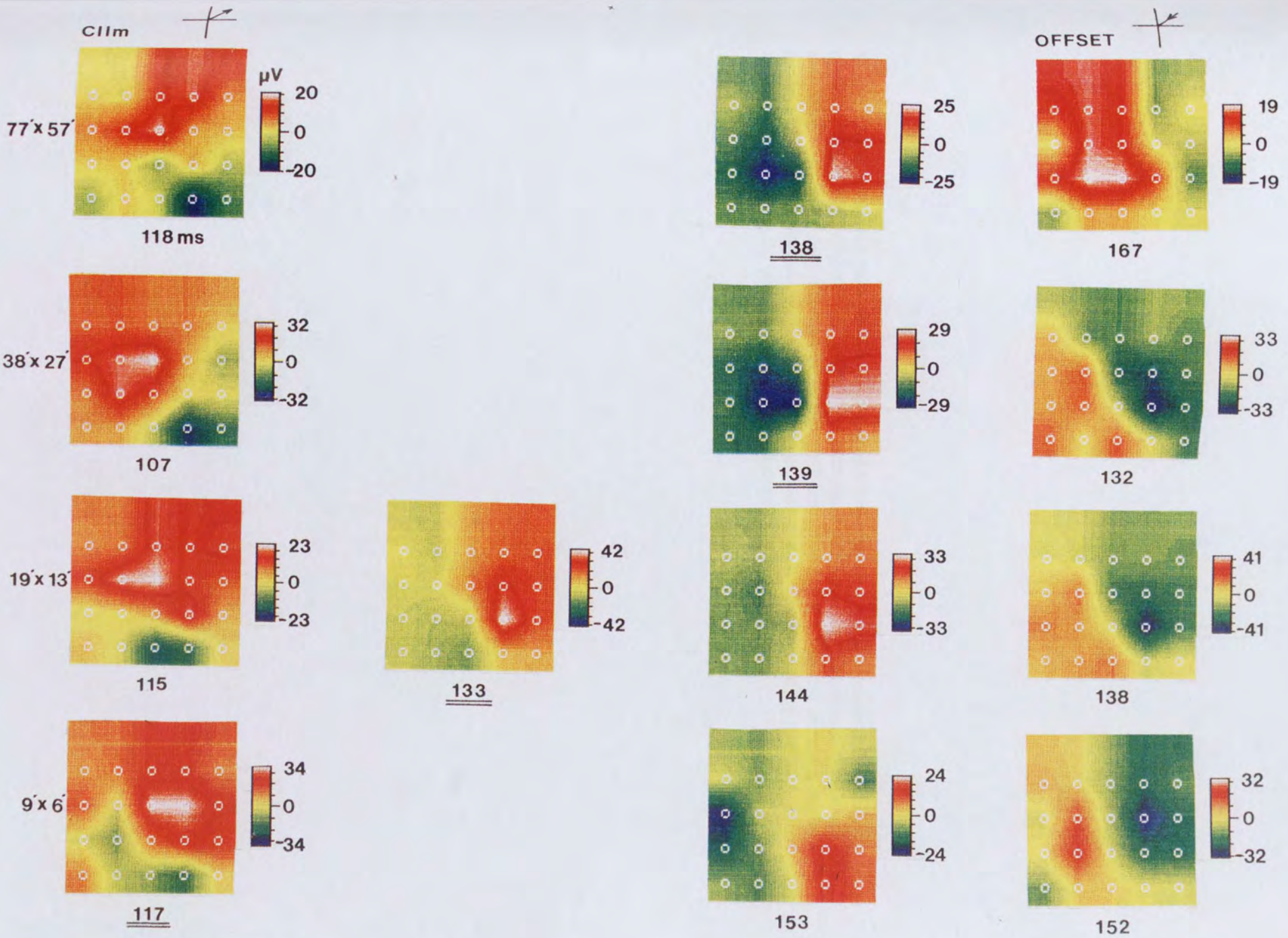
CIIm
OFFSET
μV
77'x 57'
38'x 27'
19'x 13'
9'x 6'
20
0
-20
32
-32
23
-23
34
-34
118 ms
107
115
117
133
42
-42
138
25
-25
139
29
-29
144
33
-33
153
24
-24
167
19
-19
132
33
-33
138
41
-41
152
32
-32

Figure 9.162 - Following Page - Effect of altering check size on the lower left quarter field response of subject CD, to a field size of 3°40' x 2°51'. For each check size, the topography of each of the onset and offset peaks are shown, the most prominant peak being underlined. The line drawings shown beside selected topographies indicate the direction of current flow which would be predicted from sources organized as in the cruciform model (Jeffreys and Axford 1972 a).

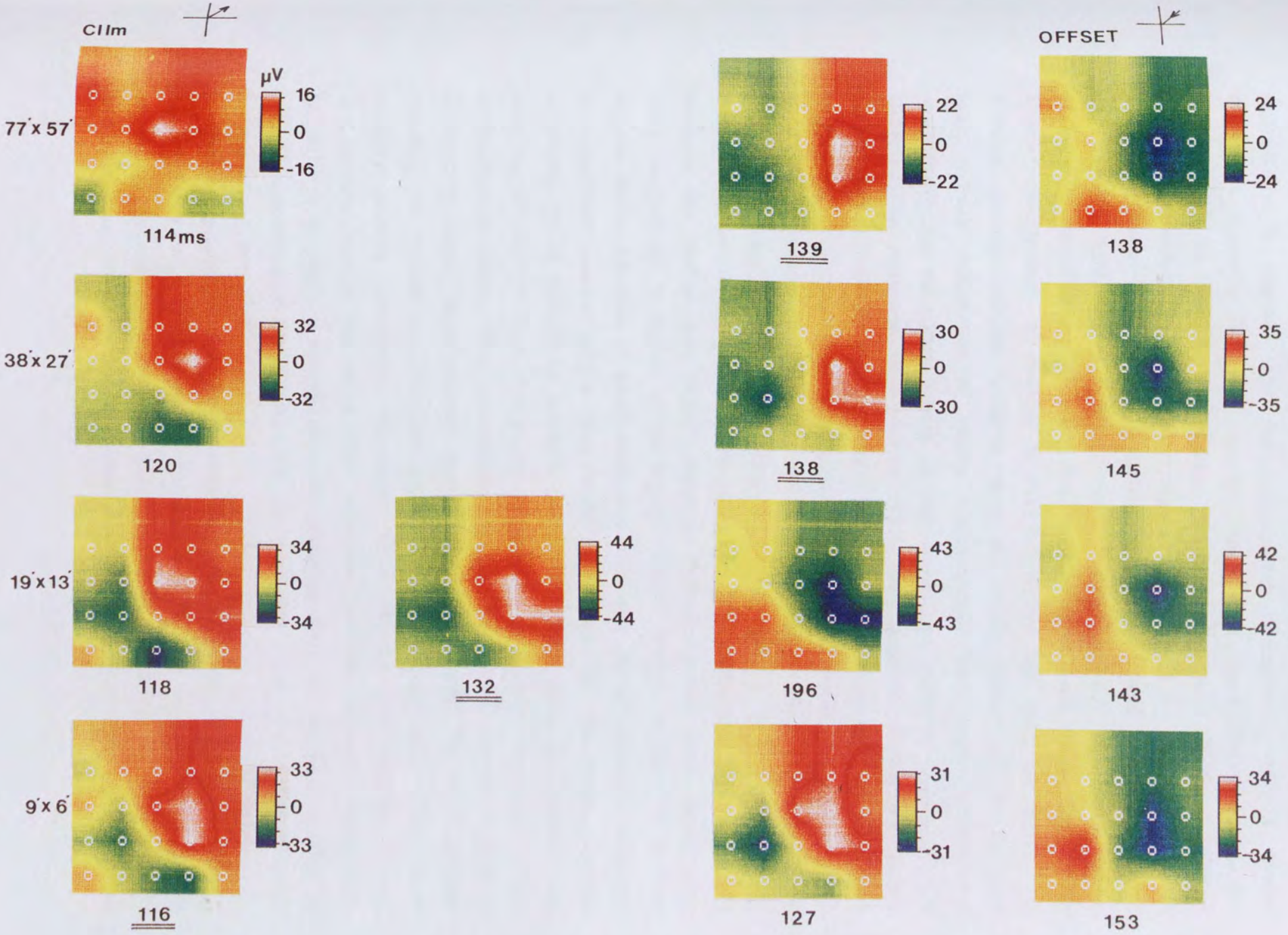
CIIm
μV
77'x 57'
16
0
-16
114ms
38'x 27'
32
0
-32
120
19'x 13'
34
0
-34
118
9'x 6'
33
0
-33
116
44
0
-44
132
OFFSET
22
0
-22
139
30
0
-30
138
43
0
-43
196
31
0
-31
127
24
0
-24
138
35
0
-35
145
42
0
-42
143
34
0
-34
153

With the 7°20'x5°43' field size and 38'x27' checks (figure 9.161), the CIIm topography is centred over the contralateral hemisphere, with a source orientation explicable from the cruciform model. As check size decreases, the positions of the positive and negative field maxima vary, consistent with a clockwise rotation of the underlying current source. The topographic distribution with 9'x6' checks is particularly complex, with areas of positive and negative field over each hemisphere. Variation of this type could reflect changes in the efficiency of octant field summation at each check size, or the relative contributions of sources in the longitudinal and calcarine fissures at different posterior/anterior locations along the medial surface of the occipital lobe. Such differences in source representation have been demonstrated anatomically for the striate cortex in and around the calcarine fissure (Polyak 1957). The responses to a 3°40'x2°51' field response (figure 9.162) are particularly difficult to interpret since all check sizes show activity over each hemisphere. Contralateral hemispheric activity is dominant, however the field areas suggest the activity of an underlying current source oriented horizontally, and not of the predicted 45° angle. Such unpredictable behaviour could result from sources active on the transitional cortical regions between the medial and lateral occipital surfaces, where inter hemispheric brain morphology is known to be highly variable (Polyak 1957). It is such regions that a stimulus of small check and field size would optimally stimulate, a superficial source origin also being suggested by the high response amplitude. It is difficult to reconcile the full field type CIIm distributions seen with the 3°40'x2°51' field size purely by cortical morphology variations. Such a distribution might occur erroneously, if the head were moved through a sufficiently large angle during probe location to result in the stimulus crossing the vertical and horizontal meridians of the visual field. This seems unlikely however considering the degree to which the head actually moved; the predictability of the larger field responses; and the response repeatability (Ahlfors et al 1992). Alternatively, the technique may be detecting activity in both hemispheres, although why this should occur only with these stimulus parameters is not clear.

The topography of the later waveform peak, seen with 77'x57' and 38'x27' checks for each field size (figure 9.161 and 9.162) is unusual as it appears unaffected by changes in stimulus parameters. In all cases, the peak displays a single area of outward and inward flowing field over the right and left

hemispheres respectively. This would be consistent with a current source oriented vertically over the midline, or slightly to the right, with current flowing down the scalp; or a current source posterior in each hemisphere, both with current flowing away from the medial surface of the brain. In either case, such a configuration could not be attributed to a lower left quadrant stimulus and the cruciform model. A similar distribution was also seen for the late peak to lower right quarter stimulation in this subject (figure 9.141). The amplitude of this peak increased as check size decreased to 19'x13' for each field size (figure 9.161 and 9.162), suggesting that either the source became progressively more superficial, or that the number of active neurones increased.

The topographies of the offset peaks were difficult to interpret with respect to any of the corresponding preceding peaks, for either field size or check size. This dissimilarity is also difficult to understand, considering the close relationship between the half and full field CIIm, CIIIm and offset distributions (chapters 5 and 6). Once more, the amplitudes increased with decreasing check size for each field, peaking with the 19'x13' checks.

9.17 - QUARTER FIELD SUMMARY.

Quarter field stimuli were studied in this chapter to test the hypothesis that by reducing the number of sources contributing to the summated response, the corresponding reduction in signal interactions would lead to more easily interpretable topographies. Although some of the CIIm responses showed orientations consistent with a striate cortex origin, variations in peak prominence; inconclusive behaviour with changing check size; and dissimilar CIIm, CIIIm and offset topographies were all unexpected complications. It would appear therefore that reducing the number of active sources leads to less predictable and more variable responses. This could reflect a reduction in signal to noise ratio, and/or an increased sensitivity to variation in cortical morphology. Of all stimuli tested, half field responses remain the most robust between subjects, possibly due to the dominance of sources on the medial surface of the longitudinal fissure which shows less intersubject morphology variation than the surfaces of the calcarine fissure (Polyak 1957).

9.21 - OCTANT FIELD STIMULATION.

It was suggested in the previous section that rotation of the half field maxima seen with many subjects, could provide evidence of a striate cortex origin for the pattern onset VEMR. Briefly, according to the cruciform model of striate cortex retinopathy (Jeffreys and Axford 1972 a), stimulation of the four octants comprising a half field, project to sources on the cortical surfaces as shown in figure 9.211A. In each case, the arrow indicates a flow of current away from the pia surface. Given uniform source activity, the fields produced by sources lining the calcarine fissure (figure 9.211A 2 and 3) would cancel, due to their opposing polarities and close proximity. The fields of sources on the medial surfaces (figure 9.211A 1 and 4) would summate, producing a scalp distribution consistent with a single, horizontally oriented current source. If the activity of one quarter of the cortex dominated the summation, (due to asynchrony between the upper and lower hemispheric activity, or to an imbalance of neuronal representation between the two), the calcarine sources would not fully cancel. Hence, the scalp distribution would suggest the activity of a source rotated clockwise from the horizontal for upper hemispheric dominance (figure 9.211B), and anti-clockwise for a dominant lower hemisphere. The influence of the calcarine sources on the half field can be examined in isolation, by comparing the responses to half field stimuli, with those from stimulation of the vertical octants of the half field only (figure 9.211C) (Jeffreys 1977, Harding et al 1994). Hence, removing the octants adjacent to the horizontal meridian of the visual field should remove any stimulation of the calcarine fissure. Stimulation of the horizontal octants of the upper and lower half fields can also be recorded to isolate activity within the calcarine fissure (figure 9.211D). The results from horizontal octants are likely to be more variable than those of the vertical octants, as the angle and shape of the calcarine fissure walls vary more than those of the longitudinal fissure (Polyak 1957).

Several authors have used octant stimuli to investigate retinotopy and source origins for the VEP to checkerboard onset (Srebro 1985, Butler et al 1987, Ossenblok and Spekreijse 1991), reversal (Halliday and Michael 1970, Michael and Halliday 1971, Blumhardt and Halliday 1979, Haimovic and Pedley 1982) and flashed pattern (Jeffreys and Axford 1972 a, Jeffreys 1977). More recently, octants have been used to study the VEMR to a checkerboard onset stimulus

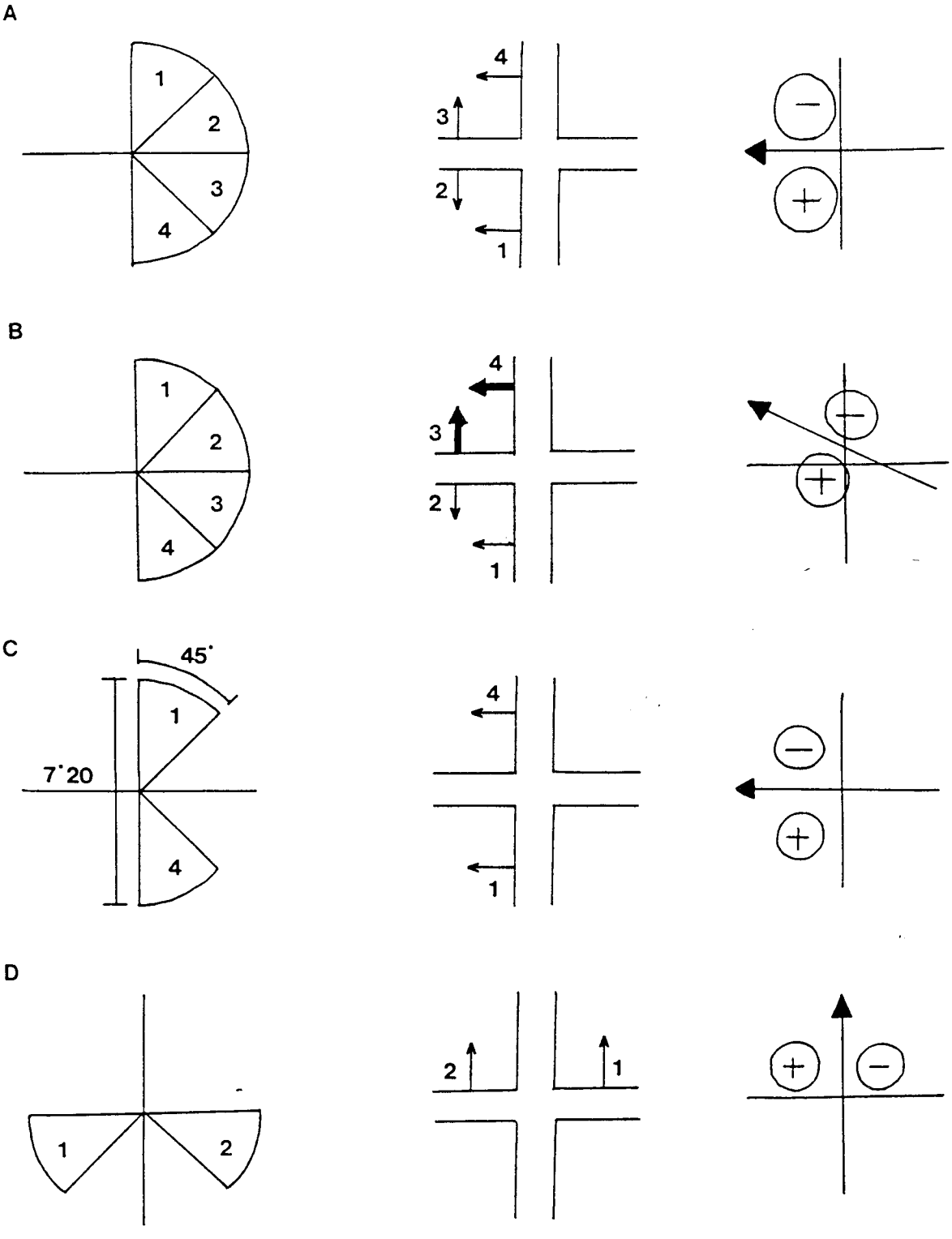

Figure 9.211 - Illustration of the striate sources which should be stimulated by half and octant field stimuli, assuming the cruciform model of striate cortex. The visual fields stimulated are shown to the left, a schematic of striate sources active are shown centrally and the resolved current sources are shown to the right. **A** - assumes that all cortical sources activated by the half field stimulus contribute equally to the summated response. **B** - shows the effect of dominant upper hemispheric sources in the summation. **C** and **D** show the expected results of vertical and horizontal octant field stimulation respectively.

(Ahlfors et al 1992). The majority of these studies were performed with single octants presented foveally or peripherally. Haimovic and Pedley (1982) investigated the effect of varying the angular size of the octant, while Jeffreys (1977) used complementary octants such as those shown here (figure 9.211C, D).

Although the octant stimulus should theoretically produce a simple, easily interpretable response, conflicting results have been reported by these authors. Jeffreys and Axford (1972 a), Jeffreys (1977) and Butler et al (1987) interpreted their results as a striate origin for the CI component; Halliday and Michael (1971) and Ossenblok and Spekreijse (1991) state that the pattern reversal P100 and onset CI respectively originated in extrastriate cortex, while Srebro (1985) and Ahlfors et al (1992) could not make any firm conclusions. These disagreements could reflect the interindividual and interhemispheric variations in striate cortex morphology (Halliday and Michael 1970, Jeffreys and Axford 1972 a, Butler et al 1987, Ossenblok and Spekreijse 1991, Ahlfors et al 1992).

9.22 - METHODS.

Left half field vertical octants were recorded on subjects SC and EW, while those of the right were recorded on subjects GR and RAA. The upper and lower field horizontal octants were also recorded for subject SC. In all cases, a check size of 38'x27' and contrast of 65% were used. The stimulus consisted of two octants, each of 45° arc, with a distance of 7°20' from the outer edge of each (figure 9.211C).

9.23 - OCTANT FIELD RESPONSES.

Octant field stimuli result in less well defined waveforms compared with the half field. This, combined with relatively low amplitudes could result from poor signal to noise ratio. Figures 9.231 and 9.232 show the CIIm responses of subject SC (figure 9.231A) and EW (figure 9.231B) to left half field vertical octants, and subjects GR (figure 9.232A) and RAA (figure 9.232B) to right half field octants. In each case, the corresponding half field CIIm topography is also shown for comparison. Figure 9.233 shows the CIIm, CIIIm and offset

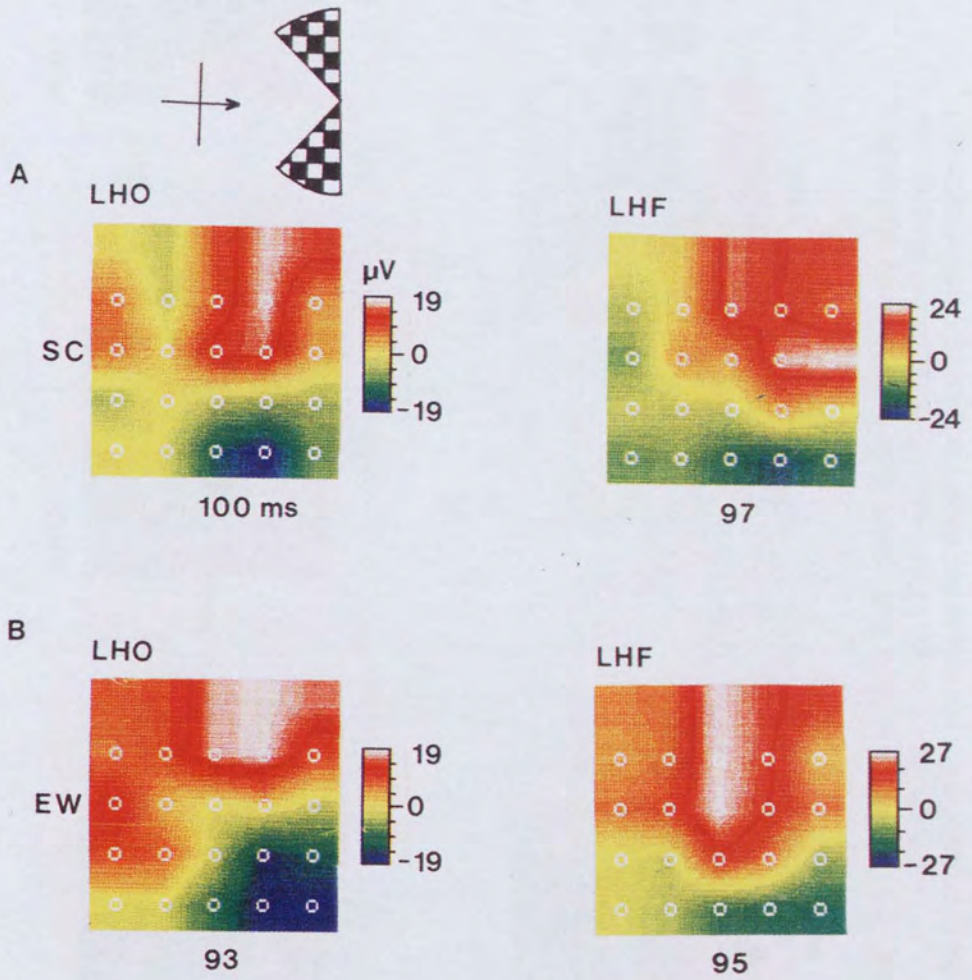

Figure 9.231 - Left half field (**LHF**) and left half octant field (**LHO**), CIIm topographic distributions of subjects SC (**A**) and EW (**B**). The diagram at the top of the page shows the arrangement of the octant field visual stimulus, with the fixation point marked (**F**).

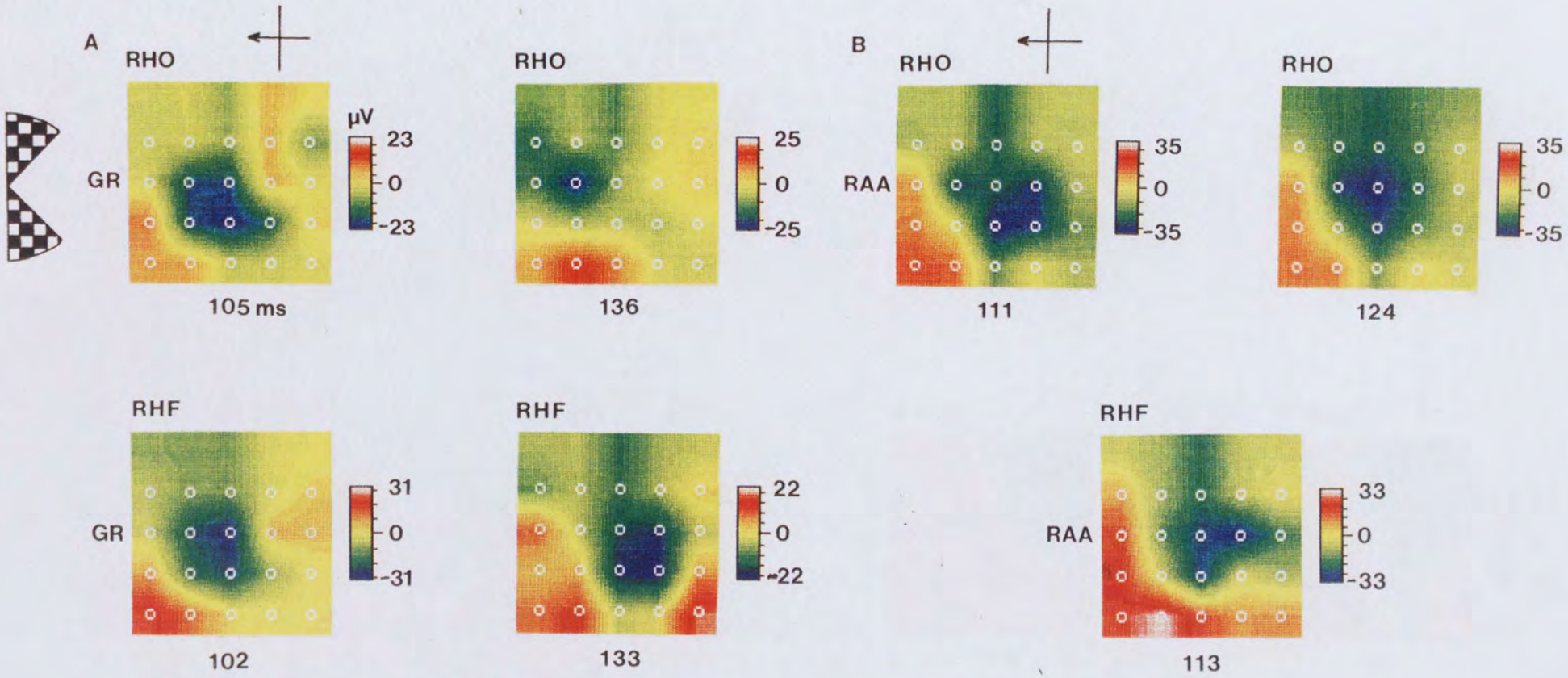

Figure 9.232 - Right half field **(RHF)** and right half octant field **(RHO)** onset topographic distributions of subjects GR **(A)** and RAA **(B)**. A single CIIm topography is not shown in either case due to problems in identification caused by the presence of two waveform peaks of similar latency and prominance. The diagram at the top of the page shows the arrangement of the octant field visual stimulus, with the fixation point marked **(F)**.

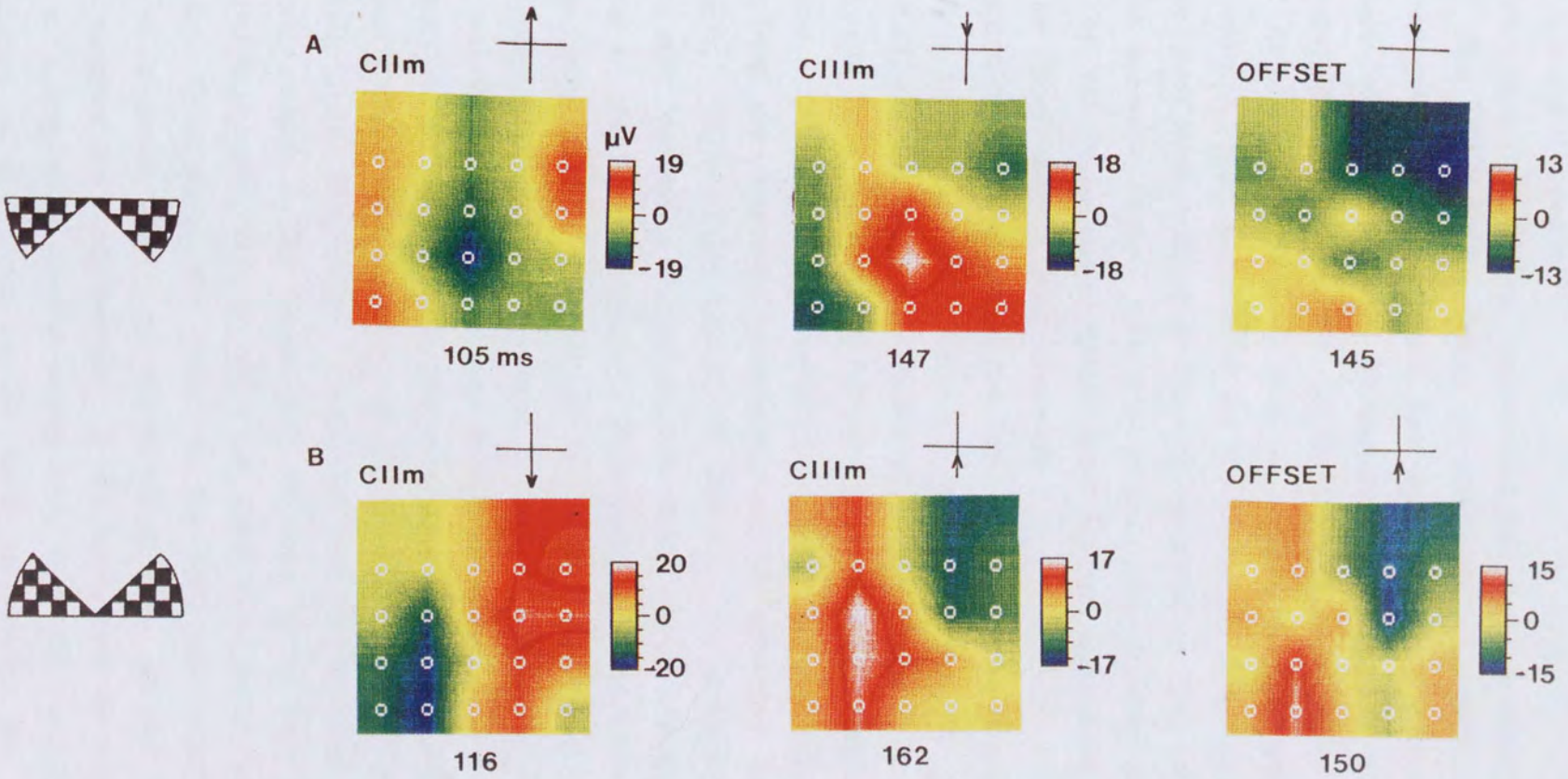

Figure 9.233 - Lower (**A**) and upper (**B**), horizontal octant field CIIm, CIIIm and offset topographies of subject SC. The diagrams to the left of the page show the arrangement of the octant field visual stimuli, with the fixation points marked (**F**).

components of subject SC to the lower (figure 9.233A) and upper field (figure 9.233B) horizontal octants.

For left visual field stimuli, octants and half fields produced peaks of similar latency. The octant field response of subject SC (figure 9.231A) shows more focally distributed maxima, rotated less with respect to each other than those of the half field, consistent with activity on the medial lobe surfaces only. The octant topography of subject EW (figure 9.231B) is likewise less rotated than the half field, however there is also an anterior displacement of the maxima by approximately 5cm, as indicated by the region of zero magnetic field. This would be consistent with domination by sources in the longitudinal fissure above the calcarine fissure. In both subjects, the positive and negative field maxima of the octant topographies have similar amplitudes, while for half fields, the upper maxima were dominant.

As seen with half field stimulation (see chapter 6), the responses to right half field octants are not as easily interpreted as those to the left. With subject GR (figure 9.232A), two half field peaks of similar latency and topography are observed, and these are matched by two peaks of similar latency separation for the octants. Both half field topographies show a clockwise rotation of the maxima from the horizontal, consistent with a dominant upper hemispheric contribution. With octant stimulation however, the topography of the first peak is almost identical to that of the half field (average SD comparison = 3.86), while that of the second displays a horizontally oriented current source. This could be explicable if the tilt of the first octant peak source occurred independently of the calcarine source activity, for example by stimulation of sources on the convexity between the longitudinal and calcarine fissures; while that of the second peak was directly caused by activity within the longitudinal fissure. The responses of subject RAA (figure 9.232B) also show a tilted half field distribution consistent with domination by the upper hemispheric sources. The octant field response shows two peaks of similar latency and topography, each of which are tilted in a similar way to that of the half field. Once more, this would be consistent with either the incomplete removal of calcarine activity by the octant stimulus, or that half field source rotations occurred for other reasons. If the latter were the case, rotation could be due to a longitudinal fissure angled away from the vertical in this subject, or stimulation of the cortex in the transition between the longitudinal and calcarine fissures. Butler et al (1987) also encountered problems with the

upper right vertical octant stimulus, which they attributed to the projection to a cortical region spanning the curvature of a cortical surface such as the lip of a gyrus or the base of a sulcus.

The CIIIm and offset waveform peaks to vertical octants were not consistent enough to analyse. As mentioned in the quarter field section, it appears that as the visual stimulus becomes more focal, the close CIIm, CIIIm and offset topographic relationship disappears. This could suggest a fundamental difference between the components, or that the later components were more susceptible to noise.

Figure 9.233A and B show the lower and upper field horizontal octant results of subject SC respectively. The upper field CIIm distribution is consistent with the activity of sources on the floor of the calcarine fissure, hence an equivalent source centred over the midline with current flowing vertically downwards. The CIIIm and offset topographies show an opposite current flow, to that of the CIIm, however each topography appears more complex. Lower field octant stimuli produce more complex CIIm, CIIIm and offset topographies than those seen with the upper field, with multiple field areas over each hemisphere. This could represent the activity of multiple cortical sources, or the effects of noise.

Where response interpretation is possible, the CIIm topographic results are in broad agreement with a striate cortex origin. Such conclusions cannot be made with confidence for the CIIIm or offset peaks however, due to their intermittent appearance. As seen with quarter fields, the use of focal field stimuli such as octants, does not improve response predictability, possibly due to the reduced signal to noise conditions obtained as the number of sources involved decrease. The effects of intersubject cortical morphology variation are also likely to be more evident when observing the activity of fewer sources.

9.31 - EFFECTS OF CENTRAL SCOTOMA.

A number of previous studies have investigated the effects of occluding parts of the checkerboard using scotomas, or annuli, (Lesevre and Joseph 1979, Lesevre 1982, Ermolaev and Kleinman 1984, Srebro 1985, Butler et al 1987, Maier et al 1987, Van Dijk and Spekreijse 1990), to a pattern reversal (Michael and Halliday 1971, Blumhardt et al 1978, Blumhardt and Halliday 1979, Haimovic

and Pedley 1982, Fukui et al 1986, Blumhardt 1987) or flashed pattern stimulus (Reitveldt et al 1967, Harter 1970, Jeffreys 1971, Jeffreys and Axford 1972 a and II). The VEMR has also been studied to grating annuli (Maclin et al 1983, Kaufman et al 1990) and the checkerboard onset (Ahlfors et al 1992). The majority of these studies have examined retinotopy and cortical source origins, while a few attempted to simulate the effects of clinical conditions such as optic neuritis, tobacco-alcohol amblyopia and neovascular maculopathy in healthy subjects (Fukui et al 1986, Blumhardt 1987, Ghilardi et al 1990). The latter of these have proved useful, since it has been shown that the VEP is modified almost identically by experimentally introduced scotomas and maculopathy (Fukui et al 1986, Blumhardt 1987).

The objective of this section is to examine how the VEMR is affected by occlusion of the central retina, and whether the results are consistent with a striate cortex origin.

9.32 - METHODS.

The full and half field responses of subject SC, and the lower left quarter field responses of subject CD were recorded to a field size of 7°20'x5°43' with 38'x27' checks at 65% contrast. Topographies were recorded with occlusion of the central 0°, 3° and 5° for full and half field stimulation and 0°, 3°, 5° and 7° quarter field, by the use of a disc placed over the monitor, centred at the point of fixation. The angle of occlusion corresponds to the disc diameter. Scotoma size was not adjusted to take account of known cortical magnification, hence increasing occlusion by the step size used here would not exclude the activity of equal volumes of cortex.

9.33 - GENERAL EFFECTS OF SCOTOMAS.

As scotoma size increased, the quality of the waveforms deteriorated progressively, showing smaller peaks of poorer definition, with the increasing presence of noise (figure 9.331). The CIIm peak remained visible regardless of the size of the scotoma, although the VEP P100 component has been shown to disappear with 4° (Reitveld et al 1967) and 8 to 10° scotomas (Blumhardt et al 1978 and Fukui et al 1986). The occlusion effects of pattern reversal stimuli have also been studied for the VEMR (Slaven 1992).

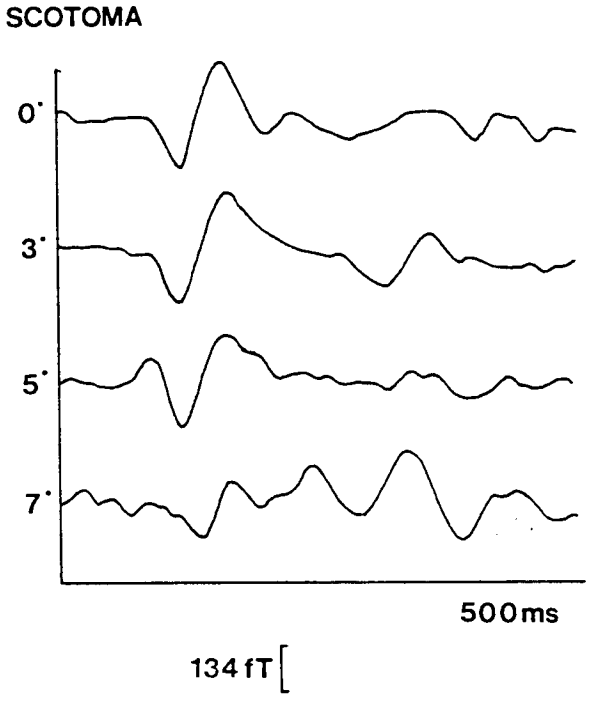

Figure 9.331 - Effect of central scotoma (0, 3, 5 and 7° diameter) on the lower left quarter field response waveforms of subject CD.

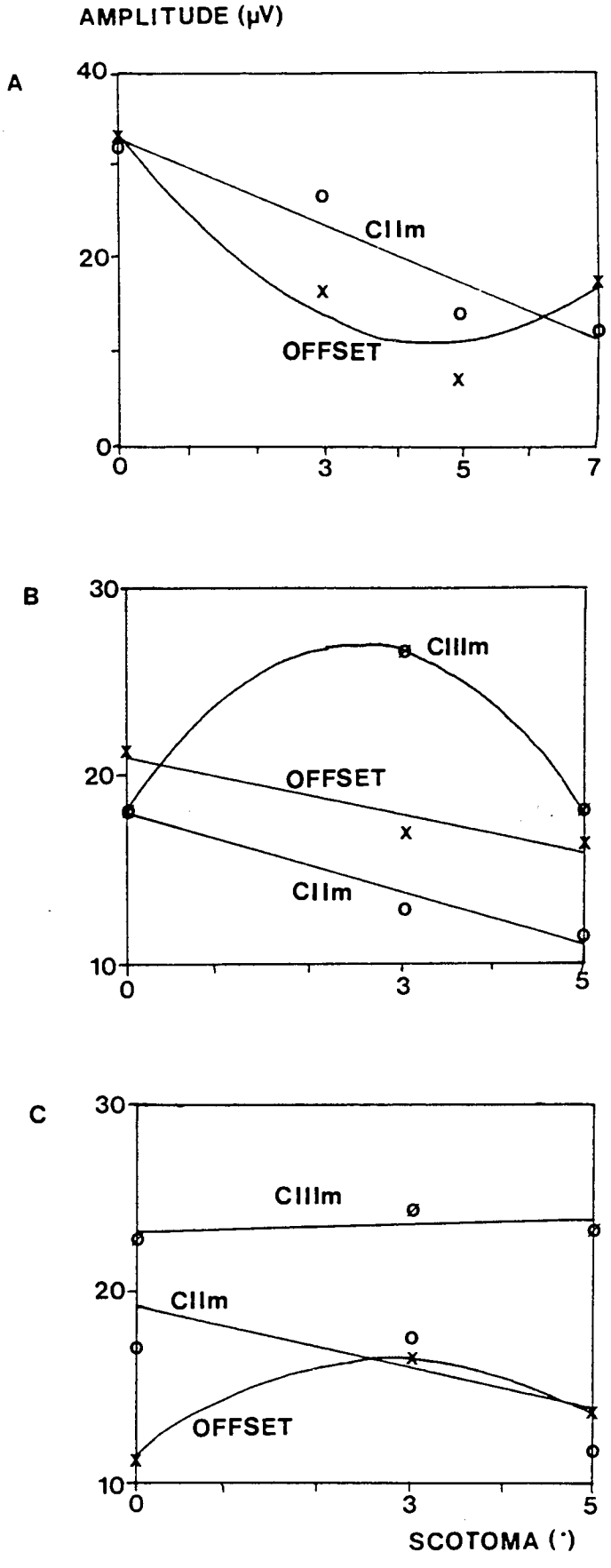

Figure 9.332 - Effect of increasing scotoma diameter on the amplitude of the lower left quarter field CIIm and offset peaks of subject CD (**A**); the full field CIIm, CIIIm and offset response of subject SC (**B**); and the right half field CIIm, CIIIm and offset responses of subject SC (**C**).

Although latency increases have been reported with increasing scotomas (Fukui et al 1986), no consistent trends were apparent with this data. Most peaks displayed an amplitude decrease with increasing occlusion (figure 9.332), the later peaks giving less consistent trends than the CIIm. Such a decline could be explained by the projection of peripheral retina to deeper portions of the calcarine fissure, and/or a decrease in the volume of active cortex due to cortical magnification effects. Such behaviour is also consistent with the pattern reversal and onset VEP findings of several authors (Reitveld et al 1967, Blumhardt et al 1978, Haimovic and Pedley 1982, Lesevre 1982, Ermolaev and Kleinman 1984, Fukui et al 1986, Maier et al 1987). A linear amplitude decrease with occlusion might have occured if the scotoma size had been adjusted for the effects of cortical magnification.

9.34 - TOPOGRAPHIC EFFECTS OF CENTRAL SCOTOMAS.

For a source of striate cortical origin, the cruciform model predicts that stimulation of progressively more peripheral retina should project to more anterior portions of the calcarine fissure (Jeffreys and Axford 1972 a). This has been observed practically by Maclin et al (1983) and Kaufman et al (1990) for the VEMR to grating annuli, who showed that increasing eccentricity produced a corresponding increase in field maxima separation. An alteration purely in depth such as this would occur for a calcarine fissure oriented perpendicular to the scalps surface, however this angle is known to vary considerably between individuals (see chapter 10). For a more acutely angled fissure, peripheral stimulation should produce deeper sources with a posterior to anterior shift in scalp distribution. Such a vertical displacement has been reported for the VEP to pattern reversal (Lesevre and Joseph 1979, Lesevre 1982) and pattern onset stimuli (Maier et al 1987), while combinations of depth and positional effects were observed for the flashed pattern VEP (Jeffreys 1971). Ahlfors et al (1992) however, found no consistent differences between foveal and peripheral octant field stimulation for the pattern onset VEMR.

Figure 9.341 shows the full field CIIm, CIIIm and offset responses of subject SC with central scotomas, while table 9.341 shows the average standard deviation values for comparisons between topographies recorded with 0 and 3°, and 3 and 5° scotomas. Of the three components, the CIIm is affected most by central occlusion, with the 3 and 5° scotoma distribution too complex to interpret. The

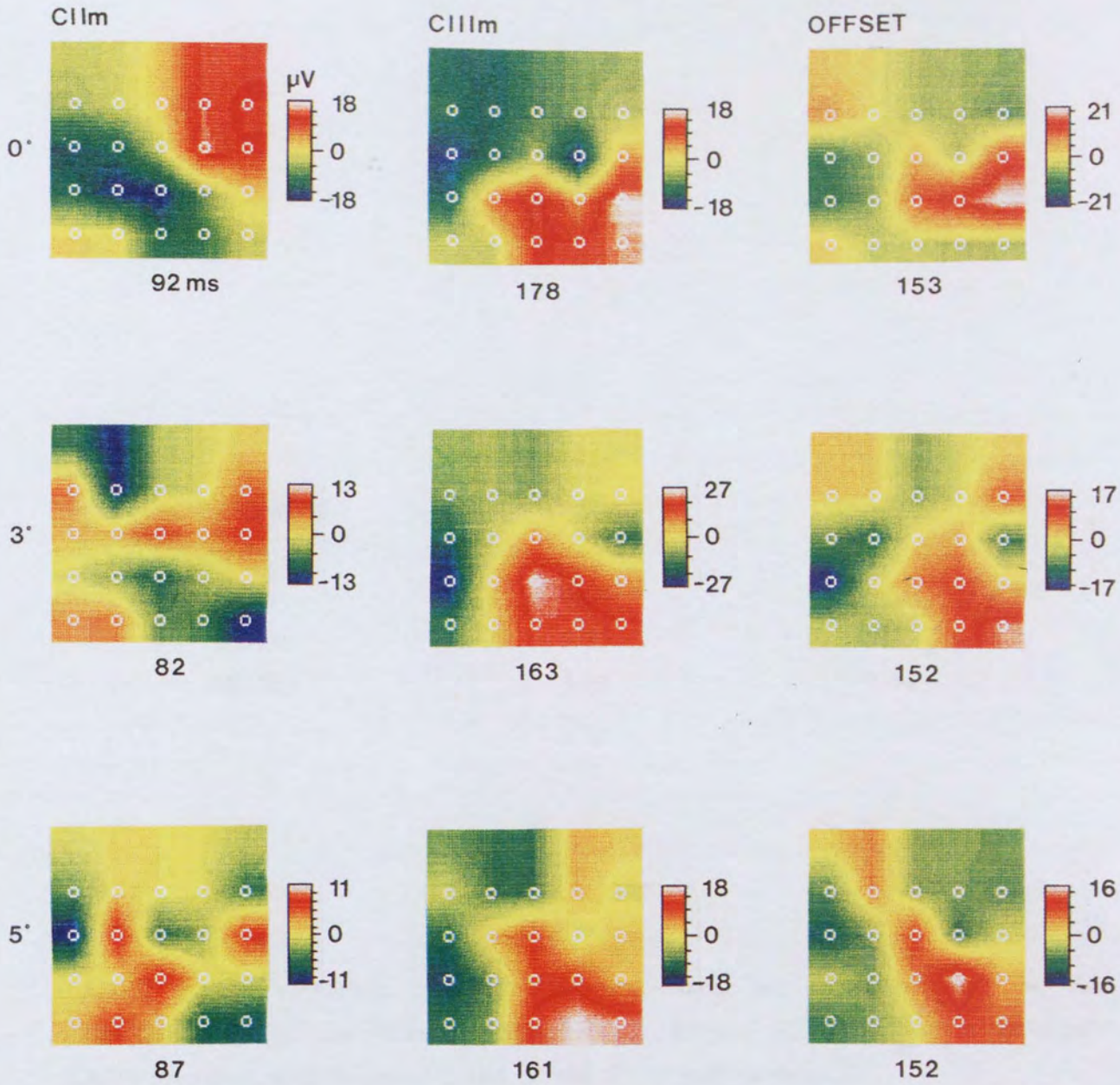

Figure 9.341 - Effect of increasing the size of central scotoma (0, 3 and 5° diameter) on the full field CIIm, CIIIm and offset topographies of subject SC.

COMPONENT	0° V's 3°	3° V's 5°
CIIm	6.06	6.56
CIIIm	5.85	5.35
OFFSET	5.35	3.64

TABLE 9.341 - Average standard deviation values for comparison of the full field CIIm, CIIIm and offset topographies of subject SC (data shown in figure 9.341) recorded with 0 and 3°, and 3 and 5° central scotoma.

CIIIm is least affected, with a recognisable distribution evident for all stimulus conditions. No systematic alteration in source depth or scalp position were apparent for any peak, consistent with the findings of Ahlfors et al (1992), although any changes might be difficult to detect considering the large number of sources activated.

Figure 9.342 shows the right half field topographies of subject SC, with response analysis provided in table 9.342. Unlike the full field distributions of figure 9.341, the half field CIIIm response becomes uninterpretable with occlusion of the central 3 and 5° of the stimulus. The offset distribution is quite consistent for all stimulus conditions (figure 9.342), as indicated by the low SD values of table 9.342. The CIIm topography is predictable with occlusion of the central 3° of the stimulus, however 5° occlusion produces a complex distribution of low amplitude. The weak ipsilateral hemispheric activity seen for the half field CIIm of this subject (see chapter 6), is evident for all CIIm scotoma responses. This suggests that the origin of such activity cannot be explicable by the projection of the central 1° of each retina to each hemisphere (Leventhal et al 1988, Victor et al 1991), leaving the possibility of a callosal transfer. The diffuse maxima of the occluded responses makes the presence of source location changes difficult to detect.

The lower left quarter field responses of subject CD are shown in figure 9.343. Once more, the CIIm topography is relatively stable with increasing occlusion, however the field maxima become increasingly diffuse and separated, consistent with an increase in cortical depth. An increase in source depth with central field occlusion could also be inferred from the progressive reduction in response amplitude, however this might also result from changes in the volume of active cortex due to cortical magnification effects. The topographic changes with increasing scotoma size are reflected by the average SD values, with the comparison between the 0 and 3° scotoma response producing an average SD of 5.44, that between 0 and 5° is 5.81, and that for 0 and 7° is 6.11. Although these values increase with occlusion, they are all less than the full field CIIm intertrial variability, reported in chapter 5 (SD = 7.39). The offset response (figure 9.343) is particularly difficult to interpret, since although the distribution produced by a stimulus with 7° scotoma shows field areas consistent with the cruciform model, reducing scotoma size produces unpredictable, complex distributions. The behaviour of the CIIm and component could therefore be explicable by a striate cortex origin, as can the

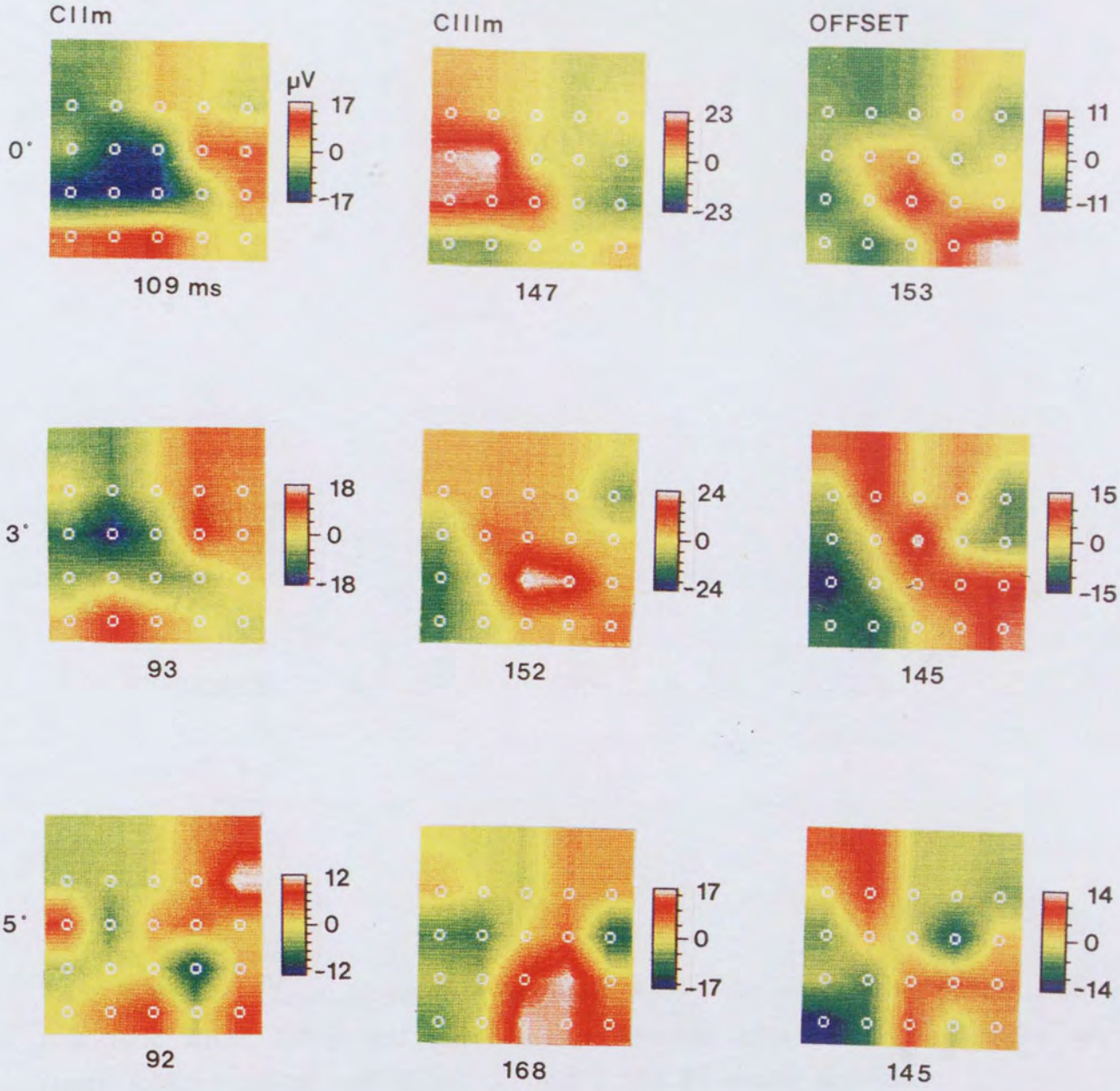

Figure 9.342 - Effect of increasing the size of central scotoma (0, 3 and 5° diameter) on the right half field CIIm, CIIIm and offset topographies of subject SC.

COMPONENT	0° V's 3°	3° V's 5°
CIIm	3.77	5.58
CIIIm	7.95	8.09
OFFSET	3.50	3.76

TABLE 9.342 - Average standard deviation values for comparison of the right half field CIIm, CIIIm and offset topographies of subject SC (data shown in figure 9.342) recorded with 0 and 3°, and 3 and 5° central scotoma.

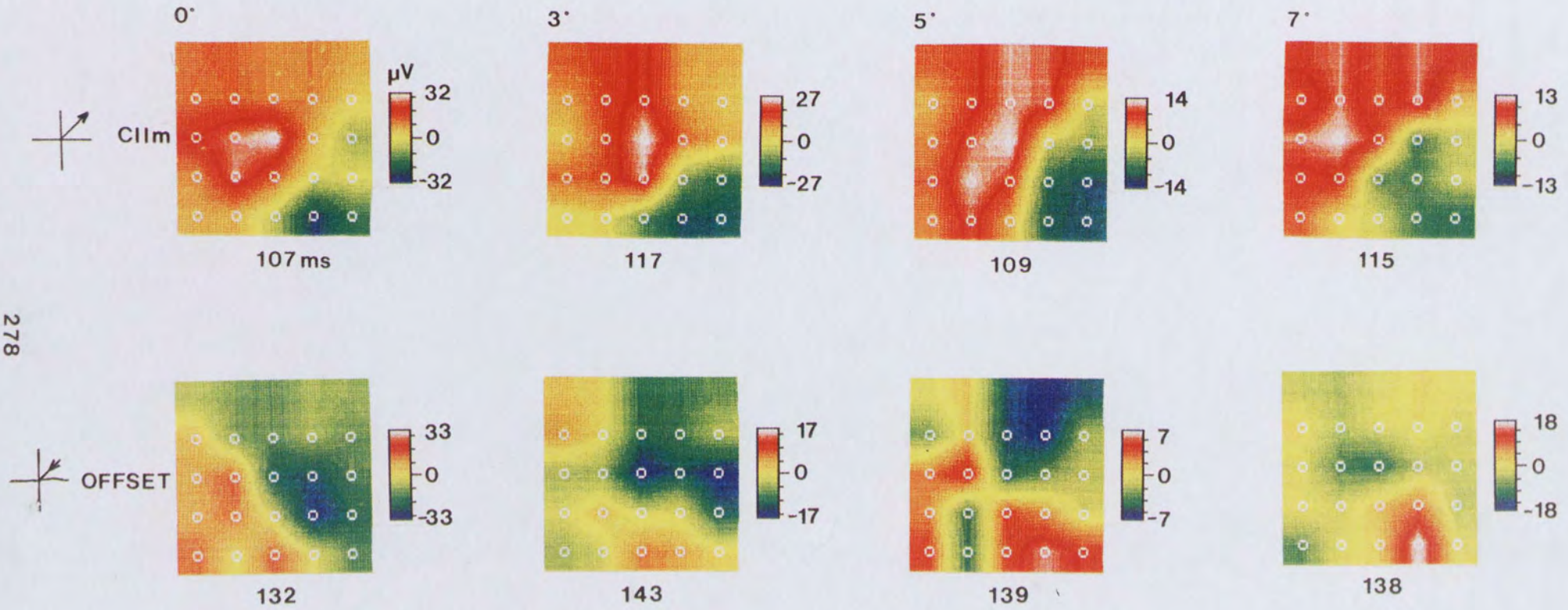

Figure 9.343 - Effect of increasing the size of central scotoma (0, 3, 5 and 7° diameter) on the lower left quarter field CIIm and offset topographies of subject CD.

results of the full and half field responses of subject SC. These results also indicate that the presence of the onset and offset VEMR components is not restricted to predominantly foveal stimuli, as has been seen previously for the VEP (Reitveld et al 1967). This is not too surprising however considering the different source orientations which may be optimally detected by the VEP and VEMR (Stok 1986).

CHAPTER 10.

10.1 - CORTICAL MORPHOLOGICAL VARIATION.

Interpretation of scalp surface electrical or magnetic field distributions by visual inspection, or source localisation algorithms requires knowledge of the anatomy of visual cortex (Myslobodsky et al 1991). The accuracy of such procedures is limited by the large intersubject cortical morphology variations with respect to the scalp surface landmarks (Brindley 1972, Srebro and Purdy 1990). Improvements can be made by the incorporation of MRI (Rogers et al 1991, Ahlfors et al 1992), or a combination of MRI and CT data for each individual (Srebro and Purdy 1990). As an approximation, authors make reference to the idealised cruciform model of striate cortex (Jeffreys and Axford 1972 a).

A quantitative study of the morphological variations in striate cortex would be of particular benefit in interpretation of MEG data, (Okada et al 1987). Few such studies have been reported however, possibly due to the usefulness clinically of the VEP, which is relatively insensitive to variations in source orientation. The positional variability of cortical sulci have been studied with respect to the 10-20 electrode placement system, using anatomical (Jasper 1958 and Blum et al 1974), X ray (Jasper 1958, Hellstrom et al 1963) and MRI techniques (Steinmetz 1989). MRI data has also been used to study anatomical (Myslobodsky et al 1991) and functional, occipital hemispheric asymmetries (Belliveau et al 1991). Post mortem studies have been reported by Brindley (1972), with possibly the most definitive study into hemispheric development and morphological variations being that of Polyak (1957). Several authors have reported physiological differences between the sexes, with males displaying on average, larger nasion to inion distances (Stockard et al 1979); larger brains relative to body length (Skullerud 1985); greater brain mass (Buchsbaum et al 1974); and increased interhemispheric structural asymmetries, with enhanced right frontal and left occipital predominance (Bear et al 1986). Such differences are thought to originate from the effects of gonadotrophic hormones on the plasticity of the brain during development (Buchsbaum et al 1974, Bear et al 1986).

The aim of this chapter is to examine some of the ways in which the intersubject and interhemispheric morphology of the striate cortex can vary,

and its possible influences upon the interpretation of MEG responses. Detailed comparisons between the findings of this study, and the topographic results of previous chapters cannot be made, since MRI scans are not available for those particular subjects. Where possible however, data from those previous chapters has been referenced, where some features of its distribution or behaviour could be explained by the general anatomical variations identified here.

10.2 - VARIATIONS IN CALCARINE FISSURE SHAPE.

Although the cruciform model assumes a horizontal calcarine fissure, uniform throughout its depth, this is rarely seen in practice, as many subjects show a curved fissure with one or more arches (Polyak 1957), the form of which varies between individuals (Belliveau et al 1991, Myslobodsky et al 1991). In some subjects, a second sulcus lies parallel to that of the calcarine sulcus, (the medial and lateral inferior or superior paracalcarine sulcus). Alternatively, the calcarine fissure can be broken into two or more segments, by the presence of a superficial cuneolingual fissure (Polyak 1957).

Figures 10.21 and 10.22 show the shape of fifty calcarine fissures obtained from published sagittal MRI scans (MRI of the Head and Neck, Lufkin RB and Hanafee WN (Eds), Raven MRI Teaching Series, 1992 and Cranial MRI - A teaching file approach, Bisese JH (Ed), McGraw Hill, 1991). All scans showing occipital lobe pathology were excluded. Ideally the study should be performed using MRI scans of normal individuals, since any pathology is likely to have some disruptive influence on cortical morphology. The use of such data was not possible for this study, although the early work reported by Jasper (1958) also used specimens in which examples showing "gross lesions or local atrophy were excluded". Of the fifty fissures, fourteen are from the left hemisphere (marked o) while the remaining thirty six are from the right. For the purpose of this chapter, the left hemispheric fissures are displayed in mirror image. Each figure shows the curvature of the scalp; a section of the nasion to inion line, presented horizontally; the calcarine fissure and a broken line representing the angle of the calcarine fissure with respect to the nasion to inion plane. The latter of these will be discussed more fully in section 10.3. The calcarine sulcus was identified with reference to the parieto-occipital sulcus, and the posterior regions of the splenum of the corpus

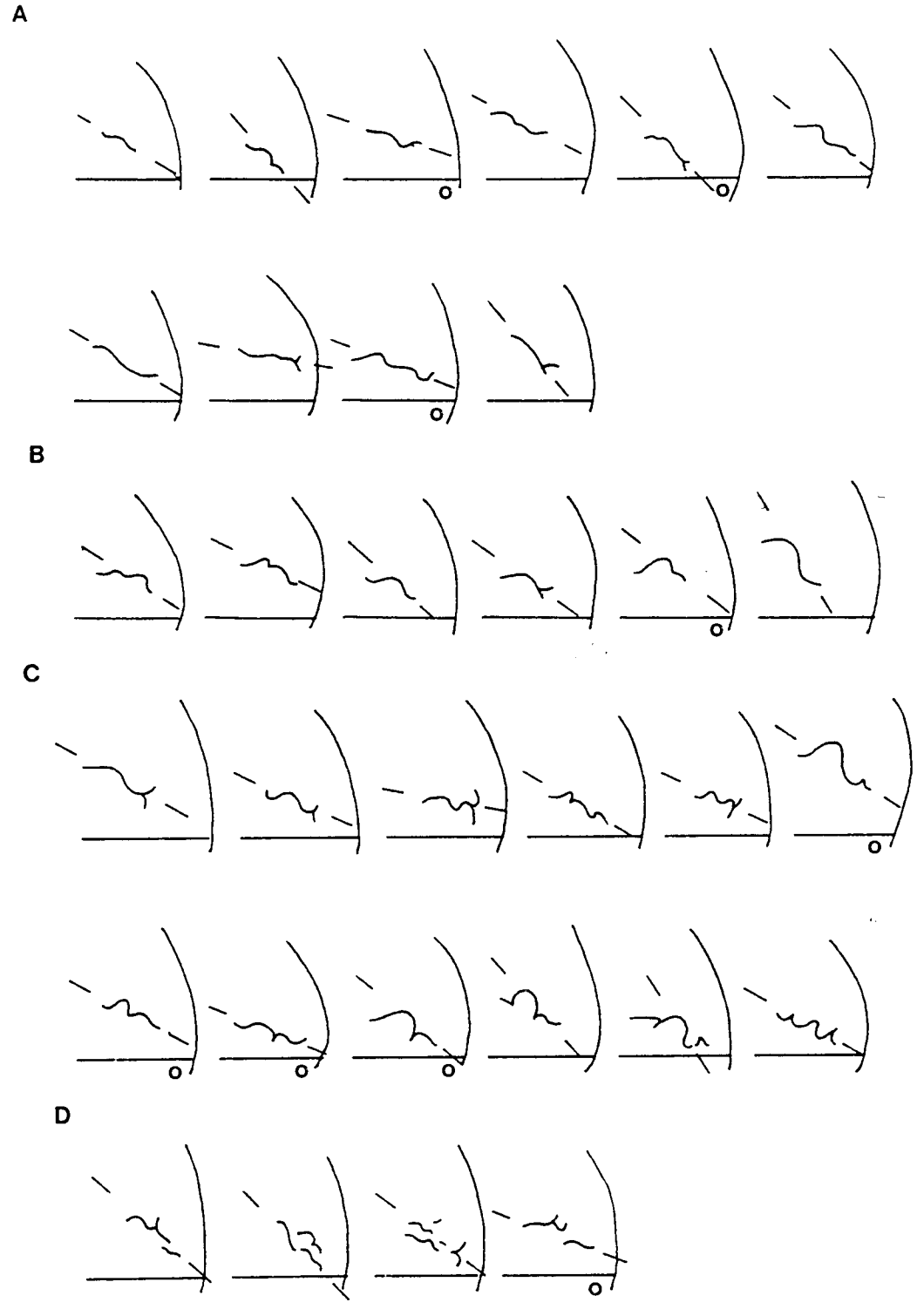

Figure 10.21 - Diagramatic representation of calcarine fissure morphology and intersubject variation. Each drawing was obtained from a sagittal MRI scan of a different subject. Each shows the curvature of the scalp to the right; a section of the nasion to inion (NI) plane (shown horizontally); the calcarine fissure; and a single line to represent the angle of the calcarine fissure with respect to the NI plane. Sections marked (o) were obtained from the left hemisphere, but are displayed in reverse. The fissures have been broadly classified either as those which are straight (**A**), those with a single arch (**B**), multiple arches (**C**) or broken fissures (**D**).

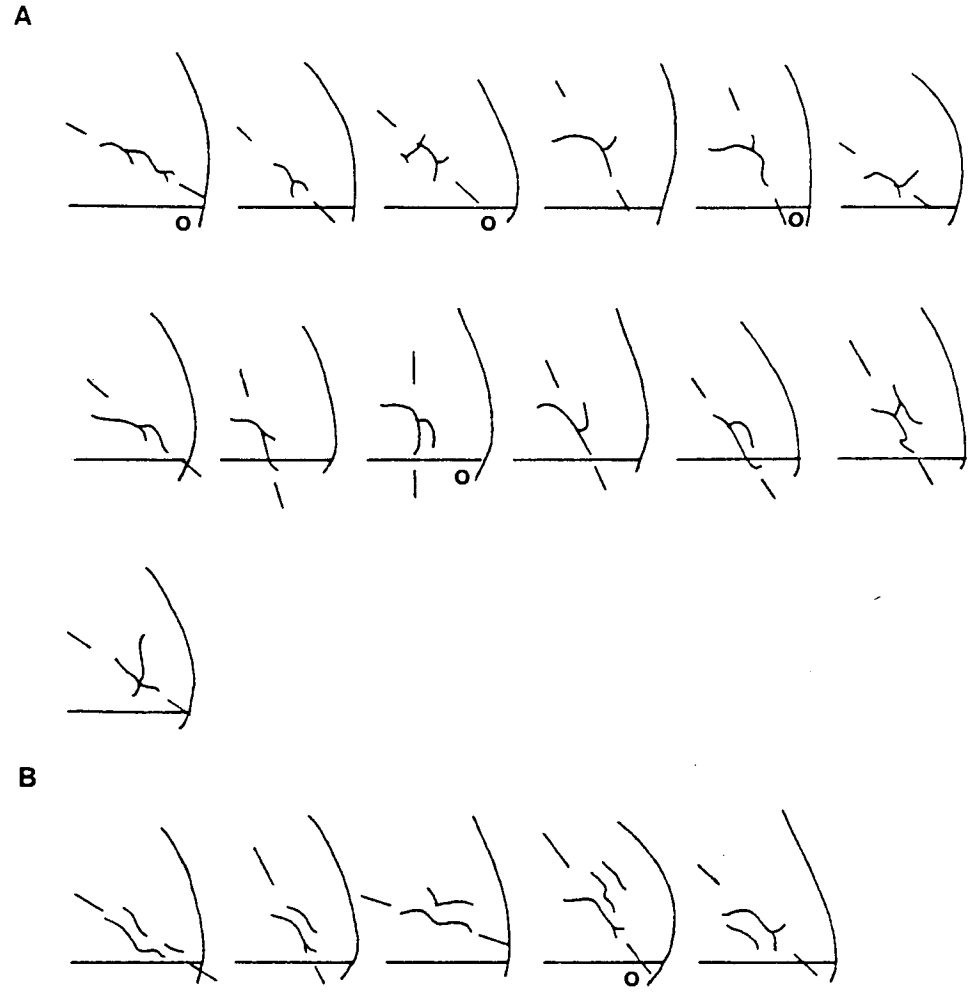

Figure 10.22 - As figure 10.21 except the fissures are classified here by the presence of branches (**A**) or multiple fissures (**B**).

collosum. The inability to adjust the depth of sagittal scan for the data studied produces a possible source of variation, since each scan might not be aligned with the crest of the cuneal and lingual gyri. Ideally, this source of error would be excluded by the collection of dedicated MRI data (Steinmetz et al 1989).

An almost infinite variety of fissure shapes can be obtained between individuals (Polyak 1957) making classification difficult, however the fifty fissures observed here were separated into six broad groupings. These are for essentially straight sulci (figure 10.21A); those showing a single arch (figure 10.21 B); those with multiple arches (figure 10.21C); those broken into two or more segments (figure 10.22D); branched fissures (figure 10.22A); and hemispheres showing multiple, parallel fissures (figure 10.22B). With straight fissures, the orientation of sources within the walls of the calcarine and longitudinal sulci would remain constant with respect to the surface of the scalp, regardless of the depth of stimulus projection. For arched fissures, the orientation of calcarine sources would vary with depth, altering their 'visibility' with respect to the magnetometer, while sources on the medial lobe surfaces would remain unchanged. Broken and branched fissures would produce unpredictable source orientations with stimuli projecting to the regions of transitional anatomy. Finally, the presence of parallel fissures would only produce problems of source interpretation if the shadow fissure lay in extrastriate regions.

10.31 - QUANTITATIVE CALCARINE VARIATION.

The height of the calcarine fissure above the inion varies between individuals (figures 10.21 and 10.22), a factor which should result in an intersubject variation in the anterior/posterior displacement of scalp field maxima. The extent of such variation cannot be measured directly from these figures, since a uniform scale was not used for their measurement. However, Steinmetz (1989) observed an absolute variation of 4 cm, while Myslobodsky et al (1991) also noticed that the right hemispheric fissure was generally higher than that of the left. Such variation can be seen for the full field CIIm topographies of figure 6.82. In particular, the transition between inward and outward flowing fields over the left hemispheres of subjects SC (6.82A), EW (6.82H) and PG (6.82I) vary by between 1 and 9cm above the inion line.

Measurements of the angle between the calcarine fissure and the nasion to inion plane are difficult to make, especially with curved sulci. To estimate this angle a single, straight line was fitted to all examples (figures 10.21 and 10.22), most easily achieved for straight fissures and those with subtle curves. For fissures with more extreme variations, the angle of the posterior sections were considered most important, since their relatively superficial depth would lead to preferential source detection (Okada et al 1987). Hence, the calcarine angle varied between 11° and 89°, with a mean value of 40° for the fifty individuals, with no significant interhemispheric variation (table 10.31). Myslobodsky et al (1991) adopted a more objective method of assessing this angle, by taking measurements between the nasion and inion line and the calcarine fissure at nine arbitrary positions. These values were plotted as a function of calcarine distance, and a regression line fitted to the data produced an angle with respect to the vertical. Their results for fourteen subjects produced an angle of 67.8° ±8.69° for the left and 73.1° ±4.29° for the right hemispheric fissures. This corresponds to an angle of 22.2° and 16.9° respectively, with respect to the nasion to inion line. Although the results of Myslobodsky et al (1991) differ from those of this study, it does not necessarily indicate that their measurement technique produced more significant results. The choice of nine arbitrary reference points might not produce a sufficiently representative sample of the fissure to assess its underlying angle, especially for convoluted sulci. The small sample size used might also have been unrepresentative. The posterior sulcal bias used here could have provided a source of variation, although there is no evidence to suggest that the angle of this section is consistently steeper than any other. Alternatively, differences in the mean fissure angle between these studies might be accounted for by the spatial distortions experienced with MRI images (Coffey et al 1992). Whichever data set is accepted, it is evident that the calcarine fissure is rarely, if ever, straight and perpendicular to the scalps surface. If it were, stimulation of deeper locations along its length would produce field maxima centred over a constant scalp position, but with increasing separation. This could explain the behaviour of the full field CIIm component of subject CD, with varying check size (chapter 8.16, figure 8.161). Such results have also been demonstrated practically for the VEMR by Maclin et al (1983) and Kaufman et al (1990). For a fissure angled at the other extreme observed here, (89°), similar stimulation would produce a scalp distribution consistent with a source of constant depth,

TABLE 10.31 - Variation in the angle of the calcarine fissure of 50 individuals measured relative to the nasion to inion plane. Results are presented for left, right and both hemispheres combined.

	LEFT HEMISPHERE	RIGHT HEMISPHERE	LEFT/RIGHT COMBINED
N	14	36	50
MIN ANGLE	19°	11°	11°
MAX ANGLE	89°	72°	89°
MEAN ANGLE	40.4°	40.1°	40.2°
S.D.	19.7°	15.0°	16.2°

S.D. = standard deviation

which migrated in a posterior to anterior direction. Such movement was seen for the full field CIIm responses of subject RAA to variations in check size (chapter 8.16, figure 8.162). This has also been observed practically for pattern reversal (Lesevre and Joseph 1979, Lesevre 1982), and pattern onset stimuli (Maier et al 1987). For a 40° fissure angle, changes in both depth and vertical displacement would be expected, as shown by the flashed pattern responses of Jeffreys (1971).

Changes in the angle of the calcarine fissure would also influence source orientations relative to the scalp, and hence those sources detectable by MEG. For a perpendicular sulcus, both longitudinal and calcarine fissure sources would be tangential with respect to the scalp, while polar sources would be predominantly radial, and therefore magnetically silent (Okada et al 1987). As the sulcus angle increased with respect to the horizontal, there would be a corresponding increase in the tangential and radial components of the polar and calcarine sources respectively (Harding et al 1991). It is unlikely that such intersubject variations in sulcal angle would be detected by a full or half field stimulus of fixed parameters, due to the domination of the response by tangentially oriented sources on the medial lobe surfaces (Jeffreys and Axford 1972 a). With quarter fields and horizontal octants however, such changes in fissure angle should become apparent in the scalp distributions, leading to more variable responses. This could explain why the results to quarter and octant field stimulation (chapter 9), displayed more variable intrasubject topographic distributions than those to full and half field stimuli (chapter 6).

10.32 - MORPHOMETRIC ANALYSIS OF SKULL SHAPE.

Textbook photographs frequently display the brain as having a horizontal calcarine fissure (figure 10.321A). If the brain is viewed in a more realistic orientation however, either on sagital MRI sections or post-mortem dissections, the fissure is far from horizontal. A post-mortem specimen is shown in figure 10.321 B, (Colour Atlas Of Anatomy 2nd Ed, McMinn RMH and Hutchings RT, Wolfe Medical Publications Ltd, 1988). In such cases, the brainstem is oriented vertically in the head, while the parietal and occipital lobes are displaced downwards from the horizontal, producing a corresponding increase in the angle of the calcarine fissure. Since the brain closely follows the interior contours of the skull, it is possible that skull shape

Figure 10.321 - Two views of the medial surface of the brain, as seen in post mortem specimens (**A**) and from MRI scans (**B**). This illustrates the influence of skull shape on the shape of the brain.

influences calcarine fissure angle. To investigate this further, a series of sagittal MRI scans from fifty individuals were examined (as used in section 10.31). If such a correlation does exist, it would prove useful for response interpretation in subjects where MRI data was unavailable.

The sagittal MRI scans were traced onto acetate sheet and photoenlarged. Since the scale of the original data were not provided, only relative measurements were used for intersubject comparison. A number of surface features were measured in an attempt to quantify changes in skull shape, particularly in the occipital regions. Firstly, the nasion to inion line was marked (N to I, in figures 10.322A, B and C) and the angle of the calcarine fissure measured with respect to it (Angle 4 figure 10.322A), as described in the previous section. The circumference over the scalp between the nasion and inion points was measured using a cartographic wheel. Points were marked above the inion at 10% intervals of the circumference (points 1, 2 and 3 of figure 10.322A), corresponding to the horizontal rows of the mapping array used throughout this thesis. Tangents to the scalp were marked at each of these points, and their angle measured with respect to a line perpendicular to the nasion to inion plane. In order to quantify the curvature of the rear portions of the skull, three different methods were used. These could be applied to any subject, by first drawing the outline of the individuals skull on paper, with the aid of a draughtsman's flexible rule.

Method 1 - (Figure 10.322B) The relative difference in prominence between the front and rear portions of the skull were assessed using reference lines drawn perpendicularly from the nasion to inion plane, separated from the scalp by a distance equivalent to 10% of the NI line (marked in figures 10.322B and C by o). The horizontal distance between the point of inflection on the crown of the skull, and the front (A) and rear (B) references were measured. From the equation :-

$$\text{Curve 1} = A / (A + B) \times 100$$

a percentage was obtained for the prominence of the frontal skull, relative to the whole length. An increase in this value would indicate a steeper occipital region, and possibly an increased distortion of the underlying cortex.

Method 2 - (Figure 10.322B) The severity of the occipital incline was measured from the equation :-

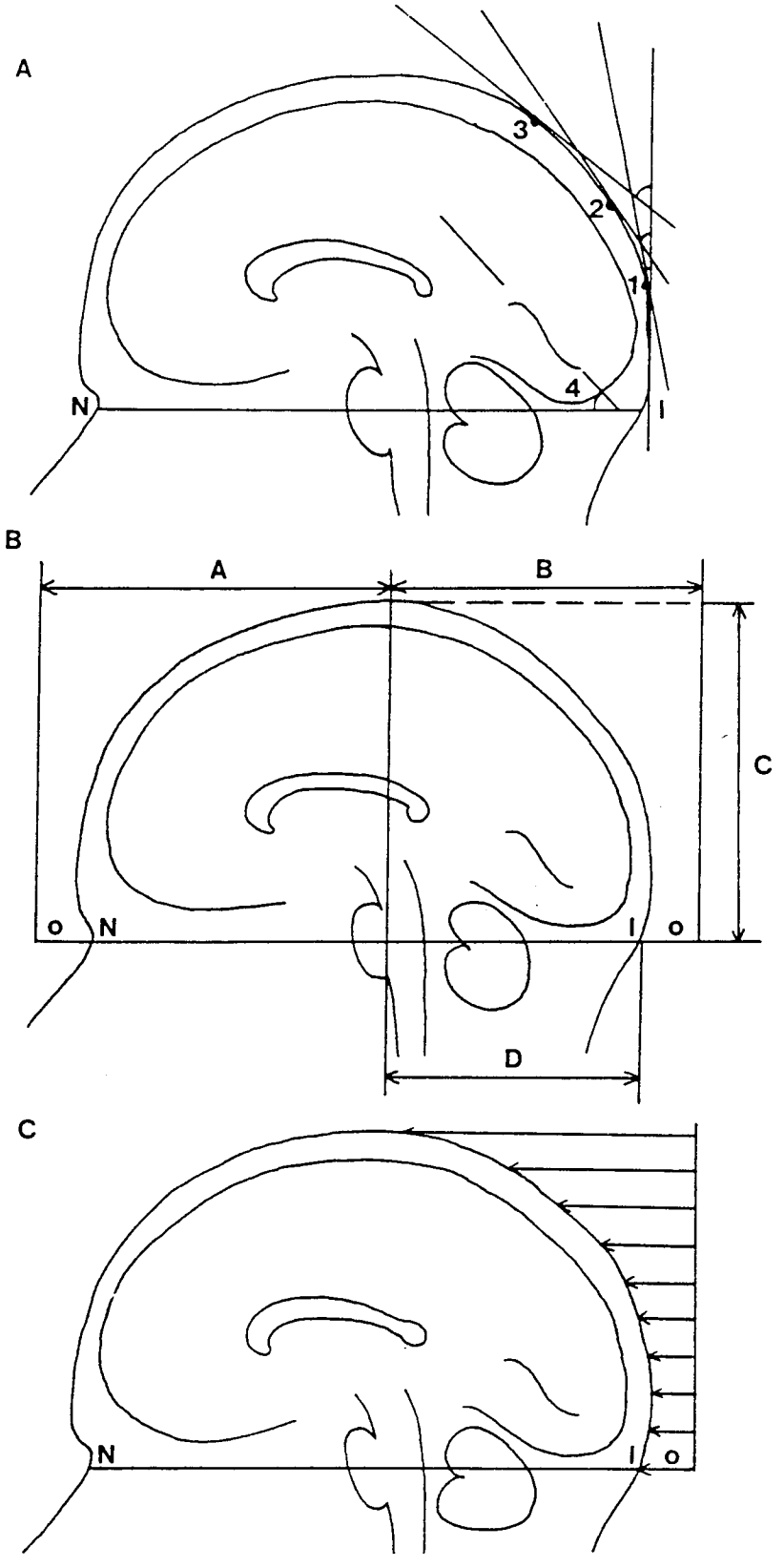

Figure 10.322 - Measurements made on the sagittal MRI data to quantify the angle of the calcarine fissure and the curvature of the scalps surface in each case. NI - nasion to inion plane.
A - 1,2 and 3 = the angle between a tangent drawn to the scalp (above the inion at 10, 20 and 30% of the half head circumference respectively), and a plane drawn perpendicular to the NI plane. 4 = the angle of the calcarine fissure with respect to the NI.
B - A and B = the distance between the point of inflection on the scalp and a plane perpendicular to the NI from the nasion and inion respectively. 0 = a distance equivalent to 10% of the NI. C = the distance from the point of inflection to the NI. D = the horizontal distance between the point of inflection and the inion.
C - horizontal distances between a plane perpendicular to the NI and the scalps surface, each made at regular intervals above the NI.

Curve 2 = C / D x 100

where C is the vertical height between the nasion to inion plane and the point of inflection of the skulls crown, while D is the horizontal distance between the inflection point and the inion. Once more, an increased value would be consistent with a steeper curvature.

Method 3 - (Figure 10.322C) Horizontal measurements were made between the rear reference line and the skulls surface, at vertical separations of 5mm. These values were plotted as a function of vertical height, and a third order polynomial produced a numerical term to describe the curvature. Unlike the previous methods, an increase in this value does not correspond to a systematic change in skull angle, but instead describes the shape of the skull.

The results of each of the above measures for the fifty individuals were plotted singularly, and in various combinations, as a function of calcarine angle. First and second order polynomial functions were fitted to the data to assess the statistical significance of any correlations. No significant first order correlations were found, however with a second order polynomial, the angle of the scalp at 20% above the inion was significantly correlated with the angle of the calcarine fissure ($p<0.05$) (Table 10.323 and figure 10.324A). Statistical significance increased by using combined measures, as shown in Table 10.323B and figures 10.323B and C. The term used in figure 10.324C produced less intersubject variability than that of figure 10.324B, showing a significant correlation of $p<0.02$.

This study illustrates that there could be a relationship between the shape of the skulls surface and the angle of the calcarine fissure. Although poor, the statistical significance of this correlation can be improved by the combination of different scalp measurements. The curvilinear trends and interindividual variability limits the practical applications of such a measure, however the results of this preliminary study provide a promising basis for a more detailed investigation.

10.4 - INTERHEMISPHERIC VARIATION.

The cruciform model assumes that a mirror symmetry exists for the morphology of the calcarine fissure between the medial surfaces of each occipital lobe (Myslobodsky et al 1991). Although such similarities can be

TABLE 10.323 - Comparisons between the angle of the calcarine fissure, measured with respect to the nasion to inion plane, and eight different methods of characterizing the shape of the scalp.

TEST	FUNCTIONS PLOTTED	R VALUE OF SECOND ORDER POLYNOMIAL	SIGNIFICANCE (P)
1	Tangent at 10%	0.08	N.S.
2	Tangent at 20%	0.29	< 0.05
3	Tangent at 30%	0.03	N.S.
4	Curve, method 1	0.09	N.S.
5	Curve, method 2	0.24	N.S.
6	Curve, method 3	0.21	N.S.
7	4 / (2 x 5)	0.30	< 0.05
8	(6 x 4) / 2	0.32	< 0.02

N.S. = Not significant

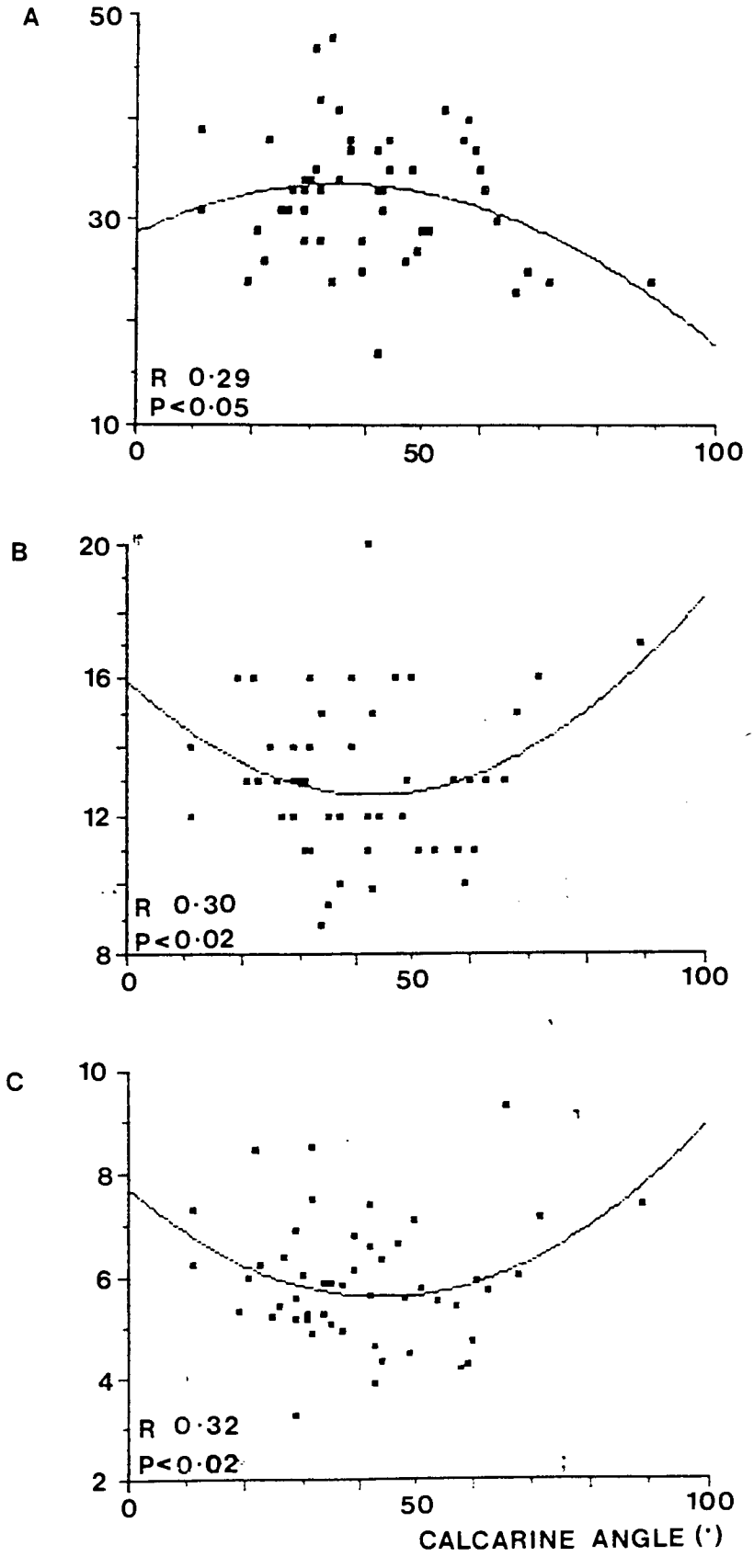

Figure 10.324 - Scatter plots to compare the angle of the calcarine fissure with three different measures of the scalps curvature. MRI data from 50 subjects is used in the analysis. In each case, the angle between the calcarine fissure and the nasion to inion plane is show along the horizontal axis. The vertical axis characterize the scalps curvature by either:-

A - Angle 2

B - The formula:- Curve #1 / (Angle 2 x Curve #2) or

C - The formula:- Curve #3 x Curve #1) / Angle 2

Where Curve #1, #2 and #3 = measurement methods 1, 2 and 3 respectively (see section 10.32) and Angle 2 = the angle at 20% above the inion (see Figure 10.322 A, angle 2).

Second order polynomials are fitted to each data set, R indicating the goodness of fit, and P the statistical significance.

seen, Polyak (1957) observed that no two hemispheres are exactly alike in all details of the calcarine fissure complex.

Figures 10.41 and 10.42 show the medial and polar aspects of each hemisphere for two post-mortem brain specimens. Initials are used to mark salient features, (C = cuneal gyrus, Cbl = cerebellum, Lc = lateral calcarine sulcus, Lg = lingual gyrus, Po = parieto-occipital fissure and Spl = splenum of corpus callosum).

For the specimen in figure 10.41, the morphology of the calcarine fissure is consistent between the medial surfaces of each hemisphere. Each fissure is relatively straight, with both cuneal and lingual gyri equally represented. In individuals where the vertical course of the fissure varies, the size of either of these gyri can be reduced or augmented (Polyak 1957). Such variation could explain the full field CIIm results for subjects SC and RAA to changes in check size (chapter 8.24, figures 8.161 and 8.162). For both subjects, the field maxima over one hemisphere rotated relative to each other as check size decreased. This would be consistent with sources in the upper surfaces of the calcarine and longitudinal fissures dominating the summation with such parameters. This might be explained by temporal summation effects (see chapter 7), or to a reduced lingual gyrus in the cortical regions optimally stimulated by small check sizes. The projection of the fissure onto the lateral surface of the pole differs between the hemispheres, with the presence of lateral calcarine sulci forming a T shaped morphology in the left and + shape in the right hemispheres. A fork in the posterior sections of the calcarine fissure such as these is a common anatomical feature (Polyak 1957, Butler et al 1987). Polyak (1957) further described how this branching can arise before the pole, at the pole or around onto the posteriolateral surface. Polar variation of this kind would only be detected by the MEG for stimuli which project to sources within the sulcal walls, and were therefore tangentially oriented. In such cases, large intersubject variations in the position and orientation of scalp fields would occur.

For the individual of figure 10.42, a less consistent morphology is evident between the hemispheres. The calcarine sulcus of the right hemisphere is broken prior to its emergence onto the posteriolateral surface, following which it curves upwards and branches downwards. A break in the calcarine fissure such as this occurs when the posterior or anterior cuneolingual gyri are not submerged, but instead appear on the medial surface of the lobe

Figure 10.41 - Medial and polar aspects of each hemisphere of a post mortem brain specimen. C - cuneal gyrus, Cbl - cerebellum, Lc - lateral calcarine sulcus, Lg - lingual gyrus, Po - parieto-occipital fissure and Spl - splenum of the corpus callosum.

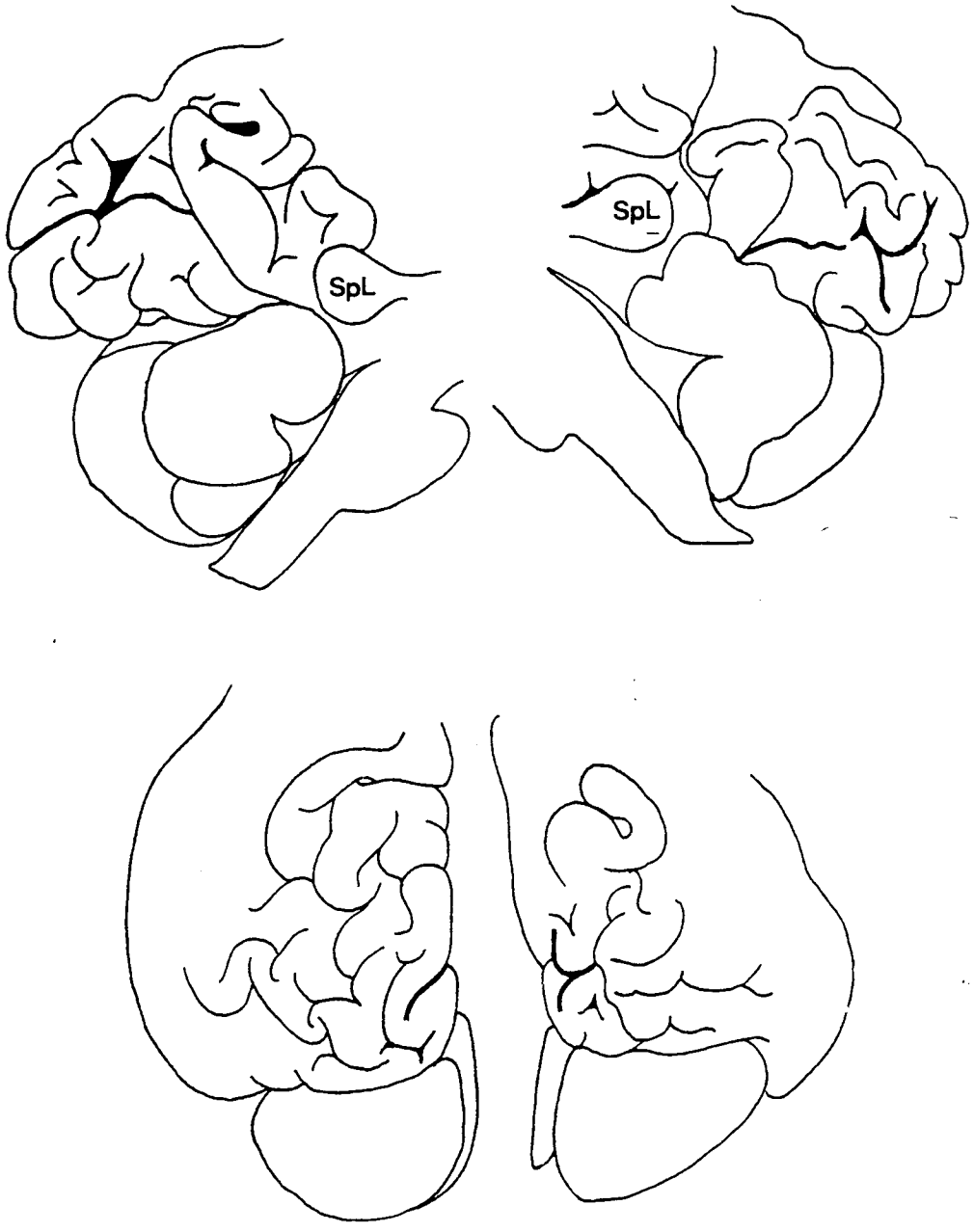

Figure 10.42 - Medial and polar aspects of each hemisphere of a post mortem brain specimen. C - cuneal gyrus, Cbl - cerebellum, Lc - lateral calcarine sulcus, Lg - lingual gyrus, Po - parieto-occipital fissure and Spl - splenum of the corpus callosum.

(Polyak 1957). Such a feature would produce problems in the interpretation of quarter or horizontal octant field stimuli projecting to this region, since only sources oriented in the medial plane would be represented. For the left hemisphere, the calcarine fissure is not broken by the posterior cuneolingual gyrus, but instead by a vertical fissure. Stimulation of this region would result in an unpredictable mixture of source orientations. The posteriolateral surface projection of the calcarine sulcus on the left hemisphere also differs from that of the right, which shows a single unbroken course.

10.5 - CHANGES IN CROSS SECTIONAL SHAPE WITH DEPTH.

The cruciform model of striate cortex assumes that the calcarine fissure of each hemisphere lie horizontally, forming the arms of a cross with respect to the vertical, longitudinal fissure (Jeffreys and Axford 1972 a). In practice, extensive interindividual and interhemispheric variations are evident. Sources of variation include fissures which are curved, branched, angled away from the horizontal, those which do not show a uniform separation between their walls and those where the fissures of each hemisphere lie at different heights.

Figures 10.51 and 10.52 show tracings of sequential, transverse vertical MRI sections for two subjects (Obtained from Dr D Beale, Walsgrave Hospital, Coventry). In each case, the scans are numbered sequentially from the pole, with a depth separation of 6mm. It is apparent that neither individual shows a classical cruciform arrangement at any depth, with almost all of the above variations appearing on one scan or another. A fissure angled away from the horizontal is often seen, with an upward displacement being the most common (figure 10.51, 1 to 3 and 10.52, 1 to 3). This should not affect full and half field distributions, due to the dominance of sources on the medial surfaces (see chapter 6). With quarter fields, or horizontal octants however, such variations would be reflected in the scalp distributions (see chapter 9). Branching of the calcarine fissure, as seen in figures 10.51 (5 to 9) and 10.52 (3 to 7), can occur by the convergence of fissures such as the calcarine and parieto-occipital. Once more, the effects of such variation would only be observed practically for stimuli which did not activate sources lining all of the fissure.

An interhemispheric variation in fissure height, such as that seen in figure 10.52 (8 to 12), would result in a corresponding asymmetry in the height of

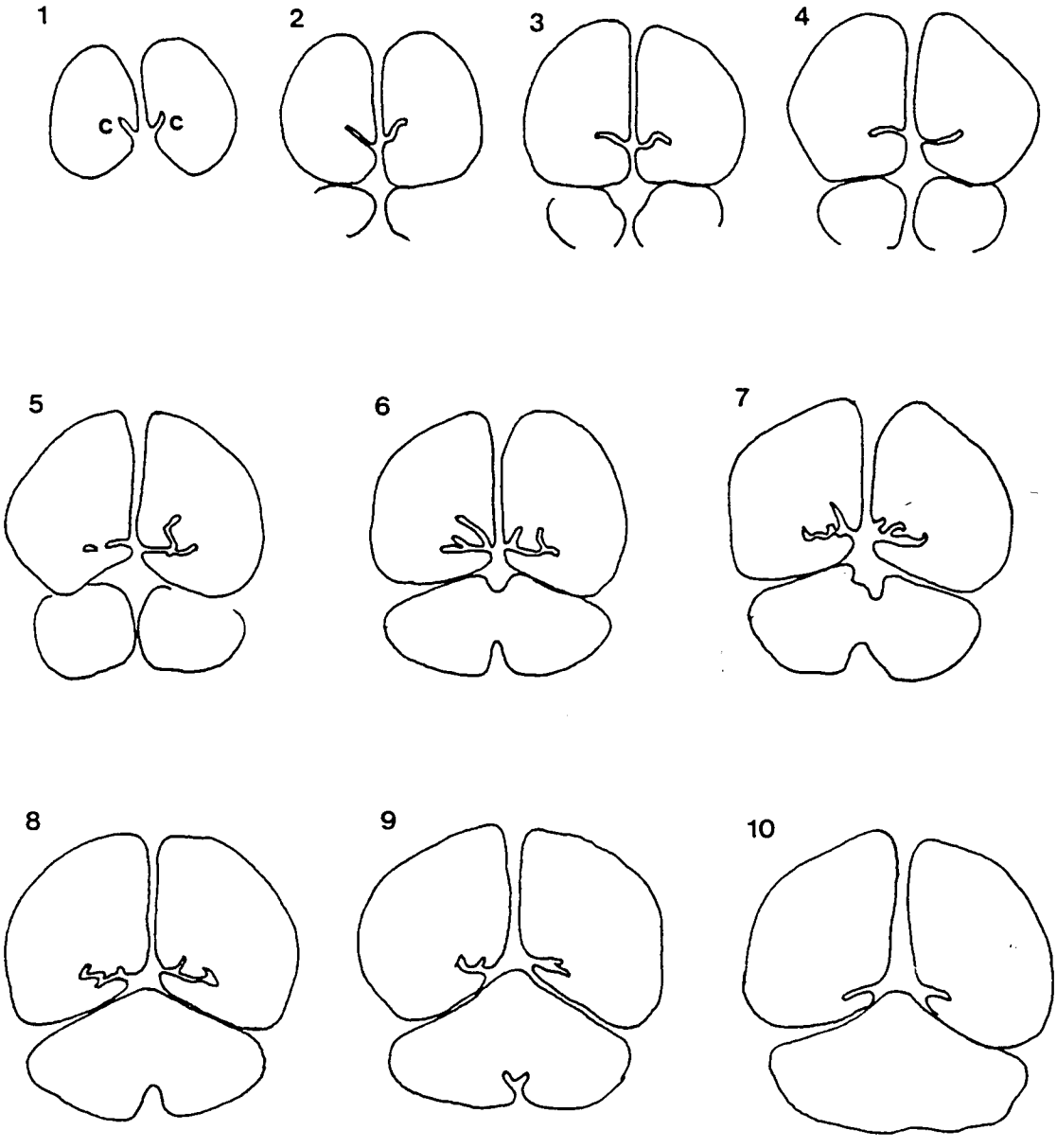

Figure 10.51 - Sequential, transverse vertical MRI sections through the occipital lobes of one subject. The sections are numbered sequentially in a posterior to anterior direction from the pole, with a depth separation of 6mm. In each case, the cross sectional shape of the calcarine fissure (c) is shown.

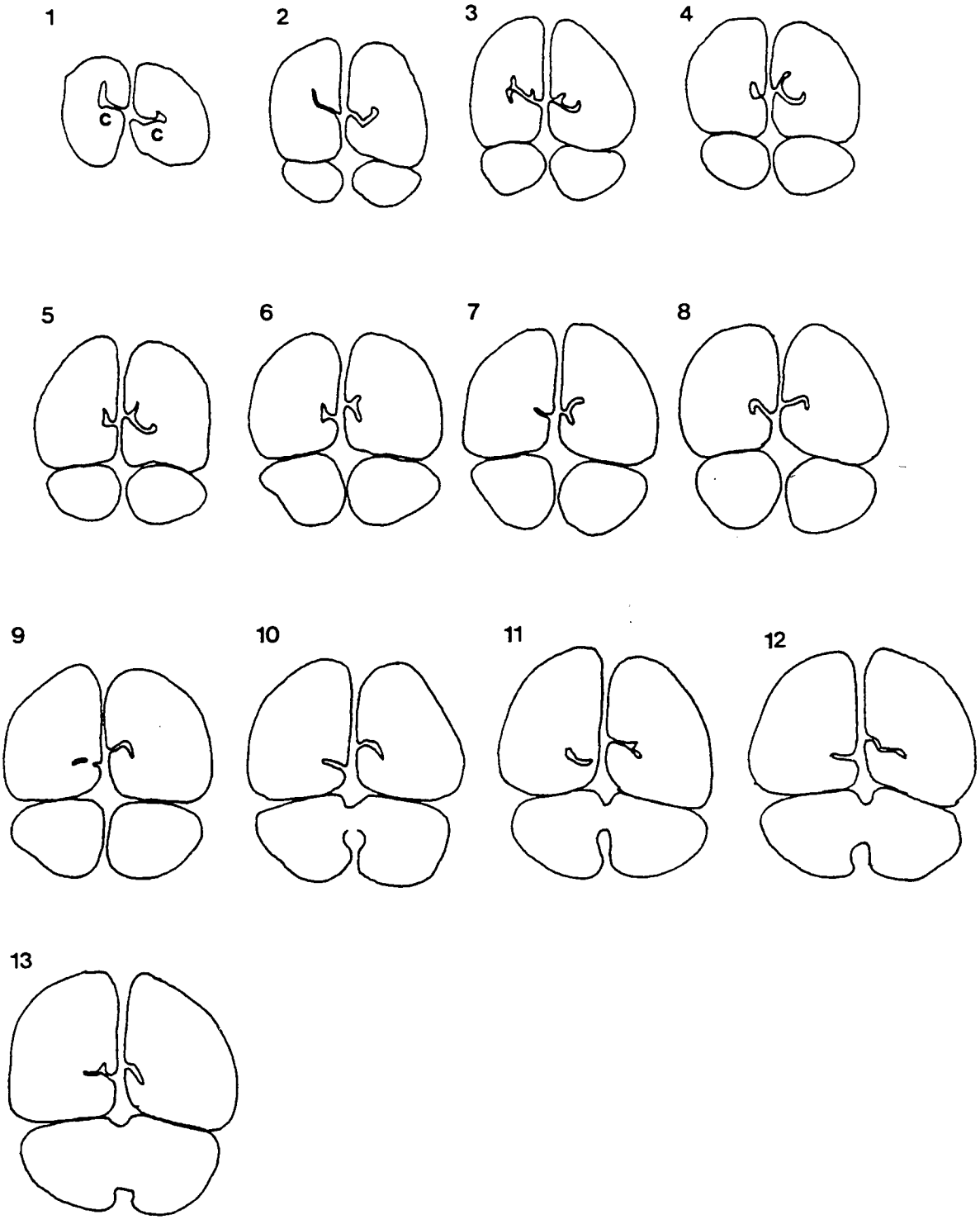

Figure 10.52 - Sequential, transverse vertical MRI sections through the occipital lobes of one subject. The sections are numbered sequentially in a posterior to anterior direction from the pole, with a depth separation of 6mm. In each case, the cross sectional shape of the calcarine fissure (c) is shown.

scalp fields. In this case, the right hemispheric fissure is higher than that of the left, a finding which was also reported by Myslobodsky et al (1991). Asymmetries in the vertical position of scalp fields, between hemispheres, are clearly evident for the full field CIIm distributions of subject SC and RAA (figure 6.82), and the full field offset response of subject EW (figure 6.83). Finally, although examples are not evident in the data of figures 10.51 and 10.52, the opposing walls of the calcarine fissure can 'open out', to form a pocket shaped recess within the hemisphere. Where this occurs, full and half field responses would also be affected, since the separation between the upper and lower calcarine sources would be too great to allow mutual cancellation of the magnetic or electric fields.

10.6 - VARIATIONS IN STRIATE CORTEX REPRESENTATION.

The shape and extent of striate cortex on the medial and lateral surfaces of the occipital lobes, provides another source of interhemispheric and intersubject variation (Brindley 1972). Most of the striate cortex lies within the calcarine fissure, on the medial aspect of each hemisphere. In the anterior sulcal areas, its presence is often confined to the lower surface of the fissure, while posteriorly, upper and lower surfaces are equally represented (Polyak 1957). Such variation might only influence the MEG response for subjects with a calcarine fissure angled acutely with respect to the scalp, due to the inverse relationship between signal strength and source depth (Wikswo 1983). In such cases, stimuli exclusively projecting to these anterior calcarine regions, such as full and half fields with central scotoma, would produce a scalp distribution consistent with upper visual field stimulation only. Examples of this are not apparent in the experimental chapters, possibly because only two subjects were studied with scotoma stimuli.

At the posterior region of the occipital lobe, striate representation may cease before the pole is reached, or extend around onto the posteriolateral surface. The extent of such projection has been shown to vary between subjects, and between the hemispheres of the same subject (Polyak 1957, Brindley 1972, Carpenter 1983). Examples of such variation are shown in figure 10.61 (A, B and C). The figure shows drawings of longitudinal sections through the occipital region of three post-mortem brain specimens, viewed from above. The shaded areas of A and B correspond to the lateral ventricles. The dashed

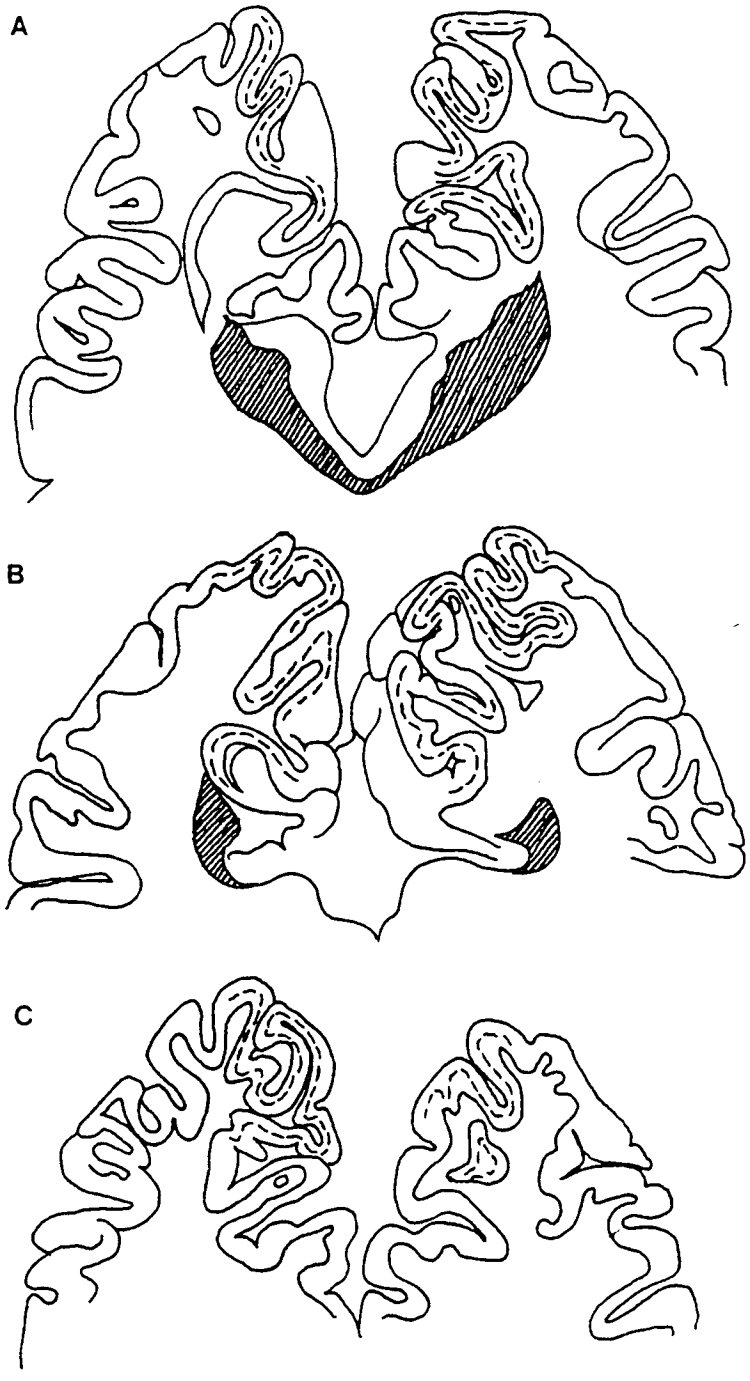

Figure 10.61 - Longitudinal sections through the occipital region of three post mortem brain specimens viewed from above. The shaded areas of A and B correspond to the lateral ventricals. The dashed line in each case indicates the regions of striate cortex, identified by the presence of the white line of Gennari.

line indicates the regions of striate cortex, identified by the presence of the white line of Gennari (Polyak 1957, Carpenter 1983). Although subjects B and C both show a symmetrical interhemispheric distribution of striate cortex, that of B extends further around onto the posteriolateral surface. An asymmetric distribution is seen for subject A, with the striate cortex stopping short of the pole in the right hemisphere, but extending around onto the lateral surface on the left. As mentioned previously, the preferential detection of tangentially oriented sources by MEG would reduce the relevance of morphological variations of the posteriolateral surfaces. Such variation would become apparent however for stimuli projecting to sources within the walls of lateral gyri, in which case large intersubject topographic variations would be expected.

10.7 - OCCIPITAL LOBE PROMINENCE.

A final source of anatomical variation which could influence the MEG response is changes in the relative depths of the left and right occipital lobe below the scalps surface. To examine such variations, a series of transverse MRI scans for 51 individuals were studied. Of the sample, 37 individuals displayed no noticeable difference in prominence between the occipital lobes (figure 10.71A); 11 displayed a more superficial right lobe (figure 10.71B) while the remaining 3 had a prominent left lobe (figure 10.71C).

Asymmetries in the relative sizes of the occipital lobes have been reported previously by Polyak (1957), Bear et al (1986) and Myslobodski et al (1991). All reported that the left hemisphere was generally larger than that of the right. Bear et al (1986) also noticed a reduction in left occipital prominence in non-right handed subjects, while Myslobodsky et al (1991) observed greater asymmetries closer to the pole. The results of this study may differ from those reported previously due to the examination of a single plane through each brain which does not take account of the three dimensional lobe variations. Where present however, such variation could theoretically result in a difference in field strength over the scalp between hemispheres. However, it is not apparent whether the relative difference in source depth would be sufficiently large to produce variations in signal strength differentiable from the effects of noise fluctuations. Evidence of differences in field strength for left and right hemispheric activity is not readily apparent in the experimental

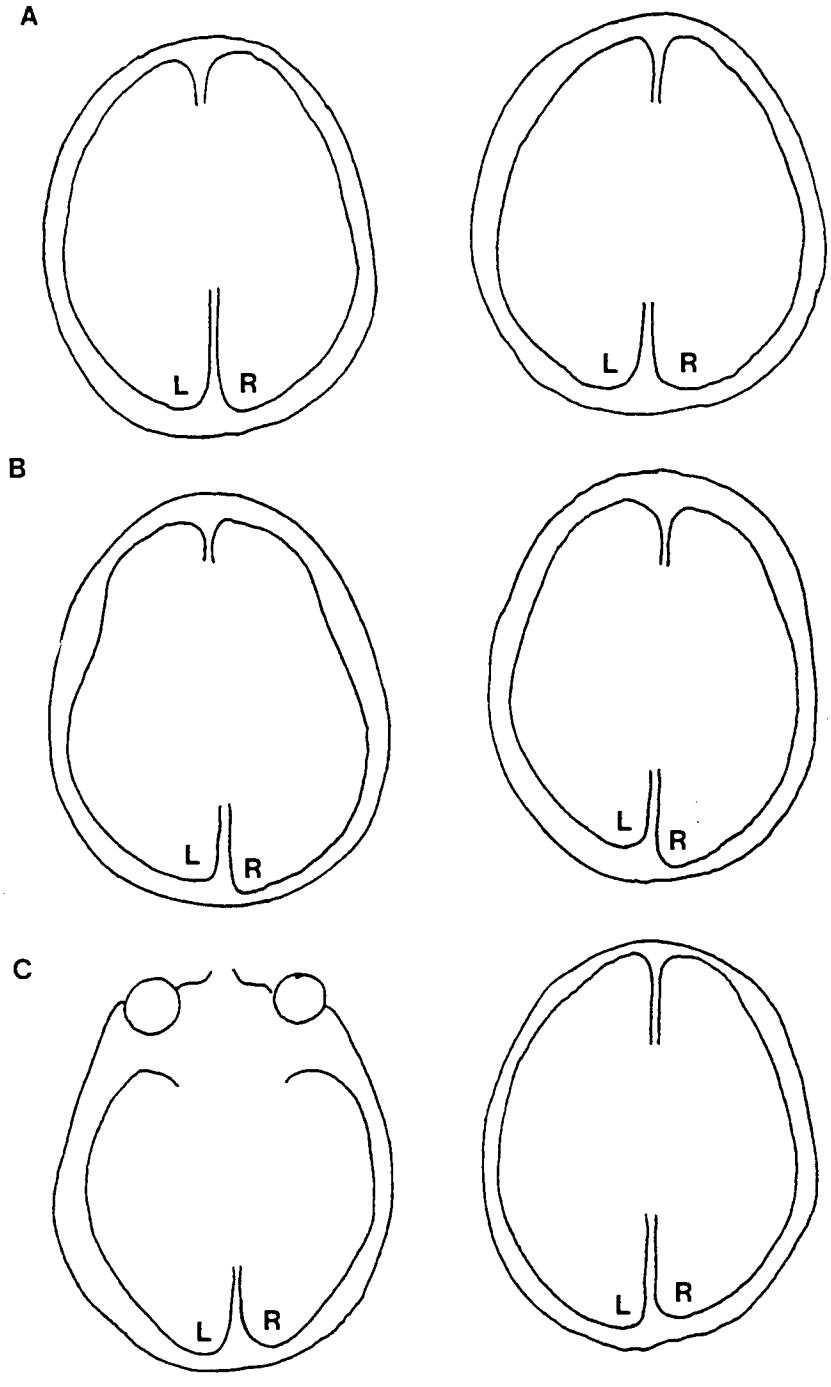

Figure 10.71 - Occipital lobe prominance, illustrated by the horizontal, transverse MRI sections of six individuals, each showing an outline of the head, and the left (L) and right (R) hemispheres within. **A** - symmetrical hemispheres. **B** - right hemisphere is closer to the scalps surface. **C** - left hemisphere is closer.

data presented in previous chapters. A possible example could for the full field offset response of subject AS (figure 8.166), where field maxima of greater amplitude were present over the left hemisphere, for all four check sizes presented.

10.8 - GENERAL CONCLUSIONS.

The results of this chapter are consistent with the observations of Polyak (1957), who demonstrated that striate cortex morphology varies greatly between individuals, and between the hemispheres of a given subject. Many of the inter and intrasubject variations identified here could help to explain the differences in topographic distribution observed in previous chapters. However, such comparisons are tentative, without having access to MRI details of the particular subjects under investigation.

Morphological variation of the calcarine fissure, should have limited effects on the VEMR topography to full or half field stimuli, if VEMR activity is assumed to originate from striate cortical regions. Hence, hemi or full field stimuli would activate sources on both upper and lower surfaces of the calcarine fissure, whose fields would mutually cancel due to their close proximity and opposite polarity. However, sources within the longitudinal fissure should summate, and the relative morphological stability of this region should result in predictable scalp topographies. This hypothesis is supported by the results to full and half field stimuli presented in chapter 6. Responses to quarter and horizontal octant stimuli were found to be more variable (see chapter 9). Hence, focal stimuli may activate cortical sources within one surface of the calcarine fissure only, removing the cancellation effect. This activity would therefore contribute more to the summated response recorded at the scalp than for full and half fields, increasing the effects of morphological variation on the resultant distribution.

It is ironic therefore that the use of a focal stimulus, which theoretically activates a select group of neural sources, might produce scalp topographies of less predictable distribution than those to gross stimuli, projecting to cortical sources of multiple orientations. In cases where focal field stimuli were required, it would be essential for localisation purposes therefore to have the MRI details of each subject available.

CHAPTER 11

GENERAL CONCLUSIONS.

The ability to detect magnetic fields outside the human body has been available since the early 1960's. Measurements of cortical activity associated with visual processing were first reported in 1975 (Cohn 1982), and although recording and analysis techniques have improved subsequently, few clinical applications of the visually evoked magnetic response (VEMR) have been introduced. Possible explanations for this lack of acceptance could include the prohibitive cost of equipment purchase and maintenance; the requirement for magnetically shielded environments; the need for technically proficient staff; and the continual changes in equipment specification resulting from rapid design improvements.

Before assessing the clinical potential of any new technique, it is first necessary to investigate the effects of stimulus, subject and recording variables on a population of 'normal' subjects. This provides a baseline against which abnormalities can be distinguished. Few such investigations have been reported however, with possibly the most complete study being that of Slaven (1992), for the VEMR to a pattern reversal stimulus.

The objectives of this study were to characterise the VEMR to a pattern onset stimulus, across a wide range of stimulus and recording conditions. It was hoped that this might provide information regarding the fundamental nature of the onset response, and suggest optimal recording strategies which could assist in future studies concerned with the techniques clinical evaluation. The major findings of the thesis are outlined below, with each referenced to the relevant chapters.

11.1 - GENERAL CHARACTERISTICS.

The VEMR to a pattern onset/offset stimulus was of sufficiently large amplitude to be recorded without the need for averaging (5.31). This was found with signal to noise conditions readily attainable in our unshielded, urban environment, so long as recordings were taken over a scalp region of maximal field strength. The typical, unaveraged onset response produced a triphasic waveform. This comprised a peak at approximately 110ms post

stimulus (the CIIm), that was preceded (the CIm) and proceeded (the CIIIm) by peaks of similar amplitude but opposite field polarity to the CIIm. Stimulus offset produced a single waveform peak after approximately 120ms, with the same field polarity to that of the CIIIm (5.33). The latency and amplitude of successive, unaveraged CIm, CIIm and CIIIm peaks fluctuated non randomly with time (5.33), although insufficient data was available to determine the exact nature of this variation. Of the three peaks, the CIm proved the most, and the CIIm the least variable. The ability to detect evoked cortical responses without the need for signal averaging could be particularly useful for studies of fundamental visual processing. Hence, the way in which the brain responds to a single stimulus event could be observed, without the loss of temporal continuity which occurs with the averaging of multiple, successive responses. A more thorough analysis of consecutive unaveraged processing events would also prove interesting for the study of how the visual system analyses repetitive stimuli.

The averaged onset waveform was biphasic, with the CIIm at approximately 110ms, followed by the CIIIm. The absence of the CIm peak was attributed to the variability of its unaveraged latency and amplitude (5.34). An average of 15 successive responses was sufficient to produce CIIm and CIIIm waveform peaks of stable latency, when recording from a scalp location of high signal to noise ratio. At more distant positions, 50 responses or more were required to attain a similar level of stability (5.36). This compares favourably with many clinical protocols used for the VEP. Waveform morphologies (5.42) and topographic distributions (5.43) were stable and reproducible when recorded over a period of 17 months. Such stability is important if clinical applications were to be considered.

An analysis of variance (ANOVA) on serial, averaged response waveforms (5.44) showed that most latency variation occurred between consecutive responses, rather than those made at different times of day, or on separate days. A more representative response would therefore be obtained from multiple responses per session, than from fewer responses recorded over a number of occasions. The partitioning of amplitude variance between responses, sessions and days was equipment specific (5.44), therefore variance data would have to be compiled following each change of equipment. Age normative latency and amplitude data would also have to be repeated, as it was found that responses recorded from two theoretically identical magnetometer

systems differed in latency, amplitude but not temporal variability. This was attributed to differences in filter performance or manufacturing tolerances (5.44). A decrease in latency and amplitude variance was achieved by increasing the amount of environmental shielding (5.5), the rate of change declining at higher shielding levels. The reason for this diminishing return was attributed to the increased importance of intrinsic subject and equipment noise as environmental noise was progressively excluded. When setting up a clinical system therefore, it might prove more cost effective to install shielding in stages, assessing response variance following each, instead of purchasing as much shielding as possibly initially.

11.2 - STIMULUS PARAMETERS.

Blurring of the stimulus produced an increase in waveform peak latency and a decrease in amplitude (5.73), being more prevalent with smaller check sizes. For clinical uses, latency variation arising from non pathologic sources needs to be minimised where possible, and so the correction of patient refractive error would be critical. That said, the VEMR appeared less sensitive to optical blur than the pattern onset visually evoked potential (5.73). Although topographic distributions became increasingly diffuse with stimulus blur, the positions of the field maxima remained constant over the scalp (5.73).

A decrease in check size produced a linear increase in amplitude of the onset and offset peaks, with a curvilinear latency change (8.15). Maximal amplitude was obtained for 6' checks, consistent with the VEP findings for optimal foveal stimulation, while latency was shortest with a check size of 50'x55' (8.15). Decreasing check size produced variations in topographic distribution explicable by increasingly shallow source depths, and/or an anterior to posterior progression down the scalp (8.16). This would be consistent with activity within the walls of the calcarine and longitudinal fissures of the occipital cortex (8.16).

An increase in stimulus contrast produced an increase in amplitude for the onset and offset peaks (8.34), inconsistent latency trends (8.35) and no appreciable effect upon topographic distribution (8.36). Unlike previous VEP studies, no amplitude saturation was observed, however this was attributed to an increase in luminance contamination at higher contrast (8.32). It might prove beneficial in future studies therefore to use high contrast stimuli, since

this would maximise signal to noise conditions without adversely affecting latencies or topographies.

Increasing occlusion of the central visual field resulted in decreased onset/offset peak amplitudes, but no clear latency trends (9.33). A recognisable CIIm and offset peak topography was still evident even following the occlusion of the central 7° of the visual field (9.34), suggesting that unlike the VEP, the VEMR cannot be produced predominantly by foveal retinal projections. If the onset VEMR were to be used for the study of foveal or macular visual field defects therefore, small field stimuli would be essential to prevent stimulation of the peripheral retinal regions.

Decreasing field size caused the latency of the onset peaks to increase, while those of the offset decreased, without consistent trends for either (8.23). The reason for such disparate latency trends is unclear, however their effects would have to be characterised with normative data, as would the effects of varying the other stimulus parameters used here. Topographically, smaller field sizes produced distributions consistent with more superficial source depths and/or an anterior to posterior movement down the scalp (8.24), which would again be consistent with an origin within the calcarine and longitudinal fissures.

11.3 - WAVEFORM PEAK IDENTIFICATION AND TOPOGRAPHIC DISTRIBUTION.

Vertical half field stimulation produced a dominant waveform peak within the first 180ms post stimulus, whose topographic distribution was consistent between individuals (the CIIm). This distribution was explicable by the activity of an equivalent current dipole in the contralateral hemisphere to that of the stimulus field, with current flowing horizontally away from the medial surface of the brain (6.31 and 6.32). The waveform peak following the CIIm, (the CIIIm), produced a topography of similar distribution, but opposite polarity to that of the CIIm. CIIIm and offset peak topographies were also similar (6.31, 6.32 and 6.4). Although both right and left half field stimuli produced predominantly contralateral hemispheric responses, 70% of the subjects also showed some ipsilateral activity with the right half field (6.31). These ipsilateral fields were of opposite polarity and lower amplitude to those seen contralaterally (6.31). Studies with left half field stimuli (6.32), octants (9.23), central scotomas (9.33) and fixation monitoring (7.6) were all

inconsistent with the inadvertent stimulation of nasal and temporal retinal regions, as an explanation for the activity in each hemisphere. Alternatively, a callosal transfer of information, predominantly from left to right hemispheres, might be responsible. If so, these results would differ from the retinocortical projection of nasal retinal regions to both hemispheres, as proposed by a number of VEP studies (6.31).

Full field stimuli produced waveform peaks with less predictable prominence and topographic distribution than those to half fields, even though the full field topographic distribution was explicable by the arithmetic summation of the constituent half (6.7 and 7.3) or quarter fields (9.15). The most prominent full field peak within the first 200ms post stimulus gave a predictable CIIm topographic distribution only for check sizes below 19'x13' (8.14) and/or field sizes above 7°20'x5°43' (8.23). This was attributed to the effects of retinocortical projections, cortical magnification and the volume of activated cortex involved (8.23). If different stimulus parameters were used, identification of this peak could only be achieved by reference to the topographic distribution of each peak, since waveform latency, prominence and polarity were all inconsistent indicators (7.3). The latency and waveform prominence of the full field CIIm peak was found to be dependant upon the temporal overlap of CIIm activity from each hemisphere, and the relative efficiency of summation at successive latencies (7.3). The interhemispheric duration of the half field CIIm/CIIIm activity differed by an average of 28ms for the two male subjects studied, and 4ms for the three females (7.6). This difference was attributed either to more detailed, or less efficient processing within one hemisphere, or to greater variation in occipital lobe morphology for males (7.6). The increased processing stability of females did not however produce a noticeable improvement in full field peak identification (7.3).

Stimulation with quarter (9.14) and octant visual fields (9.23) gave less predictable topographic distributions than those found with half fields (6.31 and 6.32). This was attributed to a reduction in signal to noise ratio, associated with the stimulation of a more select neuronal population, and/or an increased sensitivity to variations in cortical morphology. The implications of these findings upon the choice of stimulus parameters and visual field types for use with a single channel magnetometer will be outlined in section 11.7.

11.4 - COMPONENT INTERRELATIONSHIPS.

Similarities between the responses to stimulus onset and offset were found regarding half field topographic distribution (6.31 and 6.32); source localisation results (6.4); and the effects of varying check size on response amplitude (8.15). Differences were found however for latency effects with varying check size (8.15); latency (8.23) and topographic effects (8.24) with field size; latency (8.34), amplitude (8.35) and topography (8.36) with contrast; and intersubject topographic differences with quarter (9.14) and octant fields (9.23). Although such conflicting results make interpretation difficult, a common cortical origin for the responses to pattern onset and offset cannot be dismissed without further study. The opposite polarity of the onset and offset waveform peaks (5.2) provides evidence that the response is unlikely to originate due to a luminance mechanism.

A number of similarities were found between the behaviour of the CIIm and CIIIm onset peaks. Significant correlations were evident for both sequential unaveraged response latencies (5.33), and averaged latencies and amplitudes (5.42). Both CIIm and CIIIm latencies and amplitudes were affected similarly by altering the number of responses included in the average (5.36); the effects of optical blur (5.73); and the effects of varying check size (8.15). Amplitudes varied similarly for each component with changes in contrast (8.34). CIIm and CIIIm topographies were of similar distribution, but opposite polarity with half field stimuli (6.31 and 6.32); source localisation results (6.4); and changes in contrast (8.36). Differences between the two peaks were apparent for the effect of contrast on latency (8.35), and for quarter (9.14) and octant (9.23) field topographies. The differences might be attributed to the poor signal to noise conditions attainable with such stimuli. These similarities are strongly suggestive of either a common cortical origin for the two components, or an origin in closely related neuronal populations. If this were the case, the opposite direction of current flow exhibited by the two might represent different processing within the same cells, or similar processing in cell populations oriented 180° apart. If the former were the case, then the CIIm and CIIIm could represent excitatory and inhibitory afferent inputs respectively, onto the apical dendrites of the same pyramidal cell populations (6.5). Evidence for a contour specific mechanism underlying CIIm and CIIIm source activity was provided by the amplitude adaptation with increasing

pattern presentation (5.36), and increasing latency and decreased amplitudes with optical blur (5.73).

11.5 - SOURCE ORIGINS.

Many of the results from this thesis would be consistent with the activity of sources (for the CIIm, CIIIm and offset waveform peaks), within the walls of the calcarine and longitudinal fissures of the occipital cortex. This would suggest an origin from primary visual cortex, assuming the cruciform model of striate cortex representation (Jeffreys and Axford 1972 a). Such evidence includes the intersubject stability of half field topographies, their equivalent source orientation (6.31 and 6.32); the results of source localisation (6.4); and the behaviour of both full and half field topographies with varying check (8.16) and field size (8.24). Quarter (9.14) and octant field stimuli (9.23) also produced topographic distributions which changed predictably with varying stimulus parameters.

11.6 - CORTICAL MORPHOLOGY VARIATIONS.

A study of the sagittal MRI scans from fifty individuals displayed a variation in calcarine fissure angle of between 11 and 89° (mean 40°) with respect to a plane passing through the nasion and inion (10.31). None of the fissures were straight, or angled perpendicular to the scalp, as assumed by the cruciform model (10.2). Such variation could provide an explanation for the intersubject behaviour differences of CIIm topographies with changing check (8.16). A significant correlation was found between the angle of the calcarine fissure with respect to the nasion to inion plane, and the shape of the posterior regions of the scalp (10.32). If refined further, such measurements might prove useful in predicting source configurations for subjects where MRI data were not available.

Analysis of cortical morphology from MRI data and post mortem brain specimens revealed intersubject and interhemispheric variations in the shape and distribution of the calcarine fissure (10.2); its cross sectional shape with depth (10.5); the three dimensional distribution of striate cortex (10.4 and 10.6); and the relative depths of each hemisphere below the scalp (10.7). Such variation would theoretically have a greater influence on the topographic

distributions of quarter or octant field responses than those to half or full fields. Hence, full and half field stimuli would predominantly reflect the activity of sources on the medial surfaces of the occipital lobes (due to calcarine source cancellation), which show less morphological variation than the walls of the calcarine fissure. Analysis of the topographic results to full, half (see chapter 6) and focal field stimuli (see chapter 9) is consistent with this hypothesis, providing further evidence for an origin of the onset components within striate cortical regions (see chapter 10). In all situations where accurate localisation of cortical activity was required, MRI data for the particular individual would have to be obtained. If localisation accuracy was less critical, reference could be made to an average cortical model, constructed from the combined MRI data of numerous subjects. However, inter and intrasubject morphology variation such as that identified in this study would limit the accuracy of any conclusions drawn from such a model.

11.7 - CONSIDERATIONS FOR SINGLE CHANNEL RECORDING.

The results of this study raise several considerations to be borne in mind when recording with a single channel magnetometer.

Where possible, the use of a 3°x5° half field stimulus of 38' checks is preferable, since it produces a dominant waveform peak of predictable topographic distribution. The intersubject similarity in half field topography means that a single probe position, 6cm above the inion, on the midline or 3cm to the left, would fall over the area of maximal inward or outward flowing field for right and left half field stimuli respectively. The choice of this position was unaffected by variations in subject refractive error (5.73), stimulus contrast (8.36) or central occlusion of the visual field (9.34). Adjustments might be required when using different check (8.16) or field sizes (8.24). The ability to position the probe over scalp areas of maximal field strength for any given stimulus is desirable, to maximise signal to noise conditions. To achieve this with magnetometry would demand greater accuracy than that required for the VEP, since magnetic fields are more focally distributed over the scalp than electrical potentials (2.2). While this property makes magnetometry well suited for source localisation approaches, it could detract from its clinical usefulness, particularly when using a single channel system.

When using a full field stimulus with check sizes below 19'x13', or field sizes above 7°20'x5°4', the most prominent onset waveform peak represents activity consistent with the CIIm component. However, for differing stimulus parameters, peak identification could only be made with confidence by the inclusion of topographic data. Once more, this would have a greater detrimental effect on single, rather than multichannel applications.

The use of quarter or octant visual fields might be desirable in the study of focal visual field defects, however the increased intersubject topographic variation observed with such stimuli could reduce their practical application (see chapter 9).

Although optimal amplitudes were produced using 6' checks in a 7° field, these parameters are most susceptible to the effects of optical blur. If using the pattern onset VEMR to study foveal retinal activity therefore, care would be required to minimise refractive error. Stimulation of peripheral retina, using larger check sizes would be less influenced by optical blur, however additional normative data would be required to take account of the shorter latencies.

The clinical implementation of single channel magnetometry looks increasingly less likely due to the continued development of multichannel systems. This should not preclude its consideration however, since its relatively cheap and uncomplicated nature might speed the techniques mass introduction, if sufficient uses were demonstrated. That said, even single channel magnetometry is relatively expensive compared to the electrophysiological techniques currently in use, hence significant advantages and applications would be required. This might be achieved by the exploitation of MEGs reference free nature, and/or preferential sensitivity to tangentially oriented sources, such as those within fissure walls.

Although the pattern onset stimulus is used less clinically than that of the reversal or flash, with current VEP applications, this might not be the case for the MEG. The VEMR results presented in this thesis are comparable in many respects to those of the VEMR to pattern reversal and flash published by Slaven et al (1991) and Harding et al (1991), however, response amplitudes are up to five times greater with pattern onset. The resulting increase in signal to noise ratio might provide the onset stimulus with greater sensitivity to pathology, hence potentially increasing the range of conditions to which the technique might be applied.

BIBLIOGRAPHY

Adlers Physiology of the Eye: Clinical Application.
Moses RA and Hart WM (Ed)
The CV Mosby Company. St. Louis, Washington DC. Toronto. 1987, 622.

Adrian ED and Mathews BHC.
The Berger rhythm - potential changes from the occipital lobes of man.
Brain 57; 1934, 355-385.

Ahlfors SP, Ilmoniemi RJ and Hamalainen.
Estimates of visually evoked cortical currents. EEG and Clin. Neuro. 82;1992, 225-236.

Aine CJ, Bodis-Wollner I and George JS.
Generators of visually evoked neuromagnetic responses: spatial-frequency and evidence of multiple sources.
Advances in Neurology. Vol 54: Magnetoencephalography. Sato S (Ed).
Raven Press, New York. 1990, 141-156

Aine CJ, George J, Medvick P, Supek S, Flynn E and Bodis-Wollner I.
Identification of multiple sources in transient visual evoked neuromagnetic responses.
Advances in Biomagnetism. Williamson SJ et al (Eds).
Plenum Press, New York. 1989, 193-196.

Armstrong RA.
The usefulness of spatial pattern analysis in understanding the pathogenesis of neurodegenerative disorders, with particular reference to plaque formation in Alzheimers disease.
Neurodegeneration Vol 2, 1993.

Armstrong RA and Janday B.
A brief review of magnetic fields from the human visual system.
Ophthal. Physiol. Opt. Vol 9, 1989, 299-301.

Armstrong RA, Janday B, Slaven A and Harding GFA.
The use of flash and pattern evoked fields in the diagnosis of Alzheimers disease.
Advances in Biomagnetism. Williamson SJ et al (Eds).
Plenum Press, New York. 1989, 315-318.

Armstrong RA, Slaven A and Harding GFA.
Visual evoked magnetic fields to flash and pattern in 100 normal subjects.
Vision Res. Vol 31 N° 11, 1991, 1859-1864.

Armstrong P and Wastie ML.
Diagnostic imaging. (second Ed.), Blackwell, Oxford and London, 1987.

Aunon JI and McGillem CD.
Techniques for processing single evoked potentials.
Proceedings, San Diego Biomedical Symposium. Vol 14, 1975, 211-218.

Aunon JI and McGillem CD.
Detection and processing of individual components in the VEP.
Psychophysiology, Vol 16 N° 1, 1979, 71-79.

Aunon JI and Sencaj RW.
Comparison of different techniques for processing evoked potentials.
Med. and Biol. Eng. and Comput. 16; 1978, 642-650.

Bailey CH and Gouras P.
The retina and phototransduction.
Principles of Neuroscience. Kandel ER and Schwartz JH (Eds).
Elsevier USA, Ch 27; 1985, 344-355.

Balish M and Muratore R.
The inverse problem in EEG and MEG.
Advances in Neurology Vol 54: magnetoencephalography. Sato S (Ed).
Raven Press, New York. 1990, 79-88.

Barber C and Galloway NR.
Pattern evoked potentials as indicators of functional visual field asymmetries.
Doc. Ophthal. Proc. Series. Spekreijse H and Apkarian PA (Eds).
Dr. W Junk Publishers Hague/Boston/London. Vol 27; 1981, 229-237.

Barber JL, Watson JDG, Frackowiak RSJ and Zeki S.
Conscious visual perception without V1. Brain 116; 1993, 1293-1302.

Barrett G, Blumhardt L, Halliday AM and Kriss A.
A paradox in the lateralisation of the visual evoked response.
Nature 261; 1976, 253-255.

Barth DS and Sutherling W.
Neuromagnetic studies of evoked and spontaneous activity in animals.
Advances in Neurology Vol 54: magnetoencephalography. Sato S (Ed).
Raven Press, New York. 1990, 119-132.

Barth DS, Sutherling W, Broffman J and Beatty J.
Magnetic localization of a dipolar current source implanted in a sphere and a human cranium.
EEG and Clin. Neuro. 63; 1986, 260-273.

Barth DS, Sutherling W, Engal J and Beatty J.
Neuromagnetic localization of epileptiform spike activity in the human brain.
Science 218; 1982, 891-894.

Baule GM and McFee R.
Detection of the magnetic field of the heart. Am. Heart J. 66; 1963, 95-96.

Bayler DA, Fuortes MGF and O'Brian PM.
Receptive fields of cones in the retina of the turtle. J. Physiol. 214; 1971, 265-294.

Bear D, Schiff D, Saver J, Greenberg M and Freeman R.
Quantitative analysis of cerebral asymmetries, fronto-occipital correlation, sexual dimorphism and association with handedness.
Arch. Neurol. 43; 1986, 598-603.

Bedford JL.
Dual analysis of visually evoked magnetic and electrical responses.
Proc. Satellite Symposium on Neuroscience and Technology.
IEEE Eng. Med. Biol. Soc. Conference, Lyon proceedings. 1992.

Beers APA, Riemslag FCC and Spekreijse H.
Visual evoked potential estimation of visual activity with a laplacian derivation.
Docum. Ophthal. 79; 1992, 383-389.

Belliveau JW, Kennedy DN, McKinstry RC, Buchbinder BR, Weisskoff RM, Cohn MS, Vevea JM, Brady TJ and Rosen BR.
Functional mapping of the human visual cortex by magnetic resonance imaging.
Science 254; 1991, 716-719.

Blume WT, Buza RC and Okazaki H.
Anatomic correlates of the ten-twenty electrode placement system in infants.
EEG and Clin. Neuro. 36; 1974, 303-307.

Blumhardt L.
The abnormal pattern visual evoked response in neurology.
A textbook of clinical neurophysiology. Halliday AM, Butler SR and Paul R (Eds)
1987, 307-342.

Blumhardt LD, Barrett G, Halliday AM and Kriss A.
The effect of experimental scotomata on the ipsilateral and contralateral responses to pattern reversal in one half field.
EEG and Clin. Neuro. 45; 1978, 376-392.

Blumhardt LD, Barrett G, Kriss A and Halliday AM.
The pattern evoked potential in lesions of the posterior visual pathways.
Annals. NY Accad. Sci. 1982, 264-289.

Blumhardt LD and Halliday AM.
Hemisphere contributions to the composition of the pattern evoked potential waveform.
Exp. Brain Res. 36; 1979, 53-69.

Bobak P, Bodis-Wollner I and Guillory S.
The effect of blur and contrast on VEP latency: comparison between check and sinusoidal grating patterns.
EEG and Clin. Neuro. 68; 1987, 247-255.

Bodis-Wollner I, Brannan JR, Ghilardi MF and Mylin LH.
The importance of physiology to visual evoked potentials.
Visual Evoked Potentials. Desmedt JE (Ed).
Elsevier Ch 1, 1990, 1-24.

Brazier MAB.
Evoked responses recorded from the depths of the human brain.
Annals. NY Accad. Sci. 1964, 33-59.

Breitmeyer BG.
Simple reaction time as a measure of the temporal response properties of transient and sustained channels.
Vis. Res. 15;1975, 1411-1412.

Brenner D and Kaufman L.
Visualy evoked magnetic fields of the human brain.
Science 190; 1975, 480-481.

Brenner D, Lipton J, Kaufman L and Williamson SJ.
Somatically evoked magnetic fields of the human brain.
Science 199; 1978, 81-83.

Brenner D, Okada Y, Maclin E, Williamson SJ and Kaufman L.
Evoked magnetic fields reveal different visual areas in human cortex.
Biomagnetism. Erne SN, Hahlbohm H and Lubbig H (Eds).
Walter de Gruyter Berlin, 1981, 431-444.

Brindley GS.
The variability of the human striate cortex.
J. Physiol. 225; 1972, 1-3.

Buchsbaum MS, Henkin RI and Christiansen RL.
Age and sex differences in averaged evoked responses in a normal population, with observations on patients with gonadal dygenesis.
EEG and Clin. Neuro. 37; 1974, 137-144.

Butler SR, Georgiou GA, Glass A, Hancox RJ, Hopper JM and Smith KRH.
Cortical generators of the CI component of the pattern onset visual evoked potential.
EEG and Clin. Neuro. 68; 1987, 256-267.

Campbell FW and Kulikowski JJ.
The visual evoked potential as a function of contrast of a grating pattern.
J. Physiol. 222; 1972, 345-356.

Campbell FW and Maffei L.
Electrophysiological evidence for the existence of orientation and size detectors in the human visual system.
J. Physiol. 207; 1970, 635-652.

Campbell FW and Maffei L.
Contrast and spatial frequency.
Scientific American 231 N° 5; 1974.

Carpenter RHS.
Neurophysiology.
Physiological principles in medicine series.
Hardy RN, Hobsley M and Saunders HB (Eds).
Edward Arnold; 1984.

Carelli P, Modena I, Ricci GB and Romani GL.
Detection coils.
Biomagnetism: an interdisciplinary approach.
Williamson SJ, Romani GL, Kaufman L and Modena I (Eds).
New York, Plenum; 1982, 469-482.

Ciganek L.
Variability of the human visual evoked potentials: normative data.
EEG and Clin. Neuro. 27; 1969, 35-42.

Clarke J.
SQUIDs.
Scientific American 271; N° 2, 1994, 36-43.

Coffey CE, Wilkinson WE, Parashos MD, Soady SAR, Sullivan RJ, Patterson LJ, Fiegiel GS, Webb MC, Spritzer CE and Djang WT.
Quantitative cerebral anatomy of the aging human brain. Neurology 42; 1992, 527-536.

Cohen D.
Magnetoencephalography: evidence of magnetic fields produced by alpha-rhythm currents.
Science 161; 1968, 784-786.

Cohen D.
Introductory chapter.
Biomagnetism: an interdisciplinary approach.
Williamson SJ, Romani GL, Kaufman L and Modena I (Eds).
New York, Plenum; 1982, 5-16.

Cohen D and Cuffin BN.
Demonstration of useful differences between the magnetoencephalogram and electroencephalogram. EEG and Clin. Neuro. 56; 1983, 38-51.

Cohn NB, Kircher J, Emmerson RY and Dustman RE.
Pattern reversal evoked potentials: age, sex and hemispheric asymmetry.
EEG and Clin. Neuro. 62; 1985, 399-405.

Cohn SN, Syndulko K, Hansch E, Tourtellotte WW and Potvin AR.
Variability on serial testing of visual evoked potentials in patients with multiple sclerosis.
Clin. Applications of EP in Neurology. Courion J, Mauguiere F and Revol M (Eds).
Raven Press, New York, 1982.

Creel D, Spekreijse H and Reits D.
Evoked potentials in albinos: efficiacy of pattern stimuli in detecting misrouted optic fibres.
EEG and Clin. Neuro. 52; 1981, 595-603.

Creel D, Spekreijse H and Reits D.
Visual evoked potential (VEP) methods of detecting misrouted optic projections.
Doc. Ophthal. Proc. Series. Spekreijse H and Apkarian PA (Eds).
Dr. Junk Publishers, Hague/Boston/London. 27; 1981, 157-165.

Crum D.
The design and use of dewars for biomagnetic measurements.
Biomagnetism: Applications and theory.
Weinberg H, Stroink H and Katila T (Eds).
Pergammon Press, NY, 1985, 21-28.

Cuffin BN.
Effects of fissures in the brain on electroencephalograms and magnetoencephalograms.
J. Appl. Phys. 57 (1); 1985, 146-153.

Dagnelie G, DeVries MJ, Maier J and Spekreijse H.
Pattern reversal stimuli: motion or contrast?
Docum. Opthalmol. 61; 1986, 343-349.

Darcey TM, Ary JP and Fender DH.
Spatio-temporal visually evoked scalp potentials in response to partial-field patterned stimulation.
EEG and Clin. Neuro. 50; 1980, 348-355.

Davidoff J and Concar D.
Brain cells made for seeing.
New Scientist 1868; 1993, 32-36.

Davidson H.
Physiology of the eye.
Macmillan Press London. 1990, 204-210.

Dawson GD.
Cerebral responses to electrical stimulation of peripheral nerve in man.
J. Neurol. Neurosurg. and Psychiat. 10; 1947, 134-140.

Degg C, Slaven A and Armstrong RA.
Topographic mapping and source localization of the pattern onset visual evoked magnetic response.
Brain Topography 5 (1); 1992, 11-16.

Derrington AM and Lennie P.
Spatial and temporal contrast sensitivity of neurones in lateral geniculate nucleus of macaque.
J. Physiol. 357; 1984, 219.

DeValois KK, De Valois RL and Yund EW.
Responses of striate cortex cells to grating and checkerboard patterns.
J. Physiol. 291; 1979, 483-505.

DeValois RL, Albrecht DG and Thorell LG.
Spatial frequency selectivity of cells in macaque visual cortex.
Vis. Res. 22;1982, 545-559.

Donchin E.
Discriminant analysis in average evoked response studies: the study of single trial data.
EEG and Clin. Neuro. 27; 1969, 311-314.

Drasdo N.
Cortical potentials evoked by pattern presentation in the foveal region.
Evoked Potentials. Barber C (Ed).
MTP Press, Lancaster, Ch 17; 1980, 167-174.

Drasdo N.
Optical techniques for enhancing the specificity of visual evoked potentials.
Docum. Ophthal. Proc. Series. 31; 1982, 327-336.

Drasdo N.
Properties of foveal pattern stimuli which determine the morphology and scalp distribution of visual evoked potentials.
Docum. Ophthal. Proc. Series. 27; 1981, 381-390.

Drasdo N.
Receptive field densities of the ganglion cells of the human retina.
Vis. Res. 29 (8); 1989, 985-988.

Drasdo N and Edwards L.
Effects of stimulus quality in the scalp topography of the visual evoked potential.
Seeing contour and colour. Kulikowski JJ, Dickinson CM and Murray JJ (Eds).
Pergamon Press, Oxford; 1989, 504-511.

Duffy FH and Rengstorff RH.
Ametropia measurements from the visual evoked response
Am. J. of Optom. and Arch. of Am. Acad. of Optom. 48 (9); 1971, 717-728.

Duret D and Karp P.
Instrumentation for biomagnetism.
Il Nuovo Cimento. 2 (2); 1983, 123-141.

Dustman RE, Schenkenberg T, Lewis EG and Beck EC.
The cerebral evoked potential: life span changes and twin studies.
VEP in Man: New Developments. Desmedt JE (Ed).
Clarendon Press, Oxford. Ch 19; 1977, 363-377.

Dustman RE and Beck EC.
The effects of maturation and aging on the waveform of visually evoked potentials.
EEG and Clin. Neuro. 26; 1969, 2-11.

Eason RG, White CT and Bertlett N.
Effects of checkerboard pattern stimulation on evoked cortical responses in relation to check size and visual field.
Psychon. Sci. 21 (2); 1970, 113-115.

Edwards L and Drasdo N.
Scalp distribution of visual evoked potentials to foveal pattern and luminance stimuli.
Docum. Ophtalmol. 66; 1987, 301-311.

Ellingson RJ.
Cerebral electrical responses to auditory and visual stimuli in the infant (human and subhuman species).
Neurological and electroencephalographic correlative studies in infancy.
Kellaway P and Peterson I (Eds).
Grune and Stratton, New York. 1964, 78-114.

Enroth-Cugell C and Robson JG.
The contrast sensitivity of retinal ganglion cells of the cat.
J. Physiol. 187; 1966, 517-552.

Ermolaev RY and Kleinman D.
The effect of background illumination on pattern onset visual evoked potentials.
EEG and Clin. Neuro. 55; 1983, 546-556.

Ermolaev RY and Kleinman D.
The effect of eccentricity and colour on negativity in pattern onset visual evoked potentials.
EEG and Clin. Neuro. 59; 1984, 347-360.

Erne SN.
SQUID sensor.
Biomagnetism: an interdisciplinary approach.
Williamson SJ, Romani GL, Kaufman L and Modena I (Eds).
New York, Plenum; 1982, 69-83.

Estevez O and Spekreijse H.
Relationship between pattern appearance-disappearance and pattern reversal responses.
Exp. Brain Res. 19; 1974, 233-238.

Fagaly RL.
Neuromagnetic instrumentation.
Advances in Neurology. Vol 54: Magnetoencephalography. Sato S (Ed).
Raven Press, New York. 1990, 11-32.

Farrell DE.
Assessment of iron in human tissue: the magnetic biopsy.
Biomagnetism: an interdisciplinary approach.
Williamson SJ, Romani GL, Kaufman L and Modena I (Eds).
New York, Plenum Ch 13; 1982, 483-531.

Farrell DE, Tripp JH, Norgren R and Teyler TJ.
A study of the auditory evoked magnetic field of the human brain.
EEG and Clin. Neuro. 49; 1980, 31-37.

Fenici RR.
Cardiac studies: the clinical assessment of the magnetocardiogram.
Biomagnetism: an interdisciplinary approach.
Williamson SJ, Romani GL, Kaufman L and Modena I (Eds).
New York, Plenum; 1982, 287-299.

Fenwick P.
The use of MEG in neurology.
Advances in Neurology. Vol 54: Magnetoencephalography. Sato S (Ed).
Raven Press, New York. 1990, 271-282.

Flanagan JG and Harding GFA.
Multi-channel visual evoked potentials in early compressive lesions of the chiasm.
Docum. Ophthal. 69; 1988, 271-281.

Fox PT and Raichle ME.
Stimulus rate dependence of regional cerebral blood flow in human striate cortex, demonstration by positron emission tomography.
J. of Neurophys. 51 (5); 1984, 1109-1120.

Fukui R, Kato M and Kuroiwa Y.
Effect of central scotoma on pattern reversal visual evoked potentials in patients with maculopathy and healthy subjects.
EEG and Clin. Neuro. 63; 1986, 317-326.

Gallop JC.
SQUIDS, the josephson effects and superconducting electronics.
The Adam Hilger Series on measurement science and technology. 1990.

Galloway NR and Barber C.
The transient pattern onset VEP in glaucoma.
Doc. Ophthal. Proc. Series. Spekreijse H and Apkarian PA (Eds).
Dr. W Junk Publishers, Hague/Boston/London. 27; 1981, 95-101.

Ghilardi MF, Brannan JR and Bodis-Wollner I.
Clinical applications of pattern visual evoked potentials.
Visual Evoked Potentials. Desmedt JE (Ed). Ch 9; 1990, 121-146.

Gilbert MF, Hirsch JA and Wiesel TN.
Lateral interconnections in visual cortex.
The Brain. Symposia on quantitative biology Vol. LV.
Cold Spring Harbor Laboratory. 1990, 651-663

Gilbert CD and Wiesel TN.
Morphology and intracortical projections of functionally characterised neurones in the cat visual cortex. Nature 280; 1979, 120-125.

Gouras P.
Antidromic responses of orthodamatically identified ganglion cells in monkey retina.
J. Physiol. 204; 1969, 407-419.

Grynzpan F and Geselowitz DB.
Model studies of the magnetocardiogram.
Biophysics J. 13; 1973, 911-925.

Haimovic IC and Pedley TA.
Hemi-field pattern reversal visual evoked potentials II. Lesions of the chiasm and posterior visual pathways.
EEG and Clin. Neuro. 54; 1982, 121-131.

Halliday AM.
Evoked potentials in clinical testing.
Churchill Livingstone, Edinburgh. 1982.

Halliday AM, McDonald WI and Mushin J.
Delayed visual evoked response in optic neuritis.
The Lancet. 1972, 982-985.

Halliday AM and Michael WF.
Pattern evoked responses in man associated with the vertical and horizontal meridians of the visual field.
J. Physiol. 208; 1970, 499-513.

Hamalainen MS and Sarvas J.
Accurate modelling of the heads conductivity structure for neuromagnetic data analysis.
Bio-Magnetism 1987. 6th International Conference proceedings, Tokyo, Japan. 1987, 98-101.

Hammond SR, MacCallum S, Yiannikas C, Walsh JC and McLeod JG.
Variability on serial testing of pattern reversal visual evoked potential latencies from full field, half field and foveal stimulation in control subjects.
EEG and Clin. Neuro. 66; 1987, 401-408.

Harding GFA.
The visual evoked response.
Advances in Ophthalmol. 28; 1974, 2-28.

Harding GFA.
The flash evoked visual response and its use in ocular conditions.
J. of Electrophys. Technol. 8; 1982, 63-78.

Harding GFA.
Flash evoked cortical and subcortical potentials in neuro ophthalmology.
Acta. Neural. Belg. 85; 1985, 150-165.

Harding GFA.
Neurophysiology of vision and its clinical application.
Optometry. Edwards K and Llewellyn R (Eds).
Butterworth, London. Ch 3; 1988, 44-60.

Harding GFA.
The visual evoked potential in neuro-ophthalmic disorders.
Visual evoked potentials. Desmedt JE (Ed).
Elsevier. Ch 10; 1990, 147-167.

Harding GFA, Crews SJ and Good P.
The VEP as a diagnostic aid in neuro-ophthalmic disease.
In. Evoked Potentials. Barber C (Ed). MTP Press, Lancaster. 1980, 235-241.

Harding GFA, Degg C, Anderson SJ, Holliday I, Fylan F, Barnes G and Bedford J.
Topographic mapping of the pattern onset visually evoked magnetic response to stimulation of different portions of the visual field.
Invest. J. Psychophys. 16; 1994, 175-183.

Harding GFA, Doggett CE, Orwin A and Smith EJ.
Visual evoked potentials in pre-senile dementia.
Doc. Ophthal. Proc. series. 27; 1981, 193-202.

Harding GFA, Janday B and Armstrong RA.
Topographic mapping and source localization of the pattern reversal visual evoked magnetic response.
Brain Topography. 4 (1); 1991, 47-55.

Harding GFA and Rubinstein MP.
Early components of the visual evoked potential in man.
Doc. Ophthal. Proc. series. 27; 1981, 49-65.

Harding GFA and Wright CE.
Visual evoked potential in acute optic neuritis.
Optic Neuritis. Hess RF and Plant CT (Eds).
Cambridge University Press. Cambridge. 1986, 230-254.

Hari R, Joutsiniemi SL and Sarvas J.
Spatial resolution of neuromagnetic records: theoretical calculations in a spherical model.
EEG and Clin. Neuro. 71; 1988, 64-72.

Harter MR.
Evoked cortical responses to checkerboard patterns: effect of check size as a function of retinal eccentricity.
Vis. Res. 10; 1970, 1365-1376.

Harter MR.
Visually evoked cortical responses to the on and offset of patterned light in humans.
Vis. Res. 11; 1971, 685-695.

Harter MR and White CT.
Effects of contour sharpness and check-size on visually evoked cortical potentials.
Vis. Res. 8; 1968, 701-711.

Haywood M and Mills IM.
Design effects of video pattern generators on the VEP.
Evoked Potentials, Barber C (Ed), Chapter 6; 1980, 87-92.

Hellstrom B, Karlsson B and Mussbichler H.
Electrode placement in EEG of infants and its anatomical relationship studied radiographically.
EEG and Clin. Neuro. 15; 1963, 115-117.

Hodgkin AL.
Ionic movements and electrical activity in giant nerve fibres.
Proc. Royal Soc. 148; 1958, 1-37.

Hoke M, Feldmann H, Pantev C, Lutkenhoner B and Lehnertz K.
Objective evidence of tinnitus in auditory evoked magnetic fields.
Hearing Research. 37; 1989, 281-286.

Holmes G.
The organization of the visual cortex in man.
Proc. Roy. Soc. B. 132; 1945, 348-361.

Hubel DH.
Eye, brain and vision.
Sci. Am. Library.
HPHLP, New York. 1988.

Hubel DH and Wiesel TN.
Receptive fields of single neurons in the cats striate cortex.
J. Physiol. 148; 1959, 574-591.

Hubel DH and Wiesel TN.
Receptive fields, binocular interaction and functional architecture in the cats visual cortex.
J. Physiol. 160; 1962, 106-154.

Hubel DH and Wiesel TN.
Receptive fields and structural architecture of monkey striate cortex.
J. Physiol. 195; 1968, 215-243.

Hubel DH and Wiesel TN.
Functional architecture of macaque monkey visual cortex. Ferrier lecture.
Proc. R. Soc. Lond. Ser. B, 198; 1977, 1-59.

Hubel DH and Wiesel TN.
Brain mechanisms of vision. Sci. Am. 241; 1979, 150-162.

Hughes JR, Stone JL, Fino JJ and Hart LA.
Usefulness of different stimuli in visual evoked potentials.
Neurology 37; 1987, 656-662.

Ioannides AA, Bolton JPR, Hasson R and Clarke CJS.
Localised and distributed source solutions for the biomagnetic inverse problem II.
Advances in Biomagnetism. Williamson SJ et al (Eds).
Plenum Press, New York. 1989, 591-595.

Jacobson GP, Ahmad BK, Moran J, Newman CW, Tepley N and Wharton J.
Auditory evoked cortical magnetic field (M100-M200) measurements in tinnitus and normal groups.
Hearing Research. 56; 1991, 44-52.

James CR and Jeffreys DA.
Properties of individual components of pattern onset evoked potentials in man.
J. Physiol. 249; 1975, 57-58.

Jansen BH and Brandt ME.
The effect of the phase of prestimulus alpha acivity on the averaged visual evoked response.
EEG and Clin. Neuro. 80; 1991, 241-250.

Janday BS, Swithenby SJ and Thomas IM.
Combined magnetic field and electrical potential investigation of the visual pattern reversal system.
Proceedings of the 6th International conference on Biomagnetism.
Katila T, Ketani M, Williamson SJ and Venos S (Eds).
Denkai Press, Tokyo. 1988, 246-249.

Jasper HH.
The ten twenty electrode system of the international federation.
Committee on clinical examination in EEG, 1958, 371-375.

Jeffreys DA.
Cortical source locations of pattern related visual evoked potentials recorded from the human scalp.
Nature 229; 1971, 502-504.

Jeffreys DA.
The physiological significance of pattern visual evoked potentials.
Visual evoked potentials in Man. Desmedt JE (Ed).
Clarendon Press, Oxford. Ch 6; 1977, 134-167.

Jeffreys DA and Axford JG. (a)
Source locations of pattern specific components of human visual evoked potentials I. Component of striate cortical origin.
Exp. Brain Res. 16; 1972, 1-21.

Jeffreys DA and Axford JG. (b)
Source locations of pattern specific components of human visual evoked potentials II. Component of extrastriate cortical origin.
Exp. Brain Res. 16; 1972, 22.

Johnson BM, Mias M and Sadun AA.
Age related decline of human optic nerve axon populations.
Age 10; 1987, 5-9.

Josephson BD.
Supercurrents through Barriers. Advan. Phys. 14; 1965, 419-451.

Kalliomaki K, Kalliomaki PL, Aittoniemi K and Moilanen M.
Magnetopneumography: the magnetic technique for measuring lung contamination.
Biomagnetism: an interdisciplinary approach.
Williamson SJ, Romani GL, Kaufman L and Modena I (Eds).
New York, Plenum; 1982, 545-556.

Kandel ER.
Processing of form and movement in the visual system.
Principles of Neuroscience. Kandel ER and Schwartz JH (Eds).
Elsevier USA. Ch 29; 1985, 366-383.

Kaplan E, Lee BB and Shapley RM.
New views of primate retinal function.
Progress in retinal research. Osbourne N and Cohaden J (Eds).
Pergamon Press, Oxford. 1991, 273-336.

Katila T, Leinio M, Montonen J and Nenonen J.
Sensitivity limits in biomagnetic measurements.
ACTA Otolaryngol. (Stockh.), Suppl 491; 1991, 36-42.

Katila T and Varpula T.
Magnetic fields of the eye.
Biomagnetism: an interdisciplinary approach.
Williamson SJ, Romani GL, Kaufman L and Modena I (Eds).
New York, Plenum; 1982, 341-351

Kaufman L, Kaufman JH and Wang JZ.
On cortical folds and neuromagnetic fields.
EEG and Clin. Neuro. 79; 1991, 211-226.

Kaufman L and Williamson SJ.
Magnetic location of cortical activity.
Annals. NY Acad. Sci. 388; 1982, 197-213.

Kaufman L and Williamson SJ.
Neuromagnetic localization of neuronal activity in visual and extravisual cortex.
Vision and the Brain. 67; 1990, 271-287.

Kaufman L and Williamson SJ.
The evoked magnetic field of the human brain.
Annals NY Acad. Sci. 340; 1980, 45-65.

Kelly JP.
Anatomy of the central visual pathway.
Principles of Neuroscience. Kandel ER and Schwartz JH (Eds).
Elsevier USA. 28; 1985, 356-365.

Kjaer M.
The value of sequential evoked potential recordings in multiple sclerosis patients.
Clin. Appl. of EP in Neurol. Courion J, Mauguiere F and Revol M (Eds).
Raven Press, New York. 1982.

Kooi KA and Bagchi BK.
Visual evoked responses in man: normative data.
Annals NY Acad. Sci. 112; 1964, 254-269

Kouijzer WJJ, Stok CJ, Reits D, Donaiski Z, Lopes Da Silva FH and Peters MJ.
Neuromagnetic fields evoked by a patterned on-offset stimulus.
IEEE Trans. on Biomed. Eng. BME-32 (6); 1985, 455-458.

Krauskopf J, Klemic G, Lounasmaa OV, Travis D, Kaufman L and Williamson SJ.
Neuromagnetic measurements of visual responses to chromaticity and luminance.
Advances in Biomagnetism.
Williamson SJ, Hoke M, Stroink G and Kotani M (Eds), Plenum Press NY. 1989.

Kriss A.
Stimulating techniques and recording problems.
Evoked potentials in clinical testing. Halliday AM (Ed).
Churchill Livingstone, Edinburgh, London, Melbourne and New York. 2; 1982, 45-49.

Kriss A and Halliday AM.
A comparison of occipital potentials evoked by pattern onset, offset and reversal by movement.
Evoked Potentials. Barber C (Ed).
MTP Press, Lancaster. 1980, 213-218.

Kuffler SW.
Discharge patterns and functional organisation of mammalian retina.
J. Neurophys. 16; 1953, 37-68.

Kulikowski J.
Separation of occipital potentials related to the detection of pattern and movement.
Visual evoked potentials in Man. Desmedt JE (Ed).
Clarendon Press, Oxford. 1977, 184-196.

Kulikowski J and Murray IJ.
Contribution of striate cortical cells to pattern, movement and colour processing.
Models of the visual cortex. Rose D and Dobson VG (Eds).
Wiley and Sons Ltd. 25; 1985, 253-264.

Kulikowski J and Tolhurst DJ.
Psychophysical evidence for sustained and transient detectors in human vision.
J. Physiol. 232; 1973, 149-162.

Legge GE.
Sustained and transient mechanisms in humn vision: temporal and spatial properties.
Vis. Res. 18; 1978, 69-81.

Lehman D and Brown WS.
How to measure evoked EEG potentials for topography.
Evoked Potentials. Barber C (Ed), Chapter 14, 1980, 143-146.

Lehman D, Meles HP and Mir Z.
Average multichannel EEG potential fields evoked from upper and lower hemiretina: latency differences.
EEG and Clin. Neuro. 43; 1977, 725-731.

Lehman D and Skrandies W.
Multichannel evoked potential fields show different properties of human upper and lower hemiretina systems.
Exp. Brain Res. 35: 1979, 151-159.

Lehman D and Skrandies W.
Reference free identification of components of checkerboard evoked multichannel potential fields.
EEG and Clin. Neuro. 48; 1980, 609-621.

Lehmkuhle S, Kratz KE, Mangel SC and Sherman SM.
Spatial and temporal sensitivity of X and Y cells in the dorsal lateral geniculate nucleus of the cat. J. Neurophys. 43; 1980, 520-541.

Lennie P.
Signals in individual neurons.
Biomagnetism: an interdisciplinary approach.
Williamson SJ, Romani GL, Kaufman L and Modena I (Eds).
New York, Plenum; 1982, 364-374.

Lennie P.
Single unit activity, evoked potentials and perception.
Biomagnetism: an interdisciplinary approach.
Williamson SJ, Romani GL, Kaufman L and Modena I (Eds).
New York, Plenum; 1982, 364-374.

Lesevre N.
Chronotopographical analysis of the human evoked potential in relation to the visual field (data from normal individuals and hemianopic patients).
Annals NY Accad. Sci. 388; 1982, 156-182.

Lesevre N and Joseph JP.
Hypothesis concerning the most probable sites of origin of the various components of the pattern evoked potential.
Evoked potentials. Barber C (Ed). 1980, 159-166.

Lesevre N and Joseph JP.
Modifications of the pattern evoked potential (PEP) in relation to the stimulated part of the visual field (clues for the most probable origin of each component).
EEG and Clin. Neuro. 47; 1979, 183-203.

Leventhal AG.
Retinal design of the visual cortex.
Models of the visual cortex. Rose D and Dobson VG (Ed).
John Wiley and Sons Ltd. 1985, 380-389.

Leventhal AG, Ault SJ and Vitek DJ.
The nasotemporal division of the primate retina: the neural basis of macular sparing and splitting.
Science 240; 1988, 66-67.

Lewis G, Blackburn M, Naitoh P and Metcalfe M.
Few trial evoked field stability using the DC SQUID.
Biomagnetism: Applications and theory. Weinberg H, Stroink G and Katila T (Eds).
Pergamon Press, New York. 1984, 343-347.

Livingstone M.
Segregation of form, colour, movement and depth processing in the visual system: anatomy, phyiology, art and illusion.
Vision and the brain. Cohn B and Bodis-Wollner I (Eds).
Raven Press. NY. 1990, 119-138.

Livingstone M and Hubel D.
Anatomy and physiology of a colour system in primate visual cortex.
J. Neurosci. 4; 1984, 309.

Livingstone M and Hubel D.
Segregation of form, colour, movement and depth; anatomy, physiology and perception.
Science 240; 1988, 740-749.

Lovasik JV and Ahmedbhai N.
Stimulus contaminants in visual electrophysiology.
Am. J. Optom. and Physiol. Opt. 62 (5); 1985, 334-343.

Lueders H, Lesser RP and Klem G.
Pattern evoked potentials.
Current clinical neurophysiology: update on EEG and evoked potentials. Henry CE (Ed).
Elsevier North Holland, 1980, 467-521.

Lutkenhoner B, Lehnertz K, Hoke M and Pantev C.
On the biomagnetic inverse problem in the case of multiple dipoles.
Acta. Otolaryngol. (Stockh.). Suppl. 491; 1991, 94-105.

Maclin E, Okada YC, Kaufman L and Williamson SJ.
Retinotopic map on the visual cortex for eccentrically placed patterns: first non invasive measurement.
Il Nuovo Cimento 2; 1983, 410-419.

Maier J, Dagnelie G, Spekreijse H and Van Dijk BW.
Principal components analysis for source localization of VEPs in man.
Vis. Res. 27 (2); 1987, 165-177.

Makela JP and Hari R.
Long latency auditory evoked magnetic fields.
Advances in Neurology. Vol 54: Magnetoencephalography. Sato S (Ed).
Raven Press, New York. 1990, 177-192.

Manahilov V, Riemslag FCC and Spekreijse H.
The laplacian analysis of the pattern onset response in man.
EEG and Clin. Neuro. 82; 1992, 220-224.

Masland RH.
The functional architecture of the retina.
Sci. Am. 1986, 90-99.

May JG and Cullen JK.
Effects of meridional variation on steady state visual evoked potentials.
Vis Res. 19; 1979, 1395-1401.

May JG, Lovegrove WJ, Martin F and Nelson P.
Pattern elicited visual evoked potentials in good and poor readers.
Clin. Vis. Sci. 6 (2); 1991, 131-136.

McCormack G and Marg E.
Computer assisted eye examination II. Visual evoked response meridional refractometry.
Am. J. Optom. Archs. Am. Acad. Optom. 50; 1973, 889-903.

McGillem CD and Aunon JI.
Measurements of signal components in single visually evoked brain responses.
IEEE Trans. on Biomed. Eng. BME 24 (3); 1977, 232-241.

Meijs JWH, Bosch FGC, Peters MJ and Lopes Da Silva FH.
On the magnetic field distribution generated by a dipolar current source situated in a realistically shaped compartment model of the head.
EEG and Clin. Neuro. 66; 1987, 286-298.

Meredith JT and Celesia GG.
Pattern reversal visual evoked potentials and retinal eccentricity.
EEG and Clin. Neuro. 53; 1982, 243-253.

Michael WF and Halliday AM.
Differences between the occipital distribution of upper and lower field pattern evoked responses in man.
Brain Res. 32; 1971, 311-324.

Millodot M and Riggs LA.
Refraction determined electrophysiologically.
Arch. Ophthal. 84; 1970, 272-278.

Mori H and Nakaya Y.
Clinical value of magnetocardiography.
Proceedings of the 6th International conference on Biomagnetism.
Katila T, Ketani M, Williamson SJ and Venos S (Eds).
Denkai Press, Tokyo. 1987, 82-89.

Musselwhite MJ and Jeffreys DA.
Pattern evoked potentials and Blochs law.
Vis. Res. 22; 1982, 897-903.

Musselwhite MJ and Jeffreys DA.
The influence of spatial frequency on the reaction times and evoked potentials recorded to grating pattern stimuli.
Vis. Res. 25 (11); 1985, 1545-1555.

Myslobodsky MS, Glicksohn J, Coppola R and Weinberger DR.
Occipital lobe morphology in normal individuals assessed by magnetic resonance imaging (MRI).
Vis. Res. 31 (10); 1991, 1677-1685.

Narici L, Modena I, Opsomer RJ, Pizzella V, Romani GL, Torrioli G, Traversa R and Rossini PM.
Neuromagnetic somatosensory homunculus: a non invasive approach in humans.
Neuroscience Letters. 121; 1991, 51-54.

Nicholas P, Duret D, Teszner D and Tuomisto T.
Neuromagnetic measurements at hospital: instrumentation and preliminary tests.
Il Nuovo Cimento 20 (2); 1983, 184-194.

Nunez PL.
The brains magnetic field: some effects of multiple sources on localization methods.
EEG and Clin. Neuro. 63; 1986, 75-82.

Ochs AL and Aminoff MJ.
The effect of adaptation of the stimulating pattern on the latency and waveform of visual evoked potentials.
EEG and Clin. Neuro. 48; 1980, 502-508.

Okada Y.
Visual evoked field.
Biomagnetism: an interdisciplinary approach.
Williamson SJ, Romani GL, Kaufman L and Modena I (Eds).
New York, Plenum; 1982, 443-459.

Okada Y.
Neurogenesis of evoked magnetic fields.
Biomagnetism: an interdisciplinary approach.
Williamson SJ, Romani GL, Kaufman L and Modena I (Eds).
New York, Plenum; 1982, 399-408.

Okada Y.
Discrimination of localized and distributed current dipole sources and localized single and multiple sources.
Biomagnetism: Applications and theory. Weinberg H, Stroink G and Katila T (Eds).
Pergamon Press, New York. 1984.

Okada Y.
MEG as a noninvasive tool for electrophysiological characterization of auras in classic migraine.
Advances in Neurology. Vol 54: Magnetoencephalography. Sato S (Ed).
Raven Press, New York. 1990, 133-140.

Okada Y, Kaufman L, Brenner D and Williamson SJ.
Modulation transfer functions of the human visual system revealed by magnetic field measurements.
Vis. Res. 22; 1982, 319-333.

Okada Y, Lauritzen M and Nicholson C.
MEG source models and physiology.
Phys. Med. Biol. 32 (1); 1987, 43-51.

Oken BS, Chiappa KH and Gill E.
Normal temporal variability of the P100.
Clin. Neurophys. 68; 1987, 153-156.

Ono M, Kubik S. and Abernathey CD.
Atlas of the cerebral sulci.
Thieme, Stuttgart. 1990.

Onofrj M, Bodis-Wollner I and Mylin L.
Visual evoked potential diagnosis of field defects in patients with chiasmatic and retrochiasmatic lesions.
J. Neurol. Neurosurg. and Psych. 45; 1982, 294-302.

Orwin A, Wright CE, Harding GFA, Rowan DC and Rolfe EB.
Serial visual evoked potential recordings in Alzheimers disease.
British Medical Journal 293; 1986, 9-10.

Ossenblok P and Spekreijse H.
The extrastriate generators of the EP to checkerboard onset. A striate localization approach.
EEG and Clin. Neuro. 80; 1991, 181-193.

Padhiar S and Harding GFA.
Effects of time of day on the flash and pattern reversal visual evoked potential.
EEG and Clin. Neuro. 78; 1991, 87P.

Pantev C, Hoke M and Lehnertz K.
Randomized data acquisition paradigm for the measurement of auditory evoked magnetic fields.
Acta Otolaryngol. (Stockh.) Suppl 432; 1986, 21-25.

Pantev C, Hoke M, Lutkenhoner B, Lehnertz K and Kumpf W.
Tinnitus remission objectified by neuromagnetic measurements.
Hearing Res. 40; 1989, 261-264.

Parker DM and Salzen EA.
Latency changes in the human visual evoked response to sinusoidal gratings.
Vis. Res. 17; 1977, 1201-1204.

Parker DM, Salzen EA and Lishman JR.
The early wave of the visual evoked potential to sinusoidal gratings: responses to quadrant stimulation as a function of spatial frequency.
EEG and Clin. Neuro. 53; 1982, 427-435.

Parker DM, Salzen EA and Lishman JR.
Visual evoked response elicited by the onset and offset of sinusoidal gratings: latency, waveform and topographic characteristics.
Invest. Ophthal. Vis. Sci. 22 (5); 1982, 675-680.

Pelizzone M and Hari R.
Interpretation of neuromagnetic responses: two simple models for extended current sources in the human auditory cortex.
Acta Otolaryngol. (Stockh.) Suppl. 432; 1986, 15-20.

Pizzella V and Romani GL.
Principles of magnetoencephalography.
Advances in Neurology. Vol 54: Magnetoencephalography. Sato S (Ed).
Raven Press, New York. 1990, 1-10.

Plant GT, Laxer KD, Barbaro NM, Schiffman JS and Nakayama K.
Impaired visual motion perception in the contralateral hemifield following unilateral posterior cerebral lesions in humans. Brain 116; 1993, 1303-1335.

Polyak S.
The vertibrate visual system.
Heinrich Kluver (Ed). The University of Chicago Press, Chicago and London. 1953.

Quigley HA, Dunkelberger GR and Green WR.
Chronic human glaucoma causing selectively greater loss of large optic nerve fibres.
Ophthalmology 95; 1988, 357-363.

Regan D.
Human brain electrophysiology, evoked potentials and evoked magnetic fields in science and medicine.
Elsevier 1989.

Regan D and Richards W.
Independence of evoked potentials and apparent size.
Vis. Res. 11; 1971, 679-684.

Reilly EL, Kondo C, Brunberg JA and Doty DB.
Visual evoked potentials during hypothermia and prolonged circulatory arrest.
EEG and Clin. Neuro. 45; 1978, 100-106.

Reite M, Edrich J, Zimmerman JT and Zimmerman JE.
Human magnetic auditory evoked fields.
EEG and Clin. Neuro. 45; 1978, 114-117.

Ricci GB.
Italian contributions to MEG studies of the epilepsies.
Advances in Neurology. Vol 54: Magnetoencephalography. Sato S (Ed).
Raven Press, New York. 1990, 247-260.

Richer F, Barth DS and Beatty J.
Neuromagnetic localization of two components of the transient visual evoked response to patterned stimulation.
Il Nuovo Cimento 20 (2); 1983, 420-428.

Riemslag FCC, Spekreijse H and Van Walbeek H.
Pattern reversal and appearance disappearance responses in MS patients.
Doc. Ophthal. Proc. Series. 27; 1981, 215-221.

Rietveld WJ, Tordoir WEM, Hagenouw JRB, Lubbers JA and Spoor AC.
Visual evoked responses to blank and to checkerboard patterned flashes.
ACTA. Physiol. Pharmacol. Neerl 14; 1967, 259-285.

Ristanovic D and Hajdukovic R.
Effects of spatially structured stimulus fields on pattern reversal visual evoked potentials.
EEG and Clin. Neuro. 51; 1981, 599-610.

Rizzolatti G and Buchtel HA.
Hemispheric superiority in reaction time to faces, a sex difference.
Cortex. 13; 1977, 300-305.

Rogers RL, Baumann SB, Papanicolaou AC, Bourbon TW, Alagarsamy S and Eisenberg HM.
Localization of the P3 sources using MEG and MRI.
EEG and Clin. Neuro. 79; 1991, 308-321.

Romani GL.
Tonotopic organization of the human auditory cortex revealed by steady state neuromagnetic measurements.
ACTA Otolaryngol. (Stockh.) Suppl. 432; 1986, 33-34.

Romani GL and Leoni R.
Localization of cerebral sources by neuromagnetic measurements.
Biomagnetism: Applications and theory. Weinberg H, Stroink G and Katila T (Eds).
Pergamon Press, New York. 1984. 205-220.

Romani GL and Narici L.
Principles and clinical validity of the biomagnetic method.
Med. Progress through technology II 1986, 123-159.

Romani GL and Pizzella V.
Localization of brain activity with magnetoencephalography.
Advances in Neurology. Vol 54: Magnetoencephalography. Sato S (Ed).
Raven Press, New York. 1990, 67-78.

Rose DF.
Magnetic evoked responses: comparison with electrical evoked responses.
Advances in Neurology. Vol 54: Magnetoencephalography. Sato S (Ed).
Raven Press, New York. 1990, 89-94.

Rose DF and Ducla-Soares E.
Comparison of electroencephalography and magnetoencephalography.
Advances in Neurology. Vol 54: Magnetoencephalography. Sato S (Ed).
Raven Press, New York. 1990, 33-38.

Rose DF, Smith PD and Sato S.
Magnetoencephalography and epilepsy research.
Science 238; 1987, 329-335.

Rossini PM and Traversa R.
Somatosensory evoked fields in MEG: basic principles and applications.
Advances in Neurology. Vol 54: Magnetoencephalography. Sato S (Ed).
Raven Press, New York. 1990, 157-166.

Roth BJ.
Biomagnetic studies of peripheral nerves and skeletal muscle.
Advances in Neurology. Vol 54: Magnetoencephalography. Sato S (Ed).
Raven Press, New York. 1990, 101-118.

Rutten WLC, Bakker D, Kuit JH, Maes MA and Grote JJ.
The use of a SQUID magnetometer in the study and development of normal and artificial middle ear.
ACTA Otolaryngol. (Stockh.) Suppl. 432; 1986, 11-14.

Sato S.
Epilepsy research: NIH experience.
Advances in Neurology. Vol 54: Magnetoencephalography. Sato S (Ed).
Raven Press, New York. 1990, 223-230.

Schiller PH and Colby CL.
The responses of single cells in the lateral geniculate nucleus of the rhesus monkey to colour and luminance contrast. Vis. Res. 23; 1983, 1631-1641.

Schmitz L.
Magnetocardiography: the clinicians point of view.
Proceedings of the 6th International conference on Biomagnetism.
Katila T, Ketani M, Williamson SJ and Venos S (Eds).
Denkai Press, Tokyo. 1987, 66-73.

Sencaj RW and Aunon JI.
Dipole localization of average and single visual evoked potentials.
IEEE Trans. on Biomed. Eng. BME-29 (1); 1982, 26-33.

Shagass C.
Evoked brain potentials in psychiatry.
Plenum Press, NY London. 1972.

Shagass C, Amadeo M and Roemer RA.
Spatial distribution of potentials evoked by half field pattern reversal and pattern onset stimuli.
EEG and Clin. Neuro. 41; 1976, 609-622.

Shapley R, Kaplan E and Soodak RM.
Spatial summation and contrast sensitivity of X and Y cells in the LGN of the macaque.
Nature 292; 1981, 543-545.

Sherman SM.
Parallel W, X and Y cell pathways in the cat: a model for visual function.
Models of the visual cortex. Rose D and Dobson VG (Eds).
John Wiley and Sons Ltd, 1985, 71-83.

Sherman SM, Wilson JR, Kaas JH and Webb SV.
X and Y cells in the dorsal lateral geniculate nucleus of the owl monkey (Actus trivirgatus).
Science 192; 1976, 475-476.

Singer W.
Central core control of visual cortex functions.
The neurosciences fourth study program.
MIT Press, Cambridge, Massachusetts and London, England. 67; 1979, 1093-1110.

Skrandies W, Richer M and Lehman D.
Checkerboard evoked potentials: topography and latency for onset, offset and reversal.
Progress in brain research. Kornhuber HH and Decokle L (Eds).
Elsevier 54; 1980.

Skullerud K.
Variations in the size of the human brain: influence of age, sex, bodylength, body mass index, alcoholism, Alzheimer changes and cerebral atherosclerosis.
ACTA Neurologica, Scand. Suppl. 102 (71); 1985, 5-93.

Skuse NF and Burke D.
Power spectrum and optimal filtering for visual evoked potentials to pattern reversal.
EEG and Clin. Neuro. 77; 1990, 199-204.

Slaven A.
Visual evoked magnetic responses (VEMR), to flash and pattern reversal stimulation.
PhD Thesis, Aston University, Birmingham. 1993.

Slaven A, Degg C and Armstrong RA.
Topography of visual evoked magnetic responses to pattern shift, pattern onset and flash stimuli.
Ophthal. and Physiol. Optics. 11; 1991, 369.

Smith AT and Jeffreys DA.
Size and orientation specificity of transient visual evoked potentials in man.
Vis. Res. 18; 1978, 651-655.

Snyder EW, Dustman RE and Shearer DE.
Pattern reversal evoked potential amplitudes: life span changes.
EEG and Clin. Neuro. 52; 1981, 429-434.

Sokol S and Moskowitz A.
Effect of retinal blur on the peak latency of the pattern evoked potential.
Vis. Res. 21; 1981, 1279-1286.

Spalding JMK.
Wounds of the visual pathway, Part II the striate cortex.
J. Neurosurg. Psychiat. 15; 1952, 169-176.

Spekreijse H.
Localization of the electromagnetic sources of the pattern onset response in man.
Pigments to perception. Valberg A and Lee BB (Eds).
Plenum Press, New York. 1991, 211-221.

Spekreijse H, Dagnelie G, Maier J and Regan D.
Flicker and movement constituents of the pattern reversal response.
Vis. Res. 25 (9); 1985, 1297-1304.

Spekreijse H, Estevez O and Reits D.
Visual evoked potentials and the physiological analysis of visual processes in man.
Visual evoked potentials in Man. Desmedt JE (Ed).
Clarendon Press, Oxford. 1977, 16-89.

Spekreijse H, Van Der Tweel and Regan D.
Interocular sustained suppression: correlations with evoked potential amplitude and distribution.
Vis. Res. 12; 1972, 521-526.

Spekreijse H, Van Der Tweel and Zuidema TH.
Contrast evoked responses in man.
Vis. Res. 13; 1973, 1577-1601.

Spinelli D and Mecacci L.
Handedness and hemispheric asymmetry of pattern reversal visual evoked potentials.
Brain and Cognition 13; 1990, 193-210.

Squires KC and Donchin E.
Beyond averaging: the use of discriminant functions to recognize event related potentials elicited by single auditory stimuli.
EEG and Clin. Neuro. 41; 1976, 449-459.

Srebro R.
Localization of visually evoked cortical activity in humans.
J. Physiol 360; 1985, 233-246.

Srebro R and Purdy PD.
Localization of visually evoked cortical activity using magnetic resonance imaging and computerized tomography.
Vis. Res. 30; 1990, 351-358.

Steinmetz H, Furst G and Meyer BU.
Craniocerebral topography within the international 10-20 system.
EEG and Clin. Neuro. 72; 1989, 499-506.

Stockard JJ, Hughes JF and Sharbrough FW.
Visually evoked potentials to electronic pattern reversal latency variations with gender, age and technical factors.
Am. J. EEG Technol. 19; 1979, 171-204.

Stok CJ.
The inverse problem in EEG and MEG with application to visual evoked responses.
PhD Thesis, Leiden Finland. 1986.

Stok CJ, Kouijzer WJJ and Peters MJ.
Source localization based on EEG's and MEG's.
Biomagnetism: Applications and theory. Weinberg H, Stroink G and Katila T (Eds).
Pergamon Press, New York. 1984. 283-288.

Stolz G, Aschoff JC, Born J and Aschoff J.
VEP, physiological and psychological circadian variations in humans.
J. Neurol. 235; 1988, 308-313.

Sur M and Sherman SM.
Linear and nonlinear W cells in the C laminae of the cats lateral geniculate nucleus.
J. Neurophys. 47; 1982, 869-884.

Sutherling WW and Barth DS.
MEG in clinical epilepsy studies: the UCLA experience.
Advances in Neurology. Vol 54: Magnetoencephalography. Sato S (Ed).
Raven Press, New York. 1990, 231-246.

Sutherling WW, Crandell PH, Cahan LD and Barth DS.
The magnetic field of epileptic spikes agrees with intercranial localizations in complex partial epilepsy.
Neurology 38; 1988, 778-786.

Tan CT, Murray NMF, Sawyers D and Leonard TJK.
Deliberate alteration of the visual evoked potential.
J. Neurol. Neurosurg. and Psychiatry. 47; 1984, 518-523.

Teyler TJ, Cuffin BN and Cohn D.
The visual evoked magnetoencephalogram.
Life Sciences 17; 1975, 683-692.

Tolhurst DJ.
Sustained and transient channels in human vision.
Vis. Res. 15; 1975, 1151-1155.

Tootell RB, Silverman MS and DeValois RL.
Spatial frequency columns in primary visual cortex.
Science 214; 1981, 813-815.

Torok B, Meyer M and Wildberger H.
The influence of pattern size on amplitude, latency and waveform of retinal and cortical potentials elicited by checkerboard pattern reversal and stimulus onset offset.
EEG and Clin. Neuro. 84; 1992, 13-19.

Tripp JH.
Physical concepts and mathematical models.
Biomagnetism: procedings of the 3rd International workshop on Biomagnetism, Erne SN, Hahlbohm HD and Lubbig H (Eds). 1981, 207-215.

Van Dijk BW and Spekreijse H.
Localization of electric and magnetic sources of brain activity.
Visual Evoked Potentials. Desmedt JE (Ed).
Elsevier Ch 5, 1990, 57-74.

Van Essen DC.
Functional organization of primate visual cortex.
Cerebral Cortex. Peters A and Jones EG (Eds).
Plenum Press, New York. 1985; Vol. 3, 259-330.

Vassilev A, Manahilov V and Mitov D.
Spatial frequency and the pattern onset offset response.
Vis. Res. 23 (12); 1983, 1417-1422.

Vassilev A and Strashimirov D.
On the latency of human visually evoked response to sinusoidal gratings.
Vis. Res. 19; 1979, 843-845.

Vella EJ, Butler SR and Glass A.
Electrical correlate of right hemisphere function.
Nature, New Biol. 125; 1972, 236.

Victor JD, Conte MM and Iadecola C.
Ocular dependence of hemifield visual evoked potentials: relevance to bilateral cortical representation of central vision.
Clin. Vis. Sci. 6 (4); 1991, 261-276.

Vieth JB.
MEG in the study of stroke (cardiovascular accident).
Advances in Neurology. Vol 54: Magnetoencephalography. Sato S (Ed).
Raven Press, New York. 1990, 261-270.

Von Bonin G.
Essay on the cerebral cortex.
Kampmeier OF (Ed).
American lecture series. Charles Thomas, Springfield Illinois USA, 1950.

Werre PF and Smith CJ.
Variability of responses evoked by flashes in man.
EEG and Clin. Neuro. 17; 1964, 644-652.

Wikswo JP.
Cellular action currents.
Biomagnetism: an interdisciplinary approach.
Williamson SJ, Romani GL, Kaufman L and Modena I (Eds).
New York, Plenum; 1982, 173-207.

Williamson SJ, Kaufman L and Brenner D.
Latency of the neuromagnetic response of the human visual cortex.
Vis. Res. 18; 1978, 107-110.

Williamson SJ, Robinson SE and Kaufman L.
Methods and instrumentation for biomagnetism.
Proceedings of the 6th International conference on Biomagnetism.
Katila T, Ketani M, Williamson SJ and Venos S (Eds).
Denkai Press, Tokyo. 1988, 18-25.

Woody CJ.
Characterization of an adaptive filter for the analysis of variable latency neuroelectric signals.
Med. and Biomed. Eng. 5; 1967, 539-553.

Wright CE.
The clinical use of spatial and temporal aspects of vision.
PhD Thesis, Aston University, Birmingham. 1983.

Wright CE and Drasdo N.
The influence of age on the spatial and temporal contrast sensitivity function.
Docum. Ophthalmol. 59; 1985, 385-395.

Wright CE, Drasdo N and Harding GFA.
Pathology of the optic nerve and visual association areas.
Brain 110; 1987, 107-120.

Wright CE, Harding GFA and Orwin A.
Presenile dementia: the use of the flash and pattern VEP in diagnosis.
EEG and Clin. Neuro. 57; 1984, 405-415.

Wright CE, Williams DE, Drasdo N and Harding GFA.
The influence of age on the ERG and VEP.
Docum. Ophthal. 59; 1985, 365-384.

Yarranton GA.
Pattern analysis by regression.
Ecology 50 (3); 1969, 390-395.

Yoshii M, Yanashima K, Kawara T, Nozawa F and Okisaka S.
Luminance unbalanced pattern onset offset electroretinogram and visual evoked cortical potential.
Docum. Ophthal. 76; 1991, 359-366.

Zeki S.
parallelism and functional specialization in human visual cortex.
The Brain. Symposia on quantitative biology Vol. LV.
Cold Spring Harbor Laboratory. 1990, 651-663

Zeki S.
The visual image in mind and brain.
Sci. Am. Special Issue. 1992, 42-51.

Zeki S and Shipp S.
The functional logic of cortical connections.
Nature. 335; 1988, 311-317.

Zerlin S and Davis H.
The variability of single evoked vertex potentials in man.
EEG and Clin. Neuro. 23; 1967, 468-472.

Zimmerman JE.
Magnetic quantities, units, materials and measurements.
Biomagnetism: an interdisciplinary approach.
Williamson SJ, Romani GL, Kaufman L and Modena I (Eds).
New York, Plenum; 1982.

Zimmerman JE and Fredrick NV.
Miniture ultrasensitive magnetic gradiometer and its use in cardiography and its use in cardiography and other applications. Applied. Phys. Lett. 19; 1971, 16-19.

Zrenner E.
Discussion: P and M pathways I.
Pigments to perception. Valberg A and Lee BB (Eds).
Plenum Press, New York. 1991, 133-196.